

Proceedings of XIII-th International
School-Conference "Actual Problems of
Microworld Physics"

Joint Institute for Nuclear Research, Dubna

Institute for Nuclear Problems
of Belarusian State University, Belarus

B.Stepanov Institute of Physics of the National Academy
of Sciences of Belarus, Belarus

Gomel Branch of the National Academy of Sciences
of Belarus, Belarus

F.Skorina Gomel State University, Belarus

Sukhoi State Technical University of Gomel, Belarus

Gomel, Belarus, July 27 - August 7, 2015

INTERNATIONAL ADVISORY COMMITTEE

V. Matveev, JINR (Chairman), *V. Anishchik*, BSU, Belarus,
V. Baryshevsky, INP BSU, Belarus, *M. Itkis*, JINR,
P. Jenni, CERN, Switzerland, *S. Kilin*, NAS, Belarus,
W. Lohmann, DESY, Germany, *V. Savrin*, SINP MSU, Russia,
G. Shirkov, JINR, *G. Snow*, LSU, USA,
V. Strazhev, BSU, Belarus, *L. Tomilchik*, IP NAS, Belarus,
G. Tonelli, INFN and University Pisa, Italy

ORGANIZING COMMITTEE from JINR

V. Matveev (Chairman), *N. Russakovich* (Vice-chairman),
S. Pakulyak (Vice-Chairman), *V. Bednyakov*, *S. Dmitriev*, *I. Golutvin*,
V. Kekelidze, *V. Korenkov*, *E. Russakovich*, *V. Shvetsov*, *V. Voronov*

ORGANIZING COMMITTEE from BELARUS

A. Shumilin, Minsk (Chairman); *N. Shumeiko*, Minsk (Vice-Chairman);
Yu. Pleskachevsky, Gomel (Vice-Chairman); *V. Andreev*, Gomel (Rector);
V. Makarenko, Minsk (Scientific Secretary);
O. Deryuzhkova, Gomel (Scientific Secretary); *I. Feranchuk*, Minsk;
Yu. Kurochkin, Minsk; *V. Kuvshinov*, Minsk; *N. Maksimenko*, Gomel;
V. Mossolov, Minsk; *V. Orlovich*, Minsk; *N. Pershay*, Minsk;
B. Pirshtuk, Gomel; *V. Prokoshin*, Minsk; *A. Rogachev*, Gomel;
S. Sinyukovich, Minsk; *O. Solovtsova*, Gomel; *V. Stankevich*, Gomel;
S. Timoshin, Gomel; *A. Yankovich*, Gomel

EDITORIAL BOARD

V. Andreev, *A. Ilyichev*, *V. Makarenko*, *N. Maksimenko*, *E. Russakovich*,
N. Russakovich, *N. Shumeiko*, *S. Timoshin*

Contents

1. Accelerator Physics	7
Precision Higgs Boson Measurement at CLIC <i>M. Pandurović</i>	9
The Deep Inelastic Scattering on the Polarized Nucleons at Electron-Ion Collider <i>E.S. Timoshin, S.I. Timoshin</i>	24
Center-Edge Asymmetry as a Tool for Revealing Large Extra Dimensions at LHC <i>A.A. Pankov, I.A. Serenkova, A.V. Tsytrinov, V.A. Bednyakov</i>	35
High-Precision Determination of the $Z - Z'$ Mixing Angle at LHC <i>A.A. Pankov, A.V. Tsytrinov</i>	46
A Stand-alone Geant4 Simulation of an Electron Calorimeter for COMET Experiment <i>A. Melnik, Dz. Shoukavy</i>	58
2. Non-Accelerator Physics	67
Minimal Length in Quantum Theory and Gravity and Measurability <i>A.E. Shalyt-Margolin</i>	69
Evolution of Entangled States in QCD Vacuum <i>V.I. Kvashinov, E.G. Bagashov</i>	89
High Precision Method for the Linear Confining Potential in Momentum Space <i>V.V. Andreev</i>	94
New properties of conformal transformations for scalar and Dirac particles in Riemannian and Riemann-Cartan spacetimes <i>A.J. Silenko</i>	103
The Integral Equations Solution for Quantum Two Particles System with the Cornell Potential in Momentum Space <i>K.S. Babich, V.V. Andreev</i>	118
Research of the Stability of Motion of Fermions	128

<i>E.E. Kazitsky, V.I. Kuvshinov</i>	
Solution of the Schrödinger Equation for Parabolic Double-Well Potential	134
<i>V.V. Kudryashov, A.V. Baran</i>	
Dipole Spin Polarizabilities and Gyration of Spin-1 Particles in the Duffin-Kemmer-Petiau Formalism	139
<i>E.V. Vakulina, N.V. Maksimenko, S.M. Kuchin</i>	
Corrections to the Formula for Baryshevsky-Luboshitz Effect in Magnetic Field	152
<i>A.I. Sery</i>	
3. Relativistic Physics of Hadron and Nuclei	161
Hadron as Coherent State on the Horosphere of the Lobachevsky Momentum Space	163
<i>Y.A. Kurochkin, Y.A. Kulchitsky, S.N. Harkusha, N.A. Rusakovich</i>	
The QCD Analysis of the F_3 Structure Function within the Analytic Approach Based on the Inverse Mellin Transform Method	172
<i>A.V. Sidorov, O.P. Solovtsova</i>	
On Target Mass Corrections to Deep-Inelastic Structure Functions	180
<i>V.I. Lashkevich, O.P. Solovtsova</i>	
A Spin-dependent Dipole Polarizabilities and Characteristics of the Nucleon, Related with Parity Violation	188
<i>V.V. Andreev, O.M. Deryuzhkova, N.V. Maksimenko</i>	
Form Factor of the Relativistic Two-particle System in the Relativistic Quasipotential Approach: The Case of Arbitrary Masses and Vector Current	199
<i>Yu.D. Chernichenko</i>	
The Quark Potential Model in Theory of Resonances	219
<i>M.N. Sergeenko</i>	
Interactions of Strange Mesons at Low Energies	227

<i>E.Z. Avakyan, S.L. Avakyan</i>	
Low Energy Hadron Interaction of Tau Lepton	242
<i>E.Z. Avakyan, S.L. Avakyan</i>	
4. Physics In and Beyond the Frame of the Standard Model	251
Some NNLO Contribution to the Drell-Yan Differential Cross Section	253
<i>Ya. Dydyshka V. Yermolchik, J. Suarez Gonzalez</i>	
Experimental Signatures of the Gauge-Higgs Unification Models	262
<i>A.A. Babich</i>	
Electromagnetic Decays of Light Vector Mesons	275
<i>V.V. Andreev, V.Yu. Gavrish</i>	
The Polarized Semi-inclusive Lepton-Nucleon DIS with Charged Current	281
<i>E.A. Degtyareva, S.I. Timoshin</i>	
One-Loop Radiative Corrections of Two-Photon Production Processes of the Leptons at Colliders	288
<i>A. Manko, R. Shulyakovsky</i>	
5. Nuclear Energy	301
Numerical Simulation of Flow and Heat Transfer around of Spherical Fuel Elements	299
<i>L. Babichev, S. Bakhanovitch, G. Gromyko, A. Zherelo</i>	
The Estimation of Efficiency of the Control Rods in the Reactor with Sodium Coolant Using Monte Carlo Simulation	304
<i>L.F. Babichev, G.W. Karpovich</i>	
Steps in Creation of Educational and Research Web-portal of Nuclear Knowledge BelNET	310
<i>S. Charapitsa, I. Dubovskaya, I. Kimlenko, A. Kovalenko, A. Lobko, A. Mazanik, N. Polyak, T. Savitskaya, T. Sidorovich, S. Sytova, A. Timoschenko</i>	
7. List of Participants	321

1 Accelerator Physics

Precision Higgs Boson Measurement at CLIC

Mila Pandurović*, on behalf of the CLICdp collaboration

Vinča Institute of Nuclear Sciences, Belgrade, Serbia

Abstract

The design of the next generation collider in high energy physics will primarily focus on the possibility to achieve high precision of the measurements of interest. The necessary precision limits are set, in the first place, by the measurement of the Higgs boson but also by measurements that are sensitive to signs of New Physics. The Compact Linear Collider (CLIC) is an attractive option for a future multi-TeV linear electron-positron collider, with the potential to cover a rich physics program with high precision. In this lecture the CLIC accelerator, detector and backgrounds will be presented with emphasis on the capabilities of CLIC for precision Higgs physics.

1 Introduction

The particle that completed the Standard model (SM) picture, the Higgs boson, was discovered at the Large Hadron Collider (LHC) in 2012 [1][2]. Besides the measurement of the Higgs boson mass, measurements of other Higgs boson properties, like its couplings to the SM particles, require high precision in order to be sensitive to eventual signs of New Physics, as well as to understand the structure of the Higgs sector. The LHC, being the discovery machine, was designed to reach extremely high center-of-mass energy of 14 TeV at the ultimate stage of operation. Due to the composite nature of colliding particles, the actual collision occurs at the parton level. The effective center-of-mass energy available in the parton-parton collision is $\sqrt{s} \approx 3\text{TeV}$. Also, the initial state of colliding partons is not known, and

*E-mail:milap@vinca.rs

it is determined statistically from the final state. Besides, the presence of high level of QCD background and multiple pile-up events restrict the precision of all measurements. On the other hand at the lepton colliders the colliding particles, electrons and positrons, are fundamental objects. Therefore collisions have a well-known initial state and low level of background. Furthermore all of the center-of-mass energy is available for the collision. These properties make the lepton colliders suitable candidates to be the precision machines.

1.1 CLIC accelerator

The particle acceleration at CLIC is based on a new, 'two-beam' acceleration technique. Two separate beam pipes, running in the parallel to each other, are carrying two beams: the drive beam and the main beam. The drive beam is carrying power for the acceleration, with frequency of 12 GHz, high current (100 A) and low energy of (2.4 GeV -240 MeV). This power is extracted from the drive beam and converted in radio-frequent power in PETS (Power Extraction and Transfer Structures). PETS are positioned along the drive beam and paired-up with the accelerating structures which are placed along the main beam (Figure 1) [3].

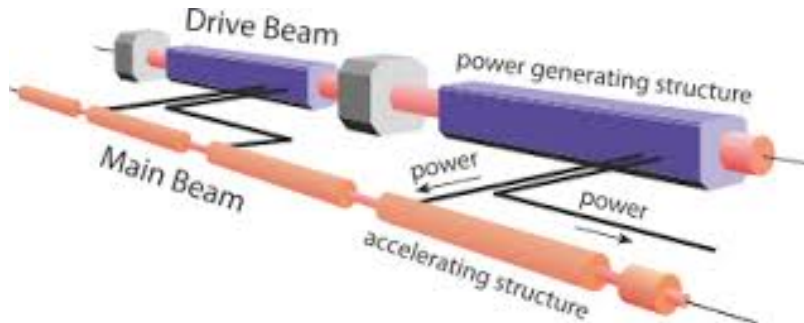


Figure 1: Two beam scheme: The beam power in the drive beam is converted to RF power in Power Extraction and Transfer Structures, and injected into accelerating structures in the main beam.

The energy extracted in the PETS is injected into accelerating structures and used to achieve the high energy (up to 1.5 TeV) in the main beam. The CLIC accelerating gradient is foreseen to be 100 MV/m.

The particles in the main beam are organized into bunches. The bunch population is $3.7 \cdot 10^9$ particles. Further, the bunches are organized into

bunch trains of 312 bunches, with the bunch separation of 0.5 ns. Bunch trains are released with $f_{rep}=50$ Hz repetition rate. The two-beam acceleration scheme is one of the subjects of the study of the CTF3 test facility at CERN.

1.2 CLIC energy staged design

The energy staged design of the CLIC collider has been optimized to maximize the physics potential of the machine and provide an early start of physics. Three distinct stages were chosen, in the way to adapt to the known physics and to eventual discoveries at the LHC.

Current studies foresee three stages, $\sqrt{s} = 380$ GeV, 1.4 TeV and 3 TeV. This would yield the collider overall length of 11.4 km, 27.2 km, and final extension to a length of 48.3 km, respectively, based on an accelerating gradient of 100 MV/m. The staging design is based on the foreseen physics program. The first stage of running, $\sqrt{s} = 380$ GeV, is devoted to the Standard model Higgs studies and exploration of the top physics, including $t\bar{t}$ threshold scan. The second stage, $\sqrt{s} = 1.4$ TeV, is chosen as it is sensitive to many of the Beyond Standard Model (BSM) models. Also the high statistics of the dominant WW-fusion Higgs production channel at this energy stage, gives access to rare Higgs processes, as well as to the Higgs self-coupling and quartic Higgs coupling. The final stage, $\sqrt{s} = 3.0$ TeV, improves the precision obtained at previous energy stages in both Higgs and BSM physics, and adds additional discovery potential.

1.3 CLIC experimental environment

One of the most important parameters of any collider experiment is its luminosity. At a linear e^+e^- collider the increase in luminosity is achieved by the optimisation of the beam parameters. The focusing of the beam, on the other hand, is limited by the energy loss by *beamstrahlung* caused by the electromagnetic interaction of the opposite beams.

1.3.1 Luminosity

The instantaneous luminosity is given by:

$$\mathcal{L} = \frac{n_b N^2 f_{rep}}{4\pi\sigma_x\sigma_y} \quad (1)$$

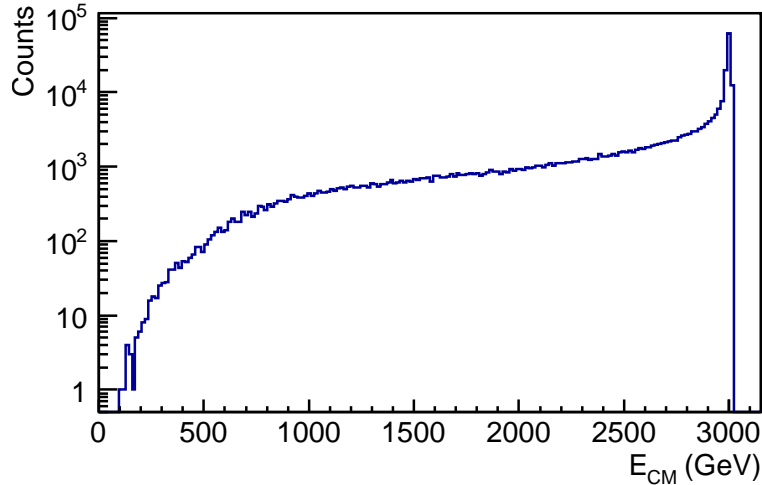


Figure 2: CLIC luminosity spectrum as a function of the effective center-of-mass energy.

where σ_x , σ_y are transverse bunch sizes, N is the bunch population and n_b is the number of bunches in a bunch train. The increase in the luminosity at linear colliders is achieved by the using high bunch population, $\mathcal{O}(10^9)$, and small beam sizes.

1.3.2 Beam-induced background

The high bunch population and small bunch size results in a strong electric field of a bunch. This is causing the particles in the colliding bunches to accelerate towards the bunch center, subsequently radiating photons. The emission of this radiation, *beamstrahlung*, has a consequence that it degrades the luminosity spectrum. Figure 2 shows the luminosity spectrum for the 3 TeV CLIC [4]. The effect is most pronounced at the highest energy stage, where around 35% of events preserve the nominal of center-of-mass energy within the less then a percent energy loss.

The energy loss by beamstrahlung is proportional to:

$$\delta E \propto \frac{N^2}{(\sigma_x + \sigma_y)\sigma_z} \quad (2)$$

The maximal length of the bunch is limited by the Hourglass effect [5], thus in order to maximize the luminosity and minimize beamstrahlung energy

loss, the flat beams, with the $\sigma_x \gg \sigma_y$ are chosen. For the final, 3 TeV energy stage the parameters foreseen are $\sigma_x=45$ nm, $\sigma_y=1$ nm.

The beamstrahlung photons can convert into electron positron pairs, or interact and produce hadrons in the final state. Such hadrons deposit 20 TeV of energy per bunch train in the central calorimeters. In addition, beamstrahlung is causing radiation damage to the very forward calorimeters.

Besides, the $\gamma\gamma \rightarrow$ hadrons background influences the event reconstruction, by the central tracker especially at the highest energy stage, where there is an average of 3.2 events per bunch crossing. This type of background is rejected using momentum and timing cuts, which drives challenging requirements on detector timing capabilities.

1.4 CLIC detector

The recent CLIC detector concept has emerged from two detector concepts parallel developed, which were based on ILC detector models, CLIC_ILD [6], and CLIC_SiD [7]. The difference between the two models are in the tracking system, where the CLIC_ILD foresees a gaseous tracking (TPC), whereas CLIC_SiD uses a silicon tracker. All other detector systems are similar. These detectors were adapted to the CLIC beam and background conditions, which are different than ILC primarily due to the higher center-of-mass energies and beam structure.

The performance of each sub-detector system is driven from the physics requirements. In the first place, precision measurement of the momentum resolution of a track ($\frac{\sigma_{p_t}}{p_t^2}$) is required for the recoil mass measurement of the Higgs boson in the Higgsstrahlung process [3]. The impact parameter resolution is necessary for heavy flavor separation (bottom/charm), and to exploit the most probable Higgs decay channel, $H \rightarrow b\bar{b}$. The required impact parameter resolution in the transverse plane is $\sigma_{r\phi} = 5 \oplus \frac{15}{p \cdot \sin^{3/2}(\theta)} [\mu m]$ [3]. Vertexing is performed with highly granulated, light-weight silicon pixel detector. Separation of the electroweak bosons requires good jet energy resolution in the calorimeters, which for the jet energies above 100 GeV is $\frac{\sigma_E}{E} < 3.5$ %.

These detectors are comprised in a strong solenoid field of 4-5 T. A muon system, implemented as an instrumented return yoke, surrounds

the whole detector. Special calorimeters for luminosity measurement and beamstrahlung monitoring are foreseen in the very forward region, down to 1.5 deg, providing additional hermeticity of the detector, which is necessary for the missing energy signature measurements in many BSM processes.

2 Higgs physics at CLIC

Measurement of properties of the Higgs boson will be a priority for CLIC. In order to estimate the physics potential of CLIC in terms of precision Higgs measurements, a comprehensive list of Higgs physics benchmark studies is currently being carried out [8]. The most important measurements are those of Higgs mass and couplings of Higgs to the SM particles, including Higgs self-coupling. The high precision measurement of the Higgs boson couplings would be a test of the SM, which predicts a strict linearity of the couplings to the corresponding masses. Any deviation from the predicted SM values would be a sign of New Physics [9].

2.1 Higgs Production at Linear Colliders

Different center-of-mass energies at CLIC give rise to different Higgs production channels. At the lowest energy stage $\sqrt{s}=380$ GeV, the leading Higgs production channel is the s-channel Higgsstrahlung process (HZ), where the Higgs boson is radiated off a Z boson. The corresponding Feynman diagram is given in Figure 3. This energy stage is in the first place dedicated to the model independent measurement of the total HZ cross-section and consequently to the absolute Higgs to Z coupling. Also at this stage the available statistics allows the determination of the cross-section of most of the Higgs decays, with the lightest accessible Higgs decay being the one to $c\bar{c}$. Besides, this energy stage allows the model independent measurement of the Higgs boson mass.

At higher energy stages, Higgs production is accessed predominantly by the t-channel WW-fusion, Figure 3 (right), where the cross-section rises logarithmically with energy. The available statistics allows more precise measurements of the Higgs couplings to be performed. The distribution of the cross-sections for the various Higgs production channels is given in Figure 4 (left), for unpolarized beams.

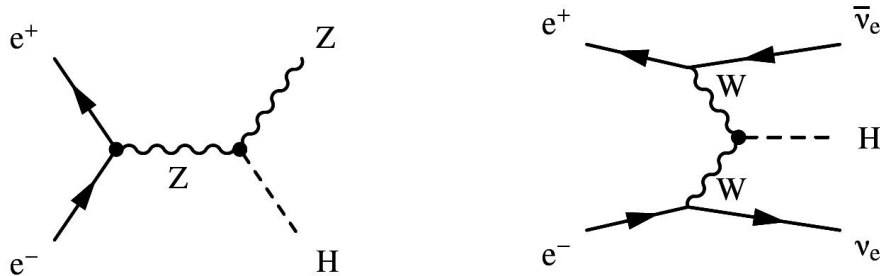


Figure 3: Feynman diagrams of the highest cross section Higgs production processes at CLIC; Higgsstrahlung (left), WW-fusion (right).

\sqrt{s}	380 GeV	1.4 TeV	3 TeV
	500 fb ⁻¹	1.5 ab ⁻¹	2 ab ⁻¹
# HZ events	68,000	20,000	11,000
# WW-fusion events	17,000	370,000	830,000
# ZZ-fusion events	3,700	37,000	84,000

Table 1: Number of Higgs events expected for the leading-order Higgs production processes for $m_H=126$ GeV, including initial state radiation and CLIC beam spectrum, for unpolarized beams.

Table 1. lists the number of Higgs events of the most relevant production processes expected in the studied CLIC staging scenario.

The cross-sections can be enhanced using polarised beams. For $P_{e^-}=80\%$ electron beam polarisation considered for CLIC, the listed numbers increase by 12% for ZH and ZZ-fusion events and 80% for WW-fusion production mechanisms.

2.2 Model independent Higgs boson measurements at linear collider

A unique feature of lepton colliders is a model independent Higgs recoil mass analysis in the Higgsstrahlung process, Figure 4 (right), which enables the measurement of the Higgs boson mass and total cross-section of the Higgsstrahlung process to be determined independently of the Higgs decay mode. The total HZ cross-section is proportional to the absolute coupling of the Z to Higgs boson and it is the starting point of the determination

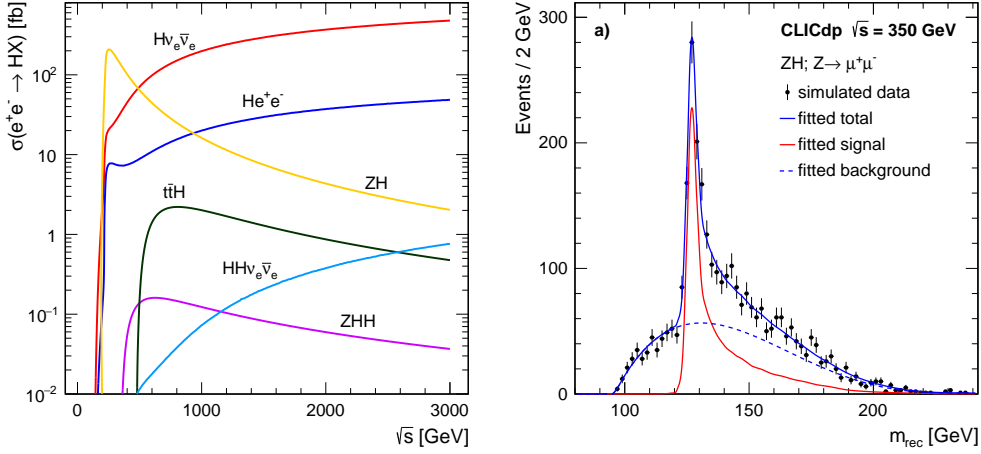


Figure 4: Left: The cross sections for the main Higgs production processes, as a function of center-of-mass energy, at an e^+e^- collider. Right: recoil mass distribution of muon pairs from Z decay at 380 GeV center-of-mass energy scaled to an integrated luminosity of 500 fb^{-1} .

of all other absolute Higgs couplings.

The Higgsstrahlung process is identified by the pair of leptons (electrons or muons) with the invariant mass consistent with the Z mass and the recoil mass (m_{rec}) consistent with the mass of the Higgs boson. The distribution of the recoil mass is constructed using only the properties of the lepton pair, invariant mass (m_Z) and energy (E_Z):

$$m_{rec}^2 = s + m_Z^2 - 2E_Z\sqrt{s} \quad (3)$$

The distribution of the recoil mass, constructed for $\sqrt{s}=380$ GeV, Figure 4 (right), features a clear peak at the Higgs mass. The high energy tail is due to emission of beamstrahlung and initial state radiation.

In the analysis of the $Z \rightarrow \mu^+\mu^-$ decay, the Higgs mass is determined with an absolute statistical precision of 120 MeV. The relative statistical error of the total cross-section of the Higgsstrahlung process $\Delta(\sigma_{HZ}) / (\sigma_{HZ})$ is determined by counting the number of events in the peak. For the combined muonic and electronic Z-decays $\Delta(\sigma_{HZ}) / (\sigma_{HZ}) \approx 4\%$, with the resulting absolute coupling of Higgs to Z boson, $g_{HZZ}^2 \approx 2\%$ [8].

The relative statistical error of the absolute Higgs to Z coupling, to-

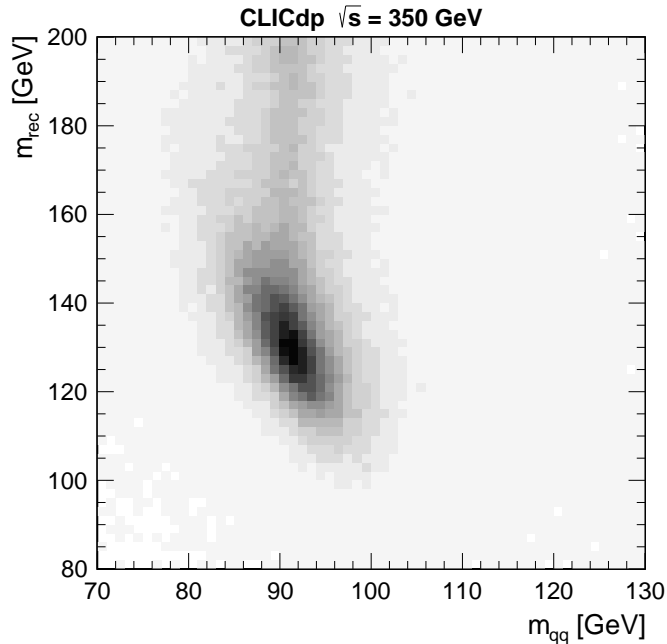


Figure 5: Reconstructed di-jet invariant mass versus reconstructed recoil mass distributions for selected $ZH \rightarrow qqX$ events at 350 GeV, given for signal events [10].

gether with the total Higgs decay width, Γ_H , limits the precision of all other absolute couplings. The leptonic Z -decays give a clear signature of Higgsstrahlung events so the selection efficiency is independent of the Higgs decay mode. On the other hand it is limited by the low Z branching fraction of 3%. It has been shown that the hadronic Z decay channel, which has a high $\text{BR}(Z \rightarrow qq \approx 69\%)$ can also be used, even though the hadronic Z reconstruction depends on the Higgs decay mode. It has been shown that careful selection criteria can be chosen, to ensure near model independence [10]. The clearest separation between signal and background is obtained from m_{qq} and the recoil mass m_{rec} , as shown in Figure 5. The signal is clearly peaked at $m_{qq} \sim m_Z$ and $m_{rec} \sim m_H$.

By combining the hadronic with leptonic channel the relative statistical error is improved to 0.8%.

The total Higgs decay width, Γ_H , is obtained through the WW -fusion Higgs production channel with the consequent Higgs decay to a W pair, $H \rightarrow WW^*$, once g_{HWW} is known:

$$\sigma(e^+e^- \rightarrow H\nu_e\bar{\nu}_e) \times (H \rightarrow WW^*) \propto \frac{g_{HWW}^4}{\Gamma_H}. \quad (4)$$

Γ_H can be used to determine the absolute value of all other measured couplings.

2.3 The measurements of cross-sections of specific Higgs decays

The measurement of absolute couplings of the Higgs to the Z boson can be used to obtain absolute couplings of Higgs to other SM particles using measurements of partial cross-sections of type $(e^+e^- \rightarrow \text{HZ}, \text{WW-fusion}) \times \text{BR}(H \rightarrow x\bar{x})$. This cross-section is proportional to the Higgs coupling to one of the vector bosons, depending on the production channel, g_{HZZ}^2 for Higgsstrahlung or g_{HWW}^2 for WW-fusion and to g_{Hxx}^2 through the decay channel $(H \rightarrow x\bar{x})$. All three energy stages are used to extract g_{Hxx}^2 and Γ_H through $\frac{g_{HZZ}^2 \cdot g_{Hxx}^2}{\Gamma_H}$, in a model independent way.

The first stage of CLIC operation, with the Higgsstrahlung as the leading Higgs production channel, enables the clean measurements of the branching fractions of the Higgs decays into the b and c quarks, τ , WW^* and gluons using the reconstruction of the recoiling Z boson and the explicit reconstruction of the Higgs boson. For these measurements precise flavor tagging for the separation of b and c jets is crucial, as well as the excellent particle flow performance for the efficient identification of τ leptons and for the reconstruction of hadronic W decays. The branching ratio of $H \rightarrow gg$ can not be directly transformed to a coupling, but provides model-dependent sensitivity to the coupling to the top quark through loop contributions, since in the SM the coupling of the Higgs to the gluon is realized through a heavy quark loop. The Higgsstrahlung process cross-section can be increased by using the polarization $P_{e^-} = -80\%$ up to 12% [8].

At the higher energy stages the leading Higgs production channel is WW-fusion. The cross-section of this production process can be increased up to 80% with the maximal polarization $P_{e^-} = -80\%$. The abundant statistic is used to improve the precision of the coupling measurements obtained at the first energy stage. Also, the higher energy stages give access to the low cross-section processes, also offering a possibility to directly measure the coupling of the Higgs to the top quark using $e^+e^- \rightarrow t\bar{t}H$ process,

which is sensitive to the top-Yukawa coupling. This process can be studied using the most favorable Higgs decay, $H \rightarrow b\bar{b}$, along with semileptonic and hadronic W decays. This complex final state, with 6 to 8 jets including four b-jets, is an excellent detector benchmark process, testing jet reconstruction, flavor tagging, lepton identification, and reconstruction of missing energy. The combined precision is $\Delta\sigma(t\bar{t}H) / \sigma(t\bar{t}H) = 8.1\%$ resulting in a precision on the top Yukawa coupling of 4.3%.

The measurement of the trilinear self-coupling provides direct experimental access to the shape of the Higgs potential. The $e^+e^- \rightarrow HH\nu_e\bar{\nu}_e$ process is available for measuring the trilinear Higgs self-coupling, with the cross-section rising with the center of mass energy. The study of this coupling using the most common Higgs decay mode $HH \rightarrow b\bar{b}b\bar{b}$ decay as the signal, achieves a precision on the Higgs trilinear self-coupling of 32% at $s = 1.4$ TeV and 16% at 3 TeV [8]. Using beam polarisation, this precision further improves to 24% and 12%, respectively.

The measurement of the quartic coupling g_{HHWW} are also possible at higher energy stages. The simulation studies have shown that the quartic coupling, using the $HH \rightarrow b\bar{b}b\bar{b}$ can be measured with a statistical uncertainty of 7% at $\sqrt{s} = 1.4$ TeV and 3% at 3 TeV, including $P_{e^-} = 80\%$ polarisation. These results could be improved by adding analyses for other Higgs decay channels such as $HH \rightarrow b\bar{b}WW^*$. The analysis of these Higgs decay channels represents a challenge for the forward jet reconstruction.

Also the sufficiently high statistics allows for the Higgs coupling measurement to the lightest SM particles, as in the Higgs decay to a pair of muons. This decay has extremely low BR of the order of 10^{-4} . The statistical precision of $\text{BR}(H \rightarrow \mu\mu) \times$ is 29% at the 1.4 TeV CLIC, and 16% at the highest energy stage 3 TeV.

The indirect couplings of Higgs to γ can also be accessed at higher energy stages. In the SM, this decay is induced via loop diagrams, dominated by heavy charged particles, mostly W bosons and t quarks. This measurement is highly sensitive to BSM physics processes, which modify the effective $H \rightarrow \gamma\gamma$ branching ratio. It has been shown that the statistical uncertainty of 15% can be obtained at the 1.4 TeV energy stage. Simulation studies of the $H \rightarrow \gamma Z$ decay channel including both hadronic and leptonic (e, μ) Z decays reach a combined precision of the Higgs production cross-section times branching ratio of 42% at 1.4 TeV [11].

2.4 Combined Higgs Fit

The best result of the Higgs couplings and decay width measurement is obtained by a simultaneous model-independent fit performed using the results of all three energy stages. The starting point of this fit is the model-independent measurement of the couplings of Higgs to Z boson g_{HZZ} . The free parameters of the fit are the uncertainties of the couplings as well as the total Higgs decay width. The relative statistical precision of the measurement of Higgs couplings to the SM particles is shown in Figure 6 (left). It has been shown that the relative statistical uncertainties can reach the percent level. The Higgs width is extracted with 3.5 % precision. Better results can be obtained by using the fit which presumes that the total Higgs decay width is constrained by the Standard model, that is, that there are no unknown decays. The fit is performed in the same manner as at the LHC experiments. The free parameters of the fit are relative partial widths of the Higgs decays with respect to corresponding SM values. The uncertainty of the total Higgs decay width does not enter the fit, but is calculated using the uncertainties of the partial widths obtained in the fit. The relative statistical uncertainty obtained by this method improves and reaches the subpercent level for the most of the measurements except the rare Higgs decays, like $H \rightarrow \gamma\gamma$ or $H \rightarrow \mu\mu$. However, the results of this fit are model dependent. The results of the model-dependent fit are shown in Figure 6 (right).

2.5 Conclusion

In this lecture, the motivation for a e^+e^- collider as a next generation facility in high energy physics is given. One of the possible options is the Compact linear collider CLIC, operating at three centre-of-mass energy stages, 380 GeV, 1.4 TeV and 3.0 TeV. The principle of CLIC particle acceleration, the detector concepts and working conditions have been presented in some detail. The focus of the lecture was put on the capability of CLIC for a comprehensive precision Higgs physics program.

The initial stage of operation, 380 GeV, allows the study of Higgs production from both the HZ and the WW-fusion process. These data would yield precise model-independent measurements of the Higgs-boson couplings. The obtained statistical precision of the absolute Higgs to Z boson coupling is $g_{HZZ} = 0.8\%$, and the total Higgs width is measured with the statistical precision of 5.0 %.

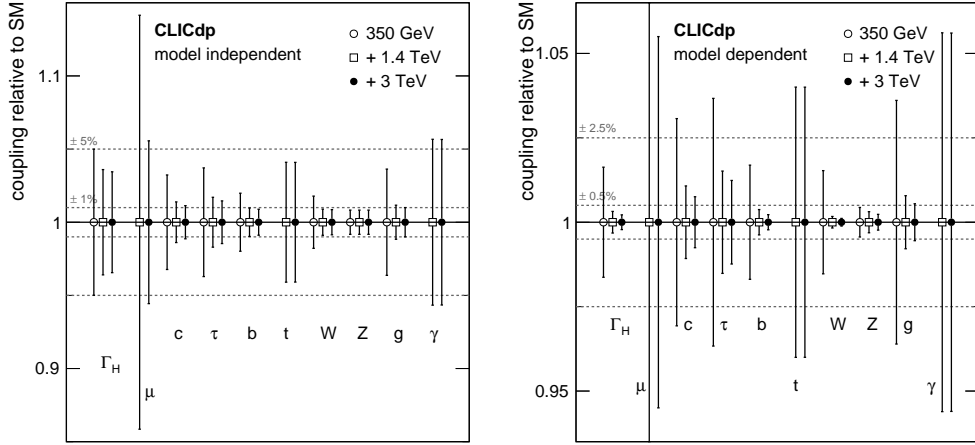


Figure 6: Illustration of the achievable precision on the Higgs couplings and decay width, obtained in a fit using three successive CLIC energy stages. Left: Model-independent fit. right: model-dependent fit. The impact of electron polarization of -80 % at $\sqrt{s}= 1.4\text{TeV}$ and 3 TeV energy stages are included as a scale factor.

The abundant Higgs boson statistics which can be obtained at CLIC above 1 TeV, where the Higgs boson is produced predominantly through the WW-fusion process, improves the precision of the absolute couplings and also gives access to rarer processes, such as $t\bar{t}H$ and Higgs selfcoupling, which serve as indirect measurements of the top Yukawa coupling and the Higgs potential, respectively. Also, higher energy stages allow the measurement of rare Higgs decays like $H \rightarrow \gamma\gamma$ or $H \rightarrow \mu\mu$.

To exploit the results obtained independently at each energy stage, the simultaneous fit of the full data sample is performed. In a model-independent fit, the majority of the accessible couplings are measured at the percent level. Using the fit which constrains the total Higgs decays width to the SM expectations, model-dependent fit, the result is improved to the sub-percent level.

References

- [1] G. Aad et al., Observation of a new particle in the search for the Standard Model Higgs boson with the ATLAS detector at the LHC, Phys.Lett. B716 (2012) 1.
- [2] S. Chatrchyan et al., Observation of a new boson at a mass of 125 GeV with the CMS experiment at the LHC, Phys.Lett. B716 (2012) 30.
- [3] M. Aicheler, P. Burrows, M. Draper, T. Garvey, P. Lebrun, K. Peach, N. Phinney, H. Schmickler, D. Schulte, N. Toge (eds.), A Multi-TeV Linear Collider based on CLIC Technology: CLIC Conceptual Design Report (CERN). CERN-2012-007, JAI-2012-001, KEK Report 2012-1, PSI-12-01, SLAC-R-985.
- [4] S. Lukić, I. Božovic-Jelisavčić, M. Pandurović and I. Smiljanić, Correction of beam-beam effects in luminosity measurement in the forward region at CLIC, JINST 8 (2013) P05008.
- [5] M. Venturini and W. Kozanecki, The hourglass effect and the measurement of the transverse size of colliding beams by luminosity scans, Proceedings IEEE Particle Accelerator Conference, SLAC-PUB-8699, (2001) 3573.
- [6] T. Abe et al. [ILD Concept Group - Linear Collider Collaboration], arXiv:1006.3396 [hep-ex].
- [7] H. Aihara, (Ed.), P. Burrows, (Ed.), M. Oreglia, (Ed.), E. L. Berger, V. Guarino, J. Repond, H. Weerts and L. Xia et al., arXiv:0911.0006 [physics.ins-det].
- [8] H. Abramowicz, et al., Physics at the CLIC e^+e^- Linear Collider - Input to the Snowmass process 2013, arXiv:1307.5288.
- [9] C. Englert, A. Freitas, M. Muhlleitner, T. Plehn, M. Rauch, M. Spira, K. Walz, Precision Measurements of Higgs Couplings: Implications for New Physics Scales, J. Phys. G 41 (2014) 113001, arXiv:1403.7191 [hep-ph].

- [10] M. A. Thomson, Model-Independent Measurement of the $e^+e^- \rightarrow HZ$ Cross Section at a Future e^+e^- Linear Collider using Hadronic Z Decays CLICdp-Pub-2015-004, [hep-ex/1509.02853].
- [11] C. Grefe, E. Sicking, Physics potential of the $\sigma(e^+e^- \rightarrow H\nu_e\bar{\nu}_e) \times BR(H \rightarrow Z\gamma)$ measurement at a 1.4 TeV Compact Linear Collider, CLICdp-Note-2014-003.

The Deep Inelastic Scattering on the Polarized Nucleons at Electron-Ion Collider

E.S.Timoshin, S.I.Timoshin

Sukhoi State Technical University of Gomel

Abstract

The contributions the individual quark and antiquark flavors, the valence quarks in the nucleon spin are obtained in the deep inelastic scattering longitudinally polarized leptons off longitudinally polarized protons, neutrons and deuterons with charged current for the experiments at Electron-Ion Collider. The radiative corrections to the measurable asymmetries are discussed.

Understanding how the nucleon spin is built up from the spin of quarks and gluons and their orbital angular momentum is one of the most challenging goals in hadron physics [1–4].

We have two pictures about the nucleon spin:

1) Jaffe-Monahar (1990)

$$\frac{1}{2} = \frac{1}{2}\Delta\Sigma + \Delta G + L_q + L_g.$$

Here $\Delta\Sigma, \Delta G$ are the quark and the gluon helicity; L_q, L_g are the orbital momentum of the quarks and the gluons.

There is the simple parton picture for the longitudinal polarization.

2) X.Ji (1996)

$$\frac{1}{2} = J_q + J_g = \frac{1}{2}\Delta\Sigma + L_q + L_g,$$

where J_q, J_g are the total angular momentum of the quarks and the gluons respectively. This decomposition the nucleon spin relate to the partons in transverse polarized nucleon.

At present we know fairly well the quark contribution

$$\Delta\Sigma = \int_0^1 dx \left[\Delta u(x) + \Delta\bar{u}(x) + \Delta d(x) + \Delta\bar{d}(x) + \Delta s(x) + \Delta\bar{s}(x) \right] \sim 30\%.$$

However, the details on the flavor and sea structure of the polarization are still necessary as and contribution from small x . We know with large uncertainties about the gluon contribution $\Delta G = \int_0^1 dx g(x) \sim 20\%$ with RHIC data [5]. There not have direct information on the quark and gluon orbital angular momentum.

The calculations L_q in lattice QCD [6–8] and in model dependent way with the pretzelosity distribution [9] give agreement results that $L_u < 0$, $L_d > 0$ and $L_u + L_d \sim 0$. Now we have new phenomenology to study nucleon structure – Generalized Parton Distributions (GPD) that provide access to orbital angular momentum in Deep Virtual Compton Scattering (DVCS) and Exclusive $J/\Psi, \rho, \varphi$ production. These studies will require high luminosity and polarized beams. The Electron-Ion Collider (EIC) proposed as a next generation facility for nuclear physics, would expand the opportunities for high-energy scattering on polarized protons, light nuclei ($D^3, He\dots$).

The machine designs are aimed to achieve:

- Polarized ($\sim 70\%$) beams of electrons, protons and light nuclei.
- High luminosity $10^{33-34} cm^{-2} s^{-1}$.
- Low x regime $x \rightarrow 10^{-4}$.
- Center of mass energies $\sim 20-100$ GeV, upgradable $\sim 140-150$ GeV. An EIC can delineate with unprecedented precision the full helicity structure of the nucleon in terms of gluons, quarks and antiquarks and their flavor.
- At EIC can to explore.
- Sea gluon $x \sim 10^{-2} - 10^{-4}$ (inclusive DIS, SIDIS at low x), spin flavor decomposition of the light quark sea.

- GPD (DVCS, Exclusive meson production) \Rightarrow angular momentum J_q, J_g :

$$J_q = \frac{1}{2} \lim_{t \rightarrow 0} \int_{-1}^1 dx \quad x \left[\overbrace{H_q(x, \xi, t) + E_g(x, \xi, t)}^{GPD} \right] = \frac{1}{2} \Delta\Sigma + L_q.$$

The first constraint on quark orbital contribution L_q to proton spin by combining the sea from EIC and valence quarks from JLab 12.

A decomposition of J_g into spin and orbital components using gauge invariant local operators (as for J_q) is impossible. The total angular momentum of gluons J_g can, in principle, be accessed in exclusive deeply virtual meson production through the relation

$$J_g = \frac{1}{2} \lim_{t \rightarrow 0} \int_0^1 dx \left[H_q(x, \xi, t) + E_g(x, \xi, t) \right].$$

The deep inelastic scattering (DIS) with charged current (CC)

$$l + N \rightarrow \nu + X \tag{1}$$

can be studied only in high-energy lepton-nucleon collision, e.g. at EIC. Data from CC DIS experiments (1) with the polarized beams provide complementary information on the nucleon spin as they probe combinations of quark flavors different from those accessible in electromagnetic DIS. Here are two independent polarized structure functions (SF)

$$g_1 \sim \Delta q + \Delta \bar{q}$$

$$g_6 \sim \Delta q - \Delta \bar{q}$$

that provide flavor separation Δq and $\Delta \bar{q}$.

Now flavor-separated parton distribution functions Δq and $\Delta \bar{q}$ are obtained exclusively from semi-inclusive DIS (SIDIS) data. However, in contrast SIDIS the inclusive CC DIS (1) not have the fragmentation functions which carry in an essential uncertainty to measurable quantities.

In this paper we study CC DIS (1) on polarized nucleons with goal to receive of an information about the spin structure of the nucleon in the experiments at EIC.

In the experiments with polarized beams the asymmetries are measured. The polarized asymmetries for CC DIS (1) in the Born approximation through SF are (the details see [10, 11]).

$$A_{l^-, l^+}(x, Q^2) = \frac{d^2\sigma_{l^-, l^+}^{\downarrow\uparrow, \uparrow\uparrow}/dxdy - d^2\sigma_{l^-, l^+}^{\downarrow\downarrow, \uparrow\downarrow}/dxdy}{d^2\sigma_{l^-, l^+}^{\downarrow\uparrow, \uparrow\uparrow}/dxdy + d^2\sigma_{l^-, l^+}^{\downarrow\downarrow, \uparrow\downarrow}/dxdy} =$$

$$= \frac{y_1^+ g_6^{l^-, l^+}(x, Q^2) \pm y_1^- g_1^{l^-, l^+}(x, Q^2)}{y_1^+ F_1^{l^-, l^+}(x, Q^2) \pm \frac{y_1^-}{2} F_3^{l^-, l^+}(x, Q^2)}$$

$$A_{\pm}(x, Q^2) = \frac{\left(d^2\sigma_{l^-}^{\downarrow\uparrow}/dxdy \pm d^2\sigma_{l^+}^{\uparrow\uparrow}/dxdy\right) - \left(d^2\sigma_{l^-}^{\downarrow\downarrow}/dxdy \pm d^2\sigma_{l^+}^{\uparrow\downarrow}/dxdy\right)}{\left(d^2\sigma_{l^-}^{\downarrow\uparrow}/dxdy \pm d^2\sigma_{l^+}^{\uparrow\uparrow}/dxdy\right) + \left(d^2\sigma_{l^-}^{\downarrow\downarrow}/dxdy \pm d^2\sigma_{l^+}^{\uparrow\downarrow}/dxdy\right)}$$

$$= \frac{y_1^+ \left[g_6^{l^-}(x, Q^2) \pm g_6^{l^+}(x, Q^2)\right] + y_1^- \left[g_1^{l^-}(x, Q^2) \mp g_1^{l^+}(x, Q^2)\right]}{y_1^+ \left[F_1^{l^-}(x, Q^2) \pm F_1^{l^+}(x, Q^2)\right] + \frac{y_1^-}{2} \left[F_3^{l^-}(x, Q^2) \mp F_3^{l^+}(x, Q^2)\right]}.$$

Here $F_{1,3}$ and $g_{1,6}$ are the spin-averaged and polarized SF; $y_1^{\pm} = 1 \pm y_1^2$, $y_1 = 1 - y$.

The polarized SF in leading order QCD (improved parton model) are

$$g_1(x, Q^2) = \sum_q \Delta q(x, Q^2) + \sum_{\bar{q}} \Delta \bar{q}(x, Q^2),$$

$$g_6(x, Q^2) = \sum_q \Delta q(x, Q^2) - \sum_{\bar{q}} \Delta \bar{q}(x, Q^2),$$

where $q = u, c, t$ ($q = d, s, b$) and $\bar{q} = \bar{d}, \bar{s}, \bar{b}$ ($\bar{q} = \bar{u}, \bar{c}, \bar{t}$) for lepton (antilepton).

The first moments polarized SF give access to the quark and antiquark contributions in the nucleon spin

$$\Gamma_{1,6}(Q^2) = \int_0^1 g_{1,6}(x, Q^2) dx = \sum_{q, \bar{q}} (\Delta q \pm \Delta \bar{q}),$$

where $\Delta q(\Delta \bar{q}) = \int_0^1 \Delta q(x)(\Delta \bar{q}(x)) dx$ is the quark (antiquark) contribution to the nucleon spin.

The proton

$$\begin{aligned}\Gamma_6^{l^-p} - \Gamma_6^{l^+p} &= (\Delta u + \Delta \bar{u}) - (\Delta d + \Delta \bar{d}) - (\Delta s + \Delta \bar{s}), \\ \Gamma_6^{l^-p} + \Gamma_6^{l^+p} &= \Delta u_V + \Delta d_V = \Delta q_V,\end{aligned}$$

where $\Delta u_V = \Delta u - \Delta \bar{u}$, $\Delta d_V = \Delta d - \Delta \bar{d}$.

$$\begin{aligned}\Gamma_1^{l^-p} + \Gamma_1^{l^+p} &= (\Delta u + \Delta \bar{u}) + (\Delta d + \Delta \bar{d}) + (\Delta s + \Delta \bar{s}), \\ \Gamma_1^{l^-p} - \Gamma_1^{l^+p} &= \Delta u_V - \Delta d_V.\end{aligned}$$

We use also the measurable quantity – the axial charge $a_3 = F + D = 1.2670 \pm 0.0035$ that in parton model: $a_3 = (\Delta u + \Delta \bar{u}) - (\Delta d + \Delta \bar{d})$.

The quark contributions to the nucleon spin:

The quark flavors

$$\begin{aligned}\Delta u + \Delta \bar{u} &= \frac{1}{2} \left(\Gamma_1^{l^-p} + \Gamma_1^{l^+p} - \Gamma_6^{l^+p} + \Gamma_6^{l^-p} \right), \\ \Delta d + \Delta \bar{d} &= \frac{1}{2} \left(\Gamma_1^{l^-p} + \Gamma_1^{l^+p} - \Gamma_6^{l^+p} + \Gamma_6^{l^-p} - 2a_3 \right), \\ \Delta s + \Delta \bar{s} &= \Gamma_6^{l^+p} - \Gamma_6^{l^-p} + a_3.\end{aligned}$$

The valence quarks

$$\begin{aligned}\Delta u_V &= \frac{1}{2} \left(\Gamma_6^{l^-p} + \Gamma_6^{l^+p} - \Gamma_1^{l^-p} + \Gamma_1^{l^+p} \right), \\ \Delta d_V &= \frac{1}{2} \left(\Gamma_1^{l^+p} - \Gamma_1^{l^-p} + \Gamma_6^{l^-p} + \Gamma_6^{l^+p} \right).\end{aligned}$$

The sea quarks

$$\begin{aligned}\Delta \bar{u} &= \frac{1}{2} \left(\Gamma_1^{l^+p} - \Gamma_6^{l^+p} \right), \\ \Delta \bar{d} &= \frac{1}{2} \left(\Gamma_1^{l^-p} - \Gamma_6^{l^+p} - a_3 \right), \\ \Delta \bar{s} &= \frac{1}{2} \left(\Gamma_6^{l^+p} - \Gamma_6^{l^-p} + a_3 \right).\end{aligned}$$

We have obtained the quark contributions for neutron and deuteron.

The neutron

$$\begin{aligned}\Delta u + \Delta \bar{u} &= \frac{1}{2} \left(\Gamma_6^{l^-n} - \Gamma_6^{l^+n} + \Gamma_1^{l^-n} + \Gamma_1^{l^+n} \right) + a_3, \\ \Delta d + \Delta \bar{d} &= \frac{1}{2} \left(\Gamma_1^{l^-n} + \Gamma_1^{l^+n} + \Gamma_6^{l^-n} - \Gamma_6^{l^+n} \right), \\ \Delta s + \Delta \bar{s} &= -a_3 - \Gamma_6^{l^-n} + \Gamma_6^{l^+n}.\end{aligned}$$

$$\begin{aligned}\Delta d_V &= \frac{1}{2} \left(\Gamma_1^{l^-n} - \Gamma_1^{l^+n} + \Gamma_6^{l^-n} + \Gamma_6^{l^+n} \right), \\ \Delta u_V &= \frac{1}{2} \left(\Gamma_6^{l^-n} + \Gamma_6^{l^+n} - \Gamma_1^{l^-n} + \Gamma_1^{l^+n} \right).\end{aligned}$$

$$\begin{aligned}\Delta \bar{s} &= \frac{1}{2} \left(-a_3 - \Gamma_6^{l^-n} + \Gamma_6^{l^+n} \right), \\ \Delta \bar{d} &= \frac{1}{2} \left(\Gamma_1^{l^+n} - \Gamma_6^{l^+n} \right), \\ \Delta \bar{u} &= \frac{1}{2} \left(\Gamma_1^{l^-n} - \Gamma_6^{l^+n} + a_3 \right).\end{aligned}$$

The deuteron

$$\begin{aligned}\Delta s + \Delta \bar{s} &= \frac{\Gamma_6^{l^+d} - \Gamma_6^{l^-d}}{1 - 1,5\omega}, \\ \Delta u_V + \Delta d_V &= \frac{\Gamma_6^{l^-d} + \Gamma_6^{l^+d}}{1 - 1,5\omega}, \\ \Delta \Sigma &= \frac{\Gamma_1^{l^-d} + \Gamma_1^{l^+d}}{1 - 1,5\omega},\end{aligned}$$

where $\omega = 0.05$ is the probability D-state in the wave function of the deuteron.

Obviously, this approach to obtain the quark polarization requires a knowledge of SF g_1, g_6 . These SF can be extracted from the measurable asymmetries A_{l^-, l^+} and A_{\pm} . In contrast electromagnetic DIS processes an extraction of polarized SF in DIS with CC (1) is a nontrivial problem, because the asymmetries A_{l^-, l^+} , A_{\pm} include two independent SF g_1 and g_6 . The ways to extract the SF g_1 and g_6 from asymmetries measured in experiments DIS with CC were proposed in our work [11, 12].

The numerical calculations the asymmetries were performed for DIS CC polarized electrons (positrons) off longitudinal polarized protons, neutrons and deuterons using parton distributions [13]. In Fig.1 we show the size of the asymmetries A_{e^-} for protons (top) and neutrons (bottom), but also A_{e^\pm} for deuterons (Fig.3). As can be seen, the asymmetries are considerable and can to access more than 50% at $x \geq 0.7$.

We calculated the QED corrections to the asymmetries in Leading Log Approximation (LLA) [14, 15].

In Fig.5 and Fig.6 we show size QED corrections in LLA to the asymmetries $A_{e^-}^p$ and $A_{e^-}^n$ respectively. They are neglectly small at $x \gtrsim 0.5$ and get noticeable in regime small x accessing of value 10 – 15% at small y .

The Next Leading Order QCD corrections to the asymmetries CC DIS are small and leading order accuracy is very good approximation [16].

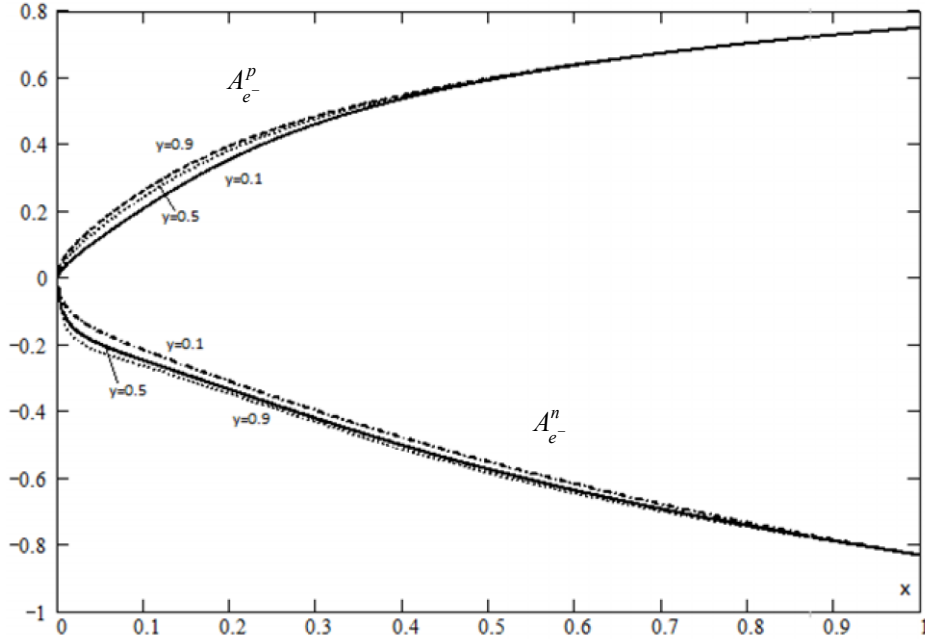


Figure 1. The asymmetries $A_{e^-}^p$ and $A_{e^-}^n$.

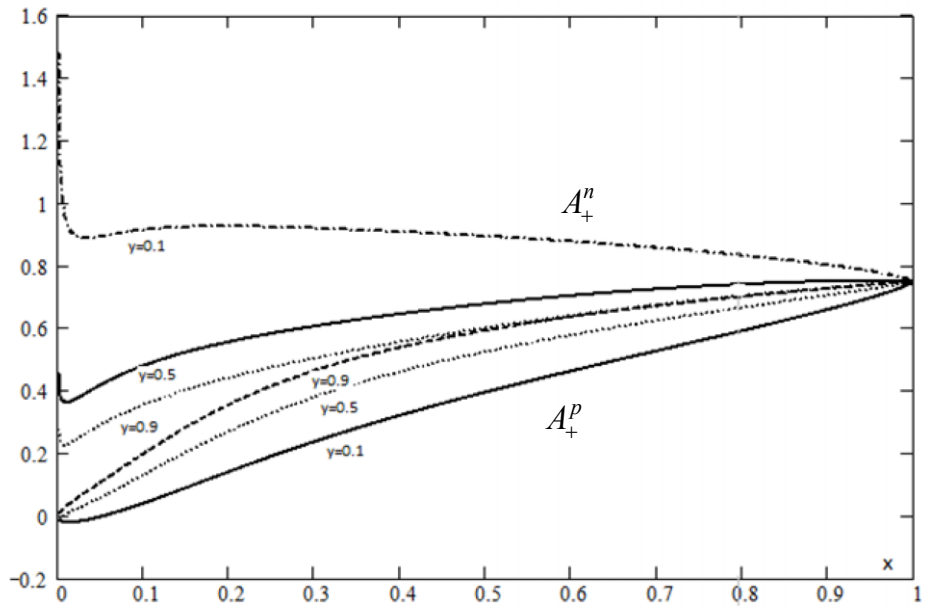


Figure 2. The asymmetries A_+^p and A_+^n

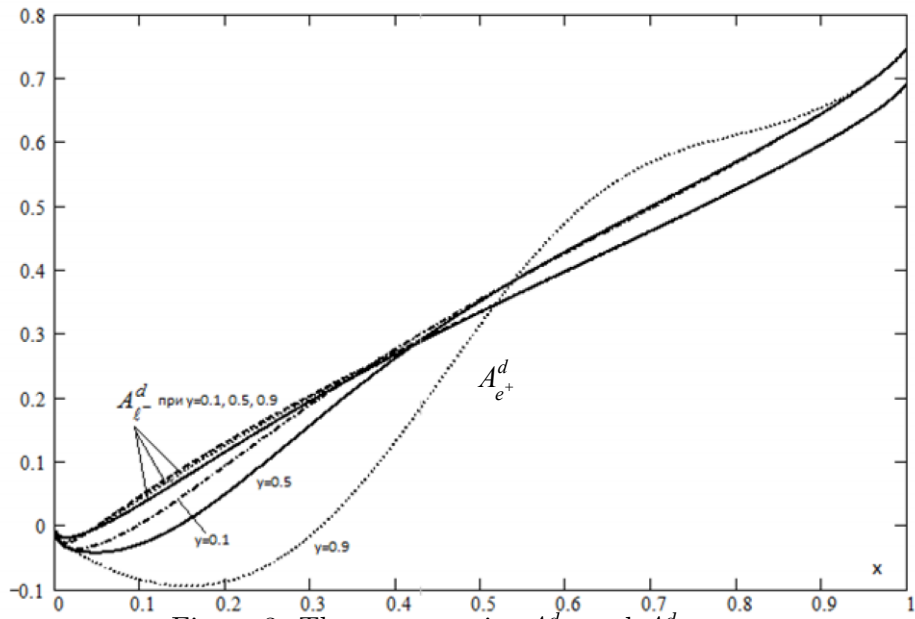


Figure 3. The asymmetries A_{e-}^d and A_{e+}^d

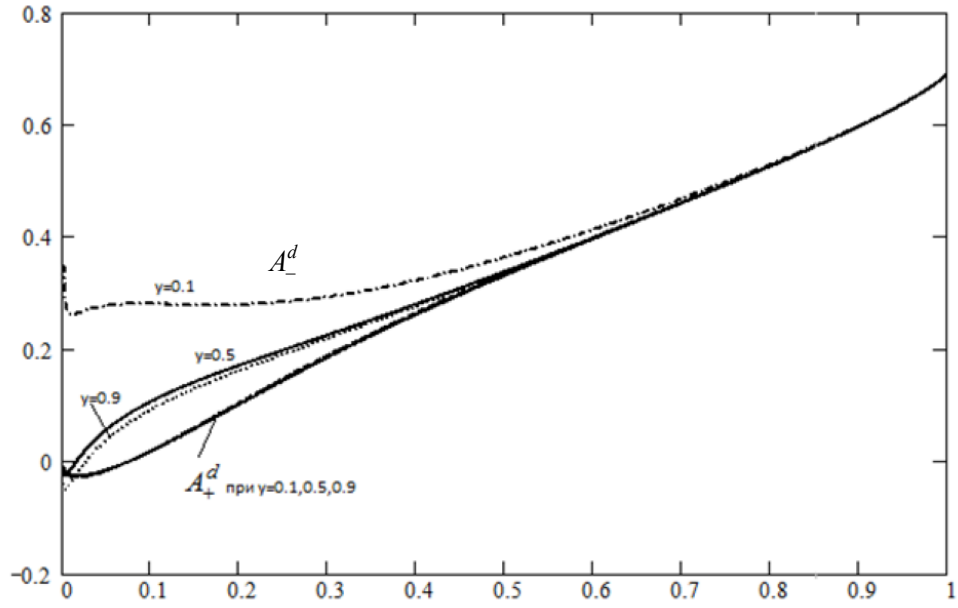


Figure 4. The asymmetries A_+^d and A_-^d

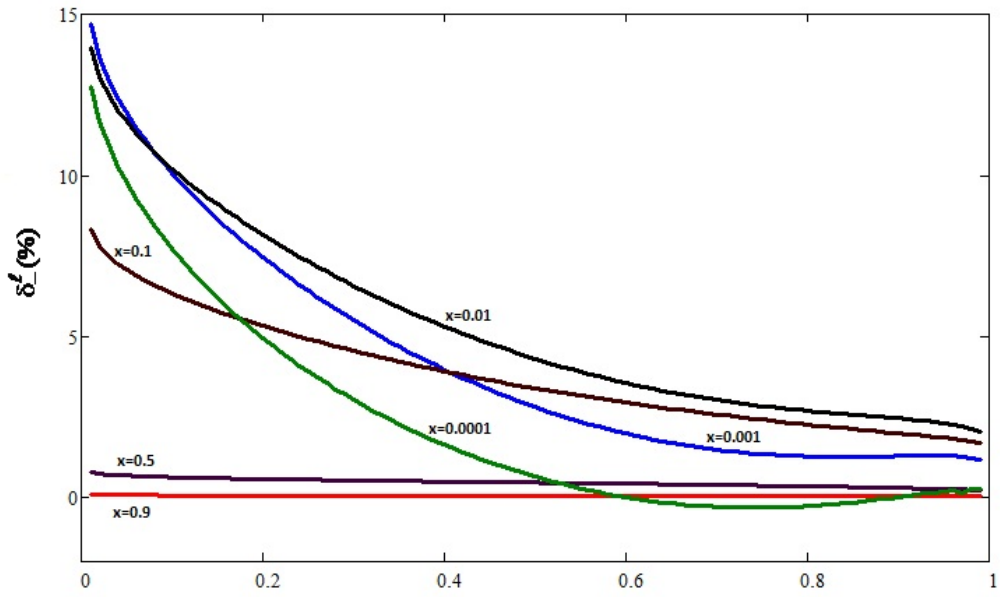


Figure 5. QED correction δ_-^l (%) to asymmetry A_{e-}^p in leading log approximation (LLA)

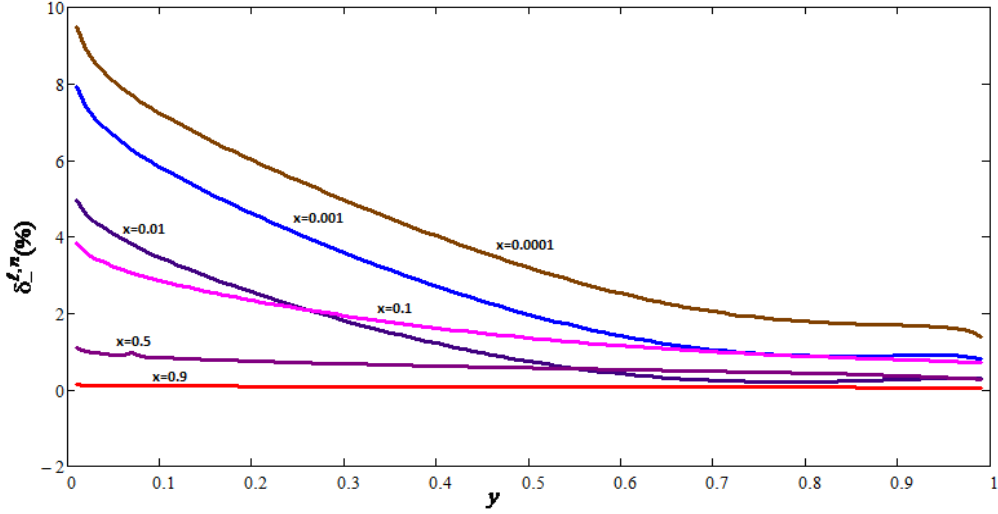


Figure 6. QED correction $\delta_-^{l,n}(\%)$ to asymmetry A_{e-}^n in LLA

Conclusion

- Data from CC DIS experiments provide complementary information on the spin structure nucleon as they probe combinations of quark flavors different from those accessible in purely electromagnetic DIS.
- CC DIS can be studied only in high-energy lepton-nucleon collisions (e.g. EIC).
- The quark contributions to the nucleon spin are obtained through the first moments of the polarized SF g_1, g_6 that can be to extract from the measurable asymmetries CC DIS.

References

- [1] Kuhn S. E. et al. Prog. Nucl. Part. Phys. 2009. V.63. P.1.
- [2] Burkardt M., et al. Rep. Progr. Phys. 2010. V.73. P.016201.
- [3] Aidara C.A. et al. Rev. Mod. Phys. 2013. V.85. P.655.
- [4] Brodsky S.J. et al. ArXiv: 1502.05728 [hep-ph].

- [5] Florian D. et al. Phys. Rev. Lett. 2014. V.113, No.1. P.012001.
- [6] Hagler P. et al. Phys. Rev. 2008. V.D77. P.094502.
- [7] Lin K. et al. PoS LATTICE 2011. 2011. P.164; arXiv:1203.6388.
- [8] Deka M. et al. ArXiv:1312.4816.
- [9] Lefky C., Prokudin A., Phys. Rev. 2015 V.D91, No.3. P.034010.
- [10] Timoshin E.S., Timoshin S.I. Nonlinear Phenomena in Complex Systems. 2014. V.17, No.1. P.64.
- [11] Timoshin E.S., Timoshin S.I. Proc. XII Int. School-Seminar "Actual Problems of Microworld Physics" (Gomel, Belarus, 2013). 2015. V.2. P.107.
- [12] Timoshin E.S., Timoshin S.I. Phys. Part. and Nuclei Lett. 2014. V.11, No.2. P.86.
- [13] Kuzela M. et al. Acta Phys. Pol. 1999. V.B30. P.1041.
- [14] De Rujula A. et al. Nucl. Phys. 1979. V.B154. P.394.
- [15] Blümlein J. Prog. Part. Nucl. Phys. 2013. V.69. P.28.
- [16] Aschenauer E.C. et al. Phys. Rev. 2013. V.D88. P.114025.

Center-Edge Asymmetry as a Tool for Revealing Large Extra Dimensions at LHC

A.A. Pankov ^{*}, I.A. Serenkova [†], A.V. Tsytrinov [‡]

*Abdus Salam ICTP Affiliated Centre
at Sukhoi State Technical University of Gomel*

V.A. Bednyakov [§]

*Joint Institute for Nuclear Research,
Moscow State Institute of Radio Engineering, Electronics*

Abstract

Arkani-Hamed, Dimopoulos and Dvali proposed a model in which gravity propagates freely in d extra compact spatial dimensions. The prospects of discovery and identification of large extra spatial dimensions effects in the processes of lepton and photon pair production at the Large Hadron Collider (LHC) were studied. These effects can be found by the specific behavior of the invariant mass distributions of the lepton and photon pairs. Identification of the effects under study can be performed with angular distributions of lepton and photon pairs. Discovery and identification reach on the mass scale parameter M_S can be obtained for graviton Kaluza – Klein towers in lepton and photon pair production processes at the LHC.

1 Introduction

Theories of low-scale quantum gravity featuring large extra spatial dimensions (LED) have attracted considerable interest because of their possible observable consequences at existing and future colliders. In scenario,

^{*}E-mail:pankov@ictp.it

[†]E-mail:inna.serenkova@cern.ch

[‡]E-mail:tsytrin@rambler.ru

[§]E-mail:Vadim.Bednyakov@cern.ch

proposed by Arkani-Hamed, Dimopoulos, and Dvali [1], the fermions and gauge bosons of the Standard Model (SM) are confined to the three ordinary spatial dimensions, which form the boundary (“the brane”) of a space with d compact spatial dimensions (“the bulk”) in which gravitons alone can propagate. In this model, the Planck scale is lowered to the electroweak scale of $\mathcal{O}(1 \text{ TeV})$, which is postulated to be the only fundamental scale in nature. The fundamental Planck scale in the extra dimensions (M_S), the characteristic size of the d extra dimensions (R) and the Planck scale on the brane are related via

$$M_{Pl}^2 \propto M_S^{d+2} R^d, \quad (1)$$

a purely classical relationship calculated by applying the $4 + d$ dimensional Gauss’s law. In this scenario, then, the weakness of gravity compared to the other SM interactions is explained by the suppression of the gravitational field flux by a factor proportional to the volume of the extra dimensions.

While direct graviton emission cross section is well defined, the cross section for virtual graviton exchange depends on a particular representation of the interaction Lagrangian and the definition of the ultraviolet cutoff on the KK modes. Three such representations have appeared nearly simultaneously [2–4]. In all of them, the effects of LED are parametrized via a single variable $\eta_G = \mathcal{F}/M_S^4$, where \mathcal{F} is a dimensionless parameter of order one reflecting the dependence of virtual G_n^* exchange on the number of extra dimensions, and M_S is the ultraviolet cutoff. Different formalisms use different definitions of \mathcal{F} , which result in different definitions of M_S :

$$\mathcal{F} = \begin{cases} 1, & \text{(GRW [3]);} \\ \frac{2}{d-2}, d > 2, & \text{(HLZ [4]);} \\ \frac{2\lambda}{\pi} = \pm \frac{2}{\pi}, & \text{(Hewett [2]).} \end{cases} \quad (2)$$

Note that \mathcal{F} depends explicitly on d only within the HLZ formalism. In both the GRW and HLZ formalisms gravity effects interfere constructively with the SM diagrams. In Hewett’s convention the sign of interference is not known, and the interference effects are parameterized via a parameter λ of order one, which is usually taken to be either $+1$ (constructive interference) or -1 (destructive interference). The parameter η_G has units of TeV^{-4} if M_S is expressed in TeV, and describes the strength of gravity in the presence of LED. The differential or total cross section in the presence

of virtual graviton exchange can be parameterized as:

$$\sigma_{\text{tot}} = \sigma_{\text{SM}} + \eta_G \sigma_{\text{int}} + \eta_G^2 \sigma_G, \quad (3)$$

where σ_{SM} is the SM cross section for the process under study and σ_{int} , σ_G are the interference and direct graviton effects, respectively.

Existing collider experimental data analysis gave no observation of LED effects, but only constraints. Indirect graviton effects at the LHC were searched for in processes of lepton and photon pair production. The corresponding constraints on M_S (HLZ) obtained from LHC data were found to be around 5.2 TeV (ATLAS) [5] and 4.8 TeV (CMS) [6] for $d = 3$.

A general feature of the different theories extending the SM of elementary particles is that new interactions involving heavy elementary objects and mass scales should exist, and manifest themselves *via* deviations of measured observables from the SM predictions. Here, we consider an alternative to LED case when the heavy intermediate states could not be produced even at the highest energy supercolliders and, correspondingly, only “virtual” effects can be expected. A description of the relevant new interaction in terms of “effective” contact-interaction (CI) is most appropriate in this case. Of course, since different interactions can give rise to similar deviations from the SM predictions, the problem is to identify, from a hypothetically measured deviation, the kind of new dynamics underlying it.

We shall here discuss the possibility of distinguishing such effects of extra dimensions from other new physics (NP) scenarios in lepton

$$p + p \rightarrow l^+ l^- + X, \quad (4)$$

where $l = e, \mu$, and photon pair production at the LHC:

$$p + p \rightarrow \gamma\gamma + X. \quad (5)$$

2 Discovery reach in the dilepton channel

At hadron colliders in the SM lepton pairs can be produced at tree-level via the following parton-level process

$$q\bar{q} \rightarrow \gamma, Z \rightarrow l^+ l^-. \quad (6)$$

Now, if gravity can propagate in extra dimensions, the possibility of KK graviton exchange opens up two tree-level channels in addition to the SM channels, namely

$$q\bar{q} \rightarrow G_n^* \rightarrow l^+l^- \quad \text{and} \quad gg \rightarrow G_n^* \rightarrow l^+l^-, \quad (7)$$

where G_n^* represents the gravitons of the KK tower.

To estimate the discovery reach of graviton towers in ADD model one can use the invariant mass distributions of lepton pairs that have significantly different behavior in the SM and the ADD model.

Discovery reach of graviton towers in the ADD model can be determined with χ^2 function defined as

$$\chi^2 = \sum_i \left(\frac{\Delta N_i}{\delta N_i} \right)^2, \quad (8)$$

where $N_i = \varepsilon_{l+l-} \mathcal{L}_{\text{int}} \sigma_i$, $\varepsilon_{l+l-} = 90\%$, $\Delta N_i = N_i^{\text{ADD}} - N_i^{\text{SM}}$, $\delta N_i = \sqrt{N_i}$. Here, \mathcal{L}_{int} is time integrated luminosity, ε_{l+l-} reconstruction efficiency of the dilepton, σ_i is integrated cross-section within the i -th bin. Summation in Eq. (8) runs over 15 bins with the width of 100 GeV in the range of 500 GeV and 2000 GeV. The results of the χ^2 analysis are demonstrated in Fig. 1. In particular, Fig. 1 shows discovery reach on cutoff scale M_S at 95% C.L. for $d = 3$ and $d = 6$ as a function of integrated luminosity of the LHC.

3 Center-edge asymmetry and identification reach in the dilepton channel

In practice the asymmetry, which is defined based on the angular distribution of the final states in scattering or decay processes, can be utilized to scrutinize underlying dynamics in new physics (NP) beyond the SM. As one of the possible NP which might be discovered early at the LHC, LED are theoretical well motivated. Once LED are discovered at the LHC, it is crucial to discriminate the different NP scenarios that can lead to the same or very similar experimental signatures. In principle such task can be accomplished by measuring the angular distribution of the lepton final states which are produced via G_n^* -mediated processes. In the real data

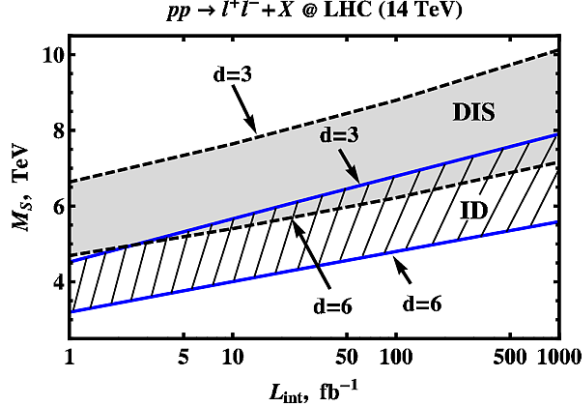


Figure 1: Discovery (gray band) and identification (hatched band) reaches on M_S (in TeV) at 95% CL as a function of integrated luminosity \mathcal{L}_{int} for different number of extra dimensions ($d = 3 - 6$) at the LHC with 14 TeV.

analysis, asymmetry is always adopted. In [7–9] center-edge asymmetry has been proposed at LHC for such kind of analysis.

The center–edge and total cross sections at the parton level can be defined as:

$$\begin{aligned}\hat{\sigma}_{\text{CE}} &\equiv \left[\int_{-z^*}^{z^*} - \left(\int_{-1}^{-z^*} + \int_{z^*}^1 \right) \right] \frac{d\hat{\sigma}}{dz} dz, \\ \hat{\sigma} &\equiv \int_{-1}^1 \frac{d\hat{\sigma}}{dz} dz,\end{aligned}\quad (9)$$

where $z = \cos \hat{\theta}$, with $\hat{\theta}$ the angle, in the c.m. frame of the two leptons, between the lepton and the proton. Here, $0 < z^* < 1$ is a parameter which defines the border between the “center” and the “edge” regions.

The center–edge asymmetry at hadron level for a given dilepton invariant mass M_{ll} can be defined as

$$A_{\text{CE}}(M_{ll}) = \frac{d\sigma_{\text{CE}}/dM_{ll}}{d\sigma/dM_{ll}}, \quad (10)$$

where a convolution over parton momenta is performed, and we obtain $d\sigma_{\text{CE}}/dM_{ll}$ and $d\sigma/dM_{ll}$ from the inclusive differential cross sections $d\sigma_{\text{CE}}/dM_{ll} dy dz$ and $d\sigma/dM_{ll} dy dz$, respectively, by integrating over z according to Eq. (9) and over rapidity y between $-Y$ and Y , with $Y = \log(\sqrt{s}/M_{ll})$.

For the SM contribution to the center–edge asymmetry, the convolution integrals, depending on the parton distribution functions, cancel, and one finds

$$A_{\text{CE}}^{\text{SM}} = \frac{1}{2}z^*(z^{*2} + 3) - 1. \quad (11)$$

This result is thus independent of the dilepton mass M_{ll} , and identical to the result for e^+e^- colliders. Hence, in the case of no cuts on the angular integration, there is a unique value, $z^* = z_0^* \simeq 0.596$, for which $A_{\text{CE}}^{\text{SM}}$ vanishes, corresponding to $\hat{\theta} = 53.4^\circ$.

The SM center-edge asymmetry of Eq. (11) is equally valid for a wide variety of NP models: composite-like contact interactions, heavy Z' bosons [10], TeV-scale gauge bosons, *etc.* However, if graviton tower exchange is possible, the graviton tensor couplings would yield a different angular distribution, leading to a different dependence of A_{CE} on z^* . In this case, the center–edge asymmetry would not vanish for the above choice of $z^* = z_0^*$. Furthermore, it would show a non-trivial dependence on M_{ll} . Thus, a value for A_{CE} different from $A_{\text{CE}}^{\text{SM}}$ would indicate non-vector-exchange of NP.

Another important difference from the SM case and NP CI-like scenarios is that the graviton also couples to gluons, and therefore it has the additional gg initial state of Eq. (7) available. In summary then, including graviton exchange and also experimental cuts relevant to the LHC detectors, the center–edge asymmetry is no longer the simple function of z^* given by Eq. (11).

We assume now that a deviation from the SM is discovered in the cross section in the form of “effective” CI. We will here investigate in which regions of the ADD parameter spaces such a deviation can be *identified* as being caused by spin-2 exchange. More precisely, we will see how the center–edge asymmetry (10) can be used to exclude spin-1 exchange interactions beyond that of the SM.

We define the bin-integrated center–edge asymmetry:

$$A_{\text{CE}}(i) = \frac{\int_i \frac{d\sigma_{\text{CE}}}{dM_{ll}} dM_{ll}}{\int_i \frac{d\sigma}{dM_{ll}} dM_{ll}}, \quad (12)$$

where i being bin in M_{ll} . To determine the underlying new physics (spin-1 vs. spin-2 couplings) one can introduce the deviation of the measured

center-edge asymmetry from that expected from pure spin-1 exchange, $A_{\text{CE}}^{\text{spin-1}}(i)$, in each i -th bin,

$$\Delta A_{\text{CE}}(i) = A_{\text{CE}}^{\text{spin-2}}(i) - A_{\text{CE}}^{\text{spin-1}}(i). \quad (13)$$

The bin-integrated statistical uncertainty is then given as

$$\delta A_{\text{CE}}(i) = \sqrt{\frac{1 - A_{\text{CE}}^2(i)}{\epsilon_{l+l-} \mathcal{L}_{\text{int}} \sigma(i)}}, \quad (14)$$

based on the number of events that are effectively detected and the A_{CE} that is actually measured. In the ADD scenario, the identification reach in M_S can be estimated from a χ^2 analysis:

$$\chi^2 = \sum_i \left[\frac{\Delta A_{\text{CE}}(i)}{\delta A_{\text{CE}}(i)} \right]^2, \quad (15)$$

where i runs over the different bins in M_{ll} . The 95% CL is then obtained by requiring $\chi^2 = 3.84$, as pertinent to a one-parameter fit.

From a conventional χ^2 analysis we find the ADD-scenario *identification* reach on M_S at the LHC. The results are summarized in Fig. 1 which shows the identification reaches for different number of extra dimensions ($d = 3, 6$) as a function of integrated luminosity \mathcal{L}_{int} .

In conclusion, a method proposed here and based on A_{CE} is suitable for actually *pinning down* the spin-2 nature of the KK gravitons up to very high M_S close to discovery reach. Therefore, the analysis sketched here can potentially represent a valuable method complementary to the direct fit to the angular distribution of the lepton pairs. We find that for $\sqrt{s} = 14$ TeV and $\mathcal{L}_{\text{int}} = 100 \text{ fb}^{-1}$ the LHC detectors will be capable of discovering and identifying graviton spin-2 exchange effects in the ADD scenario with $M_S^{\text{DIS}} = 6.2$ TeV ($M_S^{\text{ID}} = 4.8$ TeV) for $d = 6$ and $M_S^{\text{DIS}} = 8.8$ TeV ($M_S^{\text{ID}} = 6.8$ TeV) for $d = 3$.

4 Effects of LED in the diphoton channel

The process of photon pairs production

$$p + p \rightarrow \gamma\gamma + X \quad (16)$$

is one of the important processes at the hadron colliders and has been used to do precision of the SM. Also it provides a laboratory for probing new physics (CI, unparticles, supersymmetry, extra dimensions, etc.).

A unique feature of the process of photon pairs production in the ADD model compared with the lepton channel of Drell - Yan process is that intermediate states in this process can only be scalar and tensor particles whereas in dileptonic production does not exclude the possibility of the existence vector state. The Landau-Yang theorem [11, 12] forbids decays of vector particle into two photons. As an intermediate state, we consider the scalar unparticle [13, 14]. Reducing the number of hypothetical intermediate states in the Born approximation effectively leads to “enhance” the sensitivity of the observed values for dynamic parameters graviton towers and, thereby, expands the identification reach of graviton exchange towers in the ADD model.

4.1 Discovery reach

At hadron colliders in the ADD model photon pairs can be produced via the following parton-level process, namely

$$q + \bar{q} \rightarrow \gamma + \gamma \quad \text{and} \quad g + g \rightarrow \gamma + \gamma. \quad (17)$$

The differential cross section for the subprocess $q\bar{q} \rightarrow \gamma\gamma$, defined by the t - and u - channel diagrams in the SM and exchange graviton states in the s - channel, in the approximation of massless fermions can be written as:

$$\begin{aligned} \frac{d\sigma(q\bar{q} \rightarrow \gamma\gamma)}{dz} = & \frac{1}{96\pi\hat{s}} \left[2e^4 Q_q^4 \frac{1+z^2}{1-z^2} + 2\pi e^2 Q_q^2 \frac{\hat{s}^2}{M_S^4} (1+z^2) \mathcal{F} \right. \\ & \left. + \frac{\pi^2}{2} \frac{\hat{s}^4}{M_S^8} (1-z^4) \mathcal{F}^2 \right], \end{aligned} \quad (18)$$

where \mathcal{F} is defined in Eq.(2).

Here $\sqrt{\hat{s}} \equiv M_{\gamma\gamma}$ is an invariant mass of photon pairs, $z \equiv \cos \theta_{\text{cm}}$, θ_{cm} - angle in the center-of-mass photons, Q_q - quark electric charge q .

The differential cross section for the subprocess $gg \rightarrow \gamma\gamma$:

$$\frac{d\sigma(gg \rightarrow \gamma\gamma)}{dz} = \frac{\pi}{512} \frac{\hat{s}^3}{M_S^8} (1 + 6z^2 + z^4) \mathcal{F}^2, \quad (19)$$

where the factor \mathcal{F} is given in Eq.(2).

Discovery reach of graviton towers in the ADD model can be determined with χ^2 function. The requirement on the functions $\chi^2 = 3,84$ provides a limit on the parameter M_S , called as discovery reach with a confidence level is 95%.

4.2 Identification reach

The present analysis is aimed at determining an interval of values for the scale parameter M_S (at fixed d) such that, within this interval, the ADD model (which, in the following, is called a “correct” model) can be statistically separated at a preset confidence level from competing new physics models that could mimic experimentally effects of the correct model and which have a different physical nature (from Georgi’s unparticle physics model in the case being considered) at any values of their parameters. Below, we refer to such competing models as tested models and to the boundary value for the M_S range in question as the identification reach for the ADD model. In order to separate effects of the correct and tested models, we introduce the function χ^2 by analogy with that which was used to estimate the identification reaches for M_S on the basis of expression (15). For the problem at hand, the function χ^2 has the form

$$\chi^2 = \left(\frac{A_{CE}^{\text{ADD}} - A_{CE}^{\text{NG}}}{\delta A_{CE}^{\text{ADD}}} \right)^2, \quad (20)$$

where A_{CE}^{NG} is the asymmetry center-edge in the Georgi’s unparticle-physics model, $\delta A_{CE}^{\text{ADD}}$ is the respective statistical uncertainty within the correct ADD model.

In order to separate effects induced by graviton towers and Georgi’s unparticles in the process (4), we will make use of the criterion $\chi^2 = 3.84$ for the function χ^2 defined by expression (20). Results of numerical analysis for discovery and identification reach are shown in Fig. 2.

5 Conclusion

Along with contact interactions, effects of the exchange of KK graviton towers within the ADD model, which involves extra spatial dimensions, may become among the first new physics effects that would be discovered

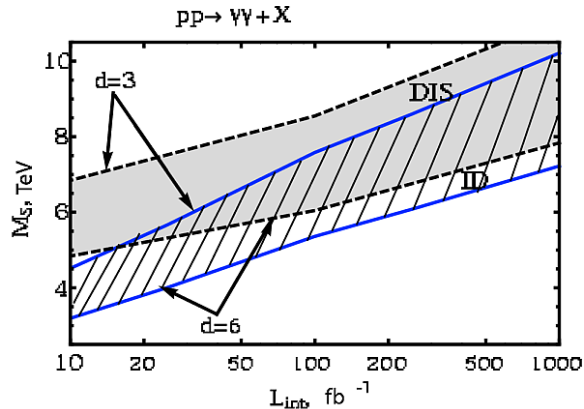


Figure 2: Discovery (gray band) and identification (hatched band) reaches on M_S (in TeV) at 95% CL as a function of integrated luminosity \mathcal{L}_{int} for different number of extra dimensions ($d = 3 - 6$) at the LHC with 14 TeV.

at the LHC. The Drell-Yan process of dilepton production is one of the most efficient channels of searches for new intermediate states owing to a strong suppression of background processes and a high efficiency of dilepton identification. In many respects, the same applies to diphoton production. If, in the dilepton and/or in the diphoton channel, experiments exhibit some indirect new physics effects, such as a deviation of the dilepton or diphoton invariant mass distribution from the respective predictions of the SM, then the next step in studying the nature of this new phenomenon will consist in determining the spin of the respective intermediate state. In the present study, we have explored prospects of the discovery and identification of indirect effects of the exchange of Kaluza-Klein graviton towers, whose existence is predicted by the ADD model featuring extra spatial dimensions, in the processes of dilepton and diphoton production in the ATLAS experiment at the LHC. Searches for these new effects are based on looking for characteristic features in the behavior of the dilepton and diphoton spectra. As for the identification of the intermediate state spin, it is being performed in terms of the center-edge asymmetry. The results of our numerical analysis aimed at the search for and the identification of effects of extra spatial dimensions in the dilepton and diphoton channels are summarized in Table. 1.

Table 1: Discovery and identification reach on M_S (in TeV) at the LHC

M_S (TeV)	l^+l^- DIS (ID)	$\gamma\gamma$ DIS (ID)
$d = 3$	8.8 (6.8)	8.5 (7.6)
$d = 6$	6.2 (4.8)	6.0 (5.4)

References

- [1] N. Arkani-Hamed, S. Dimopoulos, and G. Dvali, Phys. Lett. B **429**, 263 (1998).
- [2] J. L. Hewett, Phys. Rev. Lett. **82**, 4765 (1999).
- [3] G. F. Giudice, R. Rattazzi and J. D. Wells, Nucl. Phys. B **544**, 3 (1999).
- [4] T. Han, J. Lykken and R. Zhang, Phys. Rev. D **59**, 105006 (1999).
- [5] G. Aad [et al.] [ATLAS Collab.], Preprint ATLAS-CONF-2014-030 (2014) 18 p.
- [6] S. Chatrchyan [et .al.] [CMS Collab.], Preprint CMS-PAS-EXO-12-031 (2013) 12 p.
- [7] P. Osland, A. A. Pankov and N. Paver, Phys. Rev. D **68**, 015007 (2003).
- [8] E. W. Dvergsnes, P. Osland, A. A. Pankov and N. Paver, Phys. Rev. D **69**, 115001 (2004).
- [9] P. Osland, A. A. Pankov, N. Paver, A.V. Tsytrinov, Phys. Rev. D **78**, 035008 (2008).
- [10] A. Gulov and V. Skalozub, Int. J. Mod. Phys. A **25**, 5787 (2010).
- [11] L. D. Landau, Dokl. Akad. Nauk. SSSR, Vol. **60**, P. 207 (1948).
- [12] C. N. Yang, Phys. Rev. Vol. **77**, P. 242 (1950).
- [13] H. Georgi, Phys. Rev. Lett. **98**, 221601 (2007).
- [14] H. Georgi, Phys. Lett. B **650**, 275 (2007).

High-Precision Determination of the $Z - Z'$ Mixing Angle at LHC

A.A. Pankov*, A.V. Tsytrinov†

*Abdus Salam ICTP Affiliated Centre
at Sukhoi State Technical University of Gomel*

Abstract

We consider the expected sensitivity to Z' boson effects in the W^\pm boson pair production process at the Large Hadron Collider (LHC). The results of a model-dependent analysis of Z' boson effects are presented as constraints on the Z - Z' mixing angle ϕ and Z' boson mass. We show that the process $pp \rightarrow W^+W^- + X$ allows to place stringent constraints on the Z - Z' mixing angle.

1 Introduction

Many New Physics (NP) scenarios beyond the Standard Model (SM) [1], including superstring and left-right-symmetric models, predict the existence of new neutral gauge bosons, which might be light enough to be accessible at current and/or future colliders [2–5].

The search for these Z' particles is an important aspect of the experimental physics program of current and future high-energy colliders. Present limits from direct production at the LHC and virtual effects at LEP, through interference or mixing with the Z boson, imply that new Z' bosons are rather heavy and mix very little with the Z boson. Depending on the considered theoretical model, Z' masses of the order of 2.5–3.0 TeV [6–9] and Z - Z' mixing angles at the level of a few per mil are excluded [10–12]. The size of the mixing angle is strongly constrained by

*E-mail:pankov@ictp.it

†E-mail:tsytrin@rambler.ru

very high precision Z -pole experiments at LEP and the SLC [13]. They contain measurements from the Z line shape, from the leptonic branching ratios normalized to the total hadronic Z decay width and from leptonic forward-backward asymmetries. A Z' boson, if lighter than about 5 TeV, could be discovered at the LHC [14,15] with $\sqrt{s} = 14$ TeV in the Drell-Yan process

$$pp \rightarrow Z' \rightarrow \ell^+ \ell^- + X \quad (1)$$

with $\ell = e, \mu$. The future e^+e^- International linear collider (ILC) with high c.m. energies and longitudinally polarized beams could indicate the existence of Z' bosons via its interference effects in fermion pair production processes, with masses up to about $6 \times \sqrt{s}$ [16] while Z - Z' mixing will be constrained down to $\sim 10^{-4} - 10^{-3}$ in the process $e^+e^- \rightarrow W^+W^-$ [17,18].

After the discovery of a Z' boson at the LHC via the process (1), some diagnostics of its couplings and Z - Z' mixing needs to be done in order to identify the correct theoretical framework. In this paper we study the potential of the LHC to discover Z - Z' mixing effects in the process

$$pp \rightarrow W^+W^- + X \quad (2)$$

and compare it with that expected at the ILC.

The W^\pm boson pair production process (2) is rather important for studying the electroweak gauge symmetry at the LHC. Properties of the weak gauge bosons are closely related to electroweak symmetry breaking and the structure of the gauge sector in general. In addition, the diboson decay modes of Z' directly probe the gauge coupling strength between the new and the standard-model gauge bosons. The coupling strength strongly influences the decay branching ratios and the natural widths of the new gauge bosons. Thus, detailed examination of the process (2) will both test the gauge sector of the SM with the highest accuracy and throw light on NP that may appear beyond the SM.

Direct searches for a heavy WW resonance have been performed by the CDF and D0 collaborations at the Tevatron. The D0 collaboration explored diboson resonant production using the $\ell\nu\ell'\nu'$ and $\ell\nu jj$ final states [19]. The CDF collaboration also searched for resonant WW production in the $e\nu jj$ final state, resulting in a lower limit on the mass of an RS graviton, Z' and W' bosons [12].

The direct WW resonance search by the ATLAS Collaboration using $\ell\nu\ell'\nu'$ final-state events in 4.7 fb^{-1} pp collision data at the collider energy of 7 TeV set mass limits on such resonances [20,21]. Also, the $\ell\nu jj$ final

state allows to reconstruct the invariant mass of the system, under certain assumptions on the neutrino momentum from a W boson decay.

Here, we examine the feasibility of observing a Z' boson in the W^\pm pair production process at the LHC, which in contrast to the Drell-Yan process (1) is not the principal discovery channel, but can help to understand the origin of new gauge bosons.

2 Z' models

There are many theoretical models which predict a Z' with mass possibly in the TeV range. Popular classes of models are represented by E_6 -motivated models, the Left-Right Symmetric Model (LR), the Z' in an ‘alternative’ left-right scenario and the Sequential Standard Model (SSM), which has a heavier boson with couplings like those of the SM Z . Searching for Z' in the above models has been widely studied in the literature [2–4] and applied at LEP2, the Tevatron and the LHC. For the notation we refer to [17], where also a brief description can be found. The different models considered are: (i) Models related to the breaking of E_6 , parametrized by a parameter β , familiar cases are the Z'_χ , Z'_ψ , Z'_η and Z'_I models; (ii) Left-right models, originating from the breaking down of an $SO(10)$ grand-unification symmetry, leading to a Z'_{LR} ; (iii) The sequential Z'_{SSM} , which has couplings to fermions being the same as those of the SM Z .

The mass-squared matrix of the Z and Z' can have non-diagonal entries δM^2 , which are related to the vacuum expectation values of the fields of an extended Higgs sector:

$$M_{ZZ'}^2 = \begin{pmatrix} M_Z^2 & \delta M^2 \\ \delta M^2 & M_{Z'}^2 \end{pmatrix}. \quad (3)$$

Here, Z and Z' denote the weak gauge boson eigenstates of $SU(2)_L \times U(1)_Y$ and of the extra $U(1)'$, respectively. The mass eigenstates, Z_1 and Z_2 , diagonalizing the matrix (3), are then obtained by the rotation of the fields Z and Z' :

$$Z_1 = Z \cos \phi + Z' \sin \phi, \quad (4a)$$

$$Z_2 = -Z \sin \phi + Z' \cos \phi. \quad (4b)$$

Here, the mixing angle ϕ is expressed in terms of masses as:

$$\tan^2 \phi = \frac{M_Z^2 - M_1^2}{M_2^2 - M_Z^2} \simeq \frac{2M_Z \Delta M}{M_2^2}, \quad (5)$$

where $\Delta M = M_Z - M_1 > 0$, M_Z being the mass of the Z_1 boson in the absence of mixing, i.e., for $\phi = 0$. Once we assume the mass M_1 to be determined experimentally, the mixing depends on two free parameters, which we identify as ϕ and M_2 .

From (4), one obtains the vector and axial-vector couplings of the Z_1 and Z_2 bosons to fermions:

$$v_{1f} = v_f \cos \phi + v'_f \sin \phi, \quad a_{1f} = a_f \cos \phi + a'_f \sin \phi, \quad (6a)$$

$$v_{2f} = v'_f \cos \phi - v_f \sin \phi, \quad a_{2f} = a'_f \cos \phi - a_f \sin \phi, \quad (6b)$$

with $(v_f, a_f) = (g_L^f \pm g_R^f)/2$, and (v'_f, a'_f) similarly defined in terms of the Z' couplings. The fermionic Z' couplings can be found, e.g. in [17].

Analogously, one obtains according to the remarks above:

$$g_{WWZ_1} = \cos \phi g_{WWZ}, \quad (7a)$$

$$g_{WWZ_2} = -\sin \phi g_{WWZ}, \quad (7b)$$

where $g_{WWZ} = \cot \theta_W$.

3 Cross section

The parton model cross section for the process (2) from initial quark-antiquark states can be written as

$$\frac{d\sigma_{q\bar{q}}}{dM dy dz} = K \frac{2M}{s} \sum_q [f_{q|P_1}(\xi_1) f_{\bar{q}|P_2}(\xi_2) + f_{\bar{q}|P_1}(\xi_1) f_{q|P_2}(\xi_2)] \frac{d\hat{\sigma}_{q\bar{q}}}{dz}. \quad (8)$$

Here, s is the proton-proton center-of-mass energy squared; $z = \cos \theta$ with θ the W^- -boson-quark angle in the W^+W^- center-of-mass frame; y is the diboson rapidity; $f_{q|P_1}(\xi_1, M)$ and $f_{\bar{q}|P_2}(\xi_2, M)$ are parton distribution functions in the protons P_1 and P_2 , respectively, with $\xi_{1,2} = (M/\sqrt{s}) \exp(\pm y)$ the parton fractional momenta; finally, $d\hat{\sigma}_{q\bar{q}}/dz$ are the partonic differential cross sections. In (8), the K factor accounts for next-to-leading order QCD contributions [22,23]. For simplicity, we will use as an approximation a global flat value $K = 1.2$ [24, 25] both for the SM and Z' boson cases. For numerical computation, we use CTEQ-6L1 parton distributions [26]. Since our estimates will be at the Born level, the factorisation scale μ_F enters solely through the parton distribution functions, as the parton-level

cross section at this order does not depend on μ_F . As regards the scale dependence of the parton distributions we choose for the factorization scale the WW invariant mass, i.e., $\mu_F^2 = M^2 = \hat{s}$, with $\hat{s} = \xi_1 \xi_2 s$ the parton subprocess c.m. energy squared. We have checked that the obtained constraints presented in the following are not significantly modified when μ_F is varied in the interval $\mu_F/2$ to $2\mu_F$.

Taking into account the experimental rapidity cut relevant to the LHC experiments, ($Y_{\text{cut}} = 2.5$), one should carry out the integration over the phase space in (8) determined as [27, 28]:

$$|y| \leq Y = \min [\ln(\sqrt{s}/M), Y_{\text{cut}}] = \ln(\sqrt{s}/M), \quad (9)$$

where we do not consider low masses, $\ln(\sqrt{s}/M) < Y_{\text{cut}}$. This leads to a cut in the production angle

$$|z| \leq z_{\text{cut}} = \min [\tanh(Y_{\text{cut}} - |y|)/\beta_W, 1], \quad (10)$$

where $\beta_W = \sqrt{1 - 4M_W^2/\hat{s}}$ and M_W is the W boson mass.

The resonant Z' production cross section of process (2) needed in order to estimate the expected number of Z' events, can be derived from (8) by integrating its right-hand-side over z , the rapidity of the W^\pm -pair y and invariant mass M around the resonance peak ($M_R - \Delta M/2$, $M_R + \Delta M/2$):

$$\sigma(pp \rightarrow W^+W^- + X) = \int_{M_R - \Delta M/2}^{M_R + \Delta M/2} dM \int_{-Y}^Y dy \int_{-z_{\text{cut}}}^{z_{\text{cut}}} dz \frac{d\sigma_{q\bar{q}}}{dM dy dz}. \quad (11)$$

We adopt the parametrization of the experimental mass resolution ΔM in reconstructing the diboson invariant mass of the W^+W^- system, ΔM vs. M , as proposed in Ref. [29]. (After integration over y , interference effects vanish.)

The parton level W^\pm boson pair production can be described, within the gauge models discussed here, by the subprocesses

$$q\bar{q} \rightarrow \gamma, Z_1, Z_2 \rightarrow W^+W^-, \quad (12)$$

as well as t - and u -channel amplitudes.

The differential (unpolarized) cross section of process (12) can be written as:

$$\frac{d\hat{\sigma}_{q\bar{q}}}{dz} = \frac{1}{N_C} \frac{\beta_W}{32\pi\hat{s}} \sum_{\lambda, \lambda', \tau, \tau'} |F_{\lambda\lambda'\tau\tau'}(\hat{s}, \theta)|^2. \quad (13)$$

Here, N_C is the number of quark colors; $\lambda = -\lambda' = \pm 1/2$ are the quark helicities; the helicities of the W^- and W^+ are denoted by $\tau, \tau' = \pm 1, 0$. The helicity amplitudes $F_{\lambda\lambda'\tau\tau'}(\hat{s}, \theta)$ are summarized in Ref. [27]. There $\hat{s}, \hat{t}, \hat{u}$ are the Mandelstam variables defined as $\hat{t} = M_W^2 - \hat{s}(1 - \beta_W z)/2$, $\hat{u} = M_W^2 - \hat{s}(1 + \beta_W z)/2$; $\Gamma_{1,2}$ are $Z_{1,2}$ boson decay widths; $g_{1,f}^\lambda = v_{1,f} - 2a_{1,f}\lambda$, $g_{2,f}^\lambda = v_{2,f} - 2a_{2,f}\lambda$; and $\gamma_W = \sqrt{\hat{s}}/2M_W$. In the t - and u -channel exchanges we account for the initial $q = u, d, s, c$, only the CKM favoured quarks in the approximation of unity relevant matrix element.

In evaluation of the total width Γ_2 of the Z_2 boson we take into account its decay channels into fermions and W^\pm boson pair [30]:

$$\Gamma_2 = \sum_f \Gamma_2^{ff} + \Gamma_2^{WW} . \quad (14)$$

Further contributions of decays involving Higgs and/or gauge bosons and supersymmetric partners (including sfermions), which are not accounted for in (14), could increase Γ_2 by a model-dependent amount typically as large as 50% [30]. For definiteness the Z_2 width Γ_2 is assumed to scale with the Z_2 mass $\Gamma_2 = (M_2/M_1)\Gamma_1 \approx 0.03 M_2$. This scaling is what would be expected for the reference model SSM [31].

For illustrative purposes, the invariant mass distribution of W^\pm pairs in the process $pp \rightarrow W^+W^+ + X$ in the SM (solid black curve) and for the Z'_{SSM} model at two values of the Z - Z' mixing angle at the LHC with $\sqrt{s} = 14$ TeV is shown in Fig. 1. The W^\pm -pair invariant mass distribution ($d\sigma/dM$) is calculated with the same parton distribution functions and event selection criterion as those used in Ref. [32]. Also, the bin size ΔM of the diboson invariant mass is depicted for comparison with the Z' width. For numerical computations, we take $\Delta M = 0.03M$. The W bosons are kept on-shell and their subsequent decays are not included in the cross sections represented in Fig. 1. Here, we assumed that the invariant mass distribution of the cross section can be reconstructed from the decay products of the W^+W^- . Fig. 1 shows that at the LHC with integrated luminosity $\mathcal{L}_{\text{int}} = 100 \text{ fb}^{-1}$ the expected number of W^+W^- background events within a mass bin ΔM is of the order of a few events while the resonant yield at $\phi = 10^{-3}$ is $N_{Z'} \sim 100$.

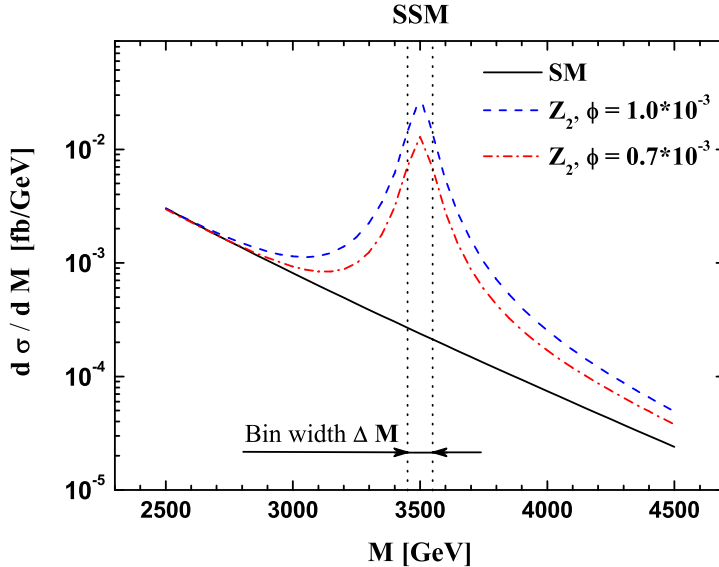


Figure 1: Invariant mass distribution of W^\pm pairs in $pp \rightarrow W^+W^- + X$ in the SM (solid curve) and for the Z'_{SSM} model ($M_{Z'} = 3.5$ TeV) with Z - Z' mixing angle of $\phi = 10^{-3}$ (dashed line) and $\phi = 0.7 \cdot 10^{-3}$ (dash-dotted line) at the LHC with $\sqrt{s} = 14$ TeV.

4 Constraints on Z'

We focus on the WW production via intermediate Z' and subsequent purely leptonic decay of on-shell W 's, that will be probed at LHC:

$$pp \rightarrow WW + X \rightarrow l\nu l'\nu' + X \quad (l, l' = e \text{ or } \mu), \quad (15)$$

and, we follow the analysis given in [27, 33, 34], to evaluate the main backgrounds and possible cuts to enhance the Z' signal to background ratio.

In our analysis, we denote by N_{SM} and $N_{Z'}$ the numbers of ‘background’ and ‘signal’ events, and we adopt the criterion $N_{Z'} = 2\sqrt{N_{\text{SM}}}$ or 3 events, whichever is larger, as the minimum signal for reach at the 95% C.L. [4]. Here, the Z' signal can be determined as

$$N_{Z'} = \mathcal{L}_{\text{int}} \times \sigma^{Z'} \times P_{\text{surv}}^{\text{EW}} \times A \times \epsilon^\ell, \quad (16)$$

with

$$\sigma^{Z'} = \sigma(pp \rightarrow Z') \times \text{Br}(Z' \rightarrow W^+W^- \rightarrow l\nu l'\nu'). \quad (17)$$

In Eq. (16), \mathcal{L}_{int} is the time-integrated luminosity, and $A \times \epsilon^\ell$ is the product of the overall acceptance times the lepton detection and reconstruction efficiencies where A represents the kinematic and geometric acceptance from the total phase space to the fiducial phase space governed by Eqs. (9) and (10), while ϵ^ℓ represents detector effects such as lepton trigger and identification efficiencies. The overall acceptance times the lepton efficiency is W^\pm invariant mass dependent and, for simplicity, we take that to be 0.5. The SM background reads:

$$N_{\text{SM}} = \mathcal{L}_{\text{int}} \left(\sigma_{\text{SM}}^{\text{EW}} P_{\text{surv}}^{\text{EW}} + \sigma_{\text{SM}}^{t\bar{t}} P_{\text{surv}}^{\text{QCD}} \right) A \epsilon^\ell \approx \mathcal{L}_{\text{int}} \sigma_{\text{SM}}^{\text{EW}} P_{\text{surv}}^{\text{EW}} A \epsilon^\ell, \quad (18)$$

where $\sigma_{\text{SM}}^{\text{EW}}$ is determined by Eqs. (11) and (13) taking into account solely the SM contribution. Also, in the latter expression for N_{SM} we take into account that for heavy $M_{Z'}$, $\sigma_{\text{SM}}^{\text{EW}} \gg \sigma_{\text{SM}}^{t\bar{t}}$ as was shown in [33].

We depict in Fig. 2 the region in parameter space to which the LHC will be able to constrain Z - Z' mixing for $\mathcal{L}_{\text{int}} = 100 \text{ fb}^{-1}$.

In particular, the discovery reach on the Z - Z' mixing and M_2 mass for Z'_{SSM} obtained from the process $pp \rightarrow WW + X \rightarrow l\nu l'\nu' + X$ ($l, l' = e$ or μ) at the LHC with $\sqrt{s} = 14 \text{ TeV}$ and $\mathcal{L}_{\text{int}} = 100 \text{ fb}^{-1}$ are depicted by the two solid lines. The form of these bounds is governed by the criterion of $N_{Z'} = 3$ and the quadratic dependence of the resonant cross section on the Z - Z' mixing angle. Also, current limits on M_2 for Z'_{SSM} derived from the Drell–Yan (l^+l^-) process at the LHC (8 TeV) (horizontal solid line) as well as those expected from the future experiments at the LHC with 14 TeV (horizontal dotted line) are shown. The combined allowed area in the (ϕ, M_2) plane obtained from the Drell–Yan and W^\pm pair production processes is shown as a hatched region. In addition, present limits on the Z - Z' mixing angle obtained from electroweak precision data analysis [10] labelled as ‘EW data’ are displayed (these have a weak mass dependence which we have not attempted to draw). For comparison, the corresponding limits obtained from W^\pm pair production at the ILC with polarized beams and for two options of energy and time-integrated luminosity (0.5 (1) TeV and 0.5 (1) ab^{-1} , respectively) are also presented [17]. Fig. 2 show that the LHC is able to not only significantly improve the current limits on the Z - Z' mixing angle, but in several cases, also allow more stringent bounds than those expected from future experiments on the WW channel at the electron–positron collider ILC [11].

In Table 1, we collect our limits on the Z' parameters for the models listed in Section II. Also shown in Table 1 are the current limits on vari-

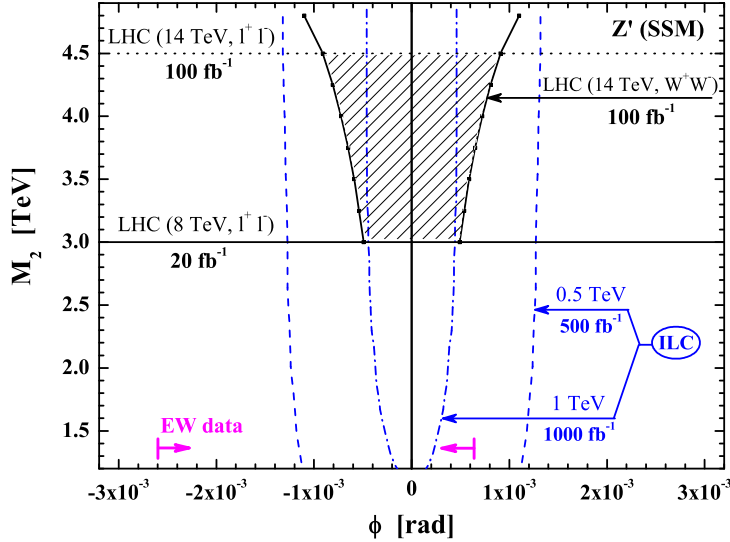


Figure 2: Reach (at 95 %C.L.) on Z - Z' mixing and M_2 mass for Z'_{SSM} obtained from the inclusive process $pp \rightarrow WW \rightarrow l\nu l'\nu'$ ($l, l' = e$ or μ) at the LHC (solid lines). The allowed domain in ϕ and M_2 is the hatched one. Current limits on M_2 for Z'_{SSM} derived from the Drell–Yan (l^+l^-) process at the LHC (8 TeV) (horizontal solid line) as well as ‘typical’ mass limits expected at the LHC (14 TeV) (horizontal dotted line) are shown. Limits on the Z - Z' mixing angle from electroweak precision data are displayed, and those expected from W^\pm pair production at the ILC with polarized beams.

ous Z' boson masses from the LEP2 and Tevatron from studies of diboson W^+W^- pair production. The limits on ϕ and M_2 at the Tevatron assume that no decay channels into exotic fermions or superpartners are open to the Z' . Otherwise, the limits would be moderately weaker. LEP2 constrains virtual and Z - Z' boson mixing effects by the angular distribution of W bosons. Table 1 shows that the limits on ϕ from the EW precision data are generally competitive with and in many cases stronger than those from the colliders, except for the ILC (1 TeV) and LHC (14 TeV) that possess high potential to improve substantially the current bounds on the Z - Z' mixing angle. We stress that these limits are highly complementary.

If a new Z' boson exists in the mass range ~ 3 – 4.5 TeV, its discovery is possible in the Drell–Yan channel. Moreover, the detection of the $Z' \rightarrow W^+W^-$ mode is eminently possible and gives valuable information

Table 1: Reach on the Z - Z' mixing angle ϕ at 95% C.L. in different processes and experiments.

collider, process	$ \phi \times$	Z'_χ $ \phi $	Z'_ψ $ \phi $	Z'_η $ \phi $	Z'_{SSM} $ \phi $	$M_{Z'}$ (TeV)
LEP2 [11], $e^+e^- \rightarrow W^+W^-$	10^{-2}	6	15	50	7	≥ 1
Tevatron [12], $p\bar{p} \rightarrow W^+W^- + X$	10^{-2}	–	–	–	2	0.4–0.9
electroweak data [10]	10^{-3}	1.6	1.8	4.7	2.6	–
ILC (0.5 TeV) [17], $e^+e^- \rightarrow W^+W^-$	10^{-3}	1.5	2.3	1.6	1.2	≥ 3
ILC (1.0 TeV) [17], $e^+e^- \rightarrow W^+W^-$	10^{-3}	0.4	0.6	0.5	0.3	≥ 3
LHC (8 TeV), $pp \rightarrow W^+W^- \rightarrow l\nu l'\nu'$	10^{-3}	–	–	–	5.2	3
LHC (14 TeV), $pp \rightarrow W^+W^- \rightarrow l\nu l'\nu'$	10^{-4}	4–8	3–6	3–6	5–9	3–4.5

on the Z - Z' mixing. It might be the only mode other than the dileptonic one, $Z' \rightarrow l^+l^-$, that is accessible. Our results demonstrate that it might be possible to detect a new heavy Z' boson from the totally leptonic or semileptonic WW channels at the LHC. The LHC at nominal energy and integrated luminosity provides the best opportunity of studying a new heavy Z' through its WW decay mode and creates the possibility of measuring (or constraining) the Z - Z' mixing, thus providing insight into the pattern of symmetry breaking.

Acknowledgments

This research has been partially supported by the Abdus Salam ICTP (TRIL Programme), the Collaborative Research Center SFB676/1-2006 of the DFG at the Department of Physics of the University of Hamburg and the Belarusian Republican Foundation for Fundamental Research.

References

- [1] J. Beringer *et al.* [PDG], Phys. Rev. D **86**, 010001 (2012).
- [2] J. L. Hewett and T. G. Rizzo, Phys. Rept. **183**, 193 (1989).
- [3] P. Langacker, Rev. Mod. Phys. **81**, 1199-1228 (2009).
- [4] A. Leike, Phys. Rept. **317**, 143-250 (1999).
- [5] A. Gulov and V. Skalozub, Int. J. Mod. Phys. A **25**, 5787 (2010).
- [6] S. Chatrchyan *et al.* [CMS Collab.], Phys. Lett. B **720**, 63 (2013).
- [7] G. Aad *et al.* [ATLAS Collab.], JHEP **1211**, 138 (2012).
- [8] G. Aad *et al.* [ATLAS Collab.], arXiv:1405.4123 [hep-ex].
- [9] [CMS Collab.], CMS-PAS-EXO-12-061.
- [10] J. Erler, P. Langacker, S. Munir, E. Rojas, JHEP **0908**, 017 (2009).
- [11] V. V. Andreev and A. A. Pankov, Phys. Atom. Nucl. **75**, 76 (2012).
- [12] T. Aaltonen *et al.* [CDF Collab.], Phys. Rev. Lett. **104**, 241801 (2010).
- [13] S. Schael *et al.* [ALEPH and DELPHI and L3 and OPAL and SLD and LEP Electroweak Working Group and SLD Electroweak Group and SLD Heavy Flavour Group Collab.], Phys. Rept. **427**, 257 (2006).
- [14] S. Godfrey and T. Martin, arXiv:1309.1688 [hep-ph].
- [15] M. Dittmar, A. Nicollerat, A. Djouadi, Phys. Lett. B **583**, 111 (2004).
- [16] T. G. Rizzo, [hep-ph/0610104].
- [17] V. V. Andreev, G. Moortgat-Pick, P. Osland, A. A. Pankov and N. Paver, Eur. Phys. J. C **72**, 2147 (2012).
- [18] B. Ananthanarayan, M. Patra, P. Poulose, JHEP **1102**, 043 (2011).
- [19] V. M. Abazov *et al.* [D0 Collab.], Phys. Rev. Lett. **107**, 011801 (2011).
- [20] G. Aad *et al.* [ATLAS Collab.], Phys. Rev. D **87**, 112006 (2013).

- [21] G. Aad *et al.* [ATLAS Collab.], Phys. Lett. B **718**, 860 (2013).
- [22] J. M. Campbell and R. K. Ellis, Phys. Rev. D **60**, 113006 (1999).
- [23] J. M. Campbell, R. K. Ellis and C. Williams, JHEP **1107**, 018 (2011).
- [24] N. Agarwal, V. Ravindran, V. K. Tiwari and A. Tripathi, Phys. Rev. D **82**, 036001 (2010).
- [25] Y. -M. Bai, L. Guo, X. -Z. Li, W. -G. Ma and R. -Y. Zhang, Phys. Rev. D **85**, 016008 (2012).
- [26] J. Pumplin, D. R. Stump, J. Huston, H. L. Lai, P. Nadolsky and W. K. Tung, JHEP **0207**, 012 (2002).
- [27] V. V. Andreev, P. Osland and A. A. Pankov, Phys. Rev. D **90**, no. 5, 055025 (2014).
- [28] P. Osland, A. Pankov, N. Paver, A. Tsytrinov, Phys. Rev. D **78**, 035008 (2008).
- [29] [ATLAS Collab.], CERN-LHCC-99-14, CERN-LHCC-99-15.
- [30] A. A. Pankov and N. Paver, Phys. Rev. D **48**, 63 (1993).
- [31] D. Benchekroun, C. Driouichi and A. Hoummada, Eur. Phys. J. direct C **3**, N3 (2001).
- [32] N. Agarwal, V. Ravindran, V. K. Tiwari and A. Tripathi, Phys. Lett. B **690**, 390 (2010).
- [33] A. Alves, O. J. P. Eboli, D. Goncalves, M. C. Gonzalez-Garcia and J. K. Mizukoshi, Phys. Rev. D **80**, 073011 (2009).
- [34] O. J. P. Eboli, C. S. Fong, J. Gonzalez-Fraile and M. C. Gonzalez-Garcia, Phys. Rev. D **83**, 095014 (2011).

A Stand-alone Geant4 Simulation of an Electron Calorimeter for COMET Experiment

A.Melnik, Dz. Shoukavy *

Institute of Physics, National Academy of Sciences of Belarus

Abstract

The simple model of electron calorimeter (ECAL) for COMET experiment based on LYSO crystal was created using GEANT4. We shown that single module can't use as the cluster for ECAL trigger. Array of 3x3 modules and 2x2 modules selected by BINP algorithm are suitable as the cluster for ECAL trigger. We found the optimal value for the threshold energy is $0,5\sigma_{noise\ module}$.

1 Introduction

On 4 July 2012, the ATLAS and CMS experiments at CERN's Large Hadron Collider (LHC) announced they had each observed a new particle – a boson consistent with the Higgs boson. The excess of signal over background was observed at a mass of around 126 GeV at 95% confidence level [1], [2]. Well known that Higgs boson plays a central role in a symmetry breaking scheme called the Brout-Englert-Higgs mechanism. The Brout-Englert-Higgs mechanism was first proposed in 1964 in two papers published independently, the first by R. Brout and F. Englert, and the second by physicist P. Higgs. This mechanism explains how elementary particles gain mass by interacting with an invisible field, now called the Higgs field that permeates all space. P. Higgs predicted a massive spin-zero boson of a new type. So the discovery of the Higgs boson by the ATLAS and CMS experiments at CERN showed that the Standard Model (SM) is correct.

*E-mail: shoukavy@ifanbel.bas-net.by

However there remain many shortcomings in the SM's description of nature. So according to the Standard Model, neutrinos are massless particles. But, neutrino oscillation experiments have shown that neutrinos have mass. There is no candidate to Dark Matter in the pure Standard Model. Also this model does not explain the nature of the confinement of quarks, why do elementary particles as much as we see and why their masses are different and so on.

So perhaps Standard Model is only a part of a bigger picture that includes new physics hidden deep in the subatomic world or in the dark recesses of the universe. Unfortunately, so far we have no evidence for physics beyond the Standard Model to explain the many remaining mysteries of the Universe. Even the most powerful particle accelerator ever built – the Large Hadron Collider at CERN – has not found any hard evidence for a new theory. New information from different experiments will help us to find more of these missing pieces. We know that lepton flavour is not conserved in neutrino oscillations and the Standard Model prediction for Charged Lepton Flavour Violation (CLFV) is $O(10^{-54})$. Therefore, if observed at any higher rate, it will be clear evidence of physics beyond the Standard Model. The COMET experiment [3],[4] will search for CLFV through the coherent neutrinoless conversion of a muon to an electron in the field of an aluminium nucleus, with a branching ratio sensitivity at a factor of 10^4 better than the current limit from SINDRUM-II at PSI [5].

2 Electron calorimeter for COMET experiment

The electron calorimeter (ECAL) of COMET experiment consists of segmented scintillating crystals. Based on the prototype ECAL results in the test experiment LYSO ($Lu_{1.8}Y_{0.2}SiO_5 : Ce$) crystal with $20 \times 20 \times 120 \text{ mm}^3$ was chosen. ECAL is placed down-stream of the straw chamber detector and serves the following purposes. One is to measure the energy of electrons with good resolution and to provide the ratio E/p for electron identification. The second is to provide additional data on hit positions of the electron tracks at the calorimeter location. This would be useful in eliminating false tracking. The last is to provide a timing signal for the electron events, and at the same time give a trigger signal that could be used to select events to be recorded for further analysis. On this regard,

fast response and high efficiency are needed.

The basic unit of the electron calorimeter is module consist of a group of 2x2 crystals that wrapped with a Mylar foil. The whole ECAL consists of 568 ($=2272/4$) modules that cover the full cross-section of the detector region ($55\pi^2 = 9503\text{mm}^3$).

3 Algorithms for ECAL trigger

The ECAL trigger is required to give a good time resolution (to keep the readout windows around the trigger time as narrow as possible) and good energy resolution (so as to select energy clusters in the signal region rather than background). Since the energy deposition will be divided among several crystals, it is necessary to do a summation over crystals to reconstruct the full energy.

Collaboration proposed to select the basic trigger unit (cell) as a group of 2x2 crystals, i.e. corresponding to one module of the ECAL. Since for online analysis we have informations from modules only that is a problem of choice of cluster. What type of cluster that can be used for data collection is better to use for ECAL trigger?

In this paper three types of clusters : 1×1 , 2×2 and 3×3 modules were considered. Let us to consider more detailed the different types of clusters and algorithms its choice.

a) 1×1 cluster. For each event it is necessary to determine unit with maximum deposited energy on it. The detector is scanned by a probe to determine this maximally energetic unit. The selected module is used as a cluster.

b) 3×3 cluster. This cluster includes the maximally energetic unit that was found as it described above, and eight surrounding this unit modules.

c) 2×2 cluster. 2×2 cluster is allocated from the 9 modules. For doing this there are two algorithms. The first one describes in Technical Design Report ([4]). First we construct the 3x3 cluster as it described above. Then we determine the total energy by using the sum of an array of 2x2 trigger cells (i.e. 4x4 crystals). All possible combinations of the sums of 2x2 trigger cells will calculated. The maximally energetic solution will be chosen and its information (energy, time and position) will be sent to global trigger for decision. This is illustrated in Fig. 1. Since this algorithm

was proposed by Budker Institute of Nuclear Physics (Novosibirsk, Russia) further we will label one as BINP algorithm.

We propose an alternative algorithm of choice the 2x2 cluster. Below we use for this algorithm short name as IP algorithm

In the IP algorithm (see Fig. 2), it is compared the energy deposited in the upper-center (module 2) and bottom-center clusters (module 8) at first. If more energy is deposited in the bottom-central module, then we should compare the bottom-left (module 7) and the bottom-right (module 9) modules and choose maximally energetic unit. For example, it will be bottom-left. Thus, we can make the supposition that the particle hit in the bottom-left of crystal of central unit (red). So in this case as the cluster we take module 5, module 8, module 7 and module 4.

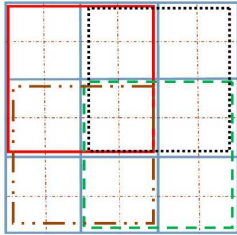


Figure 1: Crystal regions which are summed within the ECAL trigger for BINP algorithm. Illustration of the calculation of all possible combinations of the trigger cell and their summation areas.

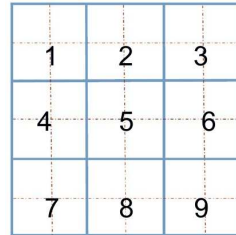


Figure 2: Crystal regions which are summed within the ECAL trigger for IP algorithm. Illustration of the calculation of all possible combinations of the trigger cell and their summation areas.

Each algorithm must be implemented for every event. For each cluster, we should determine the energy resolution and estimate deposit energy lost by the electron with a momentum of 105 MeV/c.

4 Monte-Carlo model of ECAL

The first step is creation of Monte-Carlo model of electron calorimeter using GEANT4. The ECAL is a 24×24 matrix composed of LYSO crystals with $20 \times 20 \times 120 \text{ mm}^3$. Simulated piece of calorimeter is a 1/4 part of the actual size of the ECAL. However, it is permissible for the simulation and allow to minimize amount of machine resources. It was set the main characteristics of crystals for creation of Monte-Carlo model of calorimeter,

such as the chemical composition of crystals, density, molecular density, physical condition, also their dimensions, number and location in the simulated calorimeter matrix. Each group of four crystals combined at the 2×2 unit that is wrapped with foil. The calorimeter is composed of these units and located in vacuum vessel. It is imposed a uniform magnetic field of 1 T in the space along the Oz axis. Also electronics noise in the model is taken into account as follows: in each crystal of calorimeter was added random noise that smeared by normal distribution with $\sigma_{noise} = 0.6$ MeV and average meaning of noise is zero.

The next step is setting of the source parameters. In the model is used a point isotropic source of mono-energetic electrons with the kinetic energy 104,49 MeV - that correspond to the momentum in 105 MeV/c. Electrons are emitted by the solid angle $\pm 20^\circ$. Solid angle selected in the way that to cover a large area of detector, but electrons should not hit at the extreme crystals. Distance between the source and the detector surface is 2.5 m along the axis Oz that corresponds to real distance between colimator and ECAL for COMET experiment. Implementation of the algorithm is described through the Monte-Carlo simulation of the ECAL in GEANT4 environment. Some results of modeling, comparison of results for all types of clusters and algorithms of their implementation is shown at section 5.

5 Results

First we found the distribution of total deposited energy for 105 MeV/c electron beam in trigger cells for 3x3 array using our Monte-Carlo model that described above. This is illustrated in Fig. 3. On Fig.4 the energy spectra for maximal energetic module (central module on Fig.3) is given

A trigger condition for COMET experiment would correspond to an energy deposition in the signal window $E_{min}(\sim 95 MeV) < E(\simeq 105 MeV) < E_{max}(\sim 115 MeV)$.

Thus it becomes clear that the single unit can not be used as a cluster because it does not meet to the stated requirements for the trigger condition.

Further we estimate a leak energy for different types of clusters depend on the solid angle. We considered three cases when electrons are emitted by the solid angle: $\pm 5^\circ$, $\pm 10^\circ$, $\pm 20^\circ$. Here the energy leak means the difference between the total deposited energy in the ECAL and the total deposited energy in array of 3x3 and 2x2 modules.

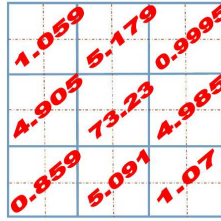


Figure 3: The distribution of total deposited energy for 3x3 cluster

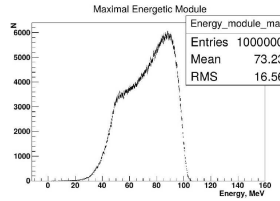


Figure 4: The energy spectra for maximal energetic module

From Fig.5 follows that IP algorithm looks more worse all. The answer is a very easy. This is due to the fact that the IP algorithm is not always correctly restore the crystal, which is hit by electron (see Fig.6).

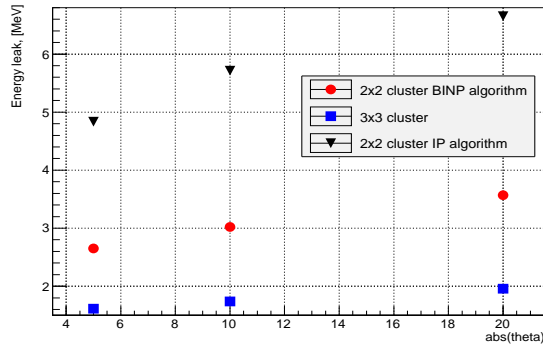


Figure 5: The leak energy for different types of clusters depend on solid angle.

Thus, we come to conclusion that the 2×2 cluster selected by IP algorithm isn't suitable as the cluster for ECAL trigger.

The next step is estimation the energy resolution by fitting Log-normal distribution for 3x3 cluster and 2x2 cluster selected by BINP algorithm and search for an optimal value of threshold energy that remove contribution of noise. Let us remember that in our Monte-Carlo model in each crystal of calorimeter was added random noise that smeared by normal distribution with $\sigma_{noise} = 0.6$ MeV and average meaning of noise is zero. In this way we simulate the electric noise that approximately expected in experiment. Thus, we add the threshold energy for trigger cell

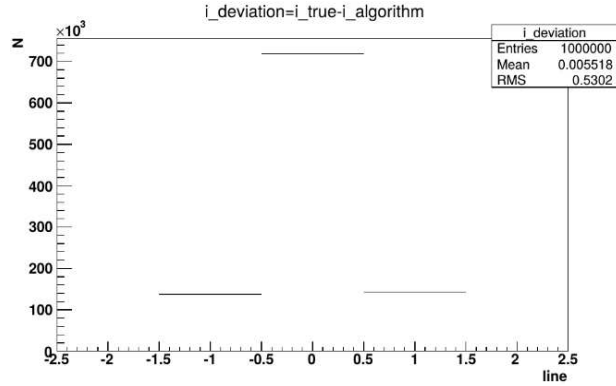


Figure 6: The difference between the true value of line for crystal which hit by electron and the reconstructing value of line.

in our model i.e we take into account events when total deposited energy in module larger than threshold. Since module consist of 4 crystals then $\sigma_{noise\ module} = \sqrt{4 \cdot \sigma_{noise\ crystal}^2} = \sqrt{4 \cdot 0.6^2} = 1.2\text{MeV}$.

We have plotted the dependence of energy resolution on threshold energy for trigger cell (see Fig.7). As it follows from Fig.7 that the optimal value for threshold energy is $E_{threshold} = 0.5\sigma_{noise\ module}$ for both types of clusters. Since in this case we have the best energy resolution of these clusters.

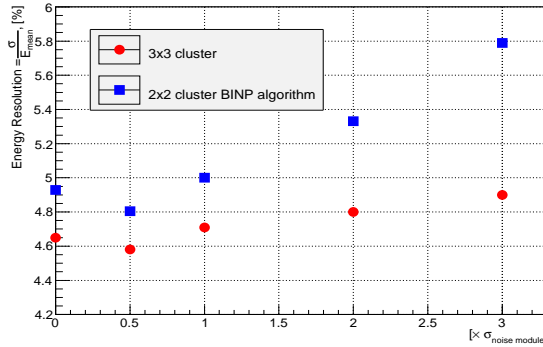


Figure 7: The dependence of energy resolution on threshold energy for module.

6 Conclusion

In this paper the simulation of an ECAL trigger algorithm for COMET experiment is performed. For this purpose we have created a simple Monte-Carlo model taking into account electronics noise using a GEANT4. We have shown that single module can't be used as a cluster for ECAL trigger due to does not meet to the stated requirements for the trigger condition. At the same time we have demonstrated that array of 3x3 modules and 2x2 cluster selected by BINP algorithm are suitable as the cluster for ECAL trigger. Also we studied the dependence of energy resolution on threshold energy for trigger cell. We found the optimal value for the threshold energy is $0.5\sigma_{moise\ module}$.

In the future we plan to divide the electronics noise in crystal into correlated and uncorrelated noise i.e. $\sigma_{moise\ crystal} = \sqrt{\sigma_{correlated}^2 + \sigma_{uncorrelated}^2}$, where $\sigma_{correlated}$ is a constant. Since we expect that impact of correlated noise on the choice of the cluster is significant.

References

- [1] G. Aad et al. (Atlas Collab.), Phys. Lett. B **716**, 1–29 (2012).
- [2] S. Chatrchyan et al. (CMS Collab.), Phys. Lett. B **716**, 30–61 (2012).
- [3] Yoshitaka Kuno on behalf of the COMET Collaboration, Prog. Theor. Exp. Phys. , 022C01 (43 pages) (2013).
- [4] COMET Collab., Technical Design Report http://comet.kek.jp/Documents_files/IPNS-Review-2014.pdf
- [5] W. Bertl et al. (SINDRUM-II Collaboration), Eur. Phys. J. C **47** 337-346 (2006)

2 Non-Accelerator Physics

Minimal Length in Quantum Theory and Gravity and Measurability

A.E.Shalyt-Margolin*

Institute for Nuclear Problems of Belarusian State University

Abstract

At the present time the majority of researchers agree that a minimal length is involved at high (Planck's) energies. But all the currently used low-energy theories (quantum mechanics and field theory, gravity, etc.) are continuous, i.e. the minimal length in them is zero. This paper presents an alternative approach when the minimal length is nonzero at all the energy scales. By this approach the definition of **measurability** and of **measurable quantities** is given. Further it is demonstrated that, provided a theory involves a minimal length, this theory must be free from such infinitesimal quantities as infinitely small variations in surface of the holographic screen, its volume, and entropy. The corresponding infinitesimal quantities in this case must be replaced by the «minimal variations possible» – finite quantities dependent on the existent energies. As a result, the initial low-energy theory (quantum theory or general relativity) inevitably must be replaced by a minimal-length theory that gives very close results but operates with absolutely other mathematical apparatus.

1 Introduction

One of the most important problems in modern fundamental physics is the problem of transition from low to high energies. Just this problem is basic for many others: divergence in a quantum field theory [1], nonrenormalisability of Einstein's gravitation theory for the standard transfer to its

*E-mail: a.shalyt@mail.ru; alexm@hep.by

quantization [2], and the like. In fact, this problem was at the root of such beautiful theories as string theory [3] and loop quantum gravity [4].

At the present time all high-energy generalizations (limits) of the basic «components» in fundamental physics (quantum theory [1] and gravity [5]) of necessity lead to a minimal length on the order of the Planck length $l_{min} \propto l_P$. This follows from a string theory [6]–[3], loop quantum gravity [4], and other approaches [9]–[17].

But it is clear that, provided a minimal length exists, it is existent at all the energy scales and not at high (Planck's) scales only.

What is inferred on this basis for real physics? At least, it is suggested that the use of infinitesimal quantities dx_μ in a mathematical apparatus of both quantum theory and gravity is incorrect, despite the fact that both these theories give the results correlating well with the experiment (for example, [18]).

Indeed, in all cases the infinitesimal quantities dx_μ bring about an infinitely small length ds [5]

$$ds^2 = g_{\mu\nu} dx_\mu dx_\nu \quad (1)$$

that is inexistent because of l_{min} .

The same is true for any function Υ dependent only on different parameters L_i whose dimensions of length of the exponents are equal to or greater than 1 $\nu_i \geq 1$

$$\Upsilon \equiv \Upsilon(L_i^{\nu_i}). \quad (2)$$

Obviously, the infinitely small variation $d\Upsilon$ of Υ is senseless as, according to (2), we have

$$d\Upsilon \equiv d\Upsilon(\nu_i L_i^{\nu_i-1} dL_i). \quad (3)$$

But, because of l_{min} , the infinitesimal quantities dL_i make no sense and hence $d\Upsilon$ makes no sense too.

Instead of these infinitesimal quantities, reasonable are «minimal variations possible» Δ_{min} of the quantity L having the dimension of length, i.e. the quantity

$$\Delta_{min} L = l_{min}. \quad (4)$$

And then

$$\Delta_{min} \Upsilon \equiv \Delta_{min} \Upsilon(\nu_i L_i^{\nu_i-1} \Delta_{min} L_i) = \Delta_{min} \Upsilon(\nu_i L_i^{\nu_i-1} l_{min}). \quad (5)$$

However, the «minimal variations possible» of any quantity having the dimensions of length (4) which are equal to $l_{min} \propto l_P$ require, according

to the Heisenberg Uncertainty Principle (HUP) [19], maximal momentum $p_{max} \propto P_{Pl}$ and energy $E_{max} \propto E_P$. Here l_P, P_{Pl}, E_P – Planck’s length, momentum, and energy, respectively.

But at low energies (far from the Planck energy) there are no such quantities and hence in essence $\Delta_{min}L = l_{min} \propto l_P$ (4) corresponds to the high-energy (Planck’s) case only.

For the energies lower than Planck’s energy, the «minimal variations possible» $\Delta_{min}L$ of the quantity L having the dimensions of length must be greater than l_{min} and dependent on the present E

$$\Delta_{min} \equiv \Delta_{min,E}, \Delta_{min,E}L > l_{min}. \quad (6)$$

Besides, as we have a minimal length unit l_{min} , it is clear that any quantity having the dimensions of length is «quantized», i.e. its value measured in the units l_{min} equals an integer number and we have

$$L = N_L l_{min}, \quad (7)$$

where N_L – positive integer number.

The problem is, how the «minimal variations possible» $\Delta_{min,E}$ (6) are dependent on the energy or, what is the same, on the scales of the measured lengths?

2 Minimal Length and Space-Time Quantum Fluctuations

To solve the above-mentioned problem, **initially** we can use the Space-Time Quantum Fluctuations (STQF) with regard to quantum theory and gravity. The definition of STQF is closely associated with the notion of «space-time foam». The notion «space-time foam», introduced by J. A. Wheeler about 60 years ago for the description and investigation of physics at Planck’s scales (Early Universe) [21],[22], is fairly settled. Despite the fact that in the last decade numerous works have been devoted to physics at Planck’s scales within the scope of this notion, for example [23]–[42], by this time still their no clear understanding of the «space-time foam» as it is.

On the other hand, it is undoubtful that a quantum theory of the Early Universe should be a deformation of the well-known quantum theory.

In my works with the colleagues [43]–[52] I has put forward one of the possible approaches to resolution of a quantum theory at Planck’s scales on the basis of the density matrix deformation.

In accordance with the modern concepts, the space-time foam [22] notion forms the basis for space-time at Planck’s scales (Big Bang). This object is associated with the quantum fluctuations generated by uncertainties in measurements of the fundamental quantities, inducing uncertainties in any distance measurement. A precise description of the space-time foam is still lacking along with an adequate quantum gravity theory. But for the description of quantum fluctuations we have a number of interesting methods (for example, [53],[32]–[42]).

In what follows, we use the terms and symbols from [34]. Then for the fluctuations $\tilde{\delta}l$ of the distance l we have the following estimate:

$$(\tilde{\delta}l)_\gamma \gtrsim l_P^\gamma l^{1-\gamma} = l_P \left(\frac{l}{l_P}\right)^{1-\gamma} = l \left(\frac{l_P}{l}\right)^\gamma = l \lambda_l^\gamma, \quad (8)$$

or that same

$$|(\tilde{\delta}l)_\gamma|_{min} = \beta l_P^\gamma l^{1-\gamma} = \beta l_P \left(\frac{l}{l_P}\right)^{1-\gamma} = \beta l \lambda_l^\gamma, \quad (9)$$

where $0 < \gamma \leq 1$, coefficient β is of order 1 and $\lambda_l \equiv l_P/l$.

From (8),(9), we can derive the quantum fluctuations for all the primary characteristics, specifically for the time $(\tilde{\delta}t)_\gamma$, energy $(\tilde{\delta}E)_\gamma$, and metrics $(\tilde{\delta}g_{\mu\nu})_\gamma$. In particular, for $(\tilde{\delta}g_{\mu\nu})_\gamma$ we can use formula (10) in [34]

$$(\tilde{\delta}g_{\mu\nu})_\gamma \gtrsim \lambda_l^\gamma. \quad (10)$$

Further in the text is assumed that the theory involves a minimal length on the order of Planck’s length

$$l_{min} \propto l_P$$

or that is the same

$$l_{min} = \xi l_P, \quad (11)$$

where the coefficient ξ is on the order of unity too.

In this case it is unimportant which is the origin of this minimal length. For simplicity, we assume that it comes from the Generalized Uncertainty

Principle (GUP) that is an extension of HUP for Planck's energies, where gravity must be taken into consideration [6]–[17]:

$$\Delta x \geq \frac{\hbar}{\Delta p} + \alpha' l_P^2 \frac{\Delta p}{\hbar}. \quad (12)$$

Here α' is the model-dependent dimensionless numerical factor.

The equation (12) leads to the minimal length $l_{min} = \xi l_P = 2\sqrt{\alpha'} l_P$. Therefore, in this case replacement of Planck's length by the minimal length in all the above formulae is absolutely correct and is used without detriment to the generality [20]

$$l_P \rightarrow l_{min}. \quad (13)$$

Thus, $\lambda_l \equiv l_{min}/l$ and then (8)–(10) upon the replacement (13) are read unchanged.

And (9) may be written as

$$|(\tilde{\delta}l)_\gamma|_{min} = \beta l \lambda_l^\gamma = \beta N_l (N_l^{-\gamma}) = \beta N_l^{1-\gamma} l_{min}. \quad (14)$$

Here one should take into account the following consideration: due to the (Integrality Condition) (7) in the right-hand side of (14) for the factor $\beta N_l^{1-\gamma}$ before l_{min} its integer part is always meant

$$\beta N_l^{1-\gamma} \mapsto [\beta N_l^{1-\gamma}] \quad (15)$$

and this goes without special mentioning for the whole text.

As noted in the overview [34], the value $\gamma = 2/3$ derived in [53] is totally consistent with the Holographic Principle [54]–[56].

The following points of importance should be noted [20]:

2.1. It is clear that **at Planck's scales, i.e. at the minimal length scales**

$$l \rightarrow l_{min} \quad (16)$$

models for different values of the parameter γ are coincident.

2.2. As noted, specifically in (7), **provided some quantity has a minimal measuring unit, values of this quantity are multiples of this unit.** Naturally, any quantity having a minimal measuring unit is uniformly discrete. The latter property is not met, in particular, by the energy E .

As $E \sim 1/l$, where l – measurable scale, **the energy E is a discrete quantity but the nonuniformly discrete one**. It is clear that the difference between the adjacent values of E is the less the lower E . In other words, for $l \gg l_{min}$ i.e.

$$E \ll E_P \quad (17)$$

E becomes a practically continuous quantity.

2.3. In fact, the parameter λ_l was introduced earlier in papers [43]–[52] as a deformation parameter on going from the canonical quantum mechanics to the quantum mechanics at Planck’s scales (early Universe) that is considered to be the quantum mechanics with the fundamental length (QMFL):

$$0 < \alpha_x = l_{min}^2/x^2 \leq 1/4, \quad (18)$$

where x is the measuring scale, $l_{min} \sim l_p$.

The deformation is understood as an extension of a particular theory by inclusion of one or several additional parameters in such a way that the initial theory appears in the limiting transition[57].

Obviously, everywhere, apart from the limiting point $\lambda_x = 1$ or $x = l_{min}$, we have

$$\lambda_x = \sqrt{\alpha_x}, \quad (19)$$

From (18) it is seen that at the limiting point $x = l_{min}$ the parameter α_x is not defined due to the appearance of singularity [43]–[52]. But at this point its definition may be extended (regularized).

The parameter α_l has the following clear physical meaning:

$$\alpha_l^{-1} \sim S^{BH}, \quad (20)$$

where

$$S^{BH} = \frac{A}{4l_p^2} \quad (21)$$

is the well-known Bekenstein-Hawking formula for the black hole entropy in the semiclassical approximation [58],[59] for the black-hole event horizon surface A , with the characteristics linear dimension («radius») $R = l$. This is especially obvious in the spherically-symmetric case.

In what follows we use both parameters: λ_x and α_x .

Turning back to the introductory section of this work and to the definition $\Delta_{min,E}L$, we assume the following:

$$|\Delta_{min,E}L| = |(\tilde{\delta}L)_\gamma|_{min}, \quad (22)$$

where $|(\tilde{\delta}L)_\gamma|_{min}$ is from formula (9), γ – fixed parameter from formulae (8), (9), and $E = c\hbar/L$.

In physics, and in thermodynamics in particular, the *extensive quantities or parameters* are those proportional to the mass of a system or to its volume. Proceeding from the definition (2) of the function $\Upsilon(L_i^{\nu_i})$, one can generalize this notion, taking as a **Generalized Extensive Quantity (GEQ)** of some spatial system Ω the function dependent only on the linear dimensions of this system, with the exponents no less than 1.

The function $\Upsilon(L_i^{\nu_i}), \nu_i \geq 1$ (2) is **GEQ** of the system Ω with the characteristic linear dimensions $L_i; i = 1, \dots, n$ or, identically, a sum of the systems $\Omega_i; i = 1, \dots, n$, each of which has its individual characteristic linear dimension L_i .

Then from the initial formulae (2)–(6) it directly follows that, provided the minimal length l_{min} is existent, **there are no** infinitesimal variations of GEQ.

In the first place, this is true for such simplest objects as the n -dimensional sphere $B_n, n \geq 2$, whose surface area (area of the corresponding hypersphere S_n) and volume V_n represent GEQs and are equal to the following:

$$S_n = nC_n R^{n-1}; V_n = C_n R^n, \quad (23)$$

where R – radius of a sphere the length of which is a characteristic linear dimension, $C_n = \pi^{n/2}/\Gamma(\frac{n}{2} + 1)$, and $\Gamma(x)$ is a gamma-function.

Of course, the same is true for the n -dimensional cube (or hypercube) A_n ; its surface area and its volume are GEQs, and a length of its edge is a characteristic linear dimension.

Provided l_{min} exists, there are no infinitesimal increments for both the surface area and volume of A_n or B_n ; only minimal variations possible for these quantities are the case.

In what follows we consider only the spatial systems whose surface areas and volumes are GEQs.

Definition 1.

1. Let us define the quantity having the dimensions of length L **measurable**, when it satisfies the relation (7).

2. Let us define any physical quantity **measurable**, when its value is consistent with point 1 of this Definition.

3 One Important Example of Gravity.

Let us consider a simple but very important example of gravity in horizon spaces.

Gravity and thermodynamics of horizon spaces and their interrelations are currently most actively studied [60]–[72]. Let us consider a relatively simple illustration – the case of a static spherically-symmetric horizon in space-time, the horizon being described by the metric

$$ds^2 = -f(r)c^2 dt^2 + f^{-1}(r)dr^2 + r^2 d\Omega^2. \quad (24)$$

The horizon location will be given by a simple zero of the function $f(r)$, at the radius $r = a$.

This case is studied in detail by T.Padmanabhan in his works [60, 71] and by the author of this paper in [73]. We use the notation system of [71]. Let, for simplicity, the space be denoted as \mathcal{H} .

It is known that for horizon spaces one can introduce the temperature that can be identified with an analytic continuation to imaginary time. In the case under consideration ([71], eq.(116))

$$k_B T = \frac{\hbar c f'(a)}{4\pi}. \quad (25)$$

Therewith, the condition $f(a) = 0$ and $f'(a) \neq 0$ must be fulfilled.

Then at the horizon $r = a$ Einstein's field equations

$$\frac{c^4}{G} \left[\frac{1}{2} f'(a) a - \frac{1}{2} \right] = 4\pi P a^2 \quad (26)$$

where $P = T_r^r$ is the trace of the momentum-energy tensor and radial pressure.

Now we proceed to the variables « α » from the formula (18) to consider (26) in a new notation, expressing a in terms of the corresponding deformation parameter α . In what follows we omit the subscript in formula (18) of α_x , where the context implies which index is the case. In particular, here we use α instead of α_a . Then we have

$$a = l_{min} \alpha^{-1/2}. \quad (27)$$

Therefore,

$$f'(a) = -2l_{min}^{-1}\alpha^{3/2}f'(\alpha). \quad (28)$$

Substituting this into (26) we obtain in the considered case of Einstein's equations in the « α -representation» the following [73]:

$$\frac{c^4}{G}(-\alpha f'(\alpha) - \frac{1}{2}) = 4\pi P\alpha^{-1}l_{min}^2. \quad (29)$$

Multiplying the left- and right-hand sides of the last equation by α , we get

$$\frac{c^4}{G}(-f'(\alpha)\alpha^2 - \frac{1}{2}\alpha) = 4\pi Pl_{min}^2. \quad (30)$$

L.h.s. of (30) is dependent on α . Because of this, r.h.s. of (30) must be dependent on α as well, i. e. $P = P(\alpha)$, i.e

$$\frac{c^4}{G}(-f'(\alpha)\alpha^2 - \frac{1}{2}\alpha) = 4\pi P(\alpha)l_{min}^2. \quad (31)$$

Note that in this specific case the parameter α within constant factors is coincident with the Gaussian curvature K_a [74] corresponding to a :

$$\frac{l_{min}^2}{a^2} = l_{min}^2 K_a. \quad (32)$$

Substituting r.h.s of (32) into (31), we obtain the Einstein equation on horizon, in this case in terms of the Gaussian curvature

$$\frac{c^4}{G}(-f'(K_a)K_a^2 - \frac{1}{2}K_a) = 4\pi P(K_a). \quad (33)$$

This means that up to the constants

$$-f'(K_a)K_a^2 - \frac{1}{2}K_a = P(K_a), \quad (34)$$

i.e. the Gaussian curvature K_a is a solution of Einstein equations in this case. Then we examine different cases of the solution (34) with due regard for considerations of formula (22).

3.1. First, let us assume that $a \gg l_{min}$. As, according (7), the radius a is quantized, we have $a = N_a l_{min}$ with the natural number $N_a \gg 1$. Then it is clear that the Gaussian curvature $K_a = 1/a^2 \approx 0$ takes a (nonuniform)

discrete series of values close to zero, and, within the factor $1/l_{min}^2$, this series represents inverse squares of natural numbers

$$(K_a) = \left(\frac{1}{N_a^2}, \frac{1}{(N_a \pm 1)^2}, \frac{1}{(N_a \pm 2)^2}, \dots \right). \quad (35)$$

Let us return to formulas (9),(22) for $l = a$

$$|((\tilde{\delta}a)_\gamma)_{min}| = \beta N_a l_{min} N_a^{-\gamma} = \beta N_a^{1-\gamma} l_{min}, \quad (36)$$

where β in this case contains the proportionality factor that relates l_{min} and l_P .

Then, according to (22), $a_{\pm 1}$ is a measurable value of the radius r following after a , and we have

$$(a_{\pm 1})_\gamma \equiv a \pm ((\tilde{\delta}a)_\gamma)_{min} = a \pm \beta N_a^{1-\gamma} l_{min} = N_a (1 \pm \beta N_a^{-\gamma}) l_{min}. \quad (37)$$

But, as $N_a \gg 1$, for sufficiently large N_a and fixed γ , the bracketed expression in r.h.s. (37) is close to 1:

$$1 \pm \beta N_a^{-\gamma} \approx 1. \quad (38)$$

Obviously, we get

$$\lim_{N_a \rightarrow \infty} (1 \pm \beta N_a^{-\gamma}) \rightarrow 1. \quad (39)$$

As a result, the Gaussian curvature $K_{a_{\pm 1}}$ corresponding to $r = a_{\pm 1}$

$$K_{a_{\pm 1}} = 1/a_{\pm 1}^2 \propto \frac{1}{N_a^2 (1 \pm \beta N_a^{-\gamma})^2} \quad (40)$$

in the case under study is only slightly different from K_a .

And this is the case for sufficiently large values of N_a , for any value of the parameter γ , for $\gamma = 1$ as well, corresponding to the absolute minimum of fluctuations $\approx l_{min}$, or more precisely – to βl_{min} . However, as all the quantities of the length dimension are quantized and the factor β is on the order of 1, actually we have $\beta = 1$.

Because of this, provided the minimal length is involved, l_{min} (9) is read as

$$|(\tilde{\delta}l)_1|_{min} = l_{min}. \quad (41)$$

But, according to (11), $l_{min} = \xi l_P$ is on the order of Planck's length, and it is clear that the fluctuation $|(\tilde{\delta}l)_1|_{min}$ corresponds to Planck's energies

and Planck's scales. The Gaussian curvature K_a , due to its smallness ($K_a \ll 1$ up to the constant factor l_{min}^{-2}) and smooth variations independent of γ (formulas (37)–(40)), is **insensitive** to the differences between various values of γ .

Consequently, for sufficiently small Gaussian curvature K_a we can take any parameter from the interval $0 < \gamma \leq 1$ as γ .

It is obvious that the case $\gamma = 1$, i. e. $|(\tilde{\delta}l)_1|_{min} = l_{min}$, is associated with infinitely small variations da of the radius $r = a$ in the Riemannian geometry.

Since then K_a is varying practically continuously, in terms of K_a up to the constant factor we can obtain the following:

$$d[L(K_a)] = d[P(K_a)], \quad (42)$$

Where have

$$L(K_a) = -f'(K_a)K_a^2 - \frac{1}{2}K_a, \quad (43)$$

i. e. l.h.s of (33) (or (34)).

But in fact, as in this case the energies are low, it is more correct to consider

$$L((K_{a\pm 1})_\gamma) - L(K_a) = [P(K_{a\pm 1})_\gamma] - [P(K_a)] \equiv F_\gamma[P(K_a)], \quad (44)$$

where $\gamma < 1$, rather than (42).

In view of the foregoing arguments 3.1, the difference between (44) and (42) is insignificant and it is perfectly correct to use (42) instead of (44).

3.2. Now we consider the opposite case or the transition to the **ultra-violet limit**

$$a \rightarrow l_{min} = \kappa l_{min}, \quad (45)$$

i.e.

$$a = \kappa l_{min}. \quad (46)$$

Here κ is on the order of 1.

Taking into consideration point 1.1) stating that in this case models for different values of the parameter γ are coincident, by formula (41) for any γ we have

$$|(\tilde{\delta}l)_\gamma|_{min} = (\tilde{\delta}l)_1|_{min} = l_{min}. \quad (47)$$

But in this case the Gaussian curvature K_a is not a «small value» continuously dependent on a , taking, according to (40), a discrete series of values $K_a, K_{a\pm 1}, K_{a\pm 2}, \dots$

Yet (26), similar to (33) ((34)), is valid in the semiclassical approximation only, i.e. at **low energies**.

Then in accordance with the above arguments, the limiting transition to **high energies** (45) gives a discrete chain of equations or a single equation with a discrete set of solutions as follows:

$$-f'(K_a)K_a^2 - \frac{1}{2}K_a = \Theta(K_a);$$

$$-f'(K_{a\pm 1})K_{a\pm 1}^2 - \frac{1}{2}K_{a\pm 1} = \Theta(K_{a\pm 1});$$

and so on. Here $\Theta(K_a)$ – some function that in the limiting transition to low energies must reproduce the low-energy result to a high degree of accuracy, i.e. $P(K_a)$ appears for $a \gg l_{min}$ from formula (34)

$$\lim_{K_a \rightarrow 0} \Theta(K_a) = P(K_a). \quad (48)$$

In general, $\Theta(K_a)$ may lack coincidence with the high-energy limit of the momentum-energy tensor trace (if any):

$$\lim_{a \rightarrow l_{min}} P(K_a). \quad (49)$$

At the same time, when we naturally assume that the Static Spherically-Symmetric Horizon Space-Time with the radius of several Planck's units (46) is nothing else but a micro black hole, then the high-energy limit (49) is existing and the replacement of $\Theta(K_a)$ by $P(K_a)$ in r.h.s. of the foregoing equations is possible to give a hypothetical gravitational equation for the event horizon micro black hole. But a question arises, for which values of the parameter a (46) (or K_a) this is valid and what is a minimal value of the parameter $\gamma = \gamma(a)$ in this case.

In all the cases under study, 3.1) and 3.2), the deformation parameter α_a (18) (λ_a (19)) is, within the constant factor, coincident with the Gaussian curvature K_a (respectively $\sqrt{K_a}$) that is in essence continuous in the low-energy case and discrete in the high-energy case.

In this way the above-mentioned example shows that, despite the absence of infinitesimal spatial-temporal increments owing to the existence of l_{min} and the essential «discreteness» of a theory, this discreteness at low energies is not «felt», the theory being actually continuous. The indicated discreteness is significant only in the case of high (Planck's) energies.

In [71] it is shown that the Einstein Equation for horizon spaces in the differential form may be written as a thermodynamic identity (the first principle of thermodynamics) ([71], formula (119)):

$$\underbrace{\frac{\hbar c f'(a)}{4\pi}}_{k_B T} \underbrace{\frac{c^3}{G\hbar} d\left(\frac{1}{4}4\pi a^2\right)}_{dS} - \underbrace{\frac{1}{2} \frac{c^4 da}{G}}_{-dE} = \underbrace{Pd\left(\frac{4\pi}{3}a^3\right)}_{P dV}. \quad (50)$$

where, as noted above, T – temperature of the horizon surface, S – corresponding entropy, E – internal energy, V – space volume.

Note that, because of the existing l_{min} , practically all quantities in (50) (except of T) represent GEQ. Apparently, the radius of a sphere $r = a$, its volume V , and entropy represent such quantities:

$$S = \frac{4\pi a^2}{4l_P^2} = \frac{\pi a^2}{l_P^2}, \quad (51)$$

within the constant factor $1/4l_P^2$ equal to a sphere with the radius a .

Because of this, there are no infinitesimal increments of these quantities, i.e. da, dV, dS . And, provided l_{min} is involved, the Einstein equation for the above-mentioned case in the differential form (50) makes no sense and is useless. If da may be, purely formally, replaced by l_{min} , then, as the quantity l_{min} is fixed, it is obvious that $\langle\langle dS \rangle\rangle$ and $\langle\langle dV \rangle\rangle$ in (50) will be growing as a and a^2 , respectively. And at low energies, i.e. for large values of $a \gg l_{min}$, this naturally leads to infinitely large rather than infinitesimal values.

In a similar way it is easily seen that the «Entropic Approach to Gravity» [75] in the present formalism is invalid within the scope of the minimal length theory. In fact, the «main instrument» in [75] is a formula for the infinitesimal variation dN in the bit numbers N on the holographic screen \mathcal{S} with the radius R and with the surface area A ([75], formula (4.18)):

$$dN = \frac{c^3}{G\hbar} dA = \frac{dA}{l_P^2}. \quad (52)$$

As $N = A/l_P^2$, and A represents GEQ, it is clear that N is also GEQ and hence neither dA nor dN makes sense.

It is obvious that infinitesimal variations of the screen surface area dA are possible only in a continuous theory involving no l_{min} .

When $l_{min} \propto l_P$ is involved, the minimal variation ΔA is evidently associated with a minimal variation in the radius R

$$R \rightarrow R \pm l_{min} \quad (53)$$

is dependent on R and growing with $\sim R$ for $R \gg l_{min}$

$$\Delta_{\pm} A(R) = A(R \pm l_{min}) - A(R) \propto \left(\frac{\pm 2R}{l_{min}} + 1\right) = \pm 2N_R + 1, \quad (54)$$

where $N_R = R/l_{min}$, as indicated above.

But, as noted above, a minimal increment of the radius R equal to $|\Delta_{min} R| = l_{min} \propto l_P$ corresponds only to the case of maximal (Planck's) energies or, what is the same, to the parameter $\gamma = 1$ in formula (22). However, in [75] the considered low energies are far from the Planck energies and hence in this case in (22) $\gamma < 1$, (53), and (54) are respectively replaced by

$$R \rightarrow R \pm N_R^{1-\gamma} l_{min} \quad (55)$$

and

$$\Delta_{\pm} A(R) = A(R \pm N_R^{1-\gamma} l_{min}) - A(R) \propto \pm N_R^{2-\gamma} + N_R^{2-2\gamma} = N_R^{2-2\gamma} (\pm N_R^{\gamma} + 1). \quad (56)$$

An increase of r.h.s in(56) with the growth of R (or identically of N_R) for $R \gg l_{min}$ is obvious.

So, if l_{min} is involved, formula (4.18) from [75] makes no sense similar to other formulae derived on its basis (4.19),(4.20),(4.22),(5.32)–(5.34), ... in [75] and similar to the derivation method for Einstein's equations proposed in this work.

Proceeding from the principal parameters of this work α_l (or λ_l), the fact is obvious and is supported by the formula (20) given in this paper, meaning that

$$\alpha_R^{-1} \sim A, \quad (57)$$

i.e. small variations of α_R (low energies) result in large variations of α_R^{-1} , as indicated by formula (54).

In fact, we have a **no-go theorems**.

4 Conclusion.

The last statements concerning dS, dN may be explicitly interpreted using the language of a quantum information theory as follows:

due to the existence of the minimal length l_{min} , the minimal area l_{min}^2 and volume l_{min}^3 are also involved, and that means «quantization» of the areas and volumes. As, up to the known constants, the «bit number» N from (52) and the entropy S from (51) are nothing else but

$$S = \frac{A}{4l_{min}^2}, N = \frac{A}{l_{min}^2}. \quad (58)$$

It is obvious that there is a «minimal measure» for the «amount of data» that may be referred to as «one bit» (or «one qubit»).

The statement that there is no such quantity as dN (and respectively dS) is equivalent to claiming the absence of 0,25 bit, 0,001 bit, and so on.

This inference completely conforms to the Hooft-Susskind Holographic Principle (HP) [54]–[56] that includes two main statements:

(a) All information contained in a particular spatial domain is concentrated at the boundary of this domain.

(b) A theory for the boundary of the spatial domain under study should contain maximally one degree of freedom per Planck's area l_P^2 .

In fact (but not explicitly) HP implicates the existence of $l_{min} = l_P$. The existence of $l_{min} \propto l_P$ totally conforms to HP, providing its generalization. Specifically, without the loss of generality, l_P^2 in point (b) may be replaced by l_{min}^2 .

So, the principal inference of this work is as follows: provided the minimal length l_{min} is involved, its existence must be taken into consideration not only at high but also at low energies, both in a quantum theory and in gravity. This becomes apparent by rejection of the infinitesimal quantities associated with the spatial-temporal variations dx_μ, \dots . In other words, with the involvement of l_{min} , the General Relativity (GR) must be replaced by a (still unframed) minimal-length gravitation theory that may be denoted as $Grav^{l_{min}}$. In their results GR and $Grav^{l_{min}}$ should be very close but, as regards their mathematical apparatus (instruments), these theories are absolutely different.

Besides, $Grav^{l_{min}}$ should offer a rather natural transition from high to low energies

$$[N_L \approx 1] \rightarrow [N_L \gg 1] \quad (59)$$

and vice versa

$$[N_L \gg 1] \rightarrow [N_L \approx 1], \quad (60)$$

where N_L – integer from formula (7) determining the characteristics scale of the lengths L (energies $E \sim 1/L \propto 1/N_L$).

It should be noted that in case $Grav^{lmin}$ the cosmological term Λ is no longer a constant $\Lambda \neq const$, (and the Bianchi identity $\nabla^\mu G_{\mu\nu} \approx 0$ [5] will appear to a high degree of accuracy only in the low-energy limit), this term is dependent on $\alpha_l(\lambda_l)$ and we have [51],[73] with the known quantum field theory

$$\Lambda(\alpha) \propto (\alpha^2 + \eta_1 \alpha^2 + \dots) \Lambda_p, \quad (61)$$

and, provided the holographic principle is valid, we get [54]–[56]

$$\Lambda^{Hol}(\alpha) \propto (\alpha + \xi_1 \alpha^2 + \dots) \Lambda_p, \quad (62)$$

where Λ_p –cosmological term at Planck’s scales.

References

- [1] M.E. Peskin, D.V. Schroeder, *An Introduction to Quantum Field Theory*, Addison-Wesley Publishing Company, 1995.
- [2] S. Weinberg, *Ultraviolet divergencies in quantum theories of gravity*, in ed. S. Hawking and W. Israel, *General Relativity*, Cambridge University Press, Cambridge, 1980.
- [3] J. Polchinski, *String Theory*, Vol. I,II, Cambridge University Press, 1998.
- [4] C. Rovelli, Loop quantum gravity: the first twenty five years *Classical and Quantum Gravity* **2011**, *28*, 153002.
- [5] R.M. Wald, *General Relativity*, The University Chicago Press Chicago and London, 1984.
- [6] G.A. Veneziano, *Europhys.Lett.* **2** (1986) 199.
- [7] D. Amati, M. Ciafaloni, G.A. Veneziano, *Phys.Lett.B.* **216** (1989) 41.
- [8] E. Witten, *Phys.Today.* **49** (1996) 24.
- [9] G. Amelino-Camelia, *Living Rev.Rel.* **16** (2013) 5.
- [10] G. Amelino-Camelia, L. Smolin, *Phys.Rev.D.* **80** (2009) 084017; G. Gubitosi et al, *JCAP.* **0908**, (2009), 021; G. Amelino-Camelia, *Int.J.Mod.Phys.D.* **14**, (2005) 2167.

- [11] S. Hossenfelder, Phys. Lett. B. **575** (2003) 85; S. Hossenfelder, Phys. Rev. D. **70** (2004) 105003; S. Hossenfelder, Class. Quant. Grav. **23** (2006) 1815.
- [12] S. Hossenfelder, Living Rev.Rel. **16** (2013) 2.
- [13] R.J. Adler, D.I. Santiago, Mod. Phys. Lett. A. **14** (1999) 1371.
- [14] D.V. Ahluwalia, Phys.Lett. **A275** (2000) 31.
- [15] D.V. Ahluwalia, Mod.Phys.Lett. **A17** (2002) 1135.
- [16] M. Maggiore, Phys.Lett. B. **319** (1993) 83.
- [17] A. Kempf, G. Mangano and R.B. Mann, Phys.Rev.D. **52** (1995) 1108.
- [18] R. Penrose, *Quantum Theory and Space-Time*, Fourth Lecture in *Stephen Hawking and Roger Penrose, The Nature of Space and Time*, Prinseton University Press, 1996.
- [19] W. Heisenberg, Zeitschrift fur Physik. **43** (1927) 172. English translation: J.A. Wheeler and H. Zurek, *Quantum Theory and Measurement* Princeton Univ. Press, 1983, pp. 62-84.
- [20] A.E. Shalyt-Margolin, *Nonlinear Phenomena in Complex Systems*, **17** (2014) No 2, 138.
- [21] J.A. Wheeler, *Geometrodynamics* (Academic Press, New York and London, 1962).
- [22] C.W. Misner, K.S. Thorne, and J.A. Wheeler, *Gravitation*, Freeman, San Francisco, (1973).
- [23] R. Garattini, Int. J. Mod. Phys. D. **4** (2002) 635.
- [24] R. Garattini, Entropy. **2** (2000) 26.
- [25] R. Garattini, Nucl.Phys.Proc.Suppl. **88** (2000) 297.
- [26] R. Garattini, Phys.Lett.B. **459** (1999) 461.
- [27] F. Scardigli, Class.Quant.Grav. **14** (1997) 1781.
- [28] F. Scardigli, Phys.Lett.B. **452** (1999) 39.

- [29] F. Scardigli, Nucl.Phys.Proc.Suppl. **88** (2000) 291.
- [30] L.J. Garay, Phys.Rev. D. **58** (1998) 124015.
- [31] L.J. Garay, Phys.Rev.Lett. **80** (1998) 2508.
- [32] Y.J. Ng, H. van Dam, Found. Phys. **30** (2000) 795.
- [33] Y.J. Ng, Int. J. Mod. Phys. D. **11** (2002) 1585.
- [34] Y.J. Ng, Mod.Phys.Lett.A. **18** (2003) 1073
- [35] Y.J. Ng, gr-qc/0401015.
- [36] Y.J. Ng, H. van Dam, Int.J.Mod.Phys.A. **20** (2005) 1328.
- [37] W.A. Christiansen, Y.J. Ng and H. van Dam, Phys.Rev.Lett. **96** (2006) 051301.
- [38] Y.J. Ng, Phys.Lett.B. **657** (2007) 10.
- [39] Y.J. Ng, AIP Conf.Proc. **1115** (2009) 74.
- [40] A.W. Christiansen, D.J.E. Floyd, Y.J. Ng, E.S. Perlman, Phys.Rev.D. **83** (2011) 084003.
- [41] G. Amelino-Camelia, Nature. **398** (1999) 216.
- [42] L. Diosi and B. Lukacs, Phys. Lett. **A142** (1989) 331.
- [43] A.E. Shalyt-Margolin and J.G. Suarez, gr-qc/0302119.
- [44] A.E. Shalyt-Margolin and J.G. Suarez, Intern. Journ. Mod. Phys. D. **12** (2003) 1265.
- [45] A.E. Shalyt-Margolin and A.Ya. Tregubovich, Mod. Phys.Lett. A. **19** (2004) 71.
- [46] A.E. Shalyt-Margolin, Mod. Phys. Lett. A. **19** (2004) 391.
- [47] A.E. Shalyt-Margolin, Mod. Phys. Lett. A. **19** (2004) 2037.
- [48] A.E. Shalyt-Margolin, Intern. Journ. Mod.Phys. D. **13** (2004) 853.
- [49] A.E. Shalyt-Margolin, Intern.Journ.Mod.Phys.A. **20** (2005) 4951.

- [50] A.E. Shalyt-Margolin, V.I. Strazhev, *Proc. Sixth International Symposium «Frontiers of Fundamental and Computational Physics»*, ed. B.G. Sidharth, Springer (2006) P. 131.
- [51] A.E. Shalyt-Margolin, *Entropy*. **12** (2010) 932.
- [52] A.E. Shalyt-Margolin, *Quantum Cosmology Research Trends*, ed. A. Reimer, *Horizons in World Physics*. **246**, Nova Science Publishers, Inc., Hauppauge, NY, (2005) P. 49.
- [53] E.P. Wigner, *Rev. Mod. Phys.* **29** (1957) 255; H. Salecker and E.P. Wigner, *Phys. Rev.* **109**, 571 (1958).
- [54] G. 't Hooft Dimensional reduction in quantum gravity. Essay dedicated to Abdus Salam *gr-qc/9310026*.
- [55] G. 't Hooft, The Holographic Principle, *hep-th/0003004*; L. Susskind, The World as a hologram. *J. Math. Phys* **1995**, *36*, 6377.
- [56] R. Bousso, *Rev. Mod. Phys* **2002**, *74*, 825.
- [57] L. Faddeev, *Priroda*. **5** (1989) 11.
- [58] J.D. Bekenstein, *Phys.Rev.D.* **7** (1973) 2333.
- [59] S. Hawking, *Phys.Rev.D.* **13** (1976) 191.
- [60] T. Padmanabhan, *Class.Quant.Grav.* **19** (2002) 5387.
- [61] T. Padmanabhan, *Int.Jorn.Mod.Phys.* **D14** (2005) 2263.
- [62] T. Padmanabhan, *Gen.Rel.Grav.* **34** (2002) 2029.
- [63] T. Padmanabhan, *Braz.J.Phys.* **35** (2005) 362.
- [64] T. Padmanabhan, *Int.J.Mod.Phys.D.* **15** (2006) 1659.
- [65] G. Mukhopadhyay, T. Padmanabhan, *Phys.Rev.D.* **74** (2006).
- [66] T. Padmanabhan, *Gen.Rel.Grav.* **40** (2008) 529.
- [67] T. Padmanabhan, A. Paranjape, *Phys.Rev.D.* **75** (2007) 064004.
- [68] T. Padmanabhan, *AIP Conference Proceedings*. **939** (2007) 114.

- [69] T. Padmanabhan, Phys.Rept. **406** (2005) 49.
- [70] A. Paranjape, S. Sarkar and T. Padmanabhan, S Phys.Rev.D. **74** (2006) 104015.
- [71] T. Padmanabhan, Rep. Prog. Phys. **74** (2010) 046901.
- [72] T. Padmanabhan, Mod.Phys.Lett.A. **25** (2010) 1129.
- [73] A.E. Shalyt-Margolin, Intern. J. Mod. Phys. D. **21** (2012) 1250013.
- [74] S. Kobayashi, K. Nomozu, *Foundations of Differential Geometry*, V.II, Interscience Publishers, 1969.
- [75] E. Verlinde, On the Origin of Gravity and the Laws of Newton, JHEP. **1104** (2011) 029.

Evolution of Entangled States in QCD Vacuum

Kuvshinov V.I.*, Bagashov E.G.

*Joint Institute for Power and Nuclear Research - Sosny,
National Academy of Sciences of Belarus*

Abstract

The interaction of single- and multiparticle quark states with QCD stochastic vacuum is considered. On the basis of the acquired results the implications for quark confinement are being made.

In multiparticle case the behaviour of entangled states is described. It is shown that the interaction with stochastic vacuum in the confinement region leads to fully mixed states and decoherence, i.e. the entanglement vanishes.

For all of the considered states purity, fidelity and von Neumann entropy are evaluated.

1 Introduction

The model of QCD stochastic vacuum is one of the phenomenological models used to explain quark confinement [1, 2, 3]. It is based on the assumption that one can calculate vacuum expectation values of gauge invariant quantities as expectation values with respect to some well-behaved stochastic gauge field, for which only the second order correlators are important and the others are negligible [3].

We consider QCD stochastic vacuum as the environment for colour quantum particles and show that the result of their interaction is decoherence, relaxation of quantum superpositions, loss of information and confinement of colour states phenomenon [4].

*E-mail: v.kuvshinov@sosny.bas-net.by

2 Interaction of Single Particle State with QCD Vacuum

Suppose we have a quark which quantum state is described by the density matrix:

$$\hat{\rho}_{in} = |\phi_{in}\rangle\langle\phi_{in}|. \quad (1)$$

As the result of the interaction of this state with stochastic QCD vacuum, the density matrix takes form [5]:

$$\hat{\rho}(L) = N_c^{-1}\hat{I} + (\hat{\rho}_{in} - N_c^{-1}\hat{I})W_{adj}(L), \quad (2)$$

where $W_{adj}(L)$ is the Wilson loop in the adjoint representation [6] and L is the space-time loop itself.

The exponential decay of Wilson loop is recognized as the condition of confinement [3], so if we choose a rectangular loop L spanning over time T and distance R , in the confinement region we get:

$$W_{adj}(L) = \exp(-\sigma_{adj}RT). \quad (3)$$

Here σ_{adj} is the QCD string tension in the adjoint representation [4]. Thus in the case of large distances and time periods we get

$$\hat{\rho}(L : RT \rightarrow \infty) = N_c^{-1}\hat{I}. \quad (4)$$

Thus the interaction of an arbitrary colour superposition represented by (1) with the QCD stochastic vacuum at large distances leads to an emergence of a fully mixed state with equal probabilities for different colours. This process can be analyzed with use of some quantum optics' quantities.

Purity P is defined as $P = \text{Tr}(\hat{\rho}^2)$ and it represents the closeness of a quantum state to a pure one. For the final state $\hat{\rho}(L)$ depicted by (2) we acquire

$$P = N_c^{-1} + (1 - N_c^{-1})W_{adj}^2(L). \quad (5)$$

Another quantity we are interested in is quantum fidelity. It is defined as [7]

$$F(\omega, \tau) = \text{Tr}(\sqrt{\sqrt{\omega}\tau\sqrt{\omega}}) \quad (6)$$

This quantity represents the square root of the probability of transition between the states described by density matrices ω and τ . In our case, for the final state $\hat{\rho}(L)$ and the initial state $\hat{\rho}_{in}$ we get

$$F(\hat{\rho}_{in}, \hat{\rho}(L)) = \text{Tr}(\hat{\rho}_{in}\sqrt{N_c^{-1} + (1 - N_c^{-1})W_{adj}(L)}). \quad (7)$$

We also consider von Neumann entropy. It shows how much quantum information is lost in the system during its departure from a pure state [8]. The definition is:

$$S = -\text{Tr} (\hat{\rho} \ln \hat{\rho}). \quad (8)$$

For the initial state $S = 0$, as the state is pure and the density matrix is idempotent. For the final state in case of $RT \rightarrow \infty$ (see (4)) we get:

$$S = -\text{Tr} (N_c^{-1} \hat{I} \ln (N_c^{-1} \hat{I})) = \ln N_c. \quad (9)$$

3 Multiparticle States

Density matrix is dependent on the quantity of degrees of freedom of a system, i.e. on the quantity of particles in the system. Accordingly, the density matrix dimensions for multiparticle states would be increased from $(N_c) \times (N_c)$ to $(N_c^{N_p}) \times (N_c^{N_p})$, where N_p is the number of particles. So the expression (2) in the multiparticle case would look like

$$\hat{\rho}(L) = N_c^{-N_p} \hat{I} + (\hat{\rho}_{in} - N_c^{-N_p} \hat{I}) W_{adj}(L). \quad (10)$$

And the expression (4) can be written as

$$\hat{\rho}(L : RT \rightarrow \infty) = N_c^{-N_p} \hat{I}. \quad (11)$$

The purity (5) would change to:

$$P = N_c^{-N_p} + (1 - N_c^{-N_p}) W_{adj}^2(L), \quad (12)$$

and the fidelity (7):

$$F = \text{Tr} (\hat{\rho}_{in} \sqrt{N_c^{-N_p} + (1 - N_c^{-N_p}) W(L)}), \quad (13)$$

with von Neumann entropy (8) being:

$$S = N_p \ln N_c. \quad (14)$$

Let us consider the following types of initial states for our system:

- By purity: 1) pure; 2) mixed.
- By separability: 1) separable; 2) non-separable (entangled).

Table 1 represents the mentioned quantum optics' characteristics for the four types of states before the interaction with vacuum:

Table 1. Purity and entropy of different states of multiparticle system before the interaction with vacuum

State:	pure separable	mixed separable	pure entangled	mixed entangled
P (purity)	1	$\frac{1}{N_c^{N_p}} \leq P < 1$	1	$\frac{1}{N_c^{N_p}} < P < 1$
S (entropy)	0	$0 < S \leq N_p \ln N_c$	0	$0 < S < N_p \ln N_c$

The same quantities after the interaction:

Table 2. Purity, fidelity and entropy of different states of multiparticle system after the interaction with vacuum

State:	pure separable	mixed separable	pure entangled	mixed entangled
P (purity)	$\frac{1}{N_c^{N_p}}$	$\frac{1}{N_c^{N_p}}$	$\frac{1}{N_c^{N_p}}$	$\frac{1}{N_c^{N_p}}$
S (entropy)	$N_p \ln N_c$	$N_p \ln N_c$	$N_p \ln N_c$	$N_p \ln N_c$
F (fidelity)	$\frac{1}{N_c^{N_p/2}}$	$\frac{1}{N_c^{N_p/2}} < F \leq 1$	$\frac{1}{N_c^{N_p/2}}$	$\frac{1}{N_c^{N_p/2}} < F < 1$

Thus we can see that the final state is defined by a number of particles (and the number of possible colours for any individual particle) in the system. But in any case the entropy during the interaction with QCD vacuum rises to its maximum value and the information is being lost in this process. In the limit $W(L) \rightarrow 0$ we get fully mixed state of a form (11).

4 Conclusion

QCD vacuum can be effectively treated as environment (in the sense of quantum statistics) for colour particles.

In the case of the interaction of stochastic QCD vacuum (only correlators of the second order are important) in confinement region (Wilson loop decays exponentially) with one-particle state the latter undergoes decoherence into a fully mixed state, along with fidelity and purity decay, and increase in von Neumann entropy.

The multi-particle case proposes additional options in terms of defining the initial state, as it might be separable or entangled, pure or mixed. It was shown, however, that after the interaction of the initial state with QCD vacuum the entanglement vanishes.

References

- [1] J. Ambjørn, P. Olesen. On the Formation of a Color Magnetic Quantum Liquid in QCD. *Nuclear Physics B*. **170**, no. 1, 60-78 (1980).
- [2] A. D. Giacomo, H. Dosch, V. I. Shevchenko, and Y. A. Simonov, *Physics Reports* **372**, no. 4, 319-368 (2002).
- [3] Y. A. Simonov. The Confinement. *Uspekhi Fizicheskikh Nauk*. **4** (1996) (in Russian).
- [4] V. Kuvshinov, P. Buividovich. White Mixed States in QCD Stochastic Vacuum. *Nonlinear Phenomena in Complex Systems*. **8**, 313-316 (2005).
- [5] V. I. Kuvshinov, E. G. Bagashov. Evolution of colour superposition in the stochastic QCD vacuum. *Nonlinear Phenom. Complex Syst.*, **16**, No. 3, 242-246 (2013).
- [6] K. G. Wilson. Confinement of Quarks. *Physics Review D*. **10**, no. 8, 2445-2459 (1974)
- [7] A. Uhlmann. The "Transition Probability" in the State Space of a *-Algebra. *Rep. Math. Phys.* **9**, 273 (1976).
- [8] J. von Neumann. *Mathematical Foundations of Quantum Mechanics* (Princeton University Press, Princeton, 1955).

High Precision Method for the Linear Confining Potential in Momentum Space

Andreev V.V *

F.Skorina Gomel State University

Abstract

This paper shows that the Schrödinger equation in the momentum representation for a linear confining potential for states with zero orbital angular momentum can be solved with high accuracy (far superior to other methods) using the special quadrature formulas for hypersingular integral.

1 Methods of solution of integral equations

After partial decomposition Schrödinger equation in the momentum space for centrally symmetric potentials, takes the form:

$$\frac{k^2}{2\mu}\phi_\ell(k) + \int_0^\infty V_\ell(k, k')\phi_\ell(k')k'^2 dk' = E\phi_\ell(k), \quad (1)$$

where $\mu = m_1 m_2 / (m_1 + m_2)$ is the reduced mass; m_1, m_2 are mass of the constituents of a bound system; \mathbf{k} is the momentum of the relative motion ($|\mathbf{k}| = k$); $\phi_\ell(k)$ is the radial part of the Fourier transform of the wave function in the coordinate representation; $V_\ell(k, k')$ is the operator ℓ -th component of the partial decomposition of the interaction potential; E is binding energy.

However, the description of bound states in the momentum representation is complicated by necessity of solving the integral equation (1),

*E-mail: vik.andreev@gsu.by

containing singular terms. So for a linear confining potential $V(r) = \sigma r$ we have that

$$V_\ell(k, k') = \frac{\sigma}{\pi(kk')^2} Q'_\ell\left(\frac{k^2 + k'^2}{2kk'}\right). \quad (2)$$

where function $Q_\ell(y)$ is Legendre polynomial of 2nd kind. Since the function Q'_ℓ hypersingular if $k = k'$, then the potential $V_\ell(k, k')$ is also hypersingular. Standard methods of numerical solution of the equation (1) with the potential (2) gives relatively low accuracy of [1, 2]. The numerical solution of the integral equation (1) can be reduced to a problem on the eigenvalues, which arises when using quadrature formulas for the integrals in the equation.

As a result, the integral equation of the form (1) can be reduced to the problem

$$\sum_{j=1}^N H(k_i, k_j) \phi(k_j) = \sum_{j=1}^N H_{ij} \phi(k_j) = E\phi(k_i), \quad (3)$$

where to obtain the eigenvalues and vectors need to know the elements of H_{ij} . And if $i \neq j$, the problem of calculating the elements H_{ij} for a linear confining potential is not complex, then the $i = j$ ($k = k'$) directly to do this is not possible, due to the presence of singularities.

2 Quadrature formula for singular integrals

Receive quadrature formula for the integral

$$I(z) = \int_{-1}^1 F(t)w(t)g(t, z) dt \quad (4)$$

where $g(t, z)$ is function is singular at $t = z$. The functions $F(t)$ and $w(t)$ is part of the kernel that does not contain the singularities for all $-1 < t, z < 1$.

For this the function $F(t)$ in (4) with the help of interpolation polynomial

$$G_i(t) = \frac{P_N^{(\alpha, \beta)}(t)}{(t - \xi_{i, N}) P_N^{(\alpha, \beta)}(\xi_{i, N})} \quad (5)$$

replaced the expansion

$$F(t) \approx \sum_{i=1}^N G_i(t) F(\xi_{i,N}) , \quad (6)$$

where $\xi_{i,N}$ are the roots of the Jacobi polynomial

$$P_N^{(\alpha,\beta)}(\xi_{i,N}) = 0 \quad (i = 1, 2, \dots, N) . \quad (7)$$

Substituting the expansion (6) in a ratio of $I(z)$ we find that the quadrature formula for the integral takes the form

$$I(z) \approx \sum_{i=1}^N \omega_i(z) F(\xi_{i,N}) , \quad (8)$$

where

$$\omega_i(z) = \frac{1}{P_N^{(\alpha,\beta)}(\xi_{i,N})} \int_{-1}^1 g(t, z) w(t) \frac{P_N^{(\alpha,\beta)}(t)}{t - \xi_{i,N}} dt . \quad (9)$$

Thus the calculation of (9) will help you find the weight coefficients for the quadrature formula (4), the singular values.

3 The analytical form of weighting factors

Consider the possibility of analytical calculation of the weighting factors for different types of singularities that is, depending on the function $g(t, z)$.

3.1 The singular Cauchy integral

The most famous option (4) in the literature is the Cauchy integral

$$g(t, z) = \frac{1}{t - z} , \quad -1 < z < 1 .$$

For this case, there are a large number of works (see for examples [3, 4, 5]), which offered various options for quadrature formulas. In this case, you can get a formula for the weighting factors (9) direct calculation of the integral

$$\omega_i^C(z) = \int_{-1}^1 \frac{w(t)}{P_N^{(\alpha,\beta)}(\xi_{i,N})} \frac{P_N^{(\alpha,\beta)}(t)}{(t - \xi_{i,N})(t - z)} dt . \quad (10)$$

With the help of identity

$$\frac{1}{(t - \xi_{i,N})(t - z)} = \frac{1}{z - \xi_{i,N}} \left[\frac{1}{t - z} - \frac{1}{t - \xi_{i,N}} \right] \quad (11)$$

coefficients (10) reducible to the form

$$\omega_i^C(z) = \begin{cases} \frac{1}{P_N^{(\alpha,\beta)}(\xi_{i,N})} \frac{\Pi_N^{(\alpha,\beta)}(z) - \Pi_N^{(\alpha,\beta)}(\xi_{i,N})}{(z - \xi_{i,N})}, & \text{if } z \neq \xi_{i,N}, \\ \frac{\Pi_N^{(\alpha,\beta)}(\xi_{i,N})}{P_N^{(\alpha,\beta)}(\xi_{i,N})}, & \text{if } z = \xi_{i,N} \end{cases}, \quad (12)$$

where

$$\Pi_n^{(\alpha,\beta)}(z) = \int_{-1}^1 w(t) \frac{P_n^{(\alpha,\beta)}(t)}{(t - z)} dt. \quad (13)$$

To calculate the coefficients of $\omega_i^C(z)$ with a high degree of accuracy to be calculated analytically integral (13) for a variety of functions $w(t)$.

The most famous variant is the version of the function $w(t)$ is weight function of the Jacobi polynomial $P_n^{(\alpha,\beta)}(t)$..

$$w(t) = w^{(\alpha,\beta)}(t) \equiv (1 - t)^\alpha (1 + t)^\beta.$$

Then the integral (13) have the form

$$\Pi_n^{(\alpha,\beta)}(z) = \mathcal{Q}_n^{(\alpha,\beta)}(z),$$

where

$$\mathcal{Q}_n^{(\alpha,\beta)}(z) = \int_{-1}^1 (1 - t)^\alpha (1 + t)^\beta \frac{P_n^{(\alpha,\beta)}(t)}{(t - z)} dt. \quad (14)$$

In the most general case for arbitrary α and β , the function $\mathcal{Q}_n^{(\alpha,\beta)}(z)$ connected with the Jacobi polynomials of the second kind $Q_n^{(\alpha,\beta)}(z)$ ratio

$$\mathcal{Q}_n^{(\alpha,\beta)}(z) = (-2)(z - 1)^\alpha (z + 1)^\beta Q_n^{(\alpha,\beta)}(z), \quad (15)$$

where

$$Q_n^{(\alpha,\beta)}(z) = 2^{\alpha+\beta+n} \frac{\Gamma(n + \alpha + 1)\Gamma(n + \beta + 1)}{\Gamma(2n + \alpha + \beta + 2)} (z + 1)^{-\beta} \times \\ \times (z - 1)^{-\alpha-n-1} {}_2F_1 \left(n + 1, n + \alpha + 1; 2n + \alpha + \beta + 2; \frac{2}{1 - z} \right).$$

3.2 Hypersingular variant

Consider hypersingular variant the integral (9), when the function is

$$g(t, z) = 1/(t - z)^2.$$

The concept of the final calculation of the integrals of this type was first introduced by Hadamard (J. Hadamard, Lectures on the Cauchy's Problem in Linear Partial Differential Equations, Yale University Press (1923).) and developed in the papers [6, 7, 8].

The final part hypersingular integral can be written as

$$\oint_{-1}^1 \frac{f(t)}{(t - z)^2} dt = \frac{d}{dz} \left[\oint_{-1}^1 \frac{f(t)}{t - z} dt \right], \quad -1 < z < 1. \quad (16)$$

Therefore, the weighting coefficients of the quadrature formula

$$\int_{-1}^1 \frac{f(t)}{(t - z)^2} dt = \sum_{i=1}^N \omega_i^H(z) f(\xi_{i,N}) \quad (17)$$

are related with coefficients (ref fz3) ratio

$$\omega_i^H(z) = \frac{d}{dz} [\omega_i^C(z)] . \quad (18)$$

Then the weights for the integral (4) function $g(t, z) = 1/(t - z)^2$ can be calculated by formulas

$$\omega_i^H(z) = \begin{cases} \frac{1}{P_N^{(\alpha,\beta)}(\xi_{i,N})} \left\{ \frac{\Pi_N^{(\alpha,\beta)}(z)}{(z - \xi_{i,N})} - \frac{\Pi_N^{(\alpha,\beta)}(z) - \Pi_N^{(\alpha,\beta)}(\xi_{i,N})}{(z - \xi_{i,N})^2} \right\}, & \text{if } z \neq \xi_{i,N}, \\ \frac{\Pi_N^{(\alpha,\beta)}(\xi_{i,N})}{2P_N^{(\alpha,\beta)}(\xi_{i,N})}, & \text{if } z = \xi_{i,N}. \end{cases} \quad (19)$$

For the Cauchy integral ($g(t, z) = 1/(t - z)$) with $\alpha = -\beta = -1/2$, we have

$$\Pi_n^{(-1/2, 1/2)}(z) = \int_{-1}^1 \sqrt{\frac{1+t}{1-t}} \frac{V_n(t)}{(t - z)} dt = \pi W_n(z), \quad (20)$$

where $V_n(z)$ and $W_n(z)$ are Chebyshev polynomials 3 and 4 of kind, respectively (see [9]).

Then the quadrature formula for the Cauchy integral is of the form:

$$\int_{-1}^1 \sqrt{\frac{1+t}{1-t}} \frac{f(t)}{(t-z)} dt \approx \sum_{i=1}^N \omega_i^C(z) f(\xi_{i,N}), \quad (21)$$

where

$$\omega_i^C(z) = \begin{cases} \frac{\pi}{V'_N(\xi_{i,N})} \frac{W_N(z) - W_N(\xi_{i,N})}{(z - \xi_{i,N})}, & \text{if } z \neq \xi_{i,N}, \\ \pi \frac{W'_N(\xi_{i,N})}{V'_N(\xi_{i,N})}, & \text{if } z = \xi_{i,N} \end{cases}. \quad (22)$$

Quadrature formula for hypersingular integral has the form:

$$\int_{-1}^1 \sqrt{\frac{1+t}{1-t}} \frac{f(t)}{(t-z)^2} dt \approx \sum_{i=1}^N \omega_i^H(z) f(\xi_{i,N}), \quad (23)$$

where

$$\omega_i^H(z) = \begin{cases} \frac{\pi}{V'_N(\xi_{i,N})} \left\{ \frac{W'_N(z)}{(z - \xi_{i,N})} - \frac{W_N(z) - W_N(\xi_{i,N})}{(z - \xi_{i,N})^2} \right\}, & \text{if } z \neq \xi_{i,N}, \\ \frac{\pi W''_N(\xi_{i,N})}{2 V'_N(\xi_{i,N})}, & \text{if } z = \xi_{i,N}. \end{cases} \quad (24)$$

Formula (24) to calculate weight coefficients allows to them with high accuracy and hence can be used to solve the Schrödinger equation with a linear confining potential in momentum space.

4 The calculation of the energy spectrum for a linear confining potential with $\ell = 0$

The Schrödinger equation with a linear confining potential

$$\frac{k^2}{2\mu} \phi_\ell(k) + \frac{\sigma}{\pi k^2} \int_0^\infty Q'_\ell(y) \phi_\ell(k') dk' = E \phi_\ell(k), \quad y = \frac{k^2 + k'^2}{2kk'}, \quad (25)$$

reducible to the form

$$\tilde{k}^2 \phi_\ell(\tilde{k}) + \frac{1}{\pi \tilde{k}^2} \int_0^\infty Q'_\ell(y) \tilde{k}' \phi_\ell(\tilde{k}') d\tilde{k}' = \varepsilon \phi_\ell(\tilde{k}) \quad (26)$$

with the help of replacements

$$k = \beta \tilde{k}, \quad E = \frac{\beta^2}{2\mu} \varepsilon, \quad \beta = (2\mu\sigma)^{1/3}. \quad (27)$$

Using the mapping

$$\tilde{k} = \beta_0 \sqrt{\frac{1+z}{1-z}}, \quad \tilde{k}' = \beta_0 \sqrt{\frac{1+t}{1-t}}, \quad (28)$$

we find that the equation (26) is transformed into

$$\frac{1}{\pi \beta_0} \left(\frac{1-z}{1+z} \right) \int_{-1}^1 Q'_\ell(y(t, z)) \frac{\phi_\ell(t) dt}{(1-t)\sqrt{1-t^2}} = \left(\varepsilon - \beta_0^2 \frac{1+z}{1-z} \right) \phi_\ell(z). \quad (29)$$

For the case of $\ell = 0$ the equation (29) after simplifications can be written as follows:

$$-\frac{1}{\pi \beta_0} (1-z)^2 \int_{-1}^1 \phi_{\ell=0}(t) \sqrt{\frac{1+t}{1-t}} \frac{dt}{(t-z)^2} = \left(\varepsilon - \beta_0^2 \frac{1+z}{1-z} \right) \phi_{\ell=0}(z). \quad (30)$$

Thus, for a linear confining potential we have hypersingular kernel $\sim 1/(t-z)^2$ and therefore for the numerical solution is necessary to use weighting factors(24).

Function $w(t)$ naturally chosen in the form

$$w(t) = \sqrt{\frac{1+t}{1-t}}.$$

As a result, the matrix for eigenvalue problems It takes the form:

$$H_{ij} = \left[\beta_0^2 \delta_{ij} \left(\frac{1 + \xi_{j,N}}{1 - \xi_{j,N}} \right) - \frac{\omega_j^H(\xi_{i,N})}{\pi \beta_0} (1 - \xi_{i,N})^2 \right], \quad (31)$$

where $z \rightarrow \xi_{i,N}$, $t \rightarrow \xi_{j,N}$, $\xi_{i,N}$ are zeros of the polynomial $V_N(t)$ and matrix $\omega_j^H(\xi_{i,N})$ is calculated using the (24).

For a linear confining potential in the $\ell = 0$ is known that

$$\varepsilon = -z_n, \quad n = 1, 2, 3 \dots \quad (32)$$

where z_n are the zeros of the Airy function $Ai(z)$. Therefore, it is possible to compare the results of numerical calculations of the matrix (31) and accurate values (see, table 1)

Table 1: Relative error of δ of the solution of equation (31) ($\beta_0 = 0,9999$)

N	$n = 1$	$= 2$	$n = 3$	$n = 4$	$n = 5$
50	3×10^{-22}	4×10^{-20}	3×10^{-17}	3×10^{-15}	8×10^{-14}
80	5×10^{-33}	2×10^{-29}	1×10^{-26}	3×10^{-24}	4×10^{-22}
100	2×10^{-39}	1×10^{-35}	1×10^{-32}	4×10^{-31}	5×10^{-28}
150	4×10^{-54}	8×10^{-50}	5×10^{-47}	1×10^{-43}	6×10^{-42}

Thus, the choice of weighting coefficients in which the singularity treated analytically and functions $w(t)$ associated with interpolating polynomials $P_N^{(\alpha,\beta)}(t)$ allows us to solve the equation (25) for $\ell = 0$ in momentum space with high accuracy.

The accuracy of calculations many orders of magnitude higher than similar calculations in momentum space [10, 11, 12, 13, 1]

5 Conclusion

I am grateful to the organizers for warm and kind hospitality throughout the Conference. The work was supported by the Belarusian Republican Foundation for Basic Research.

References

- [1] Tang, A. The Nyström plus correction method for solving bound state equations in momentum space / A. Tang, J. W. Norbury // Phys. Rev. — 2001. — Vol. E63. — P. 066703.
- [2] Norbury, J. W. Confining potential in momentum space / J. W. Norbury, D. E. Kahana, K. Maung Maung // Can. J. Phys. — 1992. — Vol. 70. — P. 86–89.

- [3] Golberg, M. A. Numerical Solution of Integral Equations / M. A. Golberg Mathematical concepts and methods in science and engineering. — New York and London: Plenum Press , 1990. — 436 P.
- [4] Kornejchuk, A.A. Quadrature formulae for singular integrals. (Russian)Zh. Vychisl. Mat. Mat. Fiz. 4, No.4, Suppl., 64-74 (1964).
- [5] Sheshko, M.A.Convergence of quadrature processes for a singular integral. (Russian) Soviet Mathematics (Izvestiya VUZ. Matematika), 1976, 20:12, 8694
- [6] Hui, C.-Y. Evaluations of hypersingular integrals using Gaussian quadrature / C.-Y. Hui, D. Shia // International Journal for Numerical Methods in Engineering. — 1999. — Vol. 44 , N 2. — P. 205–214.
- [7] Kaya, A. C. On the solution of integral equations with strongly singular kernels / A. C. Kaya, F. Erdogan // Quart. Appl. Math. — 1987. — Vol. XLV. — P. 105–122.
- [8] Kutt, H. R. On the numerical evaluation of finite part integrals involving an algebraic singularity / H. R. Kutt. — 1975. — National Research Institute for Mathematical Sciences, Pretoria.
- [9] Mason, J. C. Chebyshev polynomials / J. C. Mason, D. C. Handscomb. — Chapman& Hall/Crc , 2002. — 335 P.
- [10] Chen, J.-K. Spectral method for the Cornell and screened Cornell potentials in momentum space / J.-K. Chen // Phys. Rev. D. — Oct 2013. — Vol. 88.— P. 076006. — Erratum Phys. Rev. D 89, 099904 (2014).
- [11] Deloff, A. Quarkonium bound-state problem in momentum space revisited / A. Deloff // Annals Phys. — 2007. — Vol. 322. — P. 2315–2326.
- [12] Hersbach, H. Relativistic linear potential in momentum space / H. Hersbach // Phys. Rev. D. — Apr 1993. — Vol. 47. — P. 3027–3033 .
- [13] Linear confinement in momentum space: singularity-free bound-state equations / S. Leitão, A. Stadler, M. T. Peña, E. P. Biernat // Phys.Rev. — 2014. — Vol. D90 , N 9. — P. 096003.

New Properties of Conformal Transformations for Scalar and Dirac Particles in Riemannian and Riemann-Cartan Spacetimes

Alexander J. Silenko*

*Institute for Nuclear Problems of Belarusian State University,
Bogoliubov Laboratory of Theoretical Physics, JINR, Dubna, Russia*

Abstract

New symmetry properties are found for pointlike scalar and Dirac particles (Higgs boson and all leptons) in Riemannian and Riemann-Cartan spacetimes in the presence of electromagnetic interactions. A Hermitian form of the Klein-Gordon equation for a pointlike scalar particle in an arbitrary n -dimensional Riemannian (or Riemann-Cartan) spacetime is obtained. New conformal symmetries of initial and Hermitian forms of this equation are ascertained. In the above spacetime, general Hamiltonians in the generalized Feshbach-Villars and Foldy-Wouthuysen representations are derived. The conformal-like transformation conserving these Hamiltonians is found. Corresponding conformal symmetries of a Dirac particle are determined. It is proven that all conformal symmetries remain unchanged by an inclusion of electromagnetic interactions.

1 Introduction

A determination of symmetry properties of elementary particles is one of the most important problems of contemporary particle physics. Symmetries of basic relativistic wave equations describing pointlike particles

*E-mail:alsilenko@mail.ru

with spin 0 (Higgs boson) and 1/2 (all leptons) retain an important place among these properties. Intensive studies of such symmetries began fifty years ago with the seminal work by Penrose [1]. He discovered the conformal invariance of the covariant Klein-Gordon (KG) equation [2] for a massless scalar particle in Riemannian spacetimes and supplemented this equation with a term describing a nonminimal coupling to the scalar curvature. Chernikov and Tagirov [3] have studied the case of a nonzero mass and n -dimensional Riemannian spacetimes. The inclusion of the additional Penrose-Chernikov-Tagirov (PCT) term has been argued for both massive and massless particles [3]. Accioly and Blas [4] have performed the exact Foldy-Wouthuysen (FW) transformation for a massive spin-0 particle in static spacetimes and have found new telling arguments in favor of the predicted coupling to the scalar curvature. A derivation of the relativistic FW Hamiltonian is very important for a comparison of gravitational (and inertial) effects in classical and quantum gravity because the FW representation restores Schrödinger-like forms of Hamiltonians and equations of motion. These forms are convenient for finding a semiclassical approximation and a classical limit of relativistic quantum mechanics (see Refs. [5, 6, 7, 8, 9] and references therein).

However, the transformation method used in Ref. [4] is not applicable to either massless particles or nonstatic spacetimes. To find a specific manifestation of the conformal invariance in the FW representation which takes place just for massless particles, the generalized Feshbach-Villars (GFV) transformation [10] applicable for such particles have been performed [11]. The subsequent relativistic FW transformations has made it possible to derive the FW Hamiltonians for the both massive and massless scalar particles in general noninertial frames and stationary gravitational fields. The new manifestation of the conformal invariance for massless particles consisting in the conservation of the FW Hamiltonian and the FW wave function has been discovered. New exact FW Hamiltonians have been obtained for both massive and massless scalar particles in general static spacetimes and in frames rotating in the Kerr field approximated by a spatially isotropic metric. The high-precision expression for the FW Hamiltonian has been derived in the general case. It has also been shown that conformal transformations change only such terms in the FW Hamiltonians that are proportional to the particle mass m .

In the present work, we consider the much more general problem of scalar and Dirac particles in arbitrary gravitational (noninertial) and elec-

tromagnetic fields and find (on a quantum-mechanical level) new symmetry properties relative to conformal transformations not only in the FW representation but also in initial representations. These properties are attributed to all known pointlike scalar and Dirac particles (Higgs boson and leptons) and also to the hypothetic pseudoscalar axion.

We denote world and spatial indices by Greek and Latin letters

$$\alpha, \mu, \nu, \dots = 0, 1, 2, 3, \quad i, j, k, \dots = 1, 2, 3$$

respectively. Tetrad indices are denoted by Latin letters from the beginning of the alphabet, $a, b, c, \dots = 0, 1, 2, 3$. Temporal and spatial tetrad indices are distinguished by hats. The signature is $(+ - - -)$, and the Ricci scalar curvature is defined by $R = g^{\mu\nu} R_{\mu\nu} = g^{\mu\nu} R^{\alpha}_{\mu\alpha\nu}$, where $R^{\alpha}_{\mu\beta\nu} = \partial_{\beta}\Gamma^{\alpha}_{\mu\nu} - \dots$ is the Riemann curvature tensor. The denotation $f_{,\mu}$ means $\partial f / (\partial x^{\mu})$. We use the system of units $\hbar = 1$, $c = 1$.

2 Hermitian form of the Klein-Gordon equation and conformal symmetry for a pointlike scalar particle

The covariant KG equation with the additional PCT term [1, 3] describing a scalar particle in an n -dimensional Riemannian spacetime is given by

$$(\square + m^2 - \lambda R)\psi = 0, \quad \square \equiv \frac{1}{\sqrt{-g}}\partial_{\mu}\sqrt{-g}g^{\mu\nu}\partial_{\nu}. \quad (1)$$

Minimal (zero) coupling corresponds to $\lambda = 0$, while the PCT coupling is defined by $\lambda = (n - 2)/[4(n - 1)]$ [3]. The sign of the Penrose-Chernikov-Tagirov term depends on the definition of R . For noninertial (accelerated and rotating) frames, the spacetime is flat and $R = 0$.

For a *massless* particle, the conformal transformation

$$\tilde{g}_{\mu\nu} = O^{-2}g_{\mu\nu} \quad (2)$$

conserves the form of Eq. (1) but changes the wave function and the operators acting on it [1, 3]:

$$\square - \lambda R = O^{-\frac{n+2}{2}}(\tilde{\square} - \lambda\tilde{R})O^{\frac{n-2}{2}}, \quad \tilde{\psi} = O^{\frac{n-2}{2}}\psi. \quad (3)$$

To specify symmetry properties of the initial KG equation (1), it is instructive to present it in the Hermitian form. Amazingly, this can be achieved with the simple nonunitary transformation

$$\psi = f^{-1}\Phi, \quad f = \sqrt{g^{00}\sqrt{-g}}, \quad g = \det g_{\mu\nu}. \quad (4)$$

Since $\tilde{g} = O^{-2n}g$, Φ is invariant relative to the conformal transformation (2). This invariance takes place only for a massless particle. After the transformation (4), we multiply the obtained equation by the factor f/g^{00} and come to the Hermitian form of the KG equation:

$$\left(\frac{1}{f}\partial_\mu\sqrt{-g}g^{\mu\nu}\partial_\nu\frac{1}{f} + \frac{m^2}{g^{00}} - \frac{\lambda R}{g^{00}}\right)\Phi = 0. \quad (5)$$

The use of Eqs. (2)–(4) shows that Eq. (5) is conformally invariant for a massless particle. However, it is not conformally invariant for a massive one. To determine its conformal symmetry in the latter case, it is sufficient to find a physical quantity that when substituted for m restores the conformal invariance of Eq. (5). For this purpose, we can use the quantity m' which is equal to m in the initial spacetime and takes the form

$$\tilde{m}' = Om' \quad (6)$$

after the conformal transformation (2). The equation obtained from Eq. (5) with the substitution of m' for m ,

$$\left(\frac{1}{f}\partial_\mu\sqrt{-g}g^{\mu\nu}\partial_\nu\frac{1}{f} + \frac{m'^2}{g^{00}} - \frac{\lambda R}{g^{00}}\right)\Phi = 0, \quad (7)$$

is conformally invariant. While this equation does not describe a real particle and is not equivalent to Eq. (5), finding the appropriate substitution (6) determines the conformal symmetry of the suitable equation (5). The determination of a new symmetry property for massive particles is rather important because the only discovered pointlike scalar particle, the Higgs boson, is massive.

Thus, we can conclude that Eq. (5) is not changed by the conformal-like transformation

$$\tilde{g}_{\mu\nu} = O^{-2}g_{\mu\nu}, \quad m \rightarrow m', \quad \tilde{m}' = Om'. \quad (8)$$

In particular, this transformation does not change the wave function Φ . In the general case, we can substitute any quantity satisfying Eq. (6) for m into Eq. (5).

We can now state the conformal symmetry of the initial KG equation (1). The substitution of m' for m makes the *changed* equation conformally invariant with the following properties:

$$\begin{aligned} \square + m'^2 - \lambda R &= O^{-\frac{n+2}{2}} (\tilde{\square} + \tilde{m}'^2 - \lambda \tilde{R}) O^{\frac{n-2}{2}}, \\ \tilde{\psi} &= O^{\frac{n-2}{2}} \psi. \end{aligned} \quad (9)$$

These properties establish the conformal symmetry of the covariant KG equation (1) and the specific form of its invariance relative to the conformal-like transformation (8).

The method of the FW transformation used in Ref. [11] is applicable to nonstationary spacetimes. However, only the stationary case has been considered in this work. To make a more general investigation of symmetry properties in the FW representation, we need to present Eq. (5) in another (equivalent) form.

Let us introduce the following denotations:

$$\Gamma^i = \sqrt{-g} g^{0i}, \quad G^{ij} = g^{ij} - \frac{g^{0i} g^{0j}}{g^{00}}. \quad (10)$$

Lengthy but straightforward calculations bring Eq. (5) to the form

$$\left[(\partial_0 + \Upsilon)^2 + \partial_i \frac{G^{ij}}{g^{00}} \partial_j + \frac{m^2}{g^{00}} + \Lambda \right] \Phi = 0, \quad (11)$$

where

$$\begin{aligned} \Upsilon &= \frac{1}{2f} \{ \partial_i, \Gamma^i \} \frac{1}{f} = \frac{1}{2} \left\{ \partial_i, \frac{g^{0i}}{g^{00}} \right\}, \\ \Lambda &= -\frac{f_{,0,0}}{f} - \left(\frac{g^{0i}}{g^{00}} \right)_{,i} \frac{f_{,0}}{f} - 2 \frac{g^{0i}}{g^{00}} \frac{f_{,0,i}}{f} - \left(\frac{g^{0i}}{g^{00}} \right)_{,0} \frac{f_{,i}}{f} \\ &\quad - \frac{1}{2} \left(\frac{g^{0i}}{g^{00}} \right)_{,0,i} - \frac{1}{2f^2} \left(\frac{g^{0i}}{g^{00}} \right)_{,i} \Gamma^j - \frac{g^{0i}}{2f^2 g^{00}} \Gamma^j_{,j,i} \\ &\quad + \frac{1}{4f^2} (\Gamma^i_{,i})^2 - \left(\frac{G^{ij}}{g^{00}} \right)_{,i} \frac{f_{,j}}{f} - \frac{G^{ij}}{g^{00}} \frac{f_{,i,j}}{f} - \frac{\lambda R}{g^{00}}. \end{aligned} \quad (12)$$

This form of the KG equation is also Hermitian and the wave function is not changed as compared with Eq. (7). The replacement of m with m' makes Eq. (11) to be conformally invariant. Therefore, Eq. (11) is invariant relative to the conformal-like transformation (8).

3 Conformal symmetries of Hamiltonians

To fulfill the successive GFV and FW transformations, we use the method developed in Ref. [10] and applied to the covariant KG equation in Ref. [11]. The original Feshbach-Villars method does not work for massless particles while its generalization [10] makes it possible to extend the method to such particles.

We introduce two new functions, ϕ and χ , as follows [10, 11]:

$$\Phi = \phi + \chi, \quad i(\partial_0 + \Upsilon)\Phi = N(\phi - \chi), \quad (13)$$

where N is an arbitrary nonzero real parameter. For the Feshbach-Villars transformation, it is definite and equal to the particle mass m . These functions form the two-component wave function in the GFV representation, $\Psi = \begin{pmatrix} \phi \\ \chi \end{pmatrix}$. Equations (11) and (13) result in (cf. Ref. [11])

$$\begin{aligned} i\frac{\partial\Psi}{\partial t} &= \mathcal{H}\Psi, & \mathcal{H} &= \rho_3\frac{N^2 + T}{2N} + i\rho_2\frac{-N^2 + T}{2N} - i\Upsilon, \\ T &= \partial_i\frac{G^{ij}}{g^{00}}\partial_j + \frac{m^2}{g^{00}} + \Lambda, \end{aligned} \quad (14)$$

where \mathcal{H} is the GFV Hamiltonian and ρ_i ($i = 1, 2, 3$) are the Pauli matrices. Equation (14) is exact.

For a massless particle, this Hamiltonian is not changed by the conformal transformation (2). In the general case, it is invariant relative to the conformal-like transformation (8).

The general methods developed in Refs. [6, 8, 10] allow us to perform the FW transformation of the Hamiltonian (14) for a relativistic particle in external fields. These methods are iterative. The initial Hamiltonian can be presented in the general form

$$\begin{aligned} \mathcal{H} &= \rho_3\mathcal{M} + \mathcal{E} + \mathcal{O}, & \rho_3\mathcal{M} &= \mathcal{M}\rho_3, \\ \rho_3\mathcal{E} &= \mathcal{E}\rho_3, & \rho_3\mathcal{O} &= -\mathcal{O}\rho_3, \end{aligned} \quad (15)$$

where \mathcal{E} and \mathcal{O} denote the sums of even (diagonal) and odd (off-diagonal) operators, respectively. In the considered case, $[\mathcal{M}, \mathcal{O}] = 0$,

$$\mathcal{M} = \frac{N^2 + T}{2N}, \quad \mathcal{E} = -i\Upsilon, \quad \mathcal{O} = i\rho_2\frac{-N^2 + T}{2N}, \quad (16)$$

and the transformation operator found in Ref. [8] reduces to the form [10, 11]

$$U = \frac{\epsilon + N + \rho_1(\epsilon - N)}{2\sqrt{\epsilon N}}, \quad \epsilon = \sqrt{\mathcal{M}^2 + \mathcal{O}^2} = \sqrt{T}. \quad (17)$$

This transformation operator is ρ_3 -pseudounitary ($U^\dagger = \rho_3 U^{-1} \rho_3$).

It is important that the Hamiltonian obtained as a result of the transformation with the operator (17) does not depend on N [10]:

$$\begin{aligned} \mathcal{H}' &= \rho_3 \epsilon + \mathcal{E}' + \mathcal{O}', \quad \rho_3 \mathcal{E}' = \mathcal{E}' \rho_3, \quad \rho_3 \mathcal{O}' = -\mathcal{O}' \rho_3, \\ \mathcal{E}' &= -i\Upsilon + \frac{1}{2\sqrt{\epsilon}} [\sqrt{\epsilon}, [\sqrt{\epsilon}, \mathcal{F}]] \frac{1}{\sqrt{\epsilon}}, \\ \mathcal{O}' &= \rho_1 \frac{1}{2\sqrt{\epsilon}} [\epsilon, \mathcal{F}] \frac{1}{\sqrt{\epsilon}}, \quad \mathcal{F} = -i\partial_0 - i\Upsilon. \end{aligned} \quad (18)$$

This shows a self-consistency of the used transformation method. The *exact* intermediate Hamiltonian (18) describes massive and massless particles and is not changed by the conformal-like transformation (8).

The next transformation [10] eliminates residual odd terms and leads to the final form of the *approximate* relativistic FW Hamiltonian:

$$\mathcal{H}_{FW} = \rho_3 \epsilon - i\Upsilon - \frac{1}{2\sqrt{\epsilon}} [\sqrt{\epsilon}, [\sqrt{\epsilon}, (i\partial_0 + i\Upsilon)]] \frac{1}{\sqrt{\epsilon}}. \quad (19)$$

This final Hamiltonian is also invariant relative to the conformal-like transformation (8). As a rule, the relativistic FW Hamiltonian is expanded in powers of the Planck constant and is useful when the de Broglie wavelength is much smaller than the characteristic distance [8]. In such a Hamiltonian, terms proportional to the zeroth and first powers of the Planck constant are determined exactly while higher-order terms are not specified (see Ref. [12]). As a result, the last term in Eq. (19) can be omitted if it is proportional to the second or higher orders of \hbar .

4 Inclusion of electromagnetic interactions

Fortunately, an inclusion of electromagnetic interactions does not lead to any significant complication of the above derivations. The initial covariant KG equation takes the form

$$[g^{\mu\nu}(\nabla_\mu + ieA_\mu)(\nabla_\nu + ieA_\nu) + m^2 - \lambda R] \psi = 0, \quad (20)$$

where ∇_μ is the covariant derivative and A_μ is the electromagnetic field potential. This equation is equivalent to the following one:

$$\left(\frac{1}{\sqrt{-g}} D_\mu \sqrt{-g} g^{\mu\nu} D_\nu + m^2 - \lambda R \right) \psi = 0, \quad (21)$$

where $D_\mu = \partial_\mu + ieA_\mu$. The nonunitary transformation (4) brings it to the Hermitian form corresponding to Eq. (5):

$$\left(\frac{1}{f} D_\mu \sqrt{-g} g^{\mu\nu} D_\nu \frac{1}{f} + \frac{m^2}{g^{00}} - \frac{\lambda R}{g^{00}} \right) \Phi = 0. \quad (22)$$

It is convenient to present this equation in the equivalent form [cf. Eq. (11)]

$$\begin{aligned} & \left[(D_0 + \Upsilon')^2 + D_i \frac{G^{ij}}{g^{00}} D_j + \frac{m^2}{g^{00}} + \Lambda \right] \Phi = 0, \\ & \Upsilon' = \frac{1}{2f} \{ \partial_i, \Gamma^i \} \frac{1}{f} = \frac{1}{2} \left\{ D_i, \frac{g^{0i}}{g^{00}} \right\}, \\ & T' = D_i \frac{G^{ij}}{g^{00}} D_j + \frac{m^2}{g^{00}} + \Lambda, \end{aligned} \quad (23)$$

where G^{ij} and Λ are defined by Eqs. (10) and (12), respectively.

A repeat of the transformation given above allows us to derive the Hamiltonian in the GFV representation:

$$\mathcal{H} = \rho_3 \frac{N^2 + T'}{2N} + \rho_2 \frac{-N^2 + T'}{2N} - i\Upsilon' + eA_0. \quad (24)$$

The FW transformation can be fulfilled with the operator (17) where $\epsilon = \sqrt{T'}$. The transformed operator \mathcal{H}' is independent of N . The final approximate FW Hamiltonian is given by ($\epsilon = \sqrt{T'}$)

$$\begin{aligned} & \mathcal{H}_{FW} = \rho_3 \epsilon - i\Upsilon' + eA_0 \\ & - \frac{1}{2\sqrt{\epsilon}} \left[\sqrt{\epsilon}, \left[\sqrt{\epsilon}, (i\partial_0 + i\Upsilon' - eA_0) \right] \right] \frac{1}{\sqrt{\epsilon}}. \end{aligned} \quad (25)$$

The last term in Eq. (25) can be omitted if it is proportional to the second or higher orders of \hbar (see previous section).

All Hamiltonians obtained with the inclusion of electromagnetic interactions (\mathcal{H} , \mathcal{H}' , and \mathcal{H}_{FW}) are invariant relative to the conformal-like transformation (8). The Hamiltonians are conformally invariant for

a massless particle. Thus, this inclusion does not change the conformal symmetries of the Hamiltonians.

In Secs. 2–4, we considered a scalar particle in Riemannian spacetimes. However, all results obtained remain applicable to Riemann-Cartan spacetimes. The spacetime torsion does not affect the Hamiltonian of a massless particle and the corresponding equation of motion. In particular, the torsion couples only to the particle spin and is not attached to the orbital angular momentum of a test particle [13].

5 Conformal symmetry properties of Dirac particles

It is easy to determine the conformal symmetry properties of a pointlike Dirac particle. It has been established in Ref. [11] that the Dirac and FW Hamiltonians for a *massless* particle and the corresponding wave functions are invariant relative to the conformal transformation (2). The initial covariant Dirac equation is also conformally invariant relative to this transformation. After the conformal transformation (2), the wave function of the Dirac equation for a *massless* particle acquires the additional factor $O^{3/2}$ [11].

These results can be extended to massive particles. A pointlike particle in Riemannian spacetimes is described by the covariant Dirac equation (see Refs. [14, 15] and references therein)

$$\begin{aligned} (i\hbar\gamma^a D_a - mc)\psi &= 0, \quad D_a = e_a^\mu D_\mu, \\ D_\mu &= \partial_\mu + ieA_\mu + \frac{i}{4}\sigma^{ab}\Gamma_{\mu ab}, \end{aligned} \quad (26)$$

where D_μ is the covariant derivative, $\sigma^{ab} = i(\gamma^a\gamma^b - \gamma^b\gamma^a)/2$, and the Dirac matrices γ^a are defined in local Lorentz (tetrad) frames. The anholonomic components of the connection are [14, 15]

$$\begin{aligned} \Gamma_{\mu ab} &= -\Gamma_{\mu ba} = e_\mu^c \Gamma_{cab}, \\ \Gamma_{cab} &= \frac{1}{2}(-C_{cab} + C_{abc} - C_{bca}), \quad C_{abc} = e_a^\mu e_b^\nu (e_{c\nu,\mu} - e_{c\mu,\nu}), \end{aligned} \quad (27)$$

where e_μ^a is the tetrad and e_a^μ is the inverse tetrad. It is convenient to parametrize the spacetime metric as follows [15]:

$$ds^2 = V^2(dx^0)^2 - \delta_{\hat{i}\hat{j}} \hat{W}^{\hat{i}}_k \hat{W}^{\hat{j}}_l (dx^k - K^k dx^0)(dx^l - K^l dx^0). \quad (28)$$

The functions V and K^i , as well as the components of the 3×3 matrix $W^{\hat{i}}_{\hat{j}}$ may depend arbitrarily on x^μ . It can be proven [15] that this parametrization defines ten independent variables that describe the general spacetime metric. This is a modified version of the well-known parametrization of a metric proposed by Arnowitt *et al.* [16] and De Witt [17] in the context of the canonical formulation of the quantum gravity theory; the off-diagonal metric components $g^{0i} = K^i/V^2$ are related to the effects of rotation. The parametrization (28) is general and covers any Riemannian and Riemann-Cartan spacetimes.

The preferable choice of the tetrad [18] is the Schwinger gauge

$$\begin{aligned} e_{\hat{\mu}}^{\hat{0}} &= V \delta_{\hat{\mu}}^0, & e_{\hat{\mu}}^{\hat{i}} &= W^{\hat{i}}_{\hat{j}} (\delta_{\hat{\mu}}^j - K^j \delta_{\hat{\mu}}^0), \\ e_{\hat{0}}^{\hat{\mu}} &= \frac{1}{V} (\delta_{\hat{0}}^{\hat{\mu}} + \delta_{\hat{i}}^{\hat{\mu}} K^i), & e_{\hat{i}}^{\hat{\mu}} &= \delta_{\hat{j}}^{\hat{\mu}} W^{\hat{j}}_{\hat{i}}, \end{aligned} \quad (29)$$

where the inverse 3×3 matrix, $W^{\hat{i}}_{\hat{k}} W^{\hat{k}}_{\hat{j}} = \delta_{\hat{j}}^{\hat{i}}$, is introduced. The Schwinger gauge is characterized by the conditions $e_{\hat{i}}^{\hat{0}} = 0$, $e_{\hat{i}}^0 = 0$.

For the general metric (28) with the tetrad (29) we find explicitly [15]

$$\Gamma_{\hat{\mu}\hat{i}\hat{0}} = \frac{1}{V} W^{\hat{j}}_{\hat{i}} \partial_{\hat{j}} V e_{\hat{\mu}}^{\hat{0}} - \frac{1}{V} \mathcal{Q}_{(\hat{i}\hat{j})} e_{\hat{\mu}}^{\hat{j}}, \quad (30)$$

$$\Gamma_{\hat{\mu}\hat{i}\hat{j}} = \frac{1}{V} \mathcal{Q}_{[\hat{i}\hat{j}]} e_{\hat{\mu}}^{\hat{0}} + \left(\mathfrak{C}_{\hat{i}\hat{j}\hat{k}} + \mathfrak{C}_{\hat{i}\hat{k}\hat{j}} + \mathfrak{C}_{\hat{k}\hat{j}\hat{i}} \right) e_{\hat{\mu}}^{\hat{k}}, \quad (31)$$

where

$$\mathcal{Q}_{\hat{i}\hat{j}} = g_{\hat{i}\hat{k}} W^{\hat{l}}_{\hat{j}} \left(\dot{W}^{\hat{k}}_{\hat{l}} + K^m \partial_m W^{\hat{k}}_{\hat{l}} + W^{\hat{k}}_{\hat{m}} \partial_l K^m \right), \quad (32)$$

$$\mathfrak{C}_{\hat{i}\hat{j}}^{\hat{k}} = W^{\hat{l}}_{\hat{i}} W^{\hat{m}}_{\hat{j}} \partial_{[\hat{l}} W^{\hat{k}}_{\hat{m}]} = -\mathfrak{C}_{\hat{j}\hat{i}}^{\hat{k}}, \quad \mathfrak{C}_{\hat{i}\hat{j}\hat{k}} = g_{\hat{k}\hat{l}} \mathfrak{C}_{\hat{i}\hat{j}}^{\hat{l}}. \quad (33)$$

The dot $\dot{}$ denotes the derivative with respect to the time $t = x^0$. Here $\mathfrak{C}_{\hat{i}\hat{j}}^{\hat{k}}$ is nothing but the anholonomy object for the spatial triad $W^{\hat{i}}_{\hat{j}}$. The indices (which all run from 1 to 3) are raised and lowered with the help of the spatial part of the flat Minkowski metric $g_{ab} = \text{diag}(1, -1, -1, -1)$, $g_{\hat{i}\hat{j}} = -\delta_{\hat{i}\hat{j}}$.

In Riemann-Cartan gravity, the connection (27) should be added by a contribution of a spacetime torsion and takes the form

$$\Gamma_{\hat{\mu}ab} = \frac{1}{2} e_{\hat{\mu}}^c (-C_{cab} + C_{abc} - C_{bca}) - K_{\hat{\mu}ab}. \quad (34)$$

The post-Riemannian contortion tensor is given by [19]

$$\begin{aligned} K_{\mu ab} &= -K_{\mu ba} = \frac{1}{2}(-T_{\mu ab} + T_{ab\mu} - T_{b\mu a}), \\ T_{\mu\nu a} &= -T_{\nu\mu a} = e_{a\nu,\mu} - e_{a\mu,\nu} + \Gamma_{\mu ba}e_{\nu}^b - \Gamma_{\nu ba}e_{\mu}^b. \end{aligned} \quad (35)$$

To calculate the contribution of the spacetime torsion, it is convenient to use the components of the axial torsion vector

$$\check{T}^a = -\frac{1}{2}\eta^{abcd}T_{bcd}, \quad (36)$$

where η^{abcd} is the totally antisymmetric Levi-Civita tensor ($\eta_{\hat{0}\hat{1}\hat{2}\hat{3}} = -\eta^{\hat{0}\hat{1}\hat{2}\hat{3}} = +1$).

A direct check shows [20] that the Hamiltonian form of the initial Dirac equation (26) is characterized by a non-Hermitian Hamiltonian. To avoid this difficulty, one can define a new wave function as follows [20, 15, 19]:

$$\Psi = (\sqrt{-g}e_0^0)^{1/2} \psi. \quad (37)$$

This form of the nonunitary transformation operator is universal and is applicable to any Riemannian and Riemann-Cartan spacetimes.

For both the Riemannian and Riemann-Cartan spacetimes, the Hermitian Hamiltonian is given by [19]

$$\begin{aligned} \mathcal{H} &= \beta mV + eA_0 + \frac{1}{2}\alpha^{\hat{i}}\{\mathcal{F}^j_{\hat{i}}, \pi_j\} \\ &+ \frac{1}{2}(\mathbf{K} \cdot \boldsymbol{\pi} + \boldsymbol{\pi} \cdot \mathbf{K}) + \frac{1}{4}(\boldsymbol{\Xi} \cdot \boldsymbol{\Sigma} - \Upsilon\gamma_5), \\ \Upsilon &= -V\epsilon^{\hat{i}\hat{j}\hat{k}}\mathfrak{C}_{\hat{i}\hat{j}\hat{k}} + VT^{\hat{0}}, \quad \boldsymbol{\Xi}^{\hat{i}} = \epsilon^{\hat{i}\hat{j}\hat{k}}\mathcal{Q}_{\hat{j}\hat{k}} - VT^{\hat{i}}, \end{aligned} \quad (38)$$

where $\mathcal{F}^j_{\hat{i}} = VW^j_{\hat{i}}$, $\gamma_5 = -i\gamma^{\hat{0}}\gamma^{\hat{1}}\gamma^{\hat{2}}\gamma^{\hat{3}}$, and $\epsilon^{\hat{i}\hat{j}\hat{k}}$ is the three-dimensional totally antisymmetric Levi-Civita tensor ($\epsilon^{\hat{1}\hat{2}\hat{3}} = 1$).

The conformal transformation of the metric parameters has the form

$$\tilde{V} = O^{-1}V, \quad \widetilde{W}^{\hat{i}}_{\hat{k}} = O^{-1}W^{\hat{i}}_{\hat{k}}, \quad \widetilde{W}^{\hat{i}}_{\hat{k}} = OW^{\hat{i}}_{\hat{k}}, \quad \widetilde{\mathbf{K}} = \mathbf{K}.$$

As a result,

$$\widetilde{C}_{abc} = OC_{abc}, \quad \widetilde{\mathcal{Q}}_{\hat{i}\hat{j}} = \mathcal{Q}_{\hat{i}\hat{j}}, \quad \widetilde{\mathfrak{C}}_{\hat{i}\hat{j}\hat{k}} = O\mathfrak{C}_{\hat{i}\hat{j}\hat{k}}, \quad \widetilde{\mathcal{F}}^j_{\hat{i}} = \mathcal{F}^j_{\hat{i}}. \quad (39)$$

The conformal transformation (2) does not change the contortion tensor $K_{\mu ab}$. In compliance with this, $\widetilde{T}^a = OT^a$.

Thus, $\widetilde{\Xi} = \Xi$ and $\widetilde{\Upsilon} = \Upsilon$. The above-mentioned relations show that the *Hermitian* Dirac Hamiltonian (38) is invariant relative to the conformal transformation (2) for massless particles [11] and relative to the conformal-like transformation (8) for massive ones.

We can also note that the anholonomic components of the connection (local Lorentz connection [19]) $\Gamma_{\mu ab}$ remain unchanged by the conformal transformation. These components together with the tetrad e_μ^a form the Poincaré gauge potentials [19]. Among these potentials, only the tetrad is changed by the conformal transformation.

It is easy to find the conformal symmetry of the FW Hamiltonian. Equation (38) can be presented in the form (15) (with $\rho_3 \rightarrow \beta$), where

$$\mathcal{M} = mV, \quad \mathcal{E} = eA_0 + \frac{1}{2}(\mathbf{K} \cdot \boldsymbol{\pi} + \boldsymbol{\pi} \cdot \mathbf{K}) + \frac{1}{4}\boldsymbol{\Xi} \cdot \boldsymbol{\Sigma}, \quad \mathcal{O} = \frac{1}{2}\alpha^{\widehat{i}}\{\mathcal{F}^j_{\widehat{i}}, \pi_j\} - \Upsilon\gamma_5. \quad (40)$$

Equation (40) shows that

$$\widetilde{\mathcal{M}} = O^{-1}\mathcal{M}, \quad \widetilde{\mathcal{E}} = \mathcal{E}, \quad \widetilde{\mathcal{O}} = \mathcal{O}. \quad (41)$$

The unitary operator of the FW transformation is given by [8]

$$U = \frac{\beta\epsilon + \beta\mathcal{M} - \mathcal{O}}{\sqrt{(\beta\epsilon + \beta\mathcal{M} - \mathcal{O})^2}} \beta, \quad \epsilon = \sqrt{\mathcal{M}^2 + \mathcal{O}^2}. \quad (42)$$

This operator is invariant relative to the conformal-like transformation (8). After the first iteration with the operator (42), next iterations eliminate residual odd terms. The final approximate FW Hamiltonian is equal to [8]

$$\mathcal{H}_{FW} = \beta\epsilon + \mathcal{E} + \frac{1}{4} \left\{ \frac{1}{2\epsilon^2 + \{\epsilon, \mathcal{M}\}}, (\beta[\mathcal{O}, [\mathcal{O}, \mathcal{M}]] - [\mathcal{O}, [\mathcal{O}, \mathcal{F}]]) \right\}, \quad (43)$$

$$\mathcal{F} = \mathcal{E} - i\hbar \frac{\partial}{\partial t}.$$

Evidently, this Hamiltonian (whose explicit form is obtained in Ref. [19]) is also invariant relative to the conformal-like transformation (8) in the general case.

The wave function of the equation for the *Hermitian* Dirac Hamiltonian,

$$i \frac{\partial \Psi}{\partial t} = \mathcal{H}\Psi, \quad (44)$$

satisfies Eq. (37). It is invariant relative to the conformal-like transformation. The FW wave function also possesses this property. The use of Eq. (37) allows us to obtain the following property of the wave function of the initial Dirac equation (26) relative to the conformal-like transformation:

$$\tilde{\psi} = O^{3/2}\psi. \quad (45)$$

Contrary to the conventional conformal invariance, this property is valid for both massive and massless particles.

All properties stated in this section are valid in the presence of electromagnetic interactions.

We can conclude that the previously ascertained similarity between massless scalar and Dirac particles in Riemannian spacetimes [11] exists for any pointlike particles in both the Riemannian and Riemann-Cartan spacetimes and is not violated by electromagnetic interactions.

6 Summary

In the present work, new symmetry properties have been found for fundamental pointlike scalar and Dirac particles (Higgs boson and all leptons) in Riemannian and Riemann-Cartan spacetimes. All results are general and have been obtained in the presence of electromagnetic interactions. The KG equation for a pointlike scalar particle in arbitrary n -dimensional Riemannian (or Riemann-Cartan) spacetimes has been brought to the Hermitian form (5). This form is useful to derive the general Hamiltonians in the GFV and FW representations. The GFV Hamiltonians (14) and (24) are exact. The corresponding FW Hamiltonians (19) and (25) are approximate. They are expanded in powers of the Planck constant and are useful when the de Broglie wavelength is much smaller than the characteristic distance. Nevertheless, these Hamiltonians are rather general. They cover the nonstationary case and can be applied for a relativistic particle in arbitrarily strong gravitational and inertial fields. In the FW Hamiltonians, terms proportional to the zeroth and first powers of the Planck constant are determined exactly while higher-order terms are not specified.

New conformal symmetries of the initial and Hermitian forms of the KG equation were ascertained. When the mass is replaced with any quantity m' satisfying the conformal transformation (6), the *changed* equations become conformally invariant. This property defines the conformal symmetries of

the conventional and Hermitian KG equations. The latter equation as well as the obtained Hamiltonians in the GFV and FW representations is invariant relative to the conformal-like transformation (8).

Corresponding conformal symmetries are also determined for both massive and massless Dirac particles. The Dirac and FW Hamiltonians are invariant relative to the conformal-like transformation (8). This transformation also defines the conformal symmetry of the initial Dirac equation for a massive particle. When m' defined by Eq. (6) is substituted for m , the Dirac wave function has the property (45).

It has been proven that all conformal symmetries remain unchanged by an inclusion of electromagnetic interactions. Thus, the results obtained in the present study have allowed us to state the general properties of conformal symmetry for pointlike scalar and Dirac particles (Higgs boson and all leptons) in Riemannian and Riemann-Cartan spacetimes in the presence of electromagnetic interactions.

The work was supported in part by the Belarusian Republican Foundation for Fundamental Research (Grant No. $\Phi 14D-007$) and by the Heisenberg-Landau program of the German Ministry for Science and Technology.

References

- [1] R. Penrose, in *Relativity, Groups and Topology*, edited by C. DeWitt and B. DeWitt (Gordon and Breach, London, 1964), p. 565.
- [2] O. Klein, Z. Phys. **37**, 895 (1926); W. Gordon, Z. Phys. **40**, 117 (1926). The equation was first obtained by E. Schroedinger (unpublished) and also by V. Fock, Z. Phys. **38**, 242 (1926).
- [3] N. Chernikov and E. Tagirov, Ann. Inst. Henri Poincaré A **9**, 109 (1968).
- [4] A. Accioly and H. Blas, Phys. Rev. D **66**, 067501 (2002); Mod. Phys. Lett. A **18**, 867 (2003).
- [5] J. P. Costella and B. H. J. McKellar, Am. J. Phys. **63**, 1119 (1995); A. J. Silenko, Pis'ma Zh. Fiz. Elem. Chast. Atom. Yadra **10**, 144 (2013) [Phys. Part. Nucl. Lett. **10**, 91 (2013)].

- [6] A. J. Silenko, J. Math. Phys. **44**, 2952 (2003).
- [7] A. J. Silenko and O. V. Teryaev, Phys. Rev. D **71**, 064016 (2005).
- [8] A. J. Silenko, Phys. Rev. A **77**, 012116 (2008); **91**, 022103 (2015).
- [9] A. J. Silenko, Phys. Rev. A **91**, 012111 (2015).
- [10] A.J. Silenko, Teor. Mat. Fiz. **156**, 398 (2008) [Theor. Math. Phys. **156**, 1308 (2008)].
- [11] A. J. Silenko, Phys. Rev. D **88**, 045004 (2013).
- [12] A. J. Silenko, Teor. Mat. Fiz. **176**, 189 (2013) [Theor. Math. Phys. **176**, 987 (2013)].
- [13] F. W. Hehl, Y. N. Obukhov, D. Puetzfeld, Phys. Lett. A, **377**, 1775 (2013).
- [14] F. W. Hehl, J. Lemke, and E. W. Mielke, Two lectures on fermions and gravity, in: *Geometry and Theoretical Physics*, Proc. of the Bad Honnef School (12-16 Feb 1990), J. Debrus and A. C. Hirshfeld, eds. (Springer, New York, 1991), pp. 56-140.
- [15] Yu. N. Obukhov, A. J. Silenko, and O. V. Teryaev, Phys. Rev. D **84**, 024025 (2011); **88**, 084014 (2013).
- [16] R. Arnowitt, S. Deser, and C. W. Misner, Phys. Rev. **116**, 1322 (1959).
- [17] B. S. De Witt, Phys. Rev. **160**, 1113 (1967).
- [18] A. J. Silenko, Acta Phys. Polon. B Proc. Suppl. **1**, 87 (2008); Yu. N. Obukhov, A. J. Silenko, and O. V. Teryaev, Phys. Rev. D **80**, 064044 (2009).
- [19] Yu. N. Obukhov, A. J. Silenko, and O. V. Teryaev, Phys. Rev. D **90**, 124068 (2014).
- [20] Yu. N. Obukhov, Phys. Rev. Lett. **86**, 192 (2001); Fortschr. Phys. **50**, 711 (2002).

The Integral Equations Solution for Quantum Two Particle Systems with the Cornell Potential in Momentum Space

K.S. Babich*, V.V. Andreev

F.Skorina Gomel State University

Abstract

A new high precision method for solution of integral equations in the momentum space with Cornell potential is suggested. The method can be used effectively for the bound state equations.

1 Relativistic equation in momentum space

In the general case, the wave function (WF) of a bound system of spinor quarks with masses m_q , m_Q and respectively with 4-momentums p_1 , p_2 and helicities $\lambda_{1,2}$ in Relativistic Hamiltonian Dynamics (RHD) satisfies the three-dimensional integral equation [1]:

$$\begin{aligned} \sum_{\lambda_1, \lambda_2} \int \langle \mathbf{k}', \sigma_1, \sigma_2 \parallel \hat{V} \parallel \mathbf{k}, \lambda_1, \lambda_2 \rangle \Phi_{\lambda_1 \lambda_2}^{J\mu}(\mathbf{k}') d\mathbf{k}' = \\ = \left(M - \sqrt{\mathbf{k}^2 + m_q^2} - \sqrt{\mathbf{k}^2 + m_Q^2} \right) \Phi_{\sigma_1 \sigma_2}^{J\mu}(\mathbf{k}). \end{aligned} \quad (1)$$

The knowledge of the kernel of the RHD integral equation makes it possible to switch to the procedure of numerical solution and calculation of the spectrum of masses of the quarkonium.

In the description of the meson, as a system of a quark and an anti-quark is widely used the Cornell potential. Effective centrally symmetric

*E-mail: kbabich@gsu.by

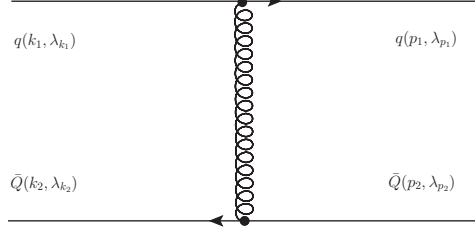


Figure 1: One-gluon exchange contribution V_{pert}

potential interaction between quarks with constituent masses m_q and m_Q contains Coulomb and linear part:

$$\hat{V}(\mathbf{r}) = -\frac{4\alpha_s}{3r} + \sigma\mathbf{r} + w, \quad \mathbf{r} = |\mathbf{r}|, \quad (2)$$

where σ , w – model parameters, α_s – QCD strong coupling constant.

This potential satisfies the requirement of quark confinement and has been widely used in calculations of the spectra of heavy mesons [2, 3].

In a common way the potential of interaction in momentum space can be constructed using the amplitude of the elastic scattering of particles that construct the system [4]

$$q_i(k_1, \lambda_{k_1}) + \bar{q}_j(k_2, \lambda_{k_2}) \rightarrow q_k(p_1, \lambda_{p_1}) + \bar{q}_l(p_2, \lambda_{p_2}), \quad (3)$$

where particle momenta and spin numbers are given between parentheses and $i, j, k, l = 1, 2, 3$ – color degrees of freedom.

For non-zero order of the perturbation theory the main contribution to the amplitude of elastic scattering T_{fi} of quark-antiquark determined by the diagram of one-gluon exchange (see Figure 1).

As a result the potential generated by diagram of gluon exchange including conservation of the currents and the running coupling constant of QCD will take the form:

$$\begin{aligned} V_{\lambda_{p_1}, \lambda_{p_2} \lambda_{k_1}, \lambda_{k_2}}^{(\text{pert})}(\mathbf{k}', \mathbf{k}) &= (-1) \frac{N_{k, k'}}{8\pi^2} \frac{4\alpha_s(q^2)}{3q^2} J^\mu(1) \widetilde{D}_{\mu\nu}(q) J^\nu(2) = \\ &= (-1) \frac{N_{k, k'}}{8\pi^2} \frac{4\alpha_s(q^2)}{3q^2} \left[j^\mu(1) j_\mu(2) - \frac{q_\mu j^\mu(1) q_\nu j^\nu(2)}{q^2} \right]. \end{aligned} \quad (4)$$

In non-relativistic limit ($\mathbf{k}^2, \mathbf{k}'^2 \ll m_q^2, m_Q^2$) potential (4) in coordinate space takes the form of the Coulomb potential [5]

$$\hat{V}_C(\mathbf{r}) = -\frac{4\alpha_s}{3r}. \quad (5)$$

Therefore we can assume (4) as relativistic generalization of the Coulomb potential (5).

The confining component of interquark potential can be derived by analyzing the Lorentz structure of the potential and experimental data on the meson mass spectrum.

The analysis results that the nonperturbative part of the interquark potential is determined as the sum of the vector ($\sim K_V(q^2)$) and scalar ($\sim K_S(q^2)$) confining parts [6]:

$$\begin{aligned}
& \langle \mathbf{k}', \lambda_{p_1}, \lambda_{p_2} \parallel \hat{V}_{conf} \parallel \mathbf{k}, \lambda_{k_1}, \lambda_{k_2} \rangle = \\
& = \frac{N_{k,k'}}{(2\pi)^3} \left[K_V(q^2) \bar{u}_{\lambda_{p_1}}(p_1) \left(\gamma^\mu + \frac{i\kappa_q}{2m_q} (k_1 - p_1)_\nu \sigma^{\mu\nu} \right) u_{\lambda_{k_1}}(k_1) \times \right. \\
& \quad \times \bar{v}_{\lambda_{k_2}}(k_2) \left(\gamma^\mu + \frac{i\kappa_Q}{2m_Q} (p_2 - k_2)_\nu \sigma^{\mu\nu} \right) v_{\lambda_{p_2}}(p_2) + \\
& \quad \left. + K_S(q^2) \bar{u}_{\lambda_{p_1}}(p_1) u_{\lambda_{k_1}}(k_1) \bar{v}_{\lambda_{k_2}}(k_2) v_{\lambda_{p_2}}(p_2) \right], \tag{6}
\end{aligned}$$

where functions

$$K_V(q^2) = \frac{8\pi A_V}{\mathbf{q}^4} + \delta(\mathbf{k}' - \mathbf{k}) B_V(\mathbf{k}), \tag{7}$$

$$K_S(q^2) = \frac{8\pi A_S}{\mathbf{q}^4} + \delta(\mathbf{k}' - \mathbf{k}) B_S(\mathbf{k}). \tag{8}$$

should provide confinement of the quarks in the meson.

Expression (6) for potential give in non-relativistic limit the linear confining potential $V(\mathbf{r}) = \sigma r + w$ with parameters

$$\sigma = (A_V - A_S), \quad w = (B_V - B_S). \tag{9}$$

Thus we can say that sum

$$\langle \mathbf{k}', \lambda_{p_1}, \lambda_{p_2} \parallel \hat{V}_{pert} + \hat{V}_{conf} \parallel \mathbf{k}, \lambda_{k_1}, \lambda_{k_2} \rangle \tag{10}$$

defined by relations (4) and (6) is relativistic generalization of the Cornell potential (2).

But in structure of (10) we meet terms which give singularities in initial equation. At this place we have strong reasons for good numerical method to stay making calculations in momentum space unlike to do different expansion by velocities and so on.

Absolute the same type of hypersingular integrals we meet in bound state problems with the Cornell potential in momentum space. Further, for simplicity, we demonstrate how to calculate numerically integrals of this type with high precision on the example of non-relativistic Schrodinger equation with the Cornell potential.

After transformation of integral $[0, \infty) \rightarrow [-1, 1]$ by making substitution $k = c \frac{1+t}{1-t}$ in

$$\frac{k^2}{2\mu} \phi_l(k) + \int_0^\infty V_l(k, k') \phi_l(k') k'^2 dk' = E \phi_l(k), \quad (11)$$

singular integrals appear [7]:

for Coulomb part

$$V^C(r) = -\frac{\alpha}{r} \Rightarrow V_l^C(k, k') = -\frac{\alpha}{\pi} \frac{Q_l(y)}{kk'} \Rightarrow \int_{-1}^1 f(t) \ln|t-z| dt \quad |z| \leq 1 \quad (12)$$

for linear part

$$V^L(r) = \frac{r}{a^2} \Rightarrow V_l^L(k, k') = \frac{Q_l'(y)}{\pi(akk')^2} \Rightarrow \int_{-1}^1 \frac{f(t)}{(t-z)^2} dt \quad |z| \leq 1, \quad (13)$$

where Q_l – Legendre polynomial of the second kind;

$$y = \frac{k^2 + k'^2}{2kk'}. \quad (14)$$

In paper [7] it was shown that “power of singularity” in integral (13) can be “reduced”

$$\int_{-1}^1 \frac{f(t)}{(t-z)^2} dt \quad |z| \leq 1, \quad \Rightarrow \quad \int_{-1}^1 \frac{f(t)}{(t-z)} dt \quad |z| \leq 1 \quad (15)$$

by making integration by parts. But instead of integral equation we receive integral-differential equation. This method has relatively low precision ($\sim 10^{-6}$).

In the same paper [7] was suggested Semispectral Chebyshev method for integrals (12) and (15).

2 New quadrature formula

In paper [8] was shown that using property $\int_0^\infty Q'_0(y) dk' = 0$ we can introduce contour-term and rewrite terms $\sim Q'_0(y)$ in a form

$$\int_0^\infty Q'_0(y) \phi_0(k') dk' \Rightarrow \int_0^\infty Q'_0(y) (\phi_0(k') - \phi_0(k)) dk' \quad (16)$$

and substitution of pure expression

$$Q'_0(y) = \frac{1}{1-y^2} = - \left(\frac{2kk'}{k'+k} \right)^2 \frac{1}{(k'-k)^2}. \quad (17)$$

leads (in the case of Non-relativistic Schödinger equation with Cornell potential) to integral like

$$\frac{4\sigma}{\pi} \int_0^\infty \frac{P_l(y)}{(k'+k)^2} \frac{[\phi_\ell(k') - \phi_\ell(k)]}{(k-k')^2} dk'; \quad (18)$$

After some calculations we have received new quadrature formula for numerical calculation of such type singular integrals which combine advantages of paper [7] and Lande subtraction method

$$\int_{-1}^1 \frac{\phi_\ell(t) - \phi_\ell(z)}{(t-z)^2} dt = \sum_{j=1}^N \omega_j(z) \phi_\ell(t_j). \quad (19)$$

$$\omega_j(z) = \frac{2}{N} \sum_{i=1}^N {}'T_{i-1}(t_j) X_{i-1}(z), \quad (20)$$

$$X_n(z) = 2 \sum_{k=0}^{n-1} {}'U_{n-1-k}(z) \left\{ T_k(z) \ln \left| \frac{1-z}{1+z} \right| + R_k(z) \right\}, \quad (21)$$

$$R_n(z) = 2 \sum_{k=0}^{n-1} {}'T_k(z) \left[\frac{(-1)^{(n-k)+1} + 1}{(n-k)} \right]. \quad (22)$$

At the same time the type of initial equation remains to be integral as before in contrast to paper [7] and accuracy of numerical calculations increases.

3 Numerical tests

3.1 Tests for integrals with exact solution

Like a pure numerical test of formula (19) lets check quadrature formula in the case of integrals that have exact solution. For the first test we took function $\phi(t) = t^4$. In this case exact solution will have the next form

$$I_1(\phi) = \int_{-1}^1 \frac{t^4 - z^4}{(t - z)^2} dt = \frac{2}{3} + 6z^2 + 4z^3 \ln \left| \frac{1 - z}{1 + z} \right|, |z| < 1. \quad (23)$$

The results of calculations is presented in Table 1.

Table 1: Numerical test of quadrature formula for the integral (23).

z	Exact value, by (23)	Quadrature form. (19)	$\delta, \%$
-0.99	-13.997086845834733	-13.997086845834787	3.807×10^{-15}
-0.7	1.2267940186741848	1.2267940186741804	3.61992×10^{-15}
-0.3	1.1398104321587945	1.1398104321587932	1.16885×10^{-15}
-0.1	0.7258639838848181	0.7258639838848198	2.29428×10^{-15}
0.0	0.6666666666666666	0.6666666666666636	4.4964×10^{-15}
0.1	0.7258639838848181	0.7258639838848202	2.90609×10^{-15}
0.5	1.6173605223326117	1.6173605223326137	1.23559×10^{-15}
0.7	1.2267940186741848	1.2267940186741875	2.17195×10^{-15}
0.99	-13.997086845834733	-13.997086845834758	1.77673×10^{-15}

For the second test lets select function $\phi(t) = e^{-t}$. Than for the integral

$$I_2(\phi) = \int_{-1}^1 \frac{e^{-t} - e^{-z}}{(t - z)^2} dt \quad (24)$$

we will have exact solution in a form

$$I_2(f_2) = \frac{e^{-1-z}}{z^2 - 1} \{e(z^2 - 1)[Ei(z+1) - Ei(z-1)] - e^{z+2}(z-1) + e^z(z+1) - 2e\}, \quad (25)$$

where $|z| < 1$, $Ei(z) = - \int_{-z}^{\infty} \frac{e^{-t}}{t} dt$ exponential integral. The results of calculations is presented in Table 2.

Table 2: Numerical test of quadrature formula for the integral (24).

z	Exact value, by (25)	Quadrature form. (19)	δ , %
-0.99	-18.597791752712833	-18.597791752712908	4.0116×10^{-15}
-0.6	-0.9833492587254643	-0.9833492587253971	6.83058×10^{-14}
-0.2	0.6793649549585903	0.6793649549585903	5.5563×10^{-15}
0.0	1.0283404811209695	1.0283404811209635	5.82998×10^{-15}
0.1	1.1445832768980895	1.1445832768980928	2.90994×10^{-15}
0.3	1.3046004784874934	1.3046004784874938	3.40402×10^{-16}
0.7	1.518977651147536	1.518977651147532	2.63125×10^{-15}
0.99	3.3470563271679046	3.3470563271677065	5.91755×10^{-14}

3.2 Non-relativistic Schrodinger equation with linear potential for the case $l = 0$

As a second numerical test we have done calculations of non-relativistic Schrodinger equation (11) with linear potential for the case $l = 0$ for which the exact solutions are well known [9].

Energy can be found by formula $\epsilon(0, s, 0) = -s^{2/3}z_\nu$, where $s \equiv 1/2\mu a$, and z_ν ($\nu = 1, 2, 3, \dots$) – zeros of Airy function $Ai(z)$. The results of this calculation is presented in Table 3. There is very good agreement between two results with excellent precision.

Table 3: Comparison of results of calculations for linear potential in momentum space by using our quadrature formula with exact value received by Airy function zeros. Number of points $N = 100$.

n	E_n (19)	E_n (exact value)	δ , %
1	2.3381074104597843	2.338107410459767	7.33×10^{-13}
2	4.0879494441309765	4.087949444130971	1.33×10^{-13}
3	5.520559828095326	5.520559828095551	4.06×10^{-12}
4	6.786708090071581	6.78670809007176	2.62×10^{-12}
5	7.944133587120411	7.944133587120854	5.58×10^{-12}
6	9.022650853340487	9.022650853340982	5.50×10^{-12}
7	10.040174341556877	10.040174341558087	1.21×10^{-11}

There is no results with accuracy better than $10^{-5} \div 10^{-6}$ in momentum space.

3.3 Comparison results in momentum space with results of in coordinate space

Like a crosscheck we also made comparison our results for solution of (11) with Cornell potential in momentum space for the first eigenvalue of energy E_1 for different values of coefficient α , with results of calculation in coordinate space by authors in [10] (see Table 4).

We should noted that our method let us repeat numbers from [10] with very good precisions already with $N = 100$ points, while that last was received on mesh $N = 300000$.

Table 4: Comparison of the results of 1S-state energy calculations for Cornell potential in momentum space by using our quadrature formula with results for coordinate space (ζ_1) in [10].

α	$E_1(1S), N = 100$	$\zeta_1(1S)$ [10], $N = 300000$	$\Delta\zeta$
0.0	2.338 107 410 459 784 3	2.338 107 410 458 750	1.0×10^{-12}
0.2	2.167 316 208 772 692 5	2.167 316 208 771 731	1.0×10^{-12}
0.4	1.988 503 899 750 148 7	1.988 503 899 749 943	9.6×10^{-13}
0.6	1.801 073 805 647 306	1.801 073 805 646 145	8.5×10^{-13}
0.8	1.604 408 543 236 034 9	1.604 408 543 235 973	6.6×10^{-13}
1.0	1.397 875 641 659 084	1.397 875 641 659 578	3.8×10^{-13}
1.2	1.180 833 939 742 701	1.180 833 939 744 863	2.1×10^{-14}
1.4	0.952 640 495 217 967 7	0.952 640 495 219 193	5.8×10^{-13}

4 Conclusions

The new high precision quadrature formula for singular integrals like in bound-state equations with the Cornell potential was suggested.

Numerical tests of quadrature formula for the cases of exact solved mathematical integrals and problems with the Cornell potential were performed and was shown the good accuracy of method.

5 Acknowledgement

Authors thanks to the Belarusian Republican Foundation for Fundamental Research for support of this work.

References

- [1] Keister, B. Relativistic Hamiltonian dynamics in nuclear and particle physics / B. Keister, W. Polyzou // “Advances in Nuclear Physics” Plenum. New York. — 1991. — Vol. 20. — P. 225–479.
- [2] Eichten, E. Spectrum of Charmed Quark-Antiquark Bound States / E. Eichten, T. Kinoshita, K. Gottfried, K.D. Lane, T.M. Yan // Phys.Rev.Lett. — 1975. — **34**. — P. 369.
- [3] Eichten, E. Charmonium: comparison with experiment / E. Eichten, K. Gottfried, T. Kinoshita, K.D. Lane, Tung-Mow Yan // Phys.Rev. — 1980. — **D21**. — P. 203.
- [4] Lucha, W. Relativistic treatment of fermion anti-fermion bound states / W. Lucha, H. Rupprecht, F. F. Schoberl // Phys. Rev. — 1991. — Vol. D44. — P. 242–249.
- [5] Lucha, W. Effective potential models for hadrons / W. Lucha, F. F. Schoberl // e-Print arXiv:hep-ph/9601263v1 (Dated: January 13, 1996)
- [6] Galkin, V. O. / V. O. Galkin, A. Y. Mishurov, R. F. Faustov // Sov. J. Nucl. Phys. — 1992. — Vol. 55. — P. 1207–1213.
- [7] Deloff, A. Semi-spectral Chebyshev method in Quantum Mechanics / A. Deloff // Annals Phys. — 2007. — Vol. 322. — P. 1373–1419.
- [8] Tang, A. MKN theory of bound states / A.Tang // e-Print arXiv: hep-ph/0103035v4.
- [9] Abramowitz, M. Handbook of Mathematical Functions / M.Abramowitz, I.Stegun // Dover, New York — 1972.
- [10] Kang, D. Precise numerical solutions of potential problems using Crank-Nicholson method / D.Kang, E.Won // e-Print arXiv: physics/060917v1 [physics.comp-ph].

Research of the Stability of Motion of Fermions

E.E. Kazitsky*, V.I. Kuvshinov†

*Joint Institute for Power and Nuclear Research - Sosny
National Academy of Science of Belarus*

1 Introduction

It is known that any particle movement can be described using respective equations in partial or total derivatives. For these equations, it is necessary to initialize. It is worth considering that there are always some interference, noise, etc. that can affect the dependence, which can be obtained from these equations. Accounting for such interference is extremely difficult due to their smallness and stochastically. It is therefore easier to determine the stability region of the corresponding equations. The movement of non-abelian gauge field is unstable at any energy density in the absence of background fields[1]. It stimulates interest in the study of stability of motion in the gauge fermion fields as fermion field can serve as a background field for the Yang-Mills theory. Besides that the definition of sustainability movement fermions due to the fact whether the system consisting of fermions, gauge and Yang-Mills fields will be stable. In this work the stability conditions for a fermion and gluons in the electromagnetic fields will be determined, as well as the interaction with the Higgs field. For this Todd criterion and generalized Hamilton equations were used. First the stability in the electromagnetic field will be investigated, then - the resistance movement in the gluon field, after that - the study of the stability in the SU (2), considering the interaction with the Higgs field.

*E-mail: egorprostoy@mail.ru

†E-mail: kuvshinov2003@gmail.com

2 Conventional signs

$\partial_\mu = \frac{\partial}{\partial x^\mu}$ is the partial derivative where $\mu \in (0, 1, 2, 3)$; ψ is wave function of the fermion; $\psi^+ = \psi^\dagger$; $\gamma_0, \gamma_1, \gamma_2, \gamma_3$ is the Dirac matrices; m is mass of the fermion; A^μ is vector potential of group $U(1)$, G_a^μ is vector potential of group $U(N)$, $a \in (0, \dots, N)$; f, g, e is coupling constants.

3 The equation for fermions in the field

As it is known we can say that fermions must be described by the Dirac equation [2, 3]

$$i\gamma_\mu \partial^\mu \psi = m\psi \quad (1)$$

Corresponding to this equation the Lagrangian has the form [4]

$$L = i\psi^+ \gamma_\mu \partial^\mu \psi - \psi^+ m\psi \quad (2)$$

In the case of a particle in a field with which the interaction takes place, the derivative is converted to an extended derivative[5]

$$\partial^\mu \rightarrow D^\mu = \partial^\mu + igA^\mu \quad (3)$$

where $A^\mu = A_n^\mu \frac{T^n}{2}$. We use matrix t^n , which obey the Lie algebra[5]

$$[T^n, T^m] = t^{nmf} T^f \quad (4)$$

T^{nmf} is a structure constant. The Lagrangian in this case takes the form

$$L = i\psi^+ \gamma_\mu D^\mu \psi - \psi^+ m\psi + L_f \quad (5)$$

L_f is Lagrangian of the gauge field. For motion in the scalar field we have

$$\partial^\mu \rightarrow D'^\mu = \partial^\mu + igA^\mu + ifa^\mu \varphi \quad (6)$$

φ is function of the scalar field, a^μ is a constant. In this ways Lagrangian is

$$L = i\psi^+ \gamma_\mu D'^\mu \psi - \psi^+ m\psi + L_f + L_s \quad (7)$$

L_s is Lagrangian of the scalar field.

4 Change of variables of wave function

We introduce the new variables in(7)

$$i\psi^+\gamma_\mu\psi = q_\mu^2 \quad (8)$$

Then a current density is written as $i\psi^+\gamma_\mu\psi = (q_0^2; q_1^2; q_2^2; q_3^2)$. For vector potential we have $A^\mu = (A_0; -A_k)$. Then $g\psi^+A^\mu\gamma_\mu\psi = gq_0^2A_0 - gq_1^2A_1 - gq_2^2A_2 - gq_3^2A_3$, $m\psi^+\psi = mq_0^2$, and $\psi^+\gamma_\mu\partial^\mu\psi = q_\mu p^\mu$

5 Toda criterion

A convenient criterion for describing the stability is Toda criterion[6]. Let us proceed from the density of the Lagrangian function to the density of the Hamilton function.

$$H = T^{00} = \frac{\partial L}{\partial p_0} - L \quad (9)$$

Next it is necessary to know the transformation matrix Y, received from the expression

$$\begin{pmatrix} \frac{d}{dt}\delta p_\mu \\ \frac{d}{dt}\delta q_\mu \end{pmatrix} = Y \begin{pmatrix} \delta q_\mu \\ \delta p_\mu \end{pmatrix} \quad (10)$$

To solve this problem it is convenient to use the equations of Hamilton, which will have the form

$$\begin{pmatrix} \frac{d}{dt}\delta p_\mu \\ \frac{d}{dt}\delta q_\mu \end{pmatrix} = I \begin{pmatrix} -\delta \frac{H}{q_\mu} \\ \delta \frac{H}{p_\mu} \end{pmatrix} \quad (11)$$

Substituting (12) to (11) we will get

$$\begin{pmatrix} \frac{d}{dt}\delta p_\mu \\ \frac{d}{dt}\delta q_\mu \end{pmatrix} = \begin{pmatrix} -\frac{\partial^2}{\partial q_\mu \partial q_\nu} & -\frac{\partial^2}{\partial q_\mu \partial p_\nu} \\ \frac{\partial^2}{\partial p_\mu \partial q_\nu} & \frac{\partial^2}{\partial p_\mu \partial p_\nu} \end{pmatrix} \begin{pmatrix} \delta q_\nu \\ \delta p_\nu \end{pmatrix} \quad (12)$$

Stability of motion defines the determinant of the matrix Y. The only imaginary eigenvalue λ indicates the stability of motion, the real one indicates the instability of of motion.

6 Massive fermions in an electromagnetic field

In the first case the group of symmetry U(1) will be considered[7]. Lagrangian which is used in the theory of fermions in an electromagnetic field has the following form

$$L = i\psi^+\gamma_\mu\partial^\mu\psi - e\psi^+\gamma_\mu A^\mu\psi - \psi^+m\psi \quad (13)$$

Hamiltonian in an explicit form

$$H = mq_0^2 + e(q_0^2A_0 - q_1^2A_1 - q_2^2A_2 - q_3^2A_3) + q_1^2p_1 - q_2^2p_2 - q_3^2p_3 \quad (14)$$

The eigenvalues will take the form

$$\lambda_0 = 0; \lambda_0 = -2(m - eA_0); \lambda_k = -eA_k \pm \sqrt{-1 + e^2A_k^2} \quad (15)$$

Motion is not stability in any field if $A_k > 0$

7 Stability of motion of fermions with two extra degrees of freedom

The case of the four space degrees of freedom and two extra degrees of freedom refers to the case of the group of symmetry SU(2)[5]. The difference is that instead of q must be written column a matrix column, consisting of wave functions, $q \rightarrow \begin{pmatrix} q_{(1)} \\ q_{(1)} \end{pmatrix}$, instead of q^+ a conjugate matrix $q^+ \rightarrow \begin{pmatrix} q_{(1)}^* & q_{(2)}^* \end{pmatrix}$, $A^\mu \rightarrow \begin{pmatrix} G_{11}^\mu & G_{12}^\mu \\ G_{21}^\mu & G_{22}^\mu \end{pmatrix}$, where $\begin{pmatrix} G_{11}^\mu & G_{12}^\mu \\ G_{21}^\mu & G_{22}^\mu \end{pmatrix} = G_a^\mu T^a$, T^a generators of the group. Lagrangian will take the form

$$L = q_{\mu(i)}p_{\mu(i)} - gq_{0(i)}^2G_{0(ii)} + gq_{1(i)}^2G_{1(ii)} + gq_{2(i)}^2G_{2(ii)} + gq_{3(i)}^2G_{3(ii)} - mq_0^2 + L_f \quad (16)$$

The eigenvalues will take the form

$$\lambda_0 = 0; \lambda_0 = -2(m - gG_0); \lambda_{k(i)} = -2(gG_{k(i)} \pm \sqrt{-1 + g^2G_{k(i)}^2}) \quad (17)$$

Motion is not stability in any field if $A_k > 0$ too.

8 Stability of motion of non-massive fermions with two extra degrees of freedom and the fermion interaction with the Higgs field

Let us take the interaction of the fermion fields with the Higgs field. To do this, the Lagrangian, which was considered in the second section, let us add the interaction potential and the Lagrangian of the Higgs field. The potential will be written in the form of the Yukawa interaction[8]

$$V_{in} = -f\psi^+\varphi\psi \quad (18)$$

where φ - the Higgs field. The Lagrangian of the Higgs field will be written as L_h . Then the total Lagrangian will take the form

$$L = q_{\mu(i)}p_{\mu(i)} - gq_{0(i)}^2G_{0(ii)} + gq_{1(i)}^2G_{1(ii)} + gq_{2(i)}^2G_{2(ii)} + gq_{3(i)}^2G_{3(ii)} - mq_0^2 - f\varphi q_0^2 + L_f + L_h \quad (19)$$

Doing all the operations which were used above for the eigenvalue we will receive the values

$$\lambda_0 = 0; \lambda_0 = -2(f\varphi - gG_0); \lambda_{k(i)} = -2(gG_{k(i)} \pm \sqrt{-1 + g^2G_{k(i)}^2}) \quad (20)$$

For stability of motion the next conditions should fulfilled

$$f\varphi - gG_0 = 0 \quad (21)$$

The Higgs field can lead to (24). In this ways motion is stability.

9 Conclusions

From (16) we see that for the sustainability movement $A_k^2 < 0$ and $\lambda_0 = 0$. That is, if there is any external of the field, the square of the spatial component of the vector potential is positive, the motion becomes unstable. This result is quite logical. A particle falling into any field tests the effect of this field, and begins to deviate from the middle of its trajectory. In the case of the group SU (2) number of degrees of freedom increases, but the expression for the vector potential remains the same. This follows from the comparison (20) and (17). The condition is also not changed. The

scalar Higgs field affects the stability that is evident from the expression (24). Also, any scalar field affects the stability. And it may lead to the stability of motion. After the analysis of the expression (31), determine the type of the vector potential and accounting Weil calibration, the size of the areas can be determined in which the motion of a particle is stable.

References

- [1] V.I. Kuvshinov, V.A. Piatrou, Stability Of Yang-Mills Fields System In The Homogeneous (Anti-) Self-Dual Background Field.
- [2] Kaku M Quntum field theory New York Oxford university press 1993.
- [3] Ryder . Quntum field theory Platon 1998, p.57.
- [4] Kaku M Quntum field theory New York Oxford university press 1993.
- [5] Peskin, M.E., Shreader D.V. - Introduction to Quantum Field Theory 2001.
- [6] Toda, M. Phys. Lett. A48, 335.
- [7] Svarc A.S. Quntum field theory and topology Science Moscow, p. 25.
- [8] H. Yukawa, On the interaction of elementary particles. (1935) Proc. Phys. Math. Soc. Japan. 17, 48.

Solution of the Schrödinger Equation for Parabolic Double-well Potential

V. V. Kudryashov*, A. V. Baran †

Institute of Physics, National Academy of Sciences of Belarus

Abstract

The smooth symmetric double-well potential is constructed by means of joining two parabolic wells and central parabolic barrier. The exact analytical solution of the Schrödinger equation is obtained.

The models with double-well potentials are used in various branches of physics and are investigated in numerous papers. For example, many references can be found in [1, 2, 3, 4]. In the present paper, we consider a symmetric potential $V(q) = V(-q)$ which has two minima at points $\pm q_0$ and maximum $V_0 = V(0)$. Without loss of generality it is possible to equate minima to zero by means of choice of an additive constant.

There is a small number of double-well potentials which permit the exact solutions to the Schrödinger equation

$$\frac{d^2\Psi(q)}{dq^2} = \frac{2m}{\hbar^2}(V(q) - E)\Psi(q). \quad (1)$$

The most studied smooth double-well potential is the quartic potential $V(q) = V_0(q^2 - q_0^2)^2/q_0^4$. For this potential, the validity of approximation methods is examined in [1, 2, 3, 4] since the exact solution of the Schrödinger equation (1) is unknown in this case. The double oscillator

$$V(q) = \frac{1}{2}m\omega^2(|q| - q_0)^2 \quad (2)$$

*E-mail: kudryash@dragon.bas-net.by

†E-mail: a.baran@dragon.bas-net.by

was considered in [5]. This quadratic potential consists of two parabolas which meet with discontinuous slope at the point $q = 0$. At the same time this model is exactly solvable. Models with quadratic and quartic double-well potentials are compared in [6].

In the present paper, we propose the generalization of formula (2). The new potential

$$V(q) = \frac{1}{2}m\omega^2 \begin{cases} q_0^2 - q^2/g, & |q| < gq_0, \\ (|q| - q_0)^2/(1 - g), & |q| > gq_0 \end{cases} \quad (3)$$

consists of two parabolic wells and central parabolic barrier. Here $0 < g < 1$. The points $q_{\mp} = \mp gq_0$ are the points of inflection where the second derivative is discontinuous. However, both the function $V(q)$ and its first derivative are continuous. In this case $V_0 = m\omega^2 q_0^2/2$. The potential (3) coincides with (2) if $g = 0$. If $q_0 = 0$, the potential (3) turns into the potential of single harmonic oscillator $m\omega^2(1 - g)^{-1}q^2/2$.

By analogy with [5] it is convenient to introduce dimensionless quantities

$$x = \sqrt{\frac{2m\omega}{\hbar}}q, \quad x_0 = \sqrt{\frac{2m\omega}{\hbar}}q_0, \quad e = \frac{E}{\hbar\omega} \quad (4)$$

and to transform the initial Schrödinger equation to the form

$$\frac{d^2\psi(x)}{dx^2} = (v(x) - e)\psi(x) \quad (5)$$

with reduced potential

$$v(x) = \frac{1}{4} \begin{cases} x_0^2 - x^2/g, & |x| < gx_0, \\ (|x| - x_0)^2/(1 - g), & |x| > gx_0. \end{cases} \quad (6)$$

Note that the value of the central maximum of the reduced potential is $v_0 = x_0^2/4$.

Fig. 1 shows the behavior of the reduced potential for different values of g in the case of $x_0 = 2.5$. Here and in all subsequent figures, we use dotted lines for $g = 0.1$, solid lines for $g = 0.5$ and dashed lines for $g = 0.9$.

In the central region $|x| < gx_0$, the Schrödinger equation (5) for the potential (6) can be rewritten in the standard form [7]

$$\frac{d^2\psi_c}{dz_c^2} = \left(-\frac{z_c^2}{4} - d_c \right) \psi_c, \quad (7)$$

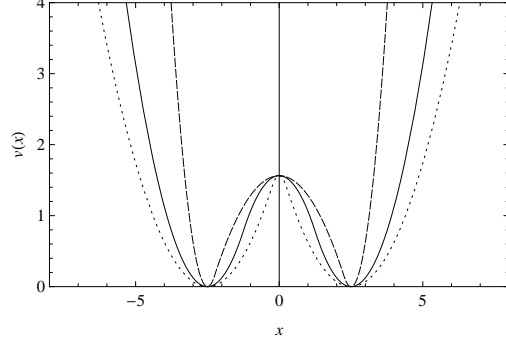


Figure 1: The reduced potential for different values of g .

where

$$z_c = \frac{x}{g^{1/4}}, \quad d_c = g^{1/2} \left(e - \frac{1}{4}x_0^2 \right). \quad (8)$$

The even $\psi_{c1}(x)$ and odd $\psi_{c2}(x)$ solutions of this equation are expressed through the confluent hypergeometric functions [7] with the help of formulas

$$\begin{aligned} \psi_{c1}(x_0, g, e, x) &= e^{-iz_c^2/4} M\left(\frac{id_c}{2} + \frac{1}{4}, \frac{1}{2}, \frac{iz_c^2}{2}\right) \\ &+ e^{iz_c^2/4} M\left(-\frac{id_c}{2} + \frac{1}{4}, \frac{1}{2}, -\frac{iz_c^2}{2}\right), \end{aligned} \quad (9)$$

$$\begin{aligned} \psi_{c2}(x_0, g, e, x) &= z_c e^{-iz_c^2/4} M\left(\frac{id_c}{2} + \frac{3}{4}, \frac{3}{2}, \frac{iz_c^2}{2}\right) \\ &+ z_c e^{iz_c^2/4} M\left(-\frac{id_c}{2} + \frac{3}{4}, \frac{3}{2}, -\frac{iz_c^2}{2}\right). \end{aligned} \quad (10)$$

It should be stressed that these solutions are real.

In both side regions $x < -gx_0$ and $x > gx_0$ adjoining to the central region from the left and from the right, the wave functions satisfy another standard equation [7]

$$\frac{d^2\psi_s}{dz_s^2} = \left(\frac{z_s^2}{4} - d_s \right) \psi_s, \quad (11)$$

where

$$z_s = \frac{(|x| - x_0)}{(1-g)^{1/4}}, \quad d_s = (1-g)^{1/2}e. \quad (12)$$

The decreasing at $|x| \rightarrow \infty$ solution of this equation can be presented through the parabolic cylinder function [7] by means of the formula

$$\psi_s(x_0, g, e, x) = D_{d_s-1/2}(z_s). \quad (13)$$

On the whole real axis $-\infty < x < \infty$, the continuous even ($i = 1$) and odd ($i = 2$) solutions of the Schrödinger equation with the symmetric smooth potential (6) can be written in the form

$$\psi_i(x_0, g, e, x) = N \begin{cases} \psi_{ci}(x_0, g, e, -gx_0)\psi_s(x_0, g, e, x), & x < -gx_0, \\ \psi_s(x_0, g, e, gx_0)\psi_{ci}(x_0, g, e, x), & -gx_0 < x < gx_0, \\ \psi_{ci}(x_0, g, e, gx_0)\psi_s(x_0, g, e, x), & x > gx_0. \end{cases} \quad (14)$$

The normalization coefficient N is determined by the condition

$$\int_{-\infty}^{\infty} \psi_i^2(x_0, g, e, x) dx = 1. \quad (15)$$

The additional requirement of continuity for the first derivative

$$\psi_i'(x_0, g, e, x) = d\psi_i(x_0, g, e, x)/dx$$

at the point $x = gx_0$ leads to the energy quantization rule for even and odd states:

$$\psi_s(x_0, g, e, gx_0)\psi_{ci}'(x_0, g, e, gx_0) = \psi_{ci}(x_0, g, e, gx_0)\psi_s'(x_0, g, e, gx_0). \quad (16)$$

Due to the symmetry of potential this rule ensures continuity of the first derivative at the point $x = -gx_0$ too. The eigenvalues e of energy are easily found as the numerical solutions of the transcendental equation (16). Substituting obtained values of e into the formula (14) we get finally the eigenfunctions for the parabolic double-well potential.

Fig. 2 demonstrates dependence of the four lowest energy levels e on x_0 for different values of g . The dash-dot line reproduces the barrier height $x_0^2/4$ in the reduced potential. There are pairs of lines which become indistinguishable at large values of x_0 . This is the evidence of double degeneration of energy levels. At $x_0 = 0$, in each pair, the values of non-degenerate lower (even) and upper (odd) levels are $(2n + 1/2)/(1 - g)^{1/2}$ and $(2n + 1 + 1/2)/(1 - g)^{1/2}$ respectively. We see that at very large x_0 , the indistinguishable levels tend to $(n + 1/2)/(1 - g)^{1/2}$.

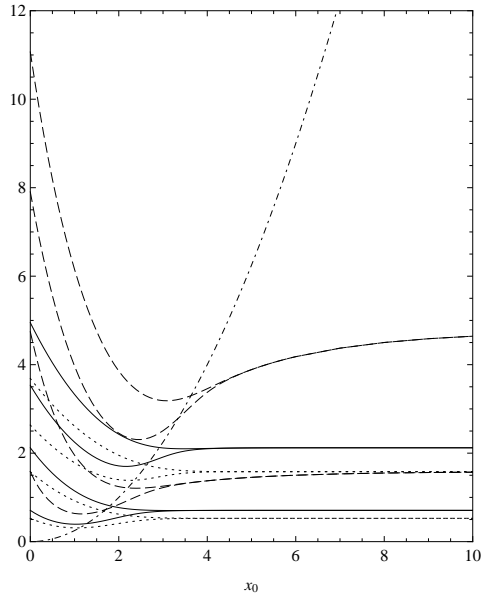


Figure 2: The dependence of e on x_0 .

Figures 3-6 show the normalized wave functions of the four lowest energy eigenstates for different values of g in the case of $x_0 = 2.5$.

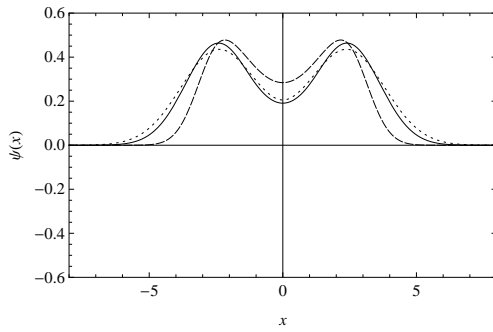


Figure 3: The ground state wave functions.

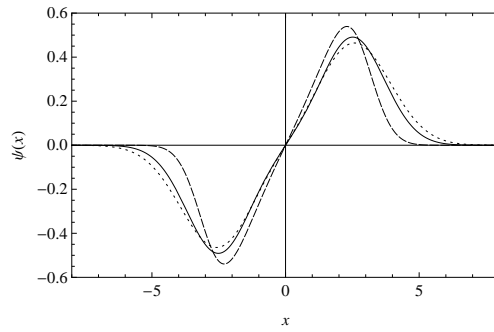


Figure 4: The first excited state wave functions.

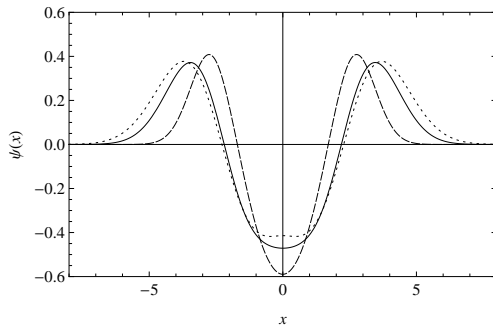


Figure 5: The second excited state wave functions.

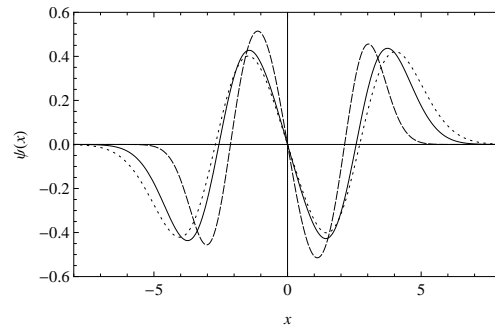


Figure 6: The third excited state wave functions.

References

- [1] L.V. Chebotarev, *Am. J. Phys.* **66**, 1086-1095 (1998).
- [2] Chang-Soo Park, *J. of the Korean Phys. Soc.* **42**, 830-834 (2003).
- [3] P. Pedram, M. Mirzaei, S.S. Gousheh, *Mol. Phys.* **108**, 1949-1955 (2010).
- [4] A.V. Turbiner, *Int. J. Mod. Phys. A* **25**, 647-658 (2010).
- [5] E. Merzbacher, *Quantum Mechanics*, 3rd Ed., John Willey and Sons, Inc., New York, 1998.
- [6] V. Jelic, F. Marsiglio, *Eur. J. Phys.* **33**, 1651-1666 (2012).
- [7] M. Abramovitz and I.A. Stegun (eds), *Handbook of Mathematical Functions*, Dover, New York, 1970.

Dipole Spin Polarizabilities and Gyration of Spin-1 Particles in the Duffin-Kemmer-Petiau Formalism

E.V. Vakulina*

*Affiliated branch of Bryansk State University
n.a. Academy Fellow I.G. Petrovskiy, Novozybkov, Russia*

N.V. Maksimenko

F. Skorina Gomel State University

S.M. Kuchin

*Affiliated branch of Bryansk State University
n.a. Academy Fellow I.G. Petrovskiy, Novozybkov, Russia*

Abstract

In this paper relativistic-invariant phenomenological Lagrangians of interaction between spin-1 particles and electromagnetic field were obtained in the Duffin-Kemmer-Petiau formalism on the basis of the covariant model that takes into account both spin polarizabilities and gyrations of the above-mentioned particles. It was shown that in the suggested covariant model with regard to the crossing symmetry, spatial parity and gauge invariance conservation laws, definite spin polarizabilities and gyrations of spin-1 particles contribute to the expansion of Compton scattering amplitude, starting from the corresponding orders on energy of photons that is in the agreement with low-energy theorems for that process.

*E-mail: elvakulina@yandex.ru

1 Introduction

With the development of the Standard Model of electroweak interaction, new electromagnetic properties of hadrons have been introduced recently. These properties, by analogy with gyration [1,2], are connected with parity violation [3,4]. In their turn, such electromagnetic characteristics as polarizabilities and gyrations are directly related to the inner structure of hadrons and the mechanism of electroweak photon-hadron interactions. For more reliable determination of polarizabilities and hadron characteristics connected with parity violation, a wide class of electrodynamic processes is used. These processes include real and virtual photons scattering, as wells as two-photon production in hadron-hadron interactions. In this context, the task of consistent relativistic-invariant determination of the contributions of polarizabilities and electroweak characteristics of particles to the electrodynamic processes' amplitudes and cross-sections is of great relevance.

The solution for this task can be found in the framework of relativistic theoretical and field approach to the description of interaction between electromagnetic field and hadrons with the account for polarizabilities (both electromagnetic and electroweak) of the latter. In papers [1, 5-9] covariant techniques describing the interaction between electromagnetic field and hadrons were presented. In such techniques the electromagnetic characteristics of particles are fundamental.

Effective covariant Lagrangian of interaction between electromagnetic field and spin-1/2 particles that takes into account the polarizabilities of the latter was introduced in [1, 10] and has been recently used for fitting the photon-proton scattering experimental data at the energies close to resonance production $\Delta(1232)$ [11]. Characterization of electrodynamic processes on the basis of relativistic theoretical and field approaches, which are focused on the obtaining of phenomenological Lagrangians, equations that describe interaction of electromagnetic field with hadrons, as well as the calculation of electrodynamic processes amplitudes consistent with the Standard Models low-energy theorems is one of the most effective methods of interaction processes investigation.

Currently there is a number of theoretical papers (see [12-16]) devoted to introduction and calculation of spin polarizabilities of spin-1/2 hadrons that contribute to the series expansion of Compton scattering amplitude at the energies of photons in the third expansion order. Along with the inves-

tigations of spin-1/2 hadrons polarizabilities, a number of papers present the results of determination and estimation of spin-1 particles polarizabilities [17-20]. Such particles are characterized by both dipole, spin and tensor polarizabilities.

Low-energy theorems play an important role in the understanding of interaction between electromagnetic field and hadrons. It is stipulated by the fact that they are based on the general concepts of quantum field theory and series expansion of Compton scattering amplitude in powers of photons energy. Currently, one of the most efficient methods of electrodynamic processes investigation is the technique that uses phenomenological Lagrangians obtained in the framework of theoretical and field approaches and consistent with the low-energy theorems that are specified by the Standard Model of electroweak interactions. Construction of such Lagrangians allows to obtain physical interpretation of electromagnetic and electroweak characteristics of hadrons.

In paper [19] low-energy theorems for Compton scattering on a spin-1 particle were obtained. On the basis of these and with the use of techniques for determination of the contribution of spin-1/2 particles polarizabilities to the amplitudes of electrodynamic processes, one can obtain relativistic-invariant effective Lagrangians and covariant spin structures of two-photon interaction amplitudes with consideration of polarizabilities and electroweak properties (gyrations) on spin-1 particles. The present paper is entirely devoted to the above-mentioned task.

In paper [21] the construction of the effective relativistic-invariant Lagrangian of interaction between electromagnetic field and particles with constant electric and magnetic dipole moments was performed with the help of dipole moments anti-symmetric tensor that is independent of electromagnetic field tensor $F_{\mu\nu}$.

The present article uses quantum-field relativistic-invariant Lagrangian, in which a tensor of induced dipole moments is introduced. It means that, in contrast to paper [21], this tensor depends on $F_{\mu\nu}$ [22]. In its turn, polarizabilities tensor [23, 24] is introduced to determine contributions of polarizabilities and gyrations to the low-energy Compton scattering amplitude with provision for particles spin degrees of freedom. Moreover, we take into account hermiticity requirements, algebra of spin operators and the behavior of tensor components under space and time inversion.

Such phenomenological approach allows to determine the effective relativistic-covariant Lagrangian using the relativistic field consideration of

the properties of C -, P - and T -transformations, as wells as the crossing symmetry. It also provides for conformance with the low-energy theorems for Compton scattering on spin-1 particles.

In the present paper the Lagrangian and the amplitude of Compton scattering on the spin-1 particles in the Duffin-Kemmer-Petiau formalism with consideration of their polarizabilities and gyrations were obtained in the framework of covariant theoretical and field approach. The technique presented in papers [5, 22, 25, 26] was used.

2 Determination of the spin structure of low-energy amplitude for spin-1 particle Compton scattering

We will follow the paper [27] in order to determine the contributions of polarizabilities and gyrations to the low-energy amplitude of electromagnetic field scattering on spin-1 particle. However, to calculate induced electric \vec{d} and magnetic \vec{m} moments in terms of the electric \vec{E} and magnetic \vec{H} vectors of electromagnetic field strength, we use the following formulas [2]:

$$\vec{d} = 4\pi\hat{\alpha}\vec{E} \quad (1)$$

$$\vec{m} = 4\pi\hat{\beta}\vec{H} \quad (2)$$

where $\hat{\alpha}$ and $\hat{\beta}$ are matrices, matrix-elements of which are the tensors of electric and magnetic polarizabilities. Diagonal elements of these matrices are expressed through scalar electric and magnetic polarizabilities:

$$\alpha_{ij} = \alpha_1\delta_{ij}$$

$$\beta_{ij} = \beta_1\delta_{ij}$$

Low-energy amplitude of electromagnetic field scattering that was obtained using formulas (1) and (2) can be presented in the following way [26]:

$$\begin{aligned} M(\vec{n}_2) = & 4\pi\omega^2\{(\vec{e}^{(\lambda_2)*}\hat{\alpha}\vec{e}^{(\lambda_1)}) + (\vec{n}_2\vec{e}^{(\lambda_1)})(\vec{n}_1\hat{\beta}\vec{e}^{(\lambda_2)*}) + \\ & + (\vec{n}_1\vec{e}^{(\lambda_2)*})(\vec{e}^{(\lambda_1)}\hat{\beta}\vec{n}_2) - (\vec{e}^{(\lambda_2)*}\vec{e}^{(\lambda_1)})(\vec{n}_1\hat{\beta}\vec{n}_2) - (\vec{n}_1\vec{n}_2)(\vec{e}^{(\lambda_1)}\hat{\beta}\vec{e}^{(\lambda_2)*}) + \\ & + [(\vec{n}_2\vec{n}_1)(\vec{e}^{(\lambda_2)*}\vec{e}^{(\lambda_1)}) - (\vec{n}_2\vec{e}^{(\lambda_1)})(\vec{n}_1\vec{e}^{(\lambda_2)*})]Sp(\hat{\beta})\}. \end{aligned} \quad (3)$$

Expression (3) includes the following designations: ω is the incident wave frequency, $\vec{n}_1 = \frac{\vec{k}_1}{|\vec{k}_1|}$, $\vec{e}^{(\lambda_1)}$ and \vec{k}_1 are correspondingly the polarization and wave vectors of the incident wave.

According to the definitions of \vec{d} and \vec{m} presented in (1) and (2), it follows that $\hat{\alpha}$ and $\hat{\beta}$ should satisfy the hermiticity requirement. Taking into account this requirement as well as the algebra of spin-1 operators \hat{S}_i [19] we can obtain the following:

$$[\hat{S}_i, \hat{S}_j] = i\delta_{ijk}\hat{S}_k, \quad (4)$$

$$\hat{S}_i\hat{S}_j\hat{S}_k = i\delta_{ijk} + \frac{1}{2}(\hat{S}_i\delta_{jk} + \hat{S}_k\delta_{ij}) + \frac{i}{2}\delta_{ikl}(\hat{S}_j\hat{S}_l + \hat{S}_l\hat{S}_j) \quad (5)$$

$\hat{\alpha}$ and $\hat{\beta}$ operators can be presented in the following way [26]:

$$\alpha_{ij} = \alpha_1\delta_{ij} + i\alpha_2\delta_{ijk}\hat{S}_k + i\chi_E\delta_{ijk}\partial_k + \bar{\alpha}(\hat{S}_i\hat{S}_j + \hat{S}_j\hat{S}_i), \quad (6)$$

$$\beta_{ij} = \beta_1\delta_{ij} + i\beta_2\delta_{ijk}\hat{S}_k + i\chi_M\delta_{ijk}\partial_k + \bar{\beta}(\hat{S}_i\hat{S}_j + \hat{S}_j\hat{S}_i), \quad (7)$$

where i, j, k and l can take the value of 1, 2 or 3, while δ_{ijk} - is the three-dimensional Levi-Civita tensor.

In formulas (6) and (7) α_1 and β_1 are scalar dipole electric and magnetic polarizabilities correspondingly, $\bar{\alpha}$ and $\bar{\beta}$ are tensor polarizabilities, α_2 and β_2 are spin dipole polarizabilities, while χ_E and χ_M are correspondingly electric and magnetic gyrations. As a consequence of crossing symmetry, α_2 , β_2 and χ_E , χ_M have non-zero contribution to the amplitude of Compton scattering in the third expansion order of the photons energy.

As it was shown in [26], by substituting formulas (6) and (7) into (3) and taking into account the contributions of α , β , $\bar{\alpha}$ and $\bar{\beta}$ polarizabilities, one can obtain the scattering amplitude in the second expansion order of the photons energy. It coincides with beyond the Born part of the amplitude and is due to the low-energy theorem [19].

Lets determine relativistic-invariant spin structures of the effective Lagrangian and the amplitudes of Compton scattering on spin-1 particles with the help of covariant representation of (6) and (7) in the Duffin-Kemmer-Petiau (DKP) formalism following paper [26].

The DKP equations for an unbounded spin-1 particle have the following form [28]:

$$(\beta_\mu\vec{\partial}_\mu + m)\psi(x) = 0, \quad (8)$$

$$\bar{\psi}(x)(\beta_\mu \vec{\partial}_\mu - m) = 0, \quad (9)$$

where $\psi(x)$ and $\bar{\psi}(x) = \psi^\dagger(x)\eta$ are ten-dimensional functions of particles, $\eta = 2(\beta_4^{(10)})^2 - I$, vectors over derivatives ∂_μ show the direction of their action, while four-dimensional vector is defined as $a_\mu\{\vec{a}, ia_0\}$. In formulas (8) and (9) β_μ are ten-dimensional DKP matrices that satisfy the following commutation rules:

$$\beta_\mu\beta_\nu\beta_\rho + \beta_\rho\beta_\nu\beta_\mu = \delta_{\mu\nu}\beta_\rho + \delta_{\rho\nu}\beta_\mu.$$

In the framework of theoretical and field covariant approach the effective Lagrangian of interaction between electromagnetic field and spin-1 particle with provision for polarizabilities has the form [5, 8, 26]:

$$L = -\frac{\pi}{2m}\bar{\psi}[\beta_\nu\hat{L}_{\nu\sigma} \overset{\leftrightarrow}{\partial}_\sigma + \hat{L}_{\nu\sigma}\beta_\nu \overset{\leftrightarrow}{\partial}_\sigma]\psi \quad (10)$$

where $\overset{\leftrightarrow}{\partial}_\sigma = \overset{\rightarrow}{\partial}_\sigma - \overset{\leftarrow}{\partial}_\sigma$.

The formula (10) for the Lagrangian includes tensor $\hat{L}_{\nu\sigma}$, which is expressed in terms of polarizabilities and gyrations as:

$$\hat{L}_{\nu\sigma}(\alpha, \chi_E) = \hat{L}_{\nu\sigma}(\alpha_1) + \hat{L}_{\nu\sigma}(\bar{\alpha}) + \hat{L}_{\nu\sigma}(\alpha_2) + \hat{L}_{\nu\sigma}(\chi_E), \quad (11)$$

$$\hat{L}_{\nu\sigma}(\beta, \chi_M) = \hat{L}_{\nu\sigma}(\beta_1) + \hat{L}_{\nu\sigma}(\bar{\beta}) + \hat{L}_{\nu\sigma}(\beta_2) + \hat{L}_{\nu\sigma}(\chi_M), \quad (12)$$

In order to determine the influence of crossing symmetry on the contributions of spin polarizabilities and gyrations to the Compton scattering amplitude in dipole representation we will transform tensors (11) as (see [22]):

$$\hat{L}_{\nu\sigma}(\alpha_1) + \hat{L}_{\nu\sigma}(\bar{\alpha}) = F_{\nu\mu}\hat{\alpha}^{\mu\rho}(\alpha_1)F_{\rho\sigma} + F_{\nu\mu}\hat{\alpha}^{\mu\rho}(\bar{\alpha})F_{\rho\sigma}, \quad (13)$$

$$\hat{L}_{\nu\sigma}(\alpha_2) + \hat{L}_{\nu\sigma}(\chi_E) = F_{\nu\mu} \overset{\leftrightarrow}{\partial}_\lambda F_{\rho\sigma}\hat{k}_{\mu\rho\lambda}(\alpha_2) + F_{\nu\mu} \overset{\leftrightarrow}{\partial}_\lambda F_{\rho\sigma}\hat{k}_{\mu\rho\lambda}(\chi_E). \quad (14)$$

Derivatives in equation (14) operate only on the tensors of electromagnetic field

$$F_{\mu\nu} = \partial_\mu A_\nu - \partial_\nu A_\mu.$$

Tensors $\hat{\alpha}^{\mu\rho}(\alpha_1)$ and $\hat{\alpha}^{\mu\rho}(\bar{\alpha})$, as well as $\hat{k}_{\mu\rho\lambda}(\alpha_2)$ and $\hat{k}_{\mu\rho\lambda}(\chi_E)$ are the covariant generalization of tensors that appear in the right part of formula (6). They have the following form:

$$\hat{\alpha}_{\mu\rho} = \alpha_1\delta_{\mu\rho} + \bar{\alpha}(\widehat{W}_\mu\widehat{W}_\rho + \widehat{W}_\rho\widehat{W}_\mu), \quad (15)$$

$$\hat{k}_{\mu\rho\lambda} = \frac{i\alpha_2}{2m}\delta_{\mu\rho\lambda k}\widehat{W}_k + \frac{i\chi_E}{2m}\delta_{\mu\rho\lambda k} \leftrightarrow \partial_k \quad (16)$$

In equations (15) and (16) the definition of covariant spin vector is used. This vector can be expressed in terms of β_ν matrices (see [28]):

$$W_\mu = -\frac{i}{4m}\delta_{\mu\chi\delta\eta}\hat{J}^{[\delta\eta]} \leftrightarrow \partial_\chi,$$

where $\hat{J}^{[\delta\eta]} = \beta_\delta\beta_\eta - \beta_\eta\beta_\delta$. All derivatives found in (15) and (16) operate on wave functions ψ and $\bar{\psi}$.

Tensor (12) is defined in a similar way. One just needs to introduce constants $\beta_1, \beta_2, \bar{\beta}$ and χ_M , in formulas (13)-(14) and make a replacement

$$F_{\nu\mu} \rightarrow \tilde{F}_{\nu\mu},$$

where

$$\tilde{F}_{\mu\nu} = \frac{i}{2}\delta_{\mu\nu\rho\sigma}F_{\rho\sigma}.$$

Lets now determine the spin structures of the amplitude of Compton scattering on spin-1 particle with provision for polarizabilities and gyrations. We will take Lagrangian (10) as a basis and follow the procedure presented in paper [28]:

$$\langle k_2, p_2 | \hat{S} | k_1, p_1 \rangle = \frac{im\delta(k_1 + p_1 - k_2 - p_2)}{(2\pi)^2\sqrt{4\omega_1\omega_2 E_1 E_2}} M, \quad (17)$$

here M is the Compton scattering amplitude that represents the sum of polarizabilities and gyrations contributions according to formulas (11) and (12).

As it was shown in [26], the contribution of α, β and $\bar{\alpha}, \bar{\beta}$ is expressed as a sum of amplitudes

$$M_1 = M_1(\alpha, \beta) + M_1(\bar{\alpha}, \bar{\beta}). \quad (18)$$

Spin structure $M(\alpha, \beta)$ in equation (18) has the following form:

$$\begin{aligned} M_1(\alpha, \beta) = & \left(-\frac{2\pi i}{m} \right) \left\{ \alpha [F_{\nu\mu}^{(2)} F_{\mu\sigma}^{(1)} + F_{\nu\mu}^{(1)} F_{\mu\sigma}^{(2)}] + \right. \\ & \left. + \beta [\tilde{F}_{\nu\mu}^{(2)} \tilde{F}_{\mu\sigma}^{(1)} + \tilde{F}_{\nu\mu}^{(1)} \tilde{F}_{\mu\sigma}^{(2)}] \right\} P_\sigma \bar{\psi}^{(r_2)}(p_2) \beta_\nu \psi^{(r_1)}(p_1). \end{aligned} \quad (19)$$

In its turn, structure $M(\bar{\alpha}, \bar{\beta})$ is determined as:

$$M_1(\bar{\alpha}, \bar{\beta}) = \left(-\frac{\pi i}{m} \right) \left\{ \bar{\alpha} [F_{\nu\mu}^{(2)} F_{\mu\sigma}^{(1)} + F_{\nu\mu}^{(1)} F_{\mu\sigma}^{(2)}] + \right. \quad (20)$$

$$\left. + \bar{\beta} [\tilde{F}_{\nu\mu}^{(2)} \tilde{F}_{\mu\sigma}^{(1)} + \tilde{F}_{\nu\mu}^{(1)} \tilde{F}_{\mu\sigma}^{(2)}] \right\} P_\sigma \bar{\psi}^{(r_2)}(p_2) [\beta_\nu \{ \widehat{W}_\mu, \widehat{W}_\rho \} + \{ \widehat{W}_\mu, \widehat{W}_\rho \} \beta_\nu] \psi^{(r_1)}(p_1).$$

Equations (19) and (20) include the following designations:

$$F_{\nu\mu}^{(2)} = k_{2\nu} e_\mu^{(\lambda_2)*} - k_{2\mu} e_\nu^{(\lambda_2)*},$$

$$F_{\mu\sigma}^{(1)} = k_{1\mu} e_\sigma^{(\lambda_1)} - k_{1\sigma} e_\mu^{(\lambda_1)},$$

where $\tilde{F}_{\nu\mu}^{(2)} = \frac{i}{2} \delta_{\nu\mu\chi\delta} F_{\chi\delta}^{(2)}$, $P_\sigma = \frac{1}{2}(p_1 + p_2)_\sigma$, p_1 and p_2 are the momenta of initial and final spin-1 particles correspondingly.

Ten-dimensional wave functions in the DKP formalism are introduced using complete matrix algebra elements ε^{AB} [28]

$$\psi^{(r)}(p) = \psi_\mu^{(r)}(p) \varepsilon^{\mu 1} + \frac{1}{2} \psi_{[\mu\nu]}^{(r)}(p) \varepsilon^{[\mu\nu] 1}.$$

In this formula

$$\psi_\mu^{(r)}(p) = \frac{i}{\sqrt{2}} \lambda_\mu^{(r)},$$

$$\psi_{[\mu\nu]}^{(r)}(p) = -\frac{1}{\sqrt{2m}} \left(p_\mu \lambda_\nu^{(r)} - \lambda_\mu^{(r)} p_\nu \right),$$

$\lambda_\mu^{(r)}$ are the components of polarization vectors of spin-1 particle, while ε^{AB} are the elements of complete matrix algebra [28]:

$$(\varepsilon^{AB})_{CD} = \delta_{AC} \delta_{BD}, \quad \varepsilon^{AB} \varepsilon^{CD} = \delta_{BC} \varepsilon^{AD},$$

where for spin-1 particle indices $A, B, C, D = \mu, [\rho\sigma]$, while square brackets stand for the anti-symmetry with respect to indices ρ and σ .

Wave functions $\bar{\psi}^{(r)}(p)$ that are conjugate with respect to $\psi^{(r)}(p)$ are expressed in the following way (taking into account η matrix):

$$\bar{\psi}^{(r)}(p) = \psi^+(p) \eta = \left(-\frac{i}{\sqrt{2}} \right) \left[\dot{\lambda}_\mu^{(r)} \varepsilon^{1\mu} + \frac{i}{2m} \varepsilon^{1[\mu\nu]} (p_\mu \dot{\lambda}_\nu^{(r)} - p_\nu \dot{\lambda}_\mu^{(r)}) \right],$$

where $\dot{\lambda}_\mu^{(r)} \{ \lambda_i^{(r)*}, \lambda_4^{(r)} \}$.

Let's now determine the spin structures of the amplitudes with provision for the contributions of spin polarizabilities α_2, β_2 and gyrations χ_E, χ_M , i.e.

$$M_2 = M_2(\alpha, \beta) + M_2(\chi_E, \chi_M).$$

Using the summands $\hat{L}_{\nu\sigma}(\alpha_2), \hat{L}_{\nu\sigma}(\chi_E), \hat{L}_{\nu\sigma}(\beta_2)$ (11) and $\hat{L}_{\nu\sigma}(\chi_M)$ (12), of the Lagrangian, as well as the previous technique for determination of polarizations contributions to the Compton scattering amplitude, one can find:

$$M_2(\alpha_2, \beta_2) = \frac{\pi}{m}(k_1 + k_2)_\lambda \delta_{\mu\rho\lambda k} \left\{ \alpha_2 [F_{\nu\mu}^{(2)} F_{\rho\sigma}^{(1)} - F_{\nu\mu}^{(1)} F_{\rho\sigma}^{(2)}] + \right. \quad (21)$$

$$\left. + \beta_2 [\tilde{F}_{\nu\mu}^{(2)} \tilde{F}_{\rho\sigma}^{(1)} - \tilde{F}_{\nu\mu}^{(1)} \tilde{F}_{\rho\sigma}^{(2)}] \right\} \bar{\psi}^{(r_2)}(p_2) [\beta_\nu \widehat{W}_k + \widehat{W}_k \beta_\nu] P_\sigma \psi^{(r_1)}(p_1).$$

Amplitude (21) in the targets rest frame and with the neglect of the target particles recoil can be expressed as:

$$M_2(\alpha_2, \beta_2) = 4i\pi(\omega_1 + \omega_2)\omega_1\omega_2 \bar{\lambda}^{(r_2)*} \left\{ \alpha_2 (\vec{S}[\vec{e}^{(\lambda_2)*} \vec{e}^{(\lambda_1)}]) + \right. \quad (22)$$

$$\left. + \beta_2 \vec{S}[\vec{n}_2 \vec{e}^{(\lambda_2)*}] [\vec{n}_1 \vec{e}^{(\lambda_1)}] \right\} \bar{\lambda}^{(r_1)}.$$

Formulas (21) and (22) imply that dipole spin polarizabilities α_2 and β_2 contribute to the amplitude of Compton scattering on spin-1 particle in the third expansion order (series expansion in the energy of photons), while the crossing symmetry requirements and parity conservation (with respect to space inversion) rules are satisfied.

Using the above-introduced technique for constructing covariant blocks of the effective Lagrangian with provision for the crossing symmetry and parity violation, we can obtain the second summand of the amplitude that depends on the contributions of electric and magnetic gyrations:

$$M_2(\chi_E, \chi_M) = \frac{2i\pi}{m^2}(k_1 + k_2)_\lambda \delta_{\mu\rho\lambda k} \left\{ \chi_E [F_{\nu\mu}^{(2)} F_{\rho\sigma}^{(1)} - F_{\nu\mu}^{(1)} F_{\rho\sigma}^{(2)}] + \right. \quad (23)$$

$$\left. + \chi_M [\tilde{F}_{\nu\mu}^{(2)} \tilde{F}_{\rho\sigma}^{(1)} - \tilde{F}_{\nu\mu}^{(1)} \tilde{F}_{\rho\sigma}^{(2)}] \right\} P_k P_\sigma \bar{\psi}^{(r_2)}(p_2) \beta_\nu \psi^{(r_1)}(p_1).$$

If we use approximation $\vec{P} = 0$, in equation (23), i.e. we consider the particle to be at rest and neglect its recoil momentum, the formula (23) can be rewritten in the following way:

$$M_2(\chi_E, \chi_M) = 4\pi\omega_1\omega_2 (\bar{\lambda}^{(r_2)*} \bar{\lambda}^{(r_1)}) \left\{ \chi_E (\vec{k}_1 + \vec{k}_2) [\vec{e}^{(\lambda_2)*} \vec{e}^{(\lambda_1)}] + \right. \quad (24)$$

$$\left. + \chi_M (\vec{k}_1 + \vec{k}_2) [\vec{\Sigma}_2 \vec{\Sigma}_1] \right\},$$

where $\vec{\Sigma}_2 = [\vec{n}_2 \vec{e}^{(\lambda_2)*}]$, $\vec{\Sigma}_1 = [\vec{n}_1 \vec{e}^{(\lambda_1)}]$.

3 Conclusion

Hence, we determined the contributions of polarizabilities to the low-energy Compton scattering amplitude with provision for the spin degrees of freedom of particles by transforming the polarizabilities tensor that satisfies both hermiticity requirement and spin algebra. This tensor is also invariant with respect to space inversion transformations.

The relativistic-covariant form of contributions of spin and tensor polarizabilities, as well as gyrations to the Compton scattering amplitude in the DKP formalism was found.

The effective Lagrangian that takes into account the changes of spin structures during space inversion transformations and considers the crossing symmetry of Compton scattering amplitude on spin-1 particle was obtained in the DKP formalism using theoretical and field relativistic generalization. The coordination of this amplitude with the low-energy theorems was performed as well.

References

- [1] Maksimenko, N. V. Phenomenological description of the polarizability of elementary particles in the field theory / Maksimenko, N. V. and Moroz, L. G. // Proc. of the XI-th International School of Young Scientists in High Energy Physics and Relativistic Nuclear Physics [in Russian], D2-11707, Joint Institute for Nuclear Research, Dubna (1979), pp. 533–543.
- [2] Fedorov, F. I. Theory of Gyrotropy [in Russian], Nauka i Tekhnika, Minsk (1976).
- [3] Bedaque, P. F. Parity violation in p Compton Scattering / P. F. Bedaque, M. J. Savage // Phys. Rev. C. 2000 V. 62 P. 018501 1–6.
- [4] Gorchtein, M. Forward Compton Scattering with neutral current: constraints from sum rules / M. Gorchtein, X. Zhang [Electronic resource]. 2015. Mode of access: <http://nucl-th/1501.0535v1>. Date of access: 22.01.2015.
- [5] Maksimenko, N. V. Covariant definition polarizability of hadrons with spin one // Doklady Akad. Of Sciences BSSR, Ser. Fiz.-Mat. Navuk, No. 6, 508–510 (1992).

- [6] Levchuk, M. I. The nucleon gyration as one of nucleon electromagnetic structure characteristics / M. I. Levchuk, L. G. Moroz // Proc. Academy of Sciences of BSSR. Ser. fiz.-mat.navuk. 1985. No. 1. P. 45–54.
- [7] Bogush, A. A., Kisel, V. V., and Moroz, L. G. On the description of the polarizability of scalar particles in the theory of relativistic wave equations in: Covariant Methods in Theoretical Physics. Physics of Elementary Particles and Theory of Relativity, [in Russian], Minsk (1981), pp. 81–90.
- [8] Andreev, V. V., Maksimenko, N. V. Polarizability of elementary particles in the theoretical-field approach // Problems of Physics, Mathematics and Technics. 2011. No. 4 (9). pp. 7–11.
- [9] Maksimenko, N. V., Deryuzhkova, O. M. Covariant gauge-invariant Lagrangian formalism taking into account polarizability of the particle // Vestsi NAN Belarusi, Ser. Fiz.-Mat. Navuk, No. 2, pp. 27–30 (2011).
- [10] Ilyichev, A. Static polarizability vertex and its applications / A. Ilyichev, S. Lukashevich, N. Maksimenko // [Electronic resource]. 2006. Mode of access: arXiv: //hep-ph/0611327v1. Date of access: 27.11.2006.
- [11] Zhang, Y. Proton Compton scattering in a unified proton - Δ^+ Model / Y. Zhang, K. Savvidy // Phys. Rev. C. 2013. Vol. 88. P. 064614-1–12.
- [12] Holstein, B. R. Hadron polarizabilities / B. R. Holstein, S. Scherer. [Electronic resource]. 2013. Mode of access: <http://hep-ph/1401.0140v1>. Date of access: 31.12.2013].
- [13] Carlson, C. E. Constraining off-shell effects using low-energy Compton scattering / C. E. Carlson, M. Vanderhaeghen // [Electronic resource]. 2011. Mode of access: <http://physics.atom-ph/1109.3779>. Date of access: 04.10.2011.
- [14] Raguza, S. Third-order spin polarizabilities of the nucleon: I / S. Raguza // Phys. Rev. D. 1993. Vol. 47. - 9. P. 3757–3767.

- [15] Raguza, S. Third-order spin polarizabilities of the nucleon: II / S. Raguza // *Phys. Rev. D.* 1994. Vol. 49. - 7. P. 3157–3159.
- [16] Low-energy Compton scattering of polarized photons on polarized nucleons / D. Babusci [et. al.] // *Rev. C.* 1998. Vol. 58. P. 1013–1041.
- [17] Chen, J. W. The polarizability of the deuteron / J. W. Chen [et. al.] // *Nucl. Phys. A.* 1998. Vol. 644. P. 221–234.
- [18] Friar, J. L. Deuteron dipole polarizability and sum rules / J. L. Friar, G. L. Payne // *Rev. C.* 2005. Vol. 72. P. 014004–1–014004–6.
- [19] Lin, K. Y. Forward dispersion relation and low-energy theorems for Compton scattering on spin 1 targets / K. Y. Lin, J. C. Chen // *J. Phys. G: Nucl. Phys.* 1975 Vol.1 P. 394–399.
- [20] F. Hagelstein. Sum Rules for Electromagnetic Moments and Polarizabilities of Spin-1 Particles in Massive Yang-Mills QED / Masterarbeit in Physik vorgelegt dem Fachbereich Physik, Mathematik und Informatik (FB 08) der Johannes Gutenberg-Universit.at Mainz am 11. März 2014.
- [21] Anandan, J. S. Classical and quantum interaction of the dipole / J. S. Anandan // *Phys. Rev. Lett.* 2000. Vol.85. P. 1354–1357
- [22] Andreev, V. V., Deryuzhkova, O. M., and Maksimenko, N. V. The covariant representation spin polarizability of the nucleon // *Problems of Physics, Mathematics and Technics.* 2014. No. 3(20). pp. 7–12.
- [23] Galynskii, M. V., Fedorov, F. I. Transformation of the beam tensor during a light-medium interaction // *Journal of Applied Spectroscopy,* 1986, Vol. 44, No. 2, pp. 200–203.
- [24] Baryshevskii, V. G. Nuclear Optics of Polarized Media [in Russian], Energoatomizdat, Moscow (1995).
- [25] Vakulina, E. V., Maksimenko, N. V. Polarizability of the pion in the formalism of Duffin Kemmer // *Problems of Physics, Mathematics and Technics.* 2013. No. 3. pp. 16–18.

- [26] Maksimenko, N.V. Spin 1 Particle Polarizability in the Duffin-Kemmer-Petiau Formalism // N.V. Maksimenko, E.V. Vakulina, S.M. Kuchin // Physics of Particles and Nuclei Letters.- 2015. - Vol. 12, No.7, P. 807–812.
- [27] Landau, L. D., Lifshitz, E. M. Course of Theoretical Physics. Volume 2. The Classical Theory of Fields 4 Edition. Butterworth-Heinemann, 1975. 402 p. Series: Course of Theoretical Physics Series (Book 2).
- [28] Bogush, A. A. Introduction to Gauge Field Theory of Electroweak Interactions [in Russian], Nauka i Tekhnika, Minsk (1987).

Corrections to the Formula for Baryshevsky-Luboshitz Effect in Magnetic Field

A.I. Sery*

Brest State A.S. Pushkin University

Abstract

In the framework of tree approximation a correction is obtained to the formula for Baryshevsky-Luboshitz rotation of the plane of linear polarization of a photon in electron gas with high degree of spin polarization of electrons in magnetic field. The frequency of photon is considered to be of the same order as the cyclotron frequency.

1 Introduction

The effect of rotation of the plane of polarization of X- and gamma-photons on spin-polarized electrons was theoretically predicted by V.G. Baryshevsky and V.L. Luboshitz in 1965 and experimentally tested at early 1970s [1, 2, 3, 4]. The effect was considered for the case when the frequency of photon was much greater than the cyclotron frequency. The effect is possible due to the dependence of Compton scattering forward amplitudes on the relative direction of spins of photon and electron. The effect is important in studying white dwarfs and neutron stars, namely, their magnetic fields and the structures of their atmospheres.

*E-mail:alexey_sery@mail.ru

2 The contribution of Faraday effect

Baryshevsky-Lubositz effect differs from another type of rotation of the plane of polarization of photons known as Faraday effect. The main differences between 2 effects are presented in Table 1.

Table 1 - The difference between Faraday and Baryshevsky-Lubositz effect.

Effect	Faraday	Baryshevsky-Lubositz
Based on	Zeeman effect	the dependence of Compton scattering forward amplitude on the directions of electron and photon spins
Spectral region	radio and visible	hard X and gamma
Can electrons be regarded as free	no	yes
Is spin polarization of electrons necessary	no	yes

The conditions for Faraday effect change significantly in the atmospheres of white dwarfs and neutron stars in comparison with terrestrial conditions because the atomic structure of matter can be destroyed by strong magnetic fields. The meaning of the term "Faraday effect" also changes (see Table 2 for details).

Table 2 - Different variants of Faraday effect.

Variant	Classic	Non-classic
1. Atomic structure	exists	doesn't exist
2a. Electron energy levels are	discrete	discrete-continuous
2b. Quantizing	Bohr-like	Landau
3. Spin degrees of freedom	are not involved	are not involved
4. Ionization at $B \ll 10^9$ Gs	is to be low	is to be high
5a. Can the effect take place at $B \geq 10^9$ Gs	no because condition 1 is not fulfilled	yes
5b. That's why at $B \geq 10^9$ Gs Baryshevsky-Luboshitz effect	is the only type of rotation	exists together with Faraday effect

In non-classic case, it's hard to consider 2 effects separately at $\hbar\omega \approx 2\mu_B B$, but Baryshevsky-Luboshitz effect dominates far from resonances (see also Table 3). The general meaning of the term "Faraday effect" includes both classic and non-classic cases.

Table 3 - Baryshevsky-Lubositz effect at different conditions.

Photon energy	$\hbar\omega \gg 2\mu_B B$	$\hbar\omega \approx 2\mu_B B$
The influence of magnetic field on the effect	can be neglected	is considerable
Spin polarization of electrons is	less then 8% in iron (experiments of 1970s)	expected to be almost 100% in astrophysics in strong magnetic fields
The order of perturbation theory on $e^2/(\hbar c)$	2	1

Baryshevsky-Lubositz effect has also some similar aspects with Baryshevsky-Podgoretsky effect [1] (see Table 4 for details).

Table 4 - Baryshevsky-Lubositz and Baryshevsky-Podgoretsky effects.

Effect	Baryshevsky-Lubositz	Baryshevsky-Podgoretsky
Particle	photon	neutron
Moving	in spin-polarized electron gas	among spin-polarized nuclei
Is spin polarization necessary	yes	yes
What takes place	rotation of the plane of linear polarization of the photon	spin precession of the neutron
Based on	the dependence of Compton scattering forward amplitude on the directions of electron and photon spins	the dependence of scattering forward amplitude on the directions of neutron and nuclear spins
Interaction	electromagnetic	strong (nuclear)
At resonances the value of	rotation changes its sign	precession changes its sign

3 General formula

In [5, 6], using the approach of [7], a formula was obtained for the calculation of Baryshevsky-Lubositz rotation angle of the plane of linear polarization of photons per unit path in electron gas with total spin polarization of electrons ($p_{0e} = 1$). After some simple rearrangements it can be written in the form:

$$\frac{d\varphi}{dl} = \frac{\pi n_e c \alpha \varepsilon_0}{\omega(\varepsilon_0 + \hbar\omega)} (E^{(+)} - E^{(-)}) Re \left(\int_{-\infty}^{+\infty} \int_{-\infty}^{+\infty} dx_1 dx_2 \bar{\Psi}_0(\xi_1) Q_{\mu\nu} \Psi_0(\xi_2) \right), \quad (1)$$

where

$$\begin{aligned} E^{(\pm)} &= e_{\mu}^{(\pm)} e_{\nu}^{\prime(\pm)*}, \varepsilon_0^2 = m^2 c^4 + p_z^2 c^2, e^{(\pm)} = \frac{1}{\sqrt{2}} \begin{bmatrix} 0 & \mp i & \cos \theta & -\sin \theta \end{bmatrix}^T, \\ \Psi_0(x) &= \frac{i\sqrt{Be}}{\sqrt{2\varepsilon_0(\varepsilon_0 + mc^2)}\sqrt{Bec\hbar}} \exp\left(-\frac{x^2}{2}\right) \begin{bmatrix} 0 & -mc^2 - \varepsilon_0 & 0 & p_z c \end{bmatrix}^T, \\ \alpha &= \frac{e^2}{\hbar c}, j_k(p) = \sqrt{\frac{eB}{\hbar c}} \left(x_k + \frac{cp}{eB}\right), \xi_k = j_k(p_y), \rho_k = j_k(g_2), \eta_k = j_k(f_2), \\ Q_{\mu\nu} &= \gamma_{\nu} G_B(g, \rho) \gamma_{\mu} + \gamma_{\mu} G_B(f, \eta) \gamma_{\nu}, \beta_1 = \frac{1}{2}(1 + i\gamma_2 \gamma_1), \beta_2 = \frac{1}{2}(1 - i\gamma_2 \gamma_1), \\ cg_0 &= \varepsilon_0 + \hbar\omega, cg_3 = p_z c + \hbar\omega \cos \theta, cf_0 = \varepsilon_0 - \hbar\omega, cf_3 = p_z c - \hbar\omega \cos \theta, \\ Y &= \gamma_0 \lambda_0 - \gamma_3 \lambda_3 + mc, G_B(\lambda, x) = \sqrt{\frac{Be}{c\hbar}} \sum_{n=0}^{\infty} \frac{\hbar c^2}{c^2 \lambda_0^2 - \varepsilon_{n\lambda}^2} D, \\ D &= U_n(x_1) U_n(x_2) Y \beta_1 + (1 - \delta_{0n}) U_{n-1}(x_1) U_{n-1}(x_2) Y \beta_2 + \\ &+ (1 - \delta_{0n}) i \sqrt{\frac{2neB\hbar}{c}} (U_{n-1}(x_1) U_n(x_2) \gamma_1 \beta_1 - U_n(x_1) U_{n-1}(x_2) \beta_1 \gamma_1), \\ \varepsilon_{ng} &\approx \sqrt{m^2 c^4 + 2ne\hbar Bc + g_3^2 c^2} - i \frac{8(2n-1)\alpha(\mu_B B)^2}{3mc^2}, \\ \varepsilon_{nf} &\approx \sqrt{m^2 c^4 + 2ne\hbar Bc + f_3^2 c^2} \end{aligned} \quad (2)$$

Here n_e is electron density, m, p_z are electron's mass and momentum along z axis, respectively; μ_B is Bohr magneton, e is electric charge, $\hbar\omega$ is photon's energy, \vec{B} is magnetic field strength, θ is the angle between the wave

vector of photon \vec{k} and \vec{B} . Transposing is denoted by T . Dirac matrices γ_k ($k = 0, 1, 2, 3$) are in standard presentation. $\varepsilon_{n\lambda}$ is energy of virtual electron on intermediate n th Landau level.

4 Summation over μ, ν

Nonzero contributions in (1) correspond to 2 cases: 1) $\mu = 1, \nu = 2$ and $\mu = 2, \nu = 1$; 2) $\mu = 1, \nu = 3$ and $\mu = 3, \nu = 1$. Only the first case was considered in [6] with the following result:

$$\begin{aligned} \frac{d\varphi}{dl} &= \frac{(\pi\hbar c)^2 n_e \alpha \cos\theta}{\hbar\omega(\varepsilon_0 + \hbar\omega)} \exp\left(-\frac{\phi}{2}\right) \sum_{n=1}^{\infty} \phi^{n-1} \text{Re}(\Xi_n(g) - \Xi_n(f)), \\ \phi &= \frac{\hbar\omega^2 \sin^2\theta}{cBe}, \quad \Xi_n(\lambda) = \frac{c\lambda_0\varepsilon_0 - \lambda_3 p_z c^2 - m^2 c^4}{c^2\lambda_0^2 - \varepsilon_{n\lambda}^2}. \end{aligned} \quad (3)$$

Considering both cases, one obtains:

$$\begin{aligned} \frac{d\varphi}{dl} &= \frac{(\pi\hbar c)^2 n_e \alpha}{\hbar\omega(\varepsilon_0 + \hbar\omega)} \exp\left(-\frac{\phi}{2}\right) \sum_{n=1}^{\infty} \phi^{n-1} \text{Re}(\Xi_n^{(+)}(g, \theta) - \Xi_n^{(-)}(f, \theta)), \\ \Xi_n^{(\pm)}(\lambda, \theta) &= \frac{(c\lambda_0\varepsilon_0 - m^2 c^4) \cos\theta - p_z c(c\lambda_3 \cos\theta \pm \sqrt{2n\hbar\omega} \sin^2\theta)}{c^2\lambda_0^2 - \varepsilon_{n\lambda}^2}. \end{aligned} \quad (4)$$

The numerical results for (3) and (4) coincide at $p_z = 0$ approximation.

5 Averaging over momenta at T=0 K

The result (3) was averaged over electron momenta p_z at T=0 K in [6]. The same averaging of (4) gives:

$$\begin{aligned} \frac{d\varphi}{dl} &= \frac{e^2 m \mu_B B}{4\hbar^3 \omega} \exp\left(-\frac{\phi}{2}\right) \sum_{n=1}^{\infty} \phi^{n-1} (R_n - S_n), \\ R_n &= \int_{-w_1}^{w_1} \frac{f_1(w) (f_2(w) \cos\theta - 2\sqrt{2nw} \sin^2\theta) dw}{f_3(w) \left(f_1^2(w) + \frac{\Gamma_n^2}{\hbar^2 \omega^2} \left(1 + 4n \frac{\mu_B B}{mc^2} + (w + t \cos\theta)^2 \right) \right)}, \\ S_n &= \int_{-w_1}^{w_1} \frac{(-f_2(w) \cos\theta + 2\sqrt{2nw} \sin^2\theta) dw}{f_3(w) (Q_n - f_2(w))}, \quad Q_n = t \sin^2\theta - 4n \frac{\mu_B B}{\hbar\omega}, \end{aligned}$$

$$\begin{aligned}
f_1(w) &= Q_n + f_2(w) + \frac{\Gamma_n^2}{4\hbar\omega mc^2}, f_2(w) = 2(\sqrt{1+w^2} - w\cos\theta), \\
f_3(w) &= \sqrt{1+w^2} + t, t = \frac{\hbar\omega}{mc^2}, w = \frac{p_z}{mc}, w_1 = \frac{\pi^2(\hbar c)^3 n_e}{(mc^2)^2 \mu_B B}. \quad (5)
\end{aligned}$$

Similarly to [6], the integrals can be taken numerically or analytically. The following notations will be used:

$$\begin{aligned}
\xi_n &= -\frac{4\cos\theta}{2+Q_n}, q_n = \frac{2-Q_n}{2+Q_n}, \nu_n = 4y_1^2 - \xi_n^2, \mu_n = 4q_n - \xi_n^2, \\
\tau_{n\pm} &= \xi_n \pm 2y_1, y_1 = \frac{w_1 + \sqrt{1+w_1^2} - 1}{w_1 + \sqrt{1+w_1^2} + 1}, \\
Y_n &= \left(\arctan\left(\frac{\tau_{n+}}{\sqrt{|\mu_n|}}\right) - \arctan\left(\frac{\tau_{n-}}{\sqrt{|\mu_n|}}\right) \right) \tilde{\theta}(\mu_n) + \\
&\quad + \ln \left| \frac{(2y_1 - \sqrt{|\mu_n|})^2 - \xi_n^2}{(2y_1 + \sqrt{|\mu_n|})^2 - \xi_n^2} \right| \tilde{\theta}(-\mu_n) \quad (6)
\end{aligned}$$

Here $\tilde{\theta}(\eta)$ is Heaviside function. Then for S_n -terms one obtains (analytical expressions for R_n -terms are very complicated):

$$\begin{aligned}
S_n &= \frac{\sqrt{2n}}{\cos\theta} \left(\tilde{I}_{1n} \sin^2\theta + 2\tilde{I}_{2n} - (Q_n + 2t) I_n \sin^2\theta \right) + \\
&\quad + \left(\tilde{I}_{1n} - Q_n I_n \right) \cos\theta, \\
\tilde{I}_{1n} &= 2 \ln \left(w_1 + \sqrt{w_1^2 + 1} \right) - \frac{4t}{\sqrt{1-t^2}} \arctan \left(y_1 \sqrt{\frac{1-t}{1+t}} \right), \\
\tilde{I}_{2n} &= -\frac{1 + \cos^2\theta}{2 \cos\theta} \ln \left| \frac{1 - y_1 \cos\theta}{1 + y_1 \cos\theta} \right| - \ln \left| \frac{1 + y_1}{1 - y_1} \right|, Q_n = -2; \\
\tilde{I}_{2n} &= \frac{8y_1}{\nu_n} \left(\frac{2 \sin^2\theta}{2 + Q_n} + q_n \right) - \ln \left| \frac{1 + y_1}{1 - y_1} \right| \\
&\quad - \frac{4\xi_n y_1}{\nu_n} \cos\theta - \ln \left| \frac{\tau_{n+}}{\tau_{n-}} \right| \cos\theta, Q_n \neq -2, \mu_n = 0; \\
\tilde{I}_{2n} &= \left(\xi_n \cos\theta - 2 \left(\frac{2 \sin^2\theta}{2 + Q_n} + q_n \right) \right) \frac{Y_n}{\sqrt{|\mu_n|}} - \ln \left| \frac{1 + y_1}{1 - y_1} \right| - \\
&\quad - \frac{1}{2} \ln \left| \frac{y_1^2 + \xi_n y_1 + q_n}{y_1^2 - \xi_n y_1 + q_n} \right| \cos\theta, Q_n \neq -2, \mu_n \neq 0. \quad (7)
\end{aligned}$$

The expressions for I_n were presented in [6].

6 Numerical results

Some numerical results are compared in Table 5.

Table 5 - The angle of rotation calculated: I) according to (3) and (4) in $p_z = 0$ approximation; II) according to (5) at $n_e = 10^{22} \text{ cm}^{-3}$.

θ , deg	$B = 10^{13} \text{ Gs}$			$B = 4 \cdot 10^{13} \text{ Gs}$		
	$\hbar\omega$, MeV	I	II	$\hbar\omega$, MeV	I	II
30	0.1125	-609.8	-609.4	0.4168	-16.3	-16.2
45	0.1097	-490.4	-490.3	0.3864	-13.4	-13.3
60	0.1072	-342.1	-342.0	0.3629	-9.5	-9.4

The difference between the result for (5) and the corresponding result in [6] is less than 10^{-10} rad/cm , i.e. much less than the accuracy of the results obtained in the first order of perturbation theory on α .

7 Summary. The main results

In the framework of tree approximation a correction is obtained to the formula for Baryshevsky-Lubositz rotation of the plane of linear polarization of a photon in electron gas with high degree of spin polarization of electrons in magnetic field. The frequency of photon is considered to be of the same order as the cyclotron frequency. The numerical difference between the $p_z = 0$ approximation and the averaging on p_z is small. The numerical contribution of $\mu = 1, \nu = 3$ and $\mu = 3, \nu = 1$ is negligibly small in comparison with the contribution of $\mu = 1, \nu = 2$ and $\mu = 2, \nu = 1$.

The research was done according to the suggestion of V.G. Baryshevsky and V.V. Tikhomirov.

References

- [1] V.G. Baryshevskii. *Nuclear Optics of Polarized Media* [in Russian] (Energoatomizdat, Moscow, 1995).
- [2] V.M. Lobashov *et al.*, [in Russian] Sov. JETP Lett. **14** (1971) 373.

- [3] V.M. Lobashov *et al.*, [in Russian] Sov. JETP **68** (1975) 1220.
- [4] P. Bock and P. Luksch, Lett. Nuovo cimento **2** (1972) 1081.
- [5] A.I. Sery. To the Problem of Compton Rotation of the plane of Polarization of X-Photons in Magnetic Field // Actual Problems of Microworld Physics: Proceedings of International School-Seminar, Gomel, Belarus, August 1 – 12, 2011, (Dubna, 2013) 230.
- [6] A.I. Sery. Resonance Width Consideration for Compton Rotation in Magnetic Field // Actual Problems of Microworld Physics: Proceedings of XII International School-Seminar, Gomel, Belarus, July 22 – August 2, 2013, (Dubna, 2015) 194.
- [7] P.I. Fomin and R.I. Kholodov, JETP. **90**, 2 (2000) 281.

3 Relativistic Physics of Hadron and Nuclei

Hadron as Coherent State on the Horosphere of the Lobachevsky Momentum Space

Y.A. Kurochkin *, Y.A. Kulchitsky, S. Harkusha
Institute of Physics, National Academy of Sciences of Belarus

N.A. Russakovich
Joint Institute for Nuclear Research, Dubna, Russian Federation

Abstract

A model of hadron (proton) as a coherent state of transverse excitations in momentum space identified with partons is presented. The features of multiparticle production resulting from the existence of theoretical and experimental constants characterizing the processes with high multiplicity at the LHC are investigated.

The investigation of the multiparticle production processes at high energies is designed to provide important information about the properties of the fundamental interactions. In this regard, the new results presented by ATLAS and CMS collaborations require a theoretical understanding both in terms of existing models and theories and search of new approaches.

Typical sizes that characterize the processes of pions production, i.e., mainly processes due to the strong interaction in the collision of two hadrons at centre-of-mass energy \sqrt{S} have the following values

$$\begin{aligned} r_{0S} &= \frac{h}{m_{\pi}c} = 1.46 \text{ fm}, \\ r_0 &\propto 2.33 \text{ fm}, \\ r &\propto \frac{hc}{\sqrt{S}}, \\ \sqrt{S} &= 7 \text{ TeV}, \\ r_{eff} &\leq r_{0S} \ln P(S). \end{aligned} \tag{1}$$

*E-mail:y.kurochkin@dragon.bas-net.by

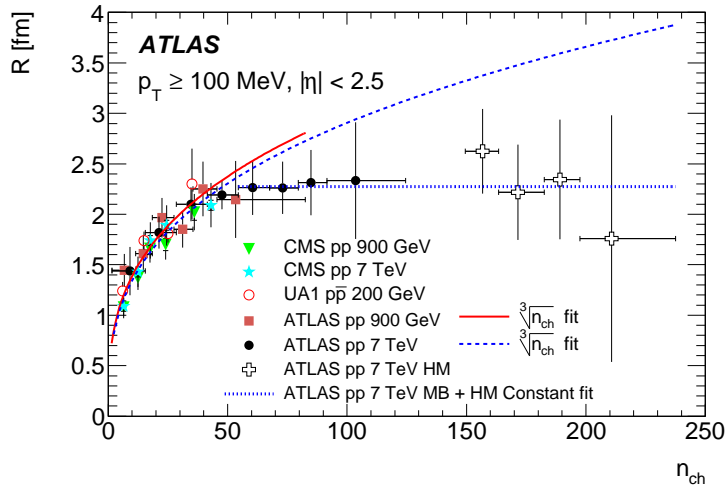


Figure 1: The dependence of the correlation radius of the pion pairs on the multiplicity of charged particles. It is evident that since the average multiplicity of charged particles 60 there is saturation - correlation radius does not change with increasing average multiplicity [1].

where r_{0S} is the radius of the strong (nuclear) interaction i.e. the Compton wavelength of a pion, r_0 is the experimental value of the correlation radius of the charged pions produced in the proton-proton collision (see figure 1), which can be regarded as the distance at which the strong interactions are weak enough for the secondary hadrons formation, r is the de Broglie wavelength corresponding to the energy of the colliding particles, the last inequality is a limit on the possible increase in the effective radius of interaction in the strong interactions of hadrons, which follows from the general principles of quantum field theory, where $P(S)$ is a polynomial of degree less than 2 [2].

The main goal of this work is to develop a model of a hadron as a coherent state of its excitations interpreted as partons and to establish restrictions on the average multiplicity of produced particles resulting from the model based on the values (1).

Let us note that there are quite a number of physical models that describe more or less various aspects of multiparticle production processes [3]. The hydrodynamic model of multiparticle production, proposed by L.D. Landau and S.Z. Belenky in [4] indicates to one characteristic dimension r_{0S} . Indeed, the hydrodynamic description of a system of particles

is the approximation followed from the kinetic equations and essentially depends on the characteristic linear dimension L of the existing problem in the study.

In this paper we suppose that the radius of nuclear forces (Compton length of the pion) $L = 1.46 \times 10^{-15}\text{m}$ is the characteristic size of investigated system.

Infinitesimal volumes used for the formulation of integral relations in hydrodynamics, thus, have to be much smaller than L^3 and much larger than the mean free path of the particles. From (1) it follows that the energy of the LHC since 7 TeV and above satisfies this condition.

Let us consider the collision of two hadrons at high energy, for example, proton-proton collision in the Large Hadron Collider. We suppose that colliding protons have a 4-momenta

$$\begin{aligned} p_1 &= (p_{01}, \vec{p}_1), p_2 = (p_{02}, \vec{p}_2), \\ p_1^2 &= \vec{p}_1^2 - p_{01}^2 = \vec{p}_2^2 - p_{02}^2 = -m_p^2, \end{aligned} \quad (2)$$

where m_p is the proton mass. We use a system of units where $c = h = 1$.

The collision is carried out at centre-of-mass energy \sqrt{S} which is determined as

$$\begin{aligned} S &= -(p_1^2 + p_2^2) = -P^2 = -P_x^2 - P_y^2 - P_z^2 + P_0^2 \\ &= -(p_{x1} + p_{x2})^2 - (p_{y1} + p_{y2})^2 - (p_{z1} + p_{z2})^2 + (p_{01} + p_{02})^2, \end{aligned} \quad (3)$$

where

$$P = (\vec{P}, iP_0) = [p_{x1} + p_{x2}, p_{y1} + p_{y2}, p_{z1} + p_{z2}, +i(p_{01} + p_{02})]. \quad (4)$$

It should be noted that in the laboratory frame (the rest system of the second proton)

$$P = (\vec{P}, iP_0) = [p_x, p_y, p_z, i(p_0 + m_p)], \quad (5)$$

where $p = (p_x, p_y, p_z, i(p_0)) = (\vec{p}, ip_0)$ is four-momentum of the incident proton.

We introduce quasi-Cartesian coordinates in Lobachevskii space realized on the upper sheet of the hyperboloid (3) in the momentum space [5] as

$$\begin{aligned}
P_z &= \frac{\sqrt{S}}{2} [e^{2q_z/\sqrt{S}} + (\frac{q_x^2 + q_y^2}{S} - 1)e^{-q_z/\sqrt{S}}], \\
P_x &= q_x e^{-q_z/\sqrt{S}}, \\
P_y &= q_y e^{-q_z/\sqrt{S}}, \\
P_0 &= \frac{\sqrt{S}}{2} [e^{2q_z/\sqrt{S}} + (\frac{q_x^2 + q_y^2}{S} + 1)e^{-q_z/\sqrt{S}}].
\end{aligned} \tag{6}$$

The formula inverse to formula (6) are

$$\begin{aligned}
q_x &= \frac{P_x \sqrt{S}}{P_0 - P_z}, \\
q_y &= \frac{P_y \sqrt{S}}{P_0 - P_z}, \\
q_z &= \sqrt{S} \ln \frac{\sqrt{S}}{P_0 - P_z}.
\end{aligned} \tag{7}$$

The metric element has the form

$$dS^2 = e^{-2q_z/\sqrt{S}}(dq_x^2 + dq_y^2) + dq_z^2 \tag{8}$$

and the volume element is

$$dV_m = \sqrt{g} dq_x dq_y dq_z = e^{-2q_z/\sqrt{S}} dq_x dq_y dq_z. \tag{9}$$

The introduced quasi-Cartesian coordinates (6) allow us to separate variables q_x , q_y , and q_z . That is impossible in four-dimensional space (3). Therefore we can consider the physics in the plane of the variables q_x , q_y only.

In addition, considering that Euclidean plane geometry is realized on horosphere of Lobachevsky space, the Fourier transformation F of the function $\phi_1(q_x, q_y)\phi_2(q_z)$ defined on that plane (horosphere) defines the function in the coordinate plane also with the Euclidean geometry. That is not correct for the variable q_z as it is evident from (9).

$$\Psi_1(x, y)\Psi_2(z) \leftrightarrow F\phi_1(q_x, q_y)\phi_2(q_z) \tag{10}$$

We note that quasi-Cartesian coordinates (6) and (7) automatically ensure the scale invariance of the theory in the plane of q_x, q_y i.e. invariance under following transformations

$$P'_x = \lambda P_x, P'_y = \lambda P_y, P'_z = \lambda P_z, P'_0 = \lambda P_0 \quad (11)$$

which is valid for any \sqrt{S} .

The fundamental role of scale invariance in processes of multiparticle production has been pointed out by V.A. Matveev, R.M. Muradyan and A.N. Tavkhelidze in [6,7].

Let us build the quantum mechanics of the system described by four-momentum (6).

Since horosphere of three-dimensional Lobachevsky space includes the geometry of the two-dimensional Euclidean space we can introduce conjugate coordinates in momentum space in the standard way [8]

$$\begin{aligned} q_x, x &= -i\hbar \frac{\partial}{\partial q_x}, \\ q_y, y &= -i\hbar \frac{\partial}{\partial q_y}. \end{aligned} \quad (12)$$

There is a Heisenberg-Weyl algebra

$$\begin{aligned} [x, q_x] &= [y, q_y] = i\hbar I, \\ [x, y] &= [q_x, q_y] = 0, \\ [x, I] &= [y, I] = [q_x, I] = [q_y, I] = 0, \end{aligned} \quad (13)$$

where I is the identity operator.

The expressions (12) and (13) allow us to construct quantum coherent states on the horosphere.

The extra dimensional constant characterizing the system is required to lead the coordinates and momenta (12) to the same dimension. It is needed for the construction of creation and annihilation operators. It is natural to take the size of hadron (proton) as such constant. This size provides, due to the uncertainty relation, nonzero components x , y , even for a hadron moving along the axis z , which in turn implies the existence of nonzero components q_x , q_y in accordance to (7).

Then the creation and annihilation operators can be written in the following manner

$$\begin{aligned} a_x &= \frac{Rq_x + i\frac{x}{R}}{\sqrt{2}}, a_x^+ = \frac{Rq_x - i\frac{x}{R}}{\sqrt{2}}, \\ a_y &= \frac{Rq_y + i\frac{y}{R}}{\sqrt{2}}, a_y^+ = \frac{Rq_y - i\frac{y}{R}}{\sqrt{2}}. \end{aligned} \quad (14)$$

Heisenberg-Weyl algebra in terms of the creation and annihilation operators is

$$[a_k, a_l^+] = \delta_{kl}I, [a_k^+, a_l^+] = [a_k, a_l] = [a_k, I] = [a_k^+, I] = 0, \quad (15)$$

where $k, l = 1, 2$ correspond to x or y and $\hbar = 1$. Coherent states are known to be defined as a state of its own annihilation operators with complex eigenvalues

$$\begin{aligned} a_x |z_1\rangle &= z_1 |z_1\rangle, \\ a_y |z_2\rangle &= z_2 |z_2\rangle. \end{aligned} \quad (16)$$

The coherent states (16) satisfy the following conditions

$$\begin{aligned} \langle z_1 | z_1 \rangle &= e^{-|z_1|^2}, \\ \langle z_2 | z_2 \rangle &= e^{-|z_2|^2}. \end{aligned} \quad (17)$$

The expression for the total space of coherent states of two-dimensional problem on the horosphere is the tensor product of states that are constructed using operators of the same mode. These coherent states are determined by the formula

$$|z_1, z_2\rangle = e^{z_1 a_x^+} e^{z_2 a_y^+} |0, 0\rangle, \quad (18)$$

where the vacuum state $|0, 0\rangle$ is determined by the condition

$$a_x |0, 0\rangle = a_y |0, 0\rangle = 0. \quad (19)$$

There is the completeness criterion for coherent states which for the states on horosphere (18) has the form

$$\int |z_1, z_2\rangle \langle z_1, z_2| d\mu(z_1, z_2) = \int |z_1\rangle \langle z_1| d\mu(z_1) \int |z_2\rangle \langle z_2| d\mu(z_2) = I \quad (20)$$

and the uncertainty relations are

$$\Delta x \Delta q_x = \frac{\hbar}{2}, \Delta y \Delta q_y = \frac{\hbar}{2}. \quad (21)$$

Thus if the uncertainty of x or y of the order R then the uncertainty of momentum will be $\hbar/2R$.

As you know, in the laboratory frame the incident particle (hadron) is flattened in the direction of the movement due to the Lorentz contraction. In this case, transverse degrees of freedom (x and y) are important since

at high energies the kinetic energy of the hadron constituents (partons) is much larger than the energy of their interaction.

Therefore hadron moving at a speed close to the speed of light can be seen as a set of almost free partons. Since components of hadron move in unison before collision therefore this state of a hadron can be considered as a coherent state of its transverse excitations i.e. partons.

The main hypothesis is that the incident particle is a coherent state of partons i.e. transverse excitations of a hadron.

It should be noted that expressions mentioned above are covariant.

Let us write expressions of coherent states in the occupation-number representation as

$$\begin{aligned} a_x^+ |z_1\rangle &= a_x^+ \sum \frac{z_1^{n_1}}{\sqrt{n_1!}} |n_1\rangle = \sum \frac{n_1 z_1^{n_1-1}}{\sqrt{n_1!}} |n_1\rangle, \\ a_y^+ |z_2\rangle &= a_y^+ \sum \frac{z_2^{n_2}}{\sqrt{n_2!}} |n_2\rangle = \sum \frac{n_2 z_2^{n_2-1}}{\sqrt{n_2!}} |n_2\rangle. \end{aligned} \quad (22)$$

The average number of quanta of excitation in each coherent state is defined by (see [9])

$$\begin{aligned} \bar{n}_1 &= e^{-|z_1|^2} \langle z_1 | a_x^+ a_x | z_1 \rangle = |z_1|^2, \\ \bar{n}_2 &= e^{-|z_2|^2} \langle z_2 | a_y^+ a_y | z_2 \rangle = |z_2|^2. \end{aligned} \quad (23)$$

The total average number of excitations in both degrees of freedom is

$$\bar{n} = \bar{n}_1 + \bar{n}_2 = e^{-z_1^2 - z_2^2} \langle z_1 z_2 | a_x^+ a_x + a_y^+ a_y | z_2 z_1 \rangle = |z_1|^2 + |z_2|^2 \quad (24)$$

and the distribution of the number of excitations for each of the degrees of freedom obeys a Poisson law

$$P(n) = \frac{e^{-\bar{n}} \bar{n}^n}{n!}, \quad (25)$$

where $\bar{n} = n_1$ or $\bar{n} = n_2$.

Therefore the number of excitations corresponding to coherent state of hadron (25) is a Poisson distribution and coincides with the multiplicity distribution in the multi-peripheral model [3].

The coordinate representation of a coherent state is given by (see [10])

$$\langle x, y | z_1, z_2 \rangle \propto e^{\frac{i\sqrt{2}}{R}(\beta_1 x + \beta_2 y)} \times e^{\frac{-1}{2R^2}[(x - \sqrt{2}R\alpha_1)^2 + (y - \sqrt{2}R\alpha_2)^2]}. \quad (26)$$

The density distribution of the coordinates is

$$|\langle x, y | z_1, z_2 \rangle|^2 \propto e^{\frac{-1}{R^2}[(x - \sqrt{2}R\alpha_1)^2 + (y - \sqrt{2}R\alpha_2)^2]}. \quad (27)$$

The corresponding momentum representation has the form

$$\langle q_x, q_y | z_1, z_2 \rangle \propto e^{iR\sqrt{2}(\alpha_1 q_x + \alpha_2 q_y)} \times e^{-\frac{R^2}{2}[(q_x - \frac{\sqrt{2}}{R}\beta_1)^2 + (q_y - \frac{\sqrt{2}}{R}\beta_2)^2]} \quad (28)$$

and therefore the density distribution is

$$|\langle q_x, q_y | z_1, z_2 \rangle|^2 \propto e^{-R^2[(q_x - \frac{\sqrt{2}}{R}\beta_1)^2 + (q_y - \frac{\sqrt{2}}{R}\beta_2)^2]}, \quad (29)$$

where the following notation is used

$$\begin{aligned} z_1 &= \alpha_1 + i\beta_1, \alpha_1 = |z_1| \cos \theta_1, \beta_1 = |z_1| \sin \theta_1, \\ z_2 &= \alpha_2 + i\beta_2, \alpha_2 = |z_2| \cos \theta_2, \beta_2 = |z_2| \sin \theta_2. \end{aligned} \quad (30)$$

According to the Gaussian distribution in (21) $\sqrt{2R}\alpha_1$ and $\sqrt{2R}\alpha_2$ are the average coordinates of the particles. We note that in this case the coordinates characterize the size of hadron. Let us estimate minimal value of \bar{n} assuming $n = n_1$ in (25). Using the size of the proton 0,84 fm (see. [11]) and the following relation

$$\sqrt{2R}\alpha_1 = \sqrt{2R}|z_1| \cos \theta_1 = \sqrt{2n}R \cos \theta_1 = r_0 \quad (31)$$

we get the minimum value $\bar{n} \approx 4$ for $\cos \theta_1 = 1$. We can obtain the number of excitations (partons) arbitrarily large varying $\cos \theta_1$.

At this stage, restrictions on the phase change can be offered only on the basis of heuristic arguments, for example, the symmetry. We consider $\theta_1 = \pi/4$ based on assumption of symmetry between the coordinate and momentum representations which follows from the explicit expressions (27) and (29). Then $\cos \theta_1 = \sin \theta_2 = 1/\sqrt{2}$ and we obtain $\bar{n} \approx 7.5$

If using the following expression $\sqrt{2n}R \cos \theta_1 = r_{0S}$ instead of (31) at the same θ_1, θ_2 we get $\bar{n} = 3$. It is obvious that $\theta_{1,2} \rightarrow \pi/2$ at high multiplicity n and correspondingly high energy.

Thus we constructed model of hadron as coherent state of excitations on the horosphere of the Lobachevsky momentum space identified with partons and hadron structure functions which depend on number of partons.

The authors would like to thank V.G. Baryshevsky and V.V. Andreev for useful discussions.

References

- [1] The ATLAS Collaboration, Two-particle Bose-Einstein correlations in pp collisions at $\sqrt{s} = 0.9$ and 7 TeV measured with the ATLAS detector, Eur. Phys. J. C 75 (2015) 466.
- [2] A.A. Logunov, M.A. Mestvirishvili, V.A. Petrov, General principles of quantum field theory and the interaction of hadrons at high energies, Proc. The general principles of quantum field theory and their consequences. M.: Nauka. 1977. Art. 183-262. [In Russian]
- [3] Yu. Nikitin, I.L. Rosenthal, Theory of multiparticle production processes, M.: Atomizdat, (1976), 230. [In Russian]
- [4] L.D. Landau and S.Z. Belenky, The hydrodynamic theory of multiparticle production. UFN, (1955), T 56, 309. [In Russian]
- [5] M.N. Olevskii, Three orthogonal systems in constant curvature spaces in which the equation $\Delta_2 U + \lambda U = 0$ allows a complete separation of variables, Math. Coll. 1950 TA 27, pp 379-426. [In Russian]
- [6] V.A. Matveev, Deep inelastic lepton-hadron processes at high energy. Interanational school for young scientists in high-energy physics. Digest of articles. Gomel 25.08.-5.09. 1973. Dubna.1973 S.81-172. [In Russian]
- [7] R.M. Muradyan, Scaling in inclusive reactions, Preprint. R2-6762, JINR Dubna, 1972. [In Russian]
- [8] Yu. Kurochkin, I.Rybak, Dz. Shoukavy, Coherent states on horosphere Lobachevsky space, Reports of the National Academy of Sciences of Belarus, (2014), T. 58, 5, pp 44-48. [In Russian]
- [9] V.P. Shelest, G.M. Zinoviev, V.A. Miransky, Models of strongly interacting particles II, M.: Atomizdat, (1976), 247 pp. [In Russian]
- [10] Perelomov A.M., Generalized coherent states and their applications, M.: Nauka. 1987. [In Russian]
- [11] R. Rohl et all, The size of proton, Nature 09250, Vol. 466, (2010), doi:10.1038, P.213-217.

The QCD analysis of the F_3 structure function within the analytic approach based on the inverse Mellin transform method

A. V. Sidorov *

Bogoliubov Laboratory of Theoretical Physics, JINR

O. P. Solovtsova †

Sukhoi State Technical University of Gomel

Abstract

We discuss the application of the analytic approach called the fractional Analytic Perturbation Theory (APT) to the QCD analysis of the non-singlet structure function $xF_3(x, Q^2)$. The inverse Mellin transform method applied for the fit of experimental data and for the Jacobi polynomial method accuracy estimates in extraction of values of the scale parameter Λ_{QCD} and the form of the xF_3 structure function. Our estimates give the accuracy of the Jacobi polynomials method for the x -shape of the structure function about 10% and for the scale parameter $\Lambda_{QCD} \sim 4\%$.

1 Introduction

Recently application of the analytic approach proposed by Shirkov and Solovtsov [1, 2], the so-called analytic perturbation theory (APT), to the QCD analysis of the nucleon structure function data with use of the well known method of the expansion of structure functions in a set of the system of orthogonal Jacobi polynomials (see Refs. [3–5]) was done [6–10].

*E-mail: Sidorov@theor.jinr.ru

†E-mail: olsol@theor.jinr.ru

The key point of APT constructions—the analytic properties of some functions (the two-point correlator of the quark currents, the moments of the structure functions and so on). A overview of the analytic approach to QCD can be found in Ref. [11]. In the framework of the APT in contrast to the infrared behavior of the perturbative (PT) running coupling, the analytic coupling has no unphysical singularities. At low Q^2 scales, instead of a rapidly changing Q^2 evolution as occurs in the PT case, the APT approach leads to a slowly changing functions (see, e.g., Refs. [12, 13]). In the asymptotic region of large Q^2 the APT and the PT approaches coincide. It should be noted that the moments of the structure functions should be analytic functions in the complex Q^2 plane with a cut along the negative real axis (see Ref. [14] for more details), the ordinary PT description violates analytic properties due to the unphysical singularities of the PT coupling. On the other hand, the APT support these analytic properties.

The data on the xF_3 structure function provides a possibility for the precise test of the perturbative QCD predictions for the Q^2 evolution of the structure function. The analysis of xF_3 structure function experimental data simplified because one do not need to parameterize gluon and sea quark contributions and could parameterize the shape of the xF_3 structure function itself at some value Q_0^2 . In this work, we apply the inverse Mellin transform method [15] to the QCD analysis of the xF_3 data. The inverse Mellin transform method rather precise and gets an accuracy about five significant digits in our case. We compare the results of both methods in order to estimate the accuracy of the Jacobi polynomial method results. In our analysis, we focus on values of the scale parameter Λ_{QCD} and the form of the $xF_3(x, Q^2)$ structure function. It should be noted that the application of the APT to the QCD analysis of the DIS data required a generalization of the APT on the case of non-integer power of QCD running coupling. Such a generalization was proposed in Refs. [16] (see also [17, 18]).

2 Description of the methods

Let us briefly discuss the inverse Mellin transform method and the method base on the expansion of the structure function on a set of the Jacobi polynomials. These methods are widely used in the deep-inelastic scattering data analysis.

2.1 Jacobi polynomials method

In this method, one can express a shape of the structure function on the x -space to values of the Mellin moments of the structure function. Then the $x F_3$ structure function can be presented as [4]

$$\begin{aligned}
 x F_3^{LT N_{max}}(x, Q^2) &= \\
 &= x^\alpha (1-x)^\beta \sum_{n=0}^{N_{max}} \Theta_n^{\alpha, \beta}(x) \sum_{j=0}^n c_j^{(n)}(\alpha, \beta) M_3(j+2, Q^2) \\
 &\hspace{15em} \text{for PT,} \tag{1} \\
 &= x^\alpha (1-x)^\beta \sum_{n=0}^{N_{max}} \Theta_n^{\alpha, \beta}(x) \sum_{j=0}^n c_j^{(n)}(\alpha, \beta) \mathcal{M}_3(j+2, Q^2) \\
 &\hspace{15em} \text{for APT.} \tag{2}
 \end{aligned}$$

Here $\Theta_n^{\alpha, \beta}$ are the Jacobi polynomials, $\alpha = 0.7$ and $\beta = 3.0$ fix the weight function of the Jacobi polynomials.

The perturbative renormalization group Q^2 evolution of the Mellin moments is well known (see, e.g., Ref. [19]) and in the leading order reads as

$$M_3^{pQCD}(N, Q^2) = \frac{[\alpha_s(Q^2)]^\nu}{[\alpha_s(Q_0^2)]^\nu} M_3(N, Q_0^2), \quad N = 2, 3, \dots, \tag{3}$$

$$\nu(N) = \gamma_{NS}^{(0), N} / 2\beta_0, \tag{4}$$

where $\alpha_s(Q^2)$ is the QCD running coupling, $\gamma_{NS}^{(0), N}$ are the non-singlet one-loop anomalous dimensions, $\beta_0 = 11 - 2n_f/3$ is the first coefficient of the renormalization group β -function, and n_f denotes the number of active flavors ($n_f = 4$ in our analysis).

In the framework of the APT, the expression (3) is converted to:

$$\mathcal{M}_3^{APT}(N, Q^2) = \frac{\mathcal{A}_\nu(Q^2)}{\mathcal{A}_\nu(Q_0^2)} \mathcal{M}_3(N, Q_0^2), \tag{5}$$

where the analytic function \mathcal{A}_ν is derived from the spectral Källén–Lehmann representation and corresponds to the discontinuity of the ν -th power of the PT running coupling.

In the leading order (*LO*), the analytic function \mathcal{A}_ν has a rather simple form (see, e.g., Ref. [18])

$$\mathcal{A}_\nu^{LO}(Q^2) = [\alpha_{\text{PT}}^{LO}]^\nu - \left(\frac{4\pi}{\beta_0}\right)^\nu \frac{\text{Li}_\delta(t)}{\Gamma(\nu)}, \quad (6)$$

$$\text{Li}_\delta(t) = \sum_{k=1}^{\infty} \frac{t^k}{k^\delta}, \quad t = \frac{\Lambda^2}{Q^2}, \quad \delta = 1 - \nu, \quad (7)$$

where the PT running coupling $\alpha_{\text{PT}}^{LO} = 4\pi/[\beta_0 \ln(Q^2/\Lambda_{\text{PT}}^2)]$ and Li_δ is the polylogarithm function. Note that the function $\mathcal{A}_{\nu=1}(Q^2)$ defines the APT running coupling, $\alpha_{\text{APT}}(Q^2)$ [20].

Unknown quantity $M_3(N, Q_0^2)$ in Eq. (3) could be parameterized as the Mellin moments of the structure function $x F_3$ at some point Q_0^2 :

$$M_3(N, Q_0^2) = \int_0^1 dx x^{N-2} x F_3(x, Q_0^2) = \int_0^1 dx x^{N-2} A x^a (1-x)^b (1+\gamma x). \quad (8)$$

In our analysis we taken into account the higher twist (HT) contribution and therefore

$$x F_3^{\text{exp}}(x, Q^2) = x F_3^{\text{LT } N_{\text{max}}}(x, Q^2) + \frac{h(x)}{Q^2}, \quad (9)$$

where $h(x)$ is a shape of the HT in the x space.

2.2 The inverse Mellin transform method

One can calculate the structure function at some Q^2 -value using the inverse Mellin transform [15]:

$$x F_3(x, Q^2) = \frac{1}{2\pi i} \int_{c-i\infty}^{c+i\infty} dn x^{-n} M_3(n, Q^2), \quad \text{PT}, \quad (10)$$

$$= \frac{1}{2\pi i} \int_{c-i\infty}^{c+i\infty} dn x^{-n} \mathcal{M}_3(n, Q^2), \quad \text{APT}. \quad (11)$$

In the PT, it is well known the analytic continuation of the anomalous dimensions on the complex plane of Mellin moments, n . In the APT case, we calculate the function $\mathcal{A}_\nu(Q^2)$ for the complex Mellin moments by the numerical summation of the set in Eq. (7). The path of integration for the inverse Mellin transform lies to the right of all singularities of the analytic continuation of moments $M_3(n, Q^2)$ or $\mathcal{M}_3(n, Q^2)$.

Table 1: The results of the QCD fit for the scale parameter Λ_{QCD} obtained in the framework of the PT and APT approaches using different methods.

Method of analysis	Λ_{PT} (MeV)	Λ_{APT} (MeV)
Inverse Mellin transform	378 ± 49	422 ± 77
Jacobi polynomials expansion	363 ± 49	407 ± 74

3 Results of fit and discussion

The results of QCD fit by using different methods are presented in Table 1 and Figs. 1–4 for $Q_0^2 = 3 \text{ GeV}^2$, $n_f = 4$, and $N_{max} = 11$. The shape of the function $h(x)$ in Eq. (9) as well as the parameters A , a , b , γ in Eq. (8), and the scale parameter Λ_{QCD} are found by fit of a combined set of the $x F_3$ -data. The kinematic region of this set is $0.5 \text{ GeV}^2 < Q^2 < 196 \text{ GeV}^2$ (see details in Ref. [9]). The description of the fitting procedure can be found in Ref. [21]. The target mass corrections are taken into account up to the terms M_N^2/Q^2 [22].

Figure 1 shows the difference in the x -space between fitting results for $x F_3$ structure function data by using the inverse Mellin transform (M) and the Jacobi polynomials expansion (J) methods. The difference $\Delta x F_3^{M-J} =$

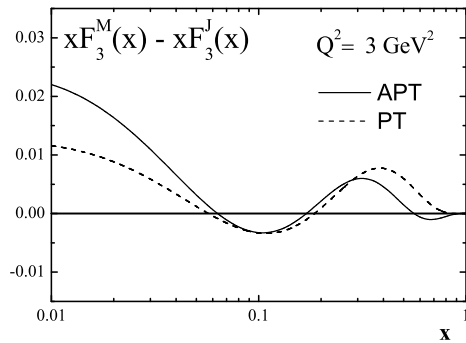


Figure 1: The difference between fitting results for the $x F_3$ structure function data by using the inverse Mellin and Jacobi methods for the APT and PT approaches.

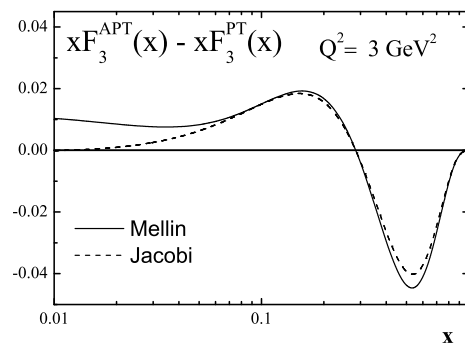


Figure 2: The difference for the $x F_3$ structure function form in the APT and PT approaches by using the inverse Mellin and the Jacobi methods.

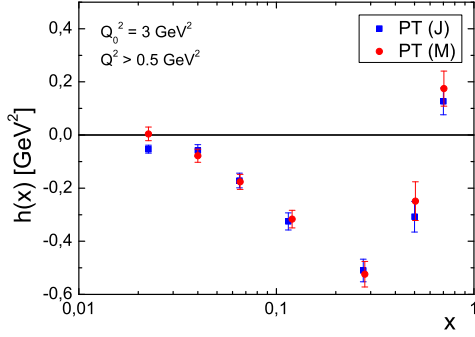


Figure 3: Result for the HT shape in the PT by using the inverse Mellin and the Jacobi methods.

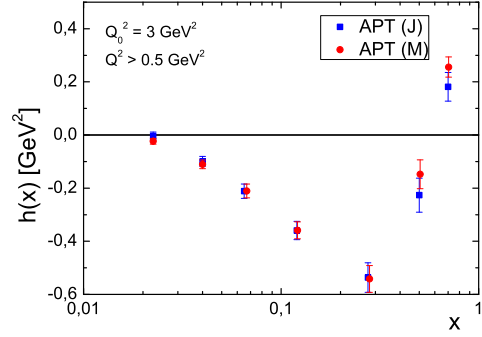


Figure 4: Result for the HT shape in the APT by using the inverse Mellin and the Jacobi methods.

$xF_3^M - xF_3^J$ presented for the APT as the solid line and for the PT as the dashed line. One can see that a value of $\Delta xF_3^{M-J} < 0.025$, which corresponds to the accuracy of the Jacobi method better than 10% for both theoretical approaches. This estimation is in qualitative agreement with the result obtained for the non-singlet xF_2 structure function [10].

Figure 2 shows the difference for the xF_3 -shape obtained in the APT (solid line) and the PT (dashed line) approaches using the inverse Mellin transform and the Jacobi polynomials methods: $\Delta xF_3^{\text{APT-PT}} = xF_3^{\text{APT}} - xF_3^{\text{PT}}$. As can be seen from this figure, the Jacobi method gives the same difference with the Mellin one at both theoretical approaches, the APT and the PT. However at small x , the Jacobi method is not sensitive to the difference of results in APT and PT approaches, while the inverse Mellin transform method reveals this difference. We found that at low $Q^2 = 1 \text{ GeV}^2$ the accuracy of the Jacobi method in the APT is two times better in comparison to the PT.

Figures 3–4 demonstrate results for the x -shape of the HT contribution. One can see, for both theoretical approaches, the APT and the PT, there is good agreement between results by using the inverse Mellin and the Jacobi methods (the exception for the lowest point in the PT).

In conclusion we stress, that the Jacobi polynomials method is fast, but gives about 10% accuracy for x -shape of the structure function and 4% accuracy for the scale parameter Λ_{QCD} .

Acknowledgments

It is a pleasure for the authors to thank D. V. Shirkov and O. V. Teryaev for interest in this work and helpful discussions. This research was supported by the JINR-BelRFFR grant F14D-007, JINR-Bulgaria Collaborative Grant and by the RFBR Grant 14-01-00647.

References

- [1] D.V. Shirkov, I.L. Solovtsov, JINR Rap. Comm. 1996. No. **2**[76]-96, 5 (1996); Phys. Rev. Lett. **79**, 1209 (1997).
- [2] K.A. Milton, I.L. Solovtsov, Phys. Rev. D **55**, 5295 (1997).
- [3] G. Parisi, N. Surlas, Nucl. Phys. B **151**, 421 (1979).
- [4] I.S. Barker, C.B. Langensiepen, G. Shaw, Nucl. Phys. **B 186**, 61 (1981);
V.G. Krivokhizhin *et al.*, Z. Phys. C **36**, 51 (1987).
- [5] V.G. Krivokhizhin *et al.*, Z. Phys. C **48**, 347 (1990);
A. Benvenuti *et al.*, Phys. Lett. B **195**, 97 (1987); Phys. Lett. B **223**, 490 (1989);
A.V. Kotikov, G. Parente, J. Sanchez-Guillen, Z. Phys. C **58**, 465 (1993);
A.L. Kataev, A.V. Sidorov, Phys. Lett. B **331**, 179 (1994).
- [6] B.G. Shaikhatdenov *et al.*, Phys. Rev. D **81**, 034008 (2010).
- [7] A.V. Kotikov, V.G. Krivokhizhin, B.G. Shaikhatdenov, Phys. Atom. Nucl. **75**, 507 (2012).
- [8] A.V. Sidorov, O.P. Solovtsova, Nonlin. Phenom. Complex Syst. **16**, 397 (2013); **18**, 222 (2015).
- [9] A.V. Sidorov, O.P. Solovtsova, Mod. Phys. Letters A **29** 1450194 (2014).
- [10] C. Ayala, S.V. Mikhailov, Phys. Rev. D **92**, 014028 (2015).
- [11] I.L. Solovtsov, D.V. Shirkov, Theor. Math. Phys. **120**, 1220 (1999).

- [12] K.A. Milton, I.L. Solovtsov, O.P. Solovtsova, Phys. Rev. D **60**, 016001 (2001).
- [13] V.L. Khandramai, R.S. Pasechnik, D.V. Shirkov, O.P. Solovtsova, O.V. Teryaev, Phys. Lett. B **706**, 340 (2012).
- [14] I.L. Solovtsov, Part. Nucl. Lett. **4**[101], 10 (2000).
- [15] M. Gluck, E. Reya, Phys. Rev. D **14**, 3034 (1976);
D.A. Kosower, Nucl. Phys. B **506**, 439 (1997);
M. Gluck, E. Reya, A. Vogt, Eur. Phys. J. C **5**, 461 (1998);
M. Stratmann, W. Vogelsang, Phys. Rev. D **64**, 114007 (2001).
- [16] A.P. Bakulev, S.V. Mikhailov, N.G. Stefanis, Phys. Rev. D **72**, 074014 (2005); *Erratum: ibid.* D **72**, 119908(E) (2005).
- [17] A.P. Bakulev, S.V. Mikhailov, N.G. Stefanis, Phys. Rev. D **75**, 056005 (2007); *Erratum: ibid.* D **77**, 079901(E) (2008).
- [18] A.P. Bakulev, Phys. Part. Nucl. **40**, 715 (2009).
- [19] A.J. Buras, Rev. Mod. Phys. **52**, 199 (1980).
- [20] D.V. Shirkov, I.L. Solovtsov, Theor. Math. Phys. **150**, 132 (2007).
- [21] A.L. Kataev *et al.*, Phys. Lett. B **417**, 374 (1998).
- [22] A.L. Kataev, G. Parente, A.V. Sidorov, Preprint ICTP IC/99/51, hep-ph/990531, Nucl. Phys. B **573**, 405 (2000).

On Target Mass Corrections to Deep-inelastic Structure Functions

V. I. Lashkevich, O. P. Solovtsova*

*International Center for Advanced Studies,
Sukhoi State Technical University of Gomel*

Abstract

We investigate target mass corrections to the unpolarized structure functions of the deep-inelastic scattering by using the traditional Georgi–Politzer method and another approaches. The recent methods for solving the ‘threshold’ problem arisen in the limit as the Bjorken variable x tends to unity are discussed. We present results of a new approach and demonstrate that, in the large- x region, target mass corrections to structure functions calculated by using this method noticeably differ that other approaches give.

1 Introduction

To compare correctly QCD predictions with experimental data of the deep-inelastic scattering at low Q^2 scales, $Q^2 \lesssim 1 - 2 \text{ GeV}^2$, it is important to take into account in the analysis additional power terms are known as target mass corrections (TMCs) arising from purely kinematic effects associated with finite mass of the nucleon target. In the QCD analysis of the deep-inelastic scattering data the operator product expansion (OPE) method is widely used. However the OPE was derived in the massless limit and if a finite mass of the nucleon target is included, then the TMCs arise. Many years ago, the OPE was used to include TMC effects systematically via the Nachtmann ξ variable [1] by Georgi and Politzer (GP) [2]. The GP method, named also as ξ -scaling method, showed the importance of the

*E-mail: solovtsova@gstu.gomel.by

accounting of TMCs. However within this method there was a problem to describe the structure functions behavior as the Bjorken variable x tends to unity. This problem was widely discussed in the literature ever since its appearance and continues to be discussed until now (see, e.g., [3–5]).

In the present work we extend our previous analysis [5] and analyze several frameworks for the TMCs in order to improve a knowledge of TMC effects for the unpolarized proton structure functions.

2 Target Mass Corrections

The inclusive cross section of the deep-inelastic scattering process can be written as $d\sigma \sim L^{\mu\nu}W_{\mu\nu}$ in terms of leptonic and hadronic tensors, $L^{\mu\nu}$ and $W_{\mu\nu}$. The hadronic tensor $W_{\mu\nu}$ is parameterized by structure functions which is defined via structure functions $F_{i=1,2,3}(x, Q^2)$.¹

2.1 Operator product expansion: GP approach

According to the GP approach the structure functions are given by [6]

$$F_1(x, Q^2) = \frac{x}{\xi\rho} F_1^0(\xi, Q^2) + \frac{\varepsilon x^2}{\rho^2} h_2(\xi, Q^2) + \frac{2\varepsilon^2 x^3}{\rho^3} g_2(\xi, q^2), \quad (1)$$

$$F_2(x, Q^2) = \frac{x^2}{\xi^2\rho^3} F_2^0(\xi, Q^2) + \frac{6\varepsilon x^3}{\rho^4} h_2(\xi, Q^2) + \frac{12\varepsilon^2 x^4}{\rho^5} g_2(\xi, q^2), \quad (2)$$

$$h_2(\xi, Q^2) = \int_{\xi}^1 \frac{F_2^0(y, Q^2)}{y^2} dy, \quad g_2(\xi, Q^2) = \int_{\xi}^1 dy \int_y^1 \frac{F_2^0(z, Q^2)}{z^2} dz,$$

$$F_3(x, Q^2) = \frac{x}{\xi\rho^2} F_3^0(\xi, Q^2) + \frac{2\varepsilon x^2}{\rho^3} h_3(\xi, q^2), \quad h_3(\xi, Q^2) = \int_{\xi}^1 \frac{F_3^0(y, Q^2)}{y} dy. \quad (3)$$

Here $x = Q^2/2\nu = Q^2/2(q \cdot P)$ is the Bjorken scaling variable, ξ is the Nachtmann variable [1]

$$\xi = \frac{2x}{1 + \sqrt{1 + 4\varepsilon x^2}} = \frac{2x}{1 + \rho}, \quad (4)$$

¹Other structure functions, $i = 4, 5, 6$, are proportional to the lepton mass and are therefore negligible for the kinematics of the deep-inelastic region.

$\rho = \sqrt{1 + 4\varepsilon x^2}$, $\varepsilon = M^2/Q^2$, M is the target mass, the functions $F_i^0(\xi, Q^2) = \lim_{M \rightarrow 0} F_i(x, Q^2)_{x=\xi}$.

The expressions (1)–(3) are known to suffer from the “threshold problem”, in which the target mass corrected structure functions do not vanish as $x \rightarrow 1$, and are in fact nonzero in the kinematically forbidden $x > 1$ region. A numerous of attempts have been made to ameliorate the threshold problem using various prescriptions.

2.2 Known approximations

Recently, Kulagin and Petti (KP) [7] showed that by expanding the target mass corrected structure functions to leading order in $1/Q^2$, the resulting functions have the correct $x \rightarrow 1$ limits (see also Ref. [8]).

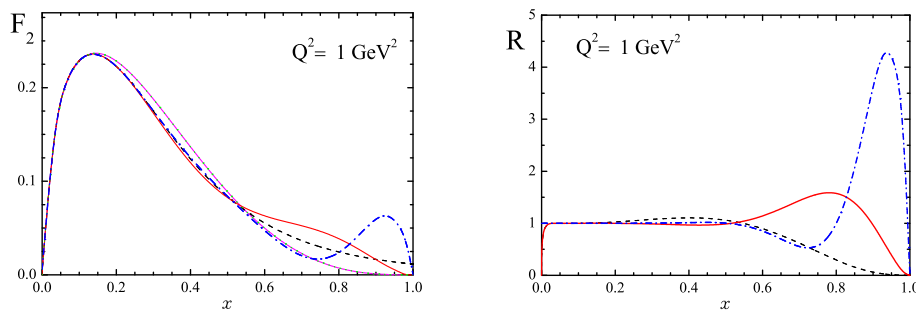


Figure 1: Left panel: The behavior of the structure function F_2 obtained vs the Bjorken variable x . The solid (red) line corresponds to result of $1/Q^2$ KP approximation, the dash-dotted (blue) line – $1/Q^4$ approximation, the dashed (black) line – the GP result, and dotted (green) line – without target mass corrections. Right panel: Ratio of the target mass corrected F_2 structure function by using the $1/Q^2$ (solid, red) and $1/Q^4$ (dash-dotted, blue) the KP approximation, and GP approximation (dashed, black) compared with the structure function without mass corrections.

While avoiding the threshold problem, this prescription, however, raises the question of whether the $1/Q^2$ approximation is sufficiently accurate for structure functions near $x \approx 1$ at moderate Q^2 . To test the convergence of the $1/Q^2$ expansion at large x , we further expand the GP result to include $\mathcal{O}(1/Q^4)$ corrections. Figure 1 illustrates the accuracy of the KP approach. In order to isolate the target mass effect from the specific form

of the structure function parametrization we take for simplicity the form $F_2 \sim (1-x)^3$. One can see that both the $1/Q^2$ and $1/Q^4$ approximations are found to reproduce the GP result well up to $x \approx 0.6$, but significant deviations are visible at larger x . The reliability of a low order $1/Q^2$ expansion is therefore questionable at large x values, and hence their efficacy in removing the $x \rightarrow 1$ threshold problem.

An alternative approach to TMCs relies on the collinear factorization (CF) formalism [9–11], which makes use of the factorization theorem to relate the hadronic tensor for lepton–hadron scattering to that for scattering from a parton. Here parton distributions are formulated directly in momentum space, avoiding the need to perform an inverse Mellin transform to obtain the PDF from its moments. The first study of TMCs within CF was made by Ellis, Furmanski, and Petronzio (EFP) [9]. Using the same notation as above, the EFP results for the target mass corrected structure functions are given by

$$F_1^{\text{EFP}}(x, Q^2) = \frac{2}{1+\rho} F_1^0(\xi, Q^2) + \frac{(\rho^2-1)}{(1+\rho)^2} h_2(\xi, Q^2), \quad (5a)$$

$$F_2^{\text{EFP}}(x, Q^2) = \frac{1}{\rho^2} F_2^0(\xi, Q^2) + \frac{3\xi(\rho^2-1)}{\rho^2(1+\rho)} h_2(\xi, Q^2), \quad (5b)$$

$$F_3^{\text{EFP}}(x, Q^2) = \frac{1}{\rho} F_3^0(\xi, Q^2) + \frac{2(\rho^2-1)}{\rho(1+\rho)^2} h_3(\xi, Q^2), \quad (5c)$$

where again the F_i^0 refer to the uncorrected structure functions. Because the massless functions F_i^0 are evaluated at ξ , the target mass corrected structure functions will suffer from the same threshold problem as in the OPE result in Eqs. (1)–(3). So, in both the EFP and OPE treatments of TMCs, the resulting structure functions are nonzero for $x > 1$.

Other approach for target mass corrected structure functions is the approach of Steffens and Melnitchouk (SM) [3] which effectively corresponds to use of a new variable

$$\xi_{SM} = x \frac{1 + \sqrt{1 + 4x^2}}{1 + \sqrt{1 + 4\epsilon x^2}}, \quad (6)$$

and the modified moments $A_n^{(\text{SM})} \equiv \int_0^{\xi_0} d\xi \xi^n F(\xi, \xi_0)$, with $\xi_0 \equiv \xi(x=1) = 2/(1 + \sqrt{1 + 4\epsilon}) < 1$ (see Refs. [5] for more details).

2.3 JLD-approach

Let us now pass to new approach which based on the Jost-Lehmann-Dyson (JLD) integral representation [12, 13]. As it was shown by Solovtsov [14] that the threshold problem is a similar to the problem that appears for an invariant charge in quantum chromodynamics, when the violation of the general principles of the theory, which are reflected in the Källén–Lehmann representation, leads to unphysical singularities. A solution of this problem was proposed proposed by Shirkov and Solovtsov² [15] (see Ref. [16] as review). By using the JLD integral representation it was shown [14] that the natural scaling variable is a new variable ξ_S ,

$$\xi_S = x \frac{\sqrt{1+4\varepsilon}}{\sqrt{1+4\varepsilon x^2}}, \quad (7)$$

which leads to the moments $\mathcal{M}_n(Q^2)$ that are analytic functions. In this case, the spectral property for the structure functions is satisfied automatically, and no problem arises in the limit as the Bjorken variable x tends to unity (see, e.g. Refs. [5]). Note the proof of the JLD representation is based on the most general principles of the theory, such as the covariance, Hermiticity, spectrality, and causality.

According to JLD-approach, instead of the function $F_i^0(\xi)$ we must use

$$F_i^0(x, Q^2) = \begin{cases} F_i^0(\xi_-) - F_i^0(1), & 0 \leq x < \bar{x}, \\ F_i^0(\xi_-) - F_i^0(\xi_+), & \bar{x} \leq x \leq 1, \end{cases} \quad (8)$$

where $\bar{x} = 1/\sqrt{1+4\varepsilon^2}$,

$$\xi_{\mp}(x) = \frac{x\sqrt{1+4\varepsilon x^2}}{1+4\varepsilon x^2+4\varepsilon^2 x^2} \cdot \left[1 + 2\varepsilon \mp 2\varepsilon \cdot \frac{\sqrt{1-x^2}}{\sqrt{1+4\varepsilon x^2}} \right]. \quad (9)$$

Follow this recipe, we transform Eqs. (1)–(3) and, for example, for the structure function F_3 it turns out:

for $x \leq \bar{x}$

$$F_3^S(x, Q^2) = \frac{x \cdot F_3^{(0)}(\xi_-(x), Q^2)}{\xi_-(x)(1+4\varepsilon x^2)} + \frac{2\varepsilon x^2}{\sqrt{(1+4\varepsilon x^2)^3}} h_3(\xi_-(x), Q^2), \quad (10a)$$

$$F_3^S(x, Q^2) = \frac{x}{(1+4\varepsilon x^2)} \left[\frac{F_3^{(0)}(\xi_-(x), Q^2)}{\xi_-(x)} - \frac{F_3^{(0)}(\xi_+(x), Q^2)}{\xi_+(x)} \right] + (10b)$$

²This analytic approach called the Analytic Perturbation Theory (APT).

$$+ \frac{2\varepsilon x^2}{\sqrt{(1+4\varepsilon x^2)^3}} [h_3(\xi_-(x), Q^2) - h_3(\xi_+(x), Q^2)]$$

for $\bar{x} \leq x \leq 1$.

3 Numerical result

In our calculations we take the distributions of light u , d and s quarks and anti-quarks from Ref. [17], where was fixed the next to leading (NLO) value of the parameter $\Lambda_{\text{QCD}} = 0.248$ GeV. We have verified that distributions provided in other papers, for example, in Refs. [18] in the region of $x > 0.2$, for which become essential the TMCs, very close to distributions given in Ref. [17].

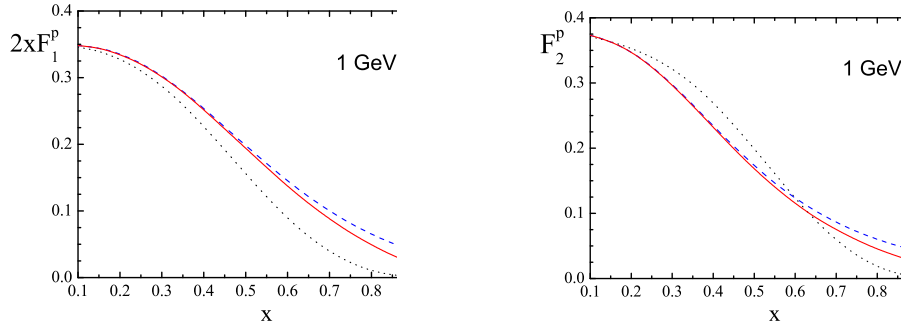


Figure 2: The behavior of the proton structure function F_1 (left panel) and F_2 (right panel) vs the Bjorken variable x at $Q^2=1$ GeV². The solid (red) line corresponds to our result obtained by using the JLD-approach, the dashed (blue) curve reflects the result obtained by standard GP method, and the dotted (green) line is the initial proton distribution [17].

Figure 2 shows the behavior of the proton structure function at $Q^2=1$ GeV² for the structure functions F_1 (left panel) and F_2 (right panel). One can see that target mass corrections to these structure functions calculated by using the JLD-approach are noticeably differ, in the large- x region, that the traditional GP method gives. The same we obtain for the proton structure function F_3 of the neutrino nucleon deep inelastic scattering obtained by using the expressions (3) and (10) (see Ref. [19] for more details).

4 Conclusion

In this report we have sought to discuss the the ‘threshold’ problem in the standard TMC analysis. Historically it has been argued that the problem in the threshold region exists because at low Q^2 the higher twist contributions cannot be neglected. The inclusion of target mass corrections in the fits of deep-inelastic scattering data is important as change the magnitude of the higher twist terms needed to describe the experimental data.

We discussed available to target mass corrections approaches and suggested to use the new JLD-approach. We observed that at low $Q^2 \sim 1 \div 2 \text{ GeV}^2$ the TMCs to structure functions calculated by using the JLD-approach noticeably differ from the standard GP-method or another approaches results. We believe that the JLD-approach including target mass effects will be useful in extracting the magnitude of the structure functions from the experimental data and to precisely extract the higher twist contribution.

Acknowledgments

We are grateful to A.V. Sidorov and D.V. Shirkov for interest in this work and helpful discussions. This work was partly supported by the RFBR grant 14-01-00647 and the BelRFFR-JINR grant F14D-007.

References

- [1] O. Nachtmann, Nucl. Phys. B **63**, 237 (1973).
- [2] H. Georgi and H.D. Politser, Phys. Rev. D **14**, 1829 (1976).
- [3] W. Melnitchouk, R. Ent, and C. Keppel, Phys. Rep. **406**, 127 (2005);
F.M. Steffens, W. Melnitchouk, Phys. Rev. C **73**, 055202 (2006);
I. Schienbein *et al.*, J. Phys. G. **35**, 053101 (2008).
- [4] A. Accardi and J.W. Qiu, JHEP **07**, 90 (2008);
A. Accardi *et al.*, Phys. Rev. D **81**, 034016 (2010).
- [5] V.I. Lashkevich and O.P. Solovtsova, Theor. Math. Phys. **160**, 1260 (2009); Nonlin. Phenom. Complex Syst. **13**, 286 (2010); Nonlin. Phenom. Complex Syst. **14**, 184 (2011).

- [6] A. De Rújula, H. Georgi, and H.D. Politzer, *Annals of Phys.* **103**, 315 (1977).
- [7] S. A. Kulagin and R. Petti, *Nucl. Phys. A* **765**, 126 (2006).
- [8] F.J. Yndurain, *The Theory of Quark and Gluon Interactions*, Springer, 2006, 476 pp.
- [9] R.K. Ellis, W. Furmnski, R.Petroncio, *Nucl. Phys. B* **212** 29 (1983).
- [10] S. Kretzer and M. H. Reno, *Phys. Rev. D* **66**, 113007 (2002).
- [11] A. Accardi and J. W. Qiu, *JHEP* **07**, 090 (2008).
- [12] R. Jost and H. Lehmann, *Nuov. Cim.* **5**, 1598 (1957).
- [13] F.J. Dyson, *Phys. Rev.* **110**, 1460 (1958).
- [14] I.L. Solovtsov, *Part. Nucl. Lett.* **4**[101], 10 (2000).
- [15] D.V. Shirkov, I.L. Solovtsov, *Phys. Rev. Lett.* **79**, 1209 (1997).
- [16] D.V. Shirkov and I.L. Solovtsov, *Theor. Math. Phys.* **150**, 132 (2007).
- [17] M. Glück, E. Reya, and A. Vong, *Z. Phys. C* **7**, 433 (1995); *Eur. Phys. J. C* **5**, 461 (1998).
- [18] A.D. Martin, R.G. Roberts, W.J. Stirling, and R.S. Thorne, *Eur. Phys. J. C* **16**, 117 (2000);
A.D. Martin, W.J. Stirling, R.S. Thorne, and G. Watt, *Eur. Phys. J. C* **63**, 189 (2009).
- [19] V.I. Lashkevich and O.P. Solovtsova, *Proc. of Annual Seminar NPC'S'2012*, Vol. **19**, 127 (2012).

A Spin-dependent Dipole Polarizabilities and Characteristics of the Nucleon, Related with Parity Violation

Andreev V.V. ^{*}, Deryuzhkova O.M. [†], Maksimenko N.V. [‡]

F.Skorina Gomel State University

1 Introduction

An important role in the understanding of the interaction of electromagnetic fields with hadrons play low-energy theorems as they are based on general principles of quantum theory and decomposition of Compton scattering amplitudes for the photon energy [1]. Currently, one of the most effective methods of investigation of electrodynamic processes is to use the effective Lagrangian obtained in the framework of field-theoretic approaches and consistent with the low-energy theorems [2]. With the development of the Standard Model of electroweak interactions in recent years introduced a new electroweak characteristics of hadrons, related to violation of P -parity [3, 4, 5].

Effective relativistic-invariant Lagrangians possible to obtain not only the physical interpretation of electromagnetic and electroweak characteristics of hadrons, but also information on the mechanisms of electromagnetic and electroweak photon-hadron interactions. For a more reliable determination of polarizabilities and the characteristics of hadrons associated with parity violation, use a wide class of electrodynamic processes in which the dispersion is realized real and virtual photons, as well as two-photon production in hadron-hadron interactions. The solution of such problems is

^{*}E-mail: vik.andreev@gsu.by

[†]E-mail: dom@gsu.by

[‡]E-mail: maksimenko@gsu.by

possible to perform in the framework of the relativistic field-theoretical approach, describe the interaction of electromagnetic fields with hadrons with regard to their electromagnetic and electroweak characteristics [6, 7].

In [8] for the construction of an effective relativistic invariant Lagrangian of the interaction of electromagnetic fields with the particles with constant electric and magnetic dipole moments introduced antisymmetric tensor of the dipole moments, which is independent of the electromagnetic field tensor $F_{\mu\nu} = \partial_\mu A_\nu - \partial_\nu A_\mu$.

In this paper, a relativistic quantum field-invariant Lagrangian to [8, 9], which defines the tensor induced dipole moments. Also provided is a variant of relativistic-invariant definition of spin dipole polarizabilities of the nucleon, which is based on the construction of the covariant induced dipole moments and phenomenological effective interaction Lagrangians of the electromagnetic field with these moments. On the basis of the relativistic properties of P -transformation, as well as cross-symmetry set covariant spin structure of the amplitude of the Compton scattering, consistent with the low-energy theorems. It is shown that the proposed model and the characteristics of the spin polarizability of the nucleon connected with parity nonconservation, contribute to the expansion of the amplitude of Compton scattering from the third order with respect to the photon energy.

2 The scattering amplitude of the electromagnetic field of the spin 1/2 particle in the dipole approximation

To get the low-energy scattering amplitude of the electromagnetic field on the spin of particles with polarizabilities will follow [10]. However, the determination of the induced electric \vec{d} and magnetic \vec{m} dipole moments of the vectors of electric \vec{E} and magnetic \vec{H} electromagnetic field strengths using the relations [11, 12]:

$$\vec{d} = 4\pi\hat{\alpha}\vec{E}, \quad (1)$$

$$\vec{m} = 4\pi\hat{\beta}\vec{H}, \quad (2)$$

where $\hat{\alpha}$ and $\hat{\beta}$ - the matrices, the matrix elements which are tensors of electric and magnetic polarizabilities. The diagonal elements of these matrices are expressed through the scalar electric and magnetic polarizability:

$$\alpha_{ij} = \alpha_1 \delta_{ij},$$

$$\beta_{ij} = \beta_1 \delta_{ij}.$$

Using (1) and (2) low-energy scattering amplitude of the electromagnetic field can be expressed through matrixes $\hat{\alpha}$ and $\hat{\beta}$ as follows [13]:

$$\begin{aligned} M(\vec{n}_2) = 4\pi\omega^2 \left\{ \left(\vec{e}^{(\lambda_2)*} \hat{\alpha} \vec{e}^{(\lambda_1)} \right) + \left(\vec{n}_2 \vec{e}^{(\lambda_1)} \right) \left(\vec{n}_1 \hat{\beta} \vec{e}^{(\lambda_2)*} \right) + \right. \\ \left. + \left(\vec{n}_1 \vec{e}^{(\lambda_2)*} \right) \left(\vec{e}^{(\lambda_1)} \hat{\beta} \vec{n}_2 \right) - \left(\vec{e}^{(\lambda_2)*} \vec{e}^{(\lambda_1)} \right) \left(\vec{n}_1 \hat{\beta} \vec{n}_2 \right) - \left(\vec{n}_1 \vec{n}_2 \right) \times \right. \\ \left. \times \left(\vec{e}^{(\lambda_1)} \hat{\beta} \vec{e}^{(\lambda_2)*} \right) + \left[\left(\vec{n}_2 \vec{n}_1 \right) \left(\vec{e}^{(\lambda_2)*} \vec{e}^{(\lambda_1)} \right) - \left(\vec{n}_2 \vec{e}^{(\lambda_1)} \right) \left(\vec{n}_1 \vec{e}^{(\lambda_2)*} \right) \right] \times \right. \\ \left. \times Sp \left(\hat{\beta} \right) \right\}. \end{aligned} \quad (3)$$

In expression (3) we have introduced the following notation: $\vec{e}^{(\lambda_1)}$ and $\vec{e}^{(\lambda_2)}$ – polarization vectors, \vec{n}_1 and \vec{n}_2 – single vectors of the falling and scattered radiation, ω – radiation frequency.

From definition \vec{d} and \vec{m} it agrees (1) and (2) follows, $\hat{\alpha}$ and $\hat{\beta}$ satisfy to the hermiticities condition.

In this case, as shown in work [14], tensors can α_{ij} and β_{ij} be presented as follows:

$$\alpha_{ij} = \alpha_1 \delta_{ij} + i\alpha_2 \varepsilon_{ijk} C_k,$$

$$\beta_{ij} = \beta_1 \delta_{ij} + i\beta_2 \varepsilon_{ijk} C_k,$$

where α_1 , α_2 , β_1 and β_2 – the real values, ε_{ijk} – a tensor Levi-Civita, C_k – pseudo-vector components.

In case of a spin particle as such pseudo-vector it is possible to choose a pseudo-vector – operator of the spin particle \vec{S} . If to consider that matrixes $\hat{\alpha}$ and $\hat{\beta}$ depend from \vec{S} , using algebra of operators 1/2-spin:

$$\left[\hat{S}_i, \hat{S}_j \right] = i\varepsilon_{ijk} \hat{S}_k,$$

$$\hat{S}_i \hat{S}_j = \frac{1}{4} \delta_{ij} + \frac{i}{2} \varepsilon_{ijk} \hat{S}_k,$$

these tensors can be presented as follows

$$\alpha_{ij} = \alpha_1 \delta_{ij} + i \alpha_2 \varepsilon_{ijk} \hat{S}_k, \quad (4)$$

$$\beta_{ij} = \beta_1 \delta_{ij} + i \beta_2 \varepsilon_{ijk} \hat{S}_k. \quad (5)$$

Substituting (4) and (5) in the equation (3), we will obtain:

$$\begin{aligned} M(\vec{n}_2) = 4\pi\omega^2 \chi_f^+ \left\{ \alpha_1 \left(\vec{e}^{(\lambda_2)*} \vec{e}^{(\lambda_1)} \right) + \beta_1 \left(\left[\vec{e}^{(\lambda_2)*} \vec{n}_2 \right] \cdot \left[\vec{e}^{(\lambda_1)} \vec{n}_1 \right] \right) + \right. \\ \left. + i \alpha_2 \left(\vec{S} \cdot \left[\vec{e}^{(\lambda_2)*} \vec{e}^{(\lambda_1)} \right] \right) + i \beta_2 \left(\vec{S} \cdot \left[\left[\vec{e}^{(\lambda_2)*} \vec{n}_2 \right] \cdot \left[\vec{e}^{(\lambda_1)} \vec{n}_1 \right] \right] \right) \right\} \chi_i, \end{aligned} \quad (6)$$

where χ_i and χ_f – spinor of an initial and final particle.

If the amplitude (6) require the condition of crossing symmetry, the equation (6) will be only the first two terms

$$M(\vec{n}_2) = 4\pi\omega^2 \left\{ \alpha_1 \left(\vec{e}^{(\lambda_2)*} \vec{e}^{(\lambda_1)} \right) + \beta_1 \left(\left[\vec{e}^{(\lambda_2)*} \vec{n}_2 \right] \cdot \left[\vec{e}^{(\lambda_1)} \vec{n}_1 \right] \right) \right\}, \quad (7)$$

which is consistent with the spin structure of the amplitude of the low-energy Compton scattering with the electric and magnetic polarizabilities [15]. In the case of Compton forward scattering amplitude has a total spin structure of the form [16]

$$M = g(\omega) \left(\vec{e}^{(\lambda_2)*} \vec{e}^{(\lambda_1)} \right) + ih(\omega) \left(\vec{S} \cdot \left[\vec{e}^{(\lambda_2)*} \vec{e}^{(\lambda_1)} \right] \right). \quad (8)$$

In this definition, the amplitude of the scalar function $g(\omega)$ is even, and $h(\omega)$ - with respect to cross-odd symmetry. Consequently, since the polarizability contribute to the amplitude (8) starting from the second-order and higher, the spin structure of the second term in (8) is determined by the contributions polarizabilities from the third-order.

We now define the Lagrangian and the Compton scattering amplitude in the covariant representation of the dipole.

3 Amplitude of low-energy Compton scattering in covariant dipole representation

In [8] for the construction of an effective relativistic invariant Lagrangian of the interaction of electromagnetic fields with the particles with constant electric and magnetic dipole moments introduced antisymmetric tensor of the dipole moments, which is independent of the electromagnetic field tensor $F_{\mu\nu}$:

$$G^{\mu\nu} = (d^\mu u^\nu - u^\mu d^\nu) + \varepsilon^{\mu\nu\rho\sigma} m_\rho u_\sigma, \quad (9)$$

where d^μ and m^μ – the components of the electric and magnetic moments presented in a covariant form; u^μ – particle 4-speed components, $\varepsilon^{\mu\nu\rho\sigma}$ – 4-dimensional tensor Levi-Civita.

An effective Lagrangians interaction of an electromagnetic field with particles with the constant dipole moments is represented as follows:

$$L = -\frac{1}{2} (e_\mu d^\mu + h_\mu m^\mu), \quad (10)$$

where $e_\mu = F_{\mu\nu} u^\nu$, $h_\mu = \tilde{F}_{\mu\nu} u^\nu$, $\tilde{F}_{\mu\nu} = \frac{1}{2} \varepsilon_{\mu\nu\rho\sigma} F^{\rho\sigma}$.

We are assuming that the form of a tensor (9) can be given and for the induced dipole moments. We will write down in a covariant form taking into account conservation law of parity and definition of a vector of Paulie-Lyubansky W^μ components of vectors of the electric and magnetic moments

$$d^\mu = 4\pi\alpha^{\mu\nu} e_\nu + 4\pi\kappa^{\mu\nu\delta} (\partial_\delta) e_\nu, \quad (11)$$

$$m^\mu = 4\pi\beta^{\mu\nu} h_\nu + 4\pi\tilde{\kappa}^{\mu\nu\delta} (\partial_\delta) h_\nu. \quad (12)$$

In equations (11) and (12) introduced the notation:

$$\alpha^{\mu\nu} = \alpha_1 g^{\mu\nu}, \kappa^{\mu\nu\delta} = \varepsilon^{\mu\nu\rho\varepsilon} W_\rho,$$

$$\beta^{\mu\nu} = \beta_1 g^{\mu\nu}, \tilde{\kappa}^{\mu\nu\delta} = \tilde{\varepsilon}^{\mu\nu\rho\delta} W_\rho.$$

In case of a particle the spin 1/2 vector \hat{W}^μ has the form:

$$\hat{W}^\mu = -\frac{1}{2m} \gamma^5 \left(\gamma^\mu \hat{p} - p^\mu \right),$$

where $\hat{p} = \gamma_\mu p^\mu$, p^μ – a particle 4-momentum, γ^μ – the matrixes satisfying to permutable ratios $\gamma^\mu \gamma^\nu + \gamma^\nu \gamma^\mu = 2g^{\mu\nu}$. Equations (11) and (12) follows

from expressions, d^μ as m^μ consist of symmetric and antisymmetric parts of the permutation of indexes μ and ν . As will be shown below, this presentation is consistent with the condition of crossing symmetry amplitude Compton scattering.

The Lagrangian (10), with which you can get the Compton scattering amplitude and align it with the low-energy theorems, within the field-theoretical covariant approach has the form [17]:

$$L(x) = \frac{i\pi}{4m} \times \left[\bar{\Psi} \gamma^\nu \hat{L}_{\nu\sigma}^{\leftrightarrow} \partial^\sigma \Psi + \bar{\Psi} \hat{L}_{\nu\sigma}^{\leftrightarrow} \gamma^\nu \partial^\sigma \Psi + \bar{\Psi} \gamma^\sigma \hat{L}_{\nu\sigma}^{\leftrightarrow} \partial^\nu \Psi + \bar{\Psi} \hat{L}_{\nu\sigma}^{\leftrightarrow} \gamma^\sigma \partial^\nu \Psi \right], \quad (13)$$

where $\Psi(x)$ is the bispinor of Dirac field, $\hat{\partial}^\nu = \vec{\partial}^\nu - \overleftarrow{\partial}^\nu$, shooters specify the directions of action of derivatives.

As was it is shown in work [13] tensor $\hat{L}_{\nu\sigma}$ in expression (13) has to be is presented definitely that Lagrangian $L(x)$ satisfied to parity conservation law, and spin structures of amplitude of Compton scattering – cross symmetry:

$$\hat{L}_{\nu\sigma} = \hat{L}_{\nu\sigma}^{(\alpha_1)} + \hat{L}_{\nu\sigma}^{(\beta_1)} + \hat{L}_{\nu\sigma}^{(\kappa)} + \hat{L}_{\nu\sigma}^{(\tilde{\kappa})}. \quad (14)$$

In turn, the tensor of (14) are consistent with the definitions (11) and (12) are as follows:

$$\hat{L}_{\nu\sigma}^{(\alpha_1)} = F_{\nu\mu} \hat{\alpha}^{\mu\rho} (\alpha_1) F_{\rho\sigma}, \quad (15)$$

$$\hat{L}_{\nu\sigma}^{(\kappa)} = F_{\nu\mu} \hat{\partial}_\delta^{\leftrightarrow} F_{\rho\sigma} \hat{\kappa}^{\mu\rho\delta} (\kappa), \quad (16)$$

where have introduced the following notations $\alpha^{\mu\nu} = \alpha_1 g^{\mu\nu}$, $\kappa^{\mu\nu\delta} (\kappa) = \varepsilon^{\mu\nu\rho\varepsilon} \hat{W}_\rho$. The derivative $\hat{\partial}_\delta^{\leftrightarrow}$ operate only to tensors of an electromagnetic field $F_{\mu\nu}$, and the operator \hat{W}_ρ operate to wave functions Ψ and $\bar{\Psi}$.

If in tensors (15) and (16) to make replacement $F_{\mu\nu} \rightarrow \tilde{F}_{\mu\nu}$, we will receive expressions for $\hat{L}_{\nu\sigma}^{(\beta_1)}$ and $\hat{L}_{\nu\sigma}^{(\tilde{\kappa})}$. Thus, effective relativistic-invariant Lagrangian, allowing to consider scalar electric and magnetic dipole polarizabilities of a nucleon, it is possible to present in the form:

$$L^{(\alpha_1)} + L^{(\beta_1)} = \frac{2\pi}{m} \left(\alpha_1 F_{\nu\mu} F_\sigma^\mu + \beta_1 \tilde{F}_{\nu\mu} \tilde{F}_\sigma^\mu \right) \theta^{\nu\sigma}, \quad (17)$$

where $\theta^{\nu\sigma} = \frac{i}{2}\bar{\Psi}\gamma^\nu\overleftrightarrow{\partial}^\sigma\Psi$.

Amplitude of Compton scattering taking into account a Lagrangian (17) has the form [18]

$$M^{(\alpha_1)} + M^{(\beta_1)} = \left(\frac{2\pi}{m}\right) \left[\alpha_1 \left(F_{\nu\mu}^{(2)} F_\sigma^{(1)\mu} + F_{\nu\mu}^{(1)} F_\sigma^{(2)\mu} \right) + \beta_1 \left(\tilde{F}_{\nu\mu}^{(2)} \tilde{F}_\sigma^{(1)\mu} + \tilde{F}_{\nu\mu}^{(1)} \tilde{F}_\sigma^{(2)\mu} \right) \right] \bar{U}^{(r_2)} \left(\vec{p}_2 \right) \gamma^\nu P^\sigma U^{(r_1)} \left(\vec{p}_1 \right). \quad (18)$$

In the equation (18) have introduced the notations:

$$F_{\mu\nu}^{(n)} = \left(k_{(n)\mu} e_\nu^{(\lambda_n)} - k_{(n)\nu} e_\mu^{(\lambda_n)} \right),$$

$\tilde{F}_{\mu\nu}^{(n)} = \frac{1}{2}\varepsilon_{\mu\nu\rho\sigma} F^{(n)\rho\sigma}$, parameter n has the values 1 and 2, $e_\mu^{(\lambda_1)}$ and $e_\mu^{(\lambda_2)*}$ are vectors of polarization of initial and final photons, $P = \frac{1}{2}(p_1 + p_2)$, k_1, p_1 and k_2, p_2 are four-momenta of initial and final photons and nucleons, $U^{(r_1)} \left(\vec{p}_1 \right)$ and $\bar{U}^{(r_2)} \left(\vec{p}_2 \right)$ are bispinors of initial and final nucleons.

Follows from (18) a ratio that the part of amplitude of Compton scattering caused by electric α_1 and magnetic β_1 scalar polarizabilities meets a condition of cross symmetry and makes a contribution, since the second order on energy of photons. In system of rest of a target and in the second order on energy of photons from (18) the ratio follows:

$$M^{(\alpha_1)} + M^{(\beta_1)} = 4\pi\omega_1\omega_2\chi_f^+ \left[\alpha_1 \left(\vec{e}^{(\lambda_2)*} \vec{e}^{(\lambda_1)} \right) + \beta_1 \left(\left[\vec{e}^{(\lambda_2)*} \vec{n}_2 \right] \cdot \left[\vec{e}^{(\lambda_1)} \vec{n}_1 \right] \right) \right] \chi_i,$$

which will be coordinated with (7).

4 Dipole spin polarizabilities and the characteristics of a nucleon, connected with violation parity

The electromagnetic characteristics of hadrons connected with not preservation of parity [3, 4] possess properties of the giration used in optics [11]. In this section we will consider relativistic-invariant determination of dipole spin polarizabilities and the giration of a nucleon connected with parity not preservation, and also we will pay attention to distinction of

their deposits to amplitude of Compton scattering. Follows from (14) a ratio that effective Lagrangian, corresponding to deposits of spin dipole polarizabilities κ and $\tilde{\kappa}$, has an appearance:

$$L^{(\kappa)} + L^{(\tilde{\kappa})} = \frac{i\pi}{4m} (\varepsilon^{\mu\rho\kappa\delta}) \left[\kappa F_{\nu\mu} \overset{\leftrightarrow}{\partial}_\delta F_{\rho\sigma} + \tilde{\kappa} \tilde{F}_{\nu\mu} \overset{\leftrightarrow}{\partial}_\delta \tilde{F}_{\rho\sigma} \right] \times \\ \times \bar{\Psi} \left[\left(\gamma^\nu \hat{W}_\kappa + \hat{W}_\kappa \gamma^\nu \right) \overset{\leftrightarrow}{\partial}^\sigma + \left(\gamma^\sigma \hat{W}_\kappa + \hat{W}_\kappa \gamma^\sigma \right) \overset{\leftrightarrow}{\partial}^\nu \right] \Psi. \quad (19)$$

The part of amplitude of Compton scattering calculated on the basis of this Lagrangian is defined as follows:

$$M^{(\kappa)} + M^{(\tilde{\kappa})} = \frac{i\pi}{4m^2} (\varepsilon^{\mu\rho\kappa\delta}) (k_1 + k_2)_\delta \left[\kappa \left(F_{\nu\mu}^{(2)} F_{\rho\sigma}^{(1)} - F_{\sigma\rho}^{(2)} F_{\mu\nu}^{(1)} \right) + \right. \\ \left. + \tilde{\kappa} \left(\tilde{F}_{\nu\mu}^{(2)} \tilde{F}_{\rho\sigma}^{(1)} - \tilde{F}_{\sigma\rho}^{(2)} \tilde{F}_{\mu\nu}^{(1)} \right) \right] \bar{U}^{(r_2)} \left(\vec{p}_2 \right) \gamma^5 [(\delta_\tau^\nu \gamma_\kappa - \delta_\kappa^\nu \gamma_\tau) P^\sigma + \\ + (\delta_\tau^\sigma \gamma_\kappa - \delta_\kappa^\sigma \gamma_\tau) P^\nu] P_\tau U^{(r_1)} \left(\vec{p}_1 \right). \quad (20)$$

Expression (20) is testified of an invariant of cross symmetry. The contribution of spin polarizabilities κ also $\tilde{\kappa}$ begins with the third order on energy of photons. If determine amplitude (20) in the rest frame and to neglect an impulse of return of a nucleon, we will obtain

$$M^{(\kappa)} + M^{(\tilde{\kappa})} = 4\pi i (\omega_1 + \omega_2) (\omega_1 \omega_2) \left\{ \kappa \left(\vec{S} \left[\vec{e} \left[\vec{e}^{(\lambda_2)*} \vec{e}^{(\lambda_1)} \right] \right) \right) + \right. \\ \left. + \tilde{\kappa} \left(\vec{S} \left[\left[\vec{e} \left[\vec{e}^{(\lambda_2)*} \vec{n}_2 \right] \cdot \left[\vec{e}^{(\lambda_1)} \vec{n}_1 \right] \right] \right) \right) \right\}. \quad (21)$$

According to from the equations (19) and (21) Lagrangian by means of which the contribution of spin dipole polarizabilities κ and $\tilde{\kappa}$ to amplitude of Compton scattering is considered is even concerning inversion of space.

By analogy with Lagrangian (19) we will construct new Lagrangian by which we will define contributions of girations (the characteristics connected with parity not preservation) to amplitude of Compton scattering. For this purpose it is enough in (19) to make replacement $\hat{W}_\kappa \rightarrow 1/m \overset{\leftrightarrow}{\partial}_\kappa$. As a result we will obtain:

$$L = \frac{i\pi}{2m^2} (\varepsilon^{\mu\rho\kappa\delta}) \left[\delta_E F_{\nu\mu} \overset{\leftrightarrow}{\partial}_\delta F_{\rho\sigma} + \delta_M \tilde{F}_{\nu\mu} \overset{\leftrightarrow}{\partial}_\delta \tilde{F}_{\rho\sigma} \right] \times \\ \times \bar{\Psi} \left[\left(\gamma^\nu \overset{\leftrightarrow}{\partial}_\kappa \overset{\leftrightarrow}{\partial}^\sigma + \gamma^\sigma \overset{\leftrightarrow}{\partial}_\kappa \overset{\leftrightarrow}{\partial}^\nu \right) \right] \Psi, \quad (22)$$

where δ_E and δ_M are electric and magnetic girations.

Amplitude of Compton scattering which is obtained on the basis of a Lagrangian (22), in system of rest of a target and in neglect an impulse of return of a target, is defined so

$$M = 4\pi\omega_1\omega_2\chi_f^+ \left\{ \delta_E \left(\left(\vec{k}_1 + \vec{k}_2 \right) \cdot \left[\vec{e}^{(\lambda_2)*} \vec{e}^{(\lambda_1)} \right] \right) + \right. \\ \left. + \delta_M \left(\left(\vec{k}_1 + \vec{k}_2 \right) \cdot \left[\vec{\Sigma}_2 \vec{\Sigma}_1 \right] \right) \right\} \chi_i, \quad (23)$$

where $\vec{\Sigma}_2 = \left[\vec{e}^{(\lambda_2)*} \vec{n}_2 \right]$, $\vec{\Sigma}_1 = \left[\vec{e}^{(\lambda_1)} \vec{n}_1 \right]$.

The ratio (23) will be coordinated with low-energy determination of amplitude (3) if to present tensors of polarizabilities through δ_E and δ_M [11]

$$\alpha_{ij} = \alpha_1 \delta_{ij} + i \delta_E \varepsilon_{ijk} \partial_k, \\ \beta_{ij} = \beta_1 \delta_{ij} + i \delta_M \varepsilon_{ijk} \partial_k,$$

where the derivative ∂_κ action to vectors of an electromagnetic field.

Thus, from the equations (21) and (23) follows:

- 1) in both amplitudes the condition of cross symmetry is satisfied;
- 2) if in the ratio (21) the invariance condition concerning inversion of space is satisfied, in the ratio (23) this condition is violated;
- 3) deposits of a giration and spin dipole polarizabilities to amplitude of Compton scattering on a nucleon begins with the third order on energy of photons.

5 Conclusion

In this work the proposal relativistic-invariant definition of spin dipole polarizabilities and girations which foundation on covariant build of the induced dipole moments and phenomenological effective Lagrangians of interaction of an electromagnetic field with these moments of a structural particle a spin 1/2 is offered. It is shown that in the offered model taking into account cross symmetry, gauge-invariant and properties of a Lagrangian to inversion of space spin dipole polarizabilities and a giration

make a contribution to decomposition of amplitude of Compton scattering since the third order on energy of photons according to low-energy theorems of Compton scattering on a nucleon.

This work was supported by the Belarusian Republican Foundation for Basic Research (grants N F14-035 and N F15D-009).

References

- [1] Maksimenko, N.V. Low-energy decomposition of amplitude of Compton scattering on a hadron and simultaneous switchboards of currents / N.V. Maksimenko, S.G. Shulga // Nuclear physics. – 1990. – Vol. 52. – N 2(8). – P. 524-534.
- [2] Hill, R.J. The NRQED lagrangian at order $\frac{1}{M^4}$ / R.J. Hill, G. Lee, G. Paz, M.P. Solon // Phys. Rev. D. – 2013. – Vol. 87. – N 5. – P. 053017-1-13.
- [3] Bedaque, P.F. Parity violation in $\gamma\vec{p}$ Compton Scattering / P.F. Bedaque, M.J. Savage // Phys. Rev. C. – 2000. – Vol. 62. – P.018501-1-6.
- [4] Gorchtein, M. Forward Compton Scattering with weak neutral current: constraints from sum rules / M. Gorchtein, X. Zhang // [Electronic resource]. – 2015. – Mode of access: <http://nucl-th/1501.0535>. – Date of access: 22.01.2015.
- [5] Gorchtein, M. CP-violation in Compton Scattering / M. Gorchtein // Phys. Rev. C. – 2008. – Vol.77. – P.065501-1-6.
- [6] Carlson, C.E. Constraining off-shell effects using low-energy Compton scattering / C.E. Carlson, M. Vanderhaeghen // [Electronic resource]. – 2011. – Mode of access: <http://physics.atom-ph/1109.3779>. – Date of access: 04.10.2011.
- [7] Krupina, N. Separation of proton polarizabilities with the beam asymmetry of Compton scattering / N. Krupina, V. Pascalutsa // Phys. Rev. Lett. – 2013. – Vol.110. – N 26. – P. 262001-1-4.
- [8] Anandan, J.S. Classical and quantum interaction of the dipole / J.S.Anandan // Phys. Rev. Lett. – 2000. – Vol. 85. – P. 1354-1357.

- [9] Silenko, A.J. Spin precession of a particle with an electric dipole moment: contributions from classical electrodynamics and from the Thomas effect / A.J. Silenko // Phys. Scr. - 2015. - Vol. 90. - P. 065303 (6pp).
- [10] Landau, L.D. Theory of field / L.D. Landau, E.M. Lifshits. – M.: Science, 1967. – 460 p.
- [11] Fedorov, F.I. Theory of gyrotropy / F.I. Fedorov. – Minsk: Science and equipment, 1976. – 456 p.
- [12] Baryshevsky, V.G. Nuclear optics of the polarized environments / V.G. Baryshevsky. – Moscow: Energoatomizdat, 1995. – 316 p.
- [13] Andreev, V.V. Covariant representation of spin polarizabilities of a nucleon / V.V. Andreev, O.M. Deryuzhkova, N.V. Maksimenko // Problems of physics, mathematics and equipment. – 2014. – N 3(20). – P. 7-12.
- [14] Galynsky, M.V. O transformation of a tensor of a bunch at interaction of light with Wednesday / M.V. Galynsky, F.I. Fedorov // ZhPS. – 1986. – Vol. 44. – N 2. – P. 288-292.
- [15] Petrunkin, V.A. The electric and magnetic polarizabilities of hadrons / V. A. Petrunkin // Elem. Chast. Atom. Yad. – 1981. – Vol. 12. – N 3. – P. 692-753.
- [16] Damashek, M. Forward Compton scattering / M. Damashek, F.J.Gilman // Phys. Rev. – 1970. – Vol. D1. – N 6. – P. 1319-1332.
- [17] Andreev, V.V. Polarizabilities of elementary particles in theoretical-field approach / V.V. Andreev, N.V. Maksimenko // Problems of physics, mathematics and equipment. – 2011. – N 4(9). – P. 7-11.
- [18] Andreev, V.V. Covariant equations of motion of a spin 1/2 particle in an electromagnetic field with allowance for polarizabilities / V.V. Andreev, O.M. Deryuzhkova, N.V. Maksimenko // Russ. Phys. Journ. – 2014. – Vol. 56. –N 9. – P. 1069-1075.

Form Factor of the Relativistic Two-particle System in the Relativistic Quasipotential Approach: The Case of Arbitrary Masses and Vector Current

Yu.D. Chernichenko,
Sukhoi State Technical University of Gomel

Abstract

A new relativistic form factor for a bound two-particle system was obtained for the case of a vector current. The present consideration was performed within the relativistic quasipotential approach based on the covariant Hamiltonian formulation of quantum field theory by going over to the three dimensional relativistic configuration representation for the case of interaction between two relativistic spinless particles of arbitrary mass.

1 Introduction

The study of hadrons electromagnetic form factors allows to obtain the information about spatial hadrons structure. The idea of the composite quark nature of hadrons and suggestion about scale invariant behavior in the region of large momentum transfers has allowed to reveal regularity of the elastic hadrons form factors behavior [1]. To describe the behavior of the form factors the different pole vector-dominance models (VDM) were used. These models successfully reproduce the behavior of the pion form factor as in space-like, so and at time-like regions [2], and behavior of the nucleon form factor in the space-like regions [3]. However the models VDM fail in description experimently of the observed for large importances of the momentum transfer of the system $-t = Q^2$ the quick decrease of electromagnetic form factor at time-like region according to the law of

dipole $\sim t^{-2}$. The reason is that the model VDM assume that the virtual photon flying in the nucleon “sees” only the vector mesons which there are the quark-antiquark bound-states while the structure of nucleon study at small distances where the momentum transfer of the system there is enough large value and quarks move quasifree (the asymptotic freedom).

However the problem of covariant description of form factor in the whole, rather than only in asymptotic region energy within the framework of relativistic quark model taking into account differences of their masses, continues remain interesting and at present. For this we must know the dynamics of the interacting quarks more in detail, in particular, we must know the covariant wave functions their of relative motion.

Within the quantum field theory the covariant wave functions of the relative motion can be obtained using the relativistic covariant two-particle quasipotential equations of Logunov–Tavkhelidze [4] and Kadyshevsky [5, 6]. The using of three-dimensional relativistic quasipotential (RQP) equation of Logunov-Tavkhelidze for description of the form factors of composite systems was executed in [7–11]. However, use of the equation Logunov-Tavkhelidze for wave function in the momentum representation has not allowed to research the behavior of the form factor in broad interval of importances of the momentum transfer of the relativistic two-particle bound system. The other model of the account of the contribution small the distances in form factor of the proton was considered in [12]. This model is based on invariant description of the structure of the particles in relativistic configurational space that was carried in [13] in the case of interaction between two relativistic spinless particles that have equal masses m in which the Compton wavelength of particle plays role of the natural scale. In this model is taken into account both the contribution to the proton form factor of vector mesons and the contribution from its the central part having radius of the Compton wavelength. The method of transition to the relativistic configurational representation in the case of interaction between two relativistic spinless particles with equal masses proposed in [13] was used in [14] to construct the three-dimensional covariant formalism for the description of relativistic two-particle systems. Within the framework of this formalism the expressions for the form factors of relativistic two-particle systems [15, 16] were obtained.

The aim of this work is to obtain the expression for the elastic form factor of relativistic two-particle system in the case of vector current on the basis of covariant Hamiltonian formulation of quantum field theory [5, 6] by

transition to the three-dimensional relativistic configurational representation for the interaction of two relativistic spinless particles having arbitrary masses m_1, m_2 [17, 18].

2 Equation for the wave function

In the case of interaction between two relativistic particles with arbitrary masses m_1 and m_2 , the RQP approach developed in [17, 18] permitted introducing the concept of an effective relativistic particle whose mass is $m' = \sqrt{m_1 m_2}$ and which plays the role of a bound two-particle system. Whereby one reduces the two-body problem in question to a one-body problem treated in terms of the RQP wave function $\Psi_{M_Q}(\Delta_{p', m' \lambda_Q})$ describing the effective relativistic particle and satisfying the fully covariant RQP Kadyshevsky equation in angular momentum space with the velocity 4-vector $\lambda_Q = (\lambda_Q^0; \boldsymbol{\lambda}_Q)$; ¹⁾ that is,

$$\begin{aligned} & (2\Delta_{q', m' \lambda_Q}^0 - 2\Delta_{p', m' \lambda_Q}^0) \Psi_{M_Q}(\Delta_{p', m' \lambda_Q}) = \\ & = \frac{2\mu}{m'} \frac{1}{(2\pi)^3} \int d\Omega_{\Delta_{k', m' \lambda_Q}} \tilde{V}(\Delta_{p', m' \lambda_Q}, \Delta_{k', m' \lambda_Q}; \Delta_{q', m' \lambda_Q}^0) \Psi_{M_Q}(\Delta_{k', m' \lambda_Q}), \end{aligned} \quad (1)$$

where $\mu = m_1 m_2 / (m_1 + m_2)$ is the ordinary reduced mass of two particles that have arbitrary masses and $d\Omega_{\Delta_{k', m' \lambda_Q}} = m' d\Delta_{k', m' \lambda_Q} / \Delta_{k', m' \lambda_Q}^0$ is the relativistic three-dimensional volume element in Lobachevsky space, all 4-momenta now belonging to the upper sheet of the mass hyperboloid:

$$\Delta_{k', m' \lambda_Q}^{02} - \Delta_{k', m' \lambda_Q}^2 = m'^2. \quad (2)$$

This sheet, embedded in 4-dimensional momentum space, serves as a model of relativistic non-Euclidean momentum space. On the mass-hyperboloid sheet (2), the Lorentz group is the motion group for this space. Upon choosing the pure Lorentz transformation (boost) $\Lambda_{\lambda_Q}^{-1}$ corresponding to the composite particle 4-velocity λ_Q , $\Lambda_{\lambda_Q}^{-1} Q = (M_Q; \mathbf{0})$, the 4-vector components $\Delta_{k', m' \lambda_Q}$ from the Lobachevsky space assume the form

$$\begin{aligned} \Delta_{k', m' \lambda_Q}^0 &= (\Lambda_{\lambda_Q}^{-1} k')^0 = k'_0 \lambda_Q^0 - \mathbf{k}' \cdot \boldsymbol{\lambda}_Q = \sqrt{m'^2 + \Delta_{k', m' \lambda_Q}^2}, \\ \Delta_{k', m' \lambda_Q} &= \Lambda_{\lambda_Q}^{-1} \mathbf{k}' = \mathbf{k}'(-) m' \boldsymbol{\lambda}_Q = \mathbf{k}' - \boldsymbol{\lambda}_Q \left(k'_0 - \frac{\mathbf{k}' \cdot \boldsymbol{\lambda}_Q}{1 + \lambda_Q^0} \right). \end{aligned} \quad (3)$$

¹⁾We use the system of units where $\hbar = c = 1$.

Equation (1) can be considered as a direct relativistic generalization of the Schrödinger equation in the spirit of Lobachevsky geometry arising on the upper mass-hyperboloid sheet (2). This equation describes scattering on the quasipotential $\tilde{V}(\mathbf{\Delta}_{p',m'\lambda_Q}, \mathbf{\Delta}_{k',m'\lambda_Q}; \Delta_{q',m'\lambda_Q}^0)$ for an effective relativistic particle that plays the role of a two-particle system, has a mass m' and a relative 3-momentum $\mathbf{\Delta}_{q',m'\lambda_Q}$, and carries the total energy of two free relativistic particles of arbitrary mass. This energy $\sqrt{s_q} = M_Q$ is proportional to the energy $\Delta_{q',m'\lambda_Q}^0$ for one effective relativistic particle of mass m' ; that is,

$$\sqrt{s_q} = \sqrt{(q_1 + q_2)^2} = \frac{m'}{\mu} \Delta_{q',m'\lambda_Q}^0, \quad \Delta_{q',m'\lambda_Q}^0 = \sqrt{m'^2 + \mathbf{\Delta}_{q',m'\lambda_Q}^2}. \quad (4)$$

In the equation (1) it is convenient to expand over the complete system of functions [17, 18]

$$\xi(\mathbf{\Delta}_{p',m'\lambda_Q}, \mathbf{r}) = \left(\frac{\Delta_{p',m'\lambda_Q}^0 - \mathbf{\Delta}_{p',m'\lambda_Q} \cdot \mathbf{n}}{m'} \right)^{-1-ir/\lambda'}, \quad (5)$$

which realize the principal series of unitary irreducible representations of the Lorentz group, i.e. the group of motions of the Lobachevsky space momentum, realized on upper sheet of the mass hyperboloid (2). The group parameter r in (5) plays the role of the modulus of the relativistic relative coordinate \mathbf{r} ($\mathbf{r} = r\mathbf{n}$, $|\mathbf{n}| = 1$), and $\lambda' = 1/m'$ is the Compton wavelength associated with the effective relativistic particle of mass m' [13, 18]. This parameter enumerates the eigenvalues of the invariant Casimir operator of the Lorentz group $\hat{C}_L = (1/4)M_{\mu\nu}M^{\mu\nu}$ ($M_{\mu\nu} = p_\mu\partial/\partial p^\nu - p_\nu\partial/\partial p^\mu$ are the group generators):

$$\hat{C}_L \xi(\mathbf{\Delta}_{p',m'\lambda_Q}, \mathbf{r}) = \left(\frac{1}{m'^2} + r^2 \right) \xi(\mathbf{\Delta}_{p',m'\lambda_Q}, \mathbf{r}), \quad 0 \leq r < \infty, \quad (6)$$

and, therefore, it is a relativistic invariant.

The functions in (5) obey the following conditions of completeness and orthogonality [18]:

$$\frac{1}{(2\pi)^3} \int d\Omega_{\mathbf{\Delta}_{p',m'\lambda_Q}} \xi(\mathbf{\Delta}_{p',m'\lambda_Q}, \mathbf{r}) \xi^*(\mathbf{\Delta}_{p',m'\lambda_Q}, \mathbf{r}') = \delta(\mathbf{r}' - \mathbf{r}), \quad (7)$$

$$\frac{1}{(2\pi)^3} \int d\mathbf{r} \xi(\mathbf{\Delta}_{q',m'\lambda_Q}, \mathbf{r}) \xi^*(\mathbf{\Delta}_{p',m'\lambda_Q}, \mathbf{r}) = \frac{\Delta_{q',m'\lambda_Q}^0}{m'} \delta(\mathbf{\Delta}_{p',m'\lambda_Q} - \mathbf{\Delta}_{q',m'\lambda_Q}),$$

and these the functions satisfy the equation in terms of finite differences [18]

$$(2\Delta_{p',m'\lambda_Q}^0 - \widehat{H}_0)\xi(\Delta_{p',m'\lambda_Q}, \mathbf{r}) = 0. \quad (8)$$

Here

$$\widehat{H}_0 = 2m' \left[\cosh \left(i\lambda' \frac{\partial}{\partial r} \right) + \frac{i\lambda'}{r} \sinh \left(i\lambda' \frac{\partial}{\partial r} \right) - \frac{\lambda'^2}{2r^2} \Delta_{\theta,\varphi} \exp \left(i\lambda' \frac{\partial}{\partial r} \right) \right] \quad (9)$$

is the operator of the free Hamiltonian, while $\Delta_{\theta,\varphi}$ is its angular part.

The wave RQP-functions in the momentum space and the \mathbf{r} -representation, called the relativistic configuration representation [17, 18], are related by

$$\begin{aligned} \psi_{M_Q}(\mathbf{r}) &= \frac{1}{(2\pi)^3} \int d\Omega_{\Delta_{p',m'\lambda_Q}} \xi(\Delta_{p',m'\lambda_Q}, \mathbf{r}) \Psi_{M_Q}(\Delta_{p',m'\lambda_Q}), \quad (10) \\ \Psi_{M_Q}(\Delta_{p',m'\lambda_Q}) &= \int d\mathbf{r} \xi^*(\Delta_{p',m'\lambda_Q}, \mathbf{r}) \psi_{M_Q}(\mathbf{r}). \end{aligned}$$

For the local quasipotential

$$\widetilde{V}(\Delta_{p',m'\lambda_Q}, \Delta_{k',m'\lambda_Q}; \Delta_{q',m'\lambda_Q}^0) \equiv \widetilde{V}((\Delta_{p',m'\lambda_Q}(-)\Delta_{k',m'\lambda_Q})^2; \Delta_{q',m'\lambda_Q}^0) \quad (11)$$

square of the vector of momentum transfer in the Lobachevsky space $\Delta_{p',k'} = \mathbf{p}'(-)\mathbf{k}'$ is the Loretz invariant that allows to present it in the form

$$\Delta_{p',k'}^2 = (\Delta_{p',k'}^0)^2 - m'^2 = (\Delta_{p',m'\lambda_Q}(-)\Delta_{k',m'\lambda_Q})^2 = \Delta_{\Delta_{p',m'\lambda_Q}, \Delta_{k',m'\lambda_Q}}^2.$$

Thus, the quasipotential (11) depends on the invariant quantity the square of vector of difference in the Lobachevsky space of two momentum vectors $\Delta_{\Delta_{p',m'\lambda_Q}, \Delta_{k',m'\lambda_Q}} = \Delta_{p',m'\lambda_Q}(-)\Delta_{k',m'\lambda_Q}$. With this quasipotential, the right-hand side of equation (1) represents a convolution in the Lobachevsky space that allows to use the expansion over the matrix elements of group of motions of this space, i.e. transformations (10). By using transformations (10) and eq. (8), equation (1) with the quasipotential (11) local in the Lobachevsky space takes the form

$$(2\Delta_{q',m'\lambda_Q}^0 - \widehat{H}_0)\psi_{M_Q}(\mathbf{r}) = \frac{2\mu}{m'} V(\mathbf{r}; \Delta_{q',m'\lambda_Q}^0) \psi_{M_Q}(\mathbf{r}), \quad (12)$$

where the quasipotential $V(\mathbf{r}; \Delta_{q',m'\lambda_{\mathcal{Q}}}^0)$ is given in terms of the same relativistic plane waves as

$$V(\mathbf{r}; \Delta_{q',m'\lambda_{\mathcal{Q}}}^0) = \frac{1}{(2\pi)^3} \int d\Omega_{\Delta_{p',k'}} \xi(\Delta_{p',k'}, \mathbf{r}) \tilde{V}((\Delta_{p',k'})^2; \Delta_{q',m'\lambda_{\mathcal{Q}}}^0).$$

For spherically symmetric potentials, expanding the quasipotential wave RQP-function $\psi_{M_{\mathcal{Q}}}(\mathbf{r})$ in the Legendre functions $P_{\mu}^{\nu}(z)$ of the first kind as

$$\psi_{M_{\mathcal{Q}}}(\mathbf{r}) = \sum_{\ell=0}^{\infty} (2\ell+1) i^{\ell} \frac{\varphi_{\ell}(r, \chi)}{r} P_{\ell}\left(\frac{\Delta_{q',m'\lambda_{\mathcal{Q}}} \cdot \mathbf{r}}{|\Delta_{q',m'\lambda_{\mathcal{Q}}}|r}\right), \quad (13)$$

we obtain equation for the partial wave function in the form

$$\left[\cosh\left(i\lambda' \frac{d}{dr}\right) + \frac{\lambda'^2 \ell(\ell+1)}{2r(r+i\lambda')} \exp\left(i\lambda' \frac{d}{dr}\right) - X(r) \right] \varphi_{\ell}(r, \chi) = 0, \quad (14)$$

where

$$X(r) = \frac{\mu}{m'^2} (M_{\mathcal{Q}} - V(r; \chi)),$$

and χ is the rapidity related with the relative 3-momentum and energy of effective relativistic particle by the formulas

$$\begin{aligned} \Delta_{q',m'\lambda_{\mathcal{Q}}} &= m' \sinh \chi \mathbf{n}_{\Delta_{q',m'\lambda_{\mathcal{Q}}}}, \quad |\mathbf{n}_{\Delta_{q',m'\lambda_{\mathcal{Q}}}}| = 1, \\ M_{\mathcal{Q}} &= \frac{m'}{\mu} \Delta_{q',m'\lambda_{\mathcal{Q}}}^0, \quad \Delta_{q',m'\lambda_{\mathcal{Q}}}^0 = m' \cosh \chi. \end{aligned}$$

3 Form factor of the relativistic two-particle system

For simplicity we consider here only the case of spinless field when the Hamiltonian density is given by the expression

$$H(x) = -z_1 \varphi_1^+(x) \varphi_1(x) A(x) - z_2 \varphi_2^+(x) \varphi_2(x) A(x). \quad (15)$$

In ref. [15] founded on refs. [7–11], the form factor of two-particle system was defined as the matrix element of the local current operator between bound states with the 4-momentum \mathcal{P} , \mathcal{Q} through the covariant wave RQP-functions satisfying eq. (1). Then, as follows from refs. [15, 16], the invariant expression in the momentum representation for the matrix element of

the local vector-current operator near poles of bound states for the interaction of two relativistic spinless particles with arbitrary masses m_1, m_2 has the form

$$\begin{aligned}
\langle \mathcal{P} | J_\nu | \mathcal{Q} \rangle = & \frac{z_1}{(2\pi)^3} \int d\tau_{\mathcal{P}} d\tau_{\mathcal{Q}} d^{(4)}k_2 d^{(4)}k_1 d^{(4)}k'_1 \theta(k_{20}) \delta(k_2^2 - m_2^2) \times \quad (16) \\
& \times \Gamma_{\mathcal{P}}^+(k'_1, k_2; \lambda_{\mathcal{P}} \tau_{\mathcal{P}}) \frac{(k_1 + k'_1)_\nu}{(\tau_{\mathcal{P}} + i\varepsilon)(\tau_{\mathcal{Q}} - i\varepsilon)} \Gamma_{\mathcal{Q}}(k_1, k_2; \lambda_{\mathcal{Q}} \tau_{\mathcal{Q}}) \theta(k_{10}) \delta(k_1^2 - m_1^2) \times \\
& \times \theta(k'_{10}) \delta(k_1'^2 - m_1^2) \delta^{(4)}(-\mathcal{Q} + k_1 + k_2 + \lambda_{\mathcal{Q}} \tau_{\mathcal{Q}}) \delta^{(4)}(\mathcal{P} - k_2 - k'_1 - \lambda_{\mathcal{P}} \tau_{\mathcal{P}}) + \\
& + (1 \leftrightarrow 2),
\end{aligned}$$

where all the momenta of the particles belong to the mass shells

$$k_i^2 = k_{i0}^2 - \mathbf{k}_i^2 = m_i^2, i = 1, 2. \quad (17)$$

As a vectors $\lambda_{\mathcal{P}}$ and $\lambda_{\mathcal{Q}}$, it is convenient to choose the 4-velocities of the system: $\lambda_{\mathcal{P}} = \mathcal{P}/\sqrt{\mathcal{P}^2}$, $\mathcal{P}^2 = (p_1 + p_2)^2 = s_p = M_{\mathcal{P}}^2$ and $\lambda_{\mathcal{Q}} = \mathcal{Q}/\sqrt{\mathcal{Q}^2}$, $\mathcal{Q}^2 = (q_1 + q_2)^2 = s_q = M_{\mathcal{Q}}^2$. This expression answers the diagram on fig. 1. Here follows to emphasize that because of transition to different own timeses of the system before ($\tau_{\mathcal{Q}} = \lambda_{\mathcal{Q}} X$, $X = x_1 + x_2$) and after interaction ($\tau_{\mathcal{P}} = \lambda_{\mathcal{P}} X$) the diagram on fig. 1 differ from diagrams, which appear in approach of the Kadyshevsky for S -matrix. The 4-velocities of the com-

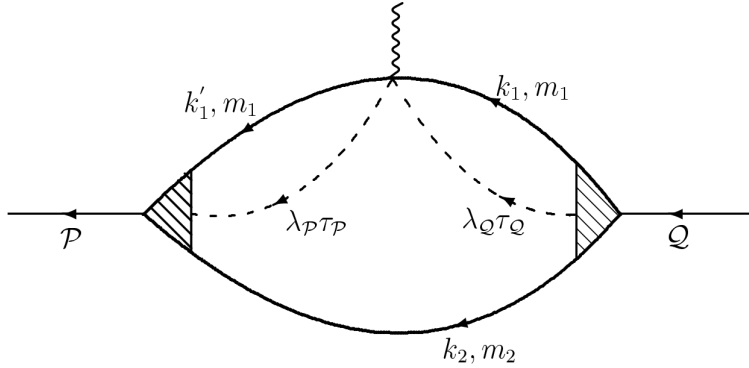


Figure 1: *The diagram for the matrix element of the local current operator between bound states with the 4-momentum \mathcal{P} , \mathcal{Q} for the interaction of two relativistic spinless particles with arbitrary masses.*

posite particle before, $\lambda_{\mathcal{Q}}$, and after interaction, $\lambda_{\mathcal{P}}$, will differ also.

In the case of equal quark masses ($m_1 = m_2 = m$) and for real-valued wave functions, expression (16) for the matrix element of the vector-current operator satisfies the transverseness condition

$$(\mathcal{P} - \mathcal{Q})^\nu \langle \mathcal{P} | J_\nu | \mathcal{Q} \rangle = 0, \quad (18)$$

This circumstance was used in [16]. In the case of unequal quark masses ($m_1 \neq m_2$), expression (16) for the matrix element of the vector-current operator features additionally its transverse component, which breaks the transverseness condition in (18). Therefore, the 4-vector in expression (16) can be represented in the form

$$\langle \mathcal{P} | J_\nu | \mathcal{Q} \rangle = F^{(+)}(t)(\mathcal{P} + \mathcal{Q})_\nu + iF^{(-)}(t)(\mathcal{P} - \mathcal{Q})_\nu. \quad (19)$$

In the case of unequal masses ($m_1 \neq m_2$), expression (16) for the matrix element of the local vector-current operator can be reduced to a one-body problem. The respective expression will be the convolution of the RQP wave functions for a single effective relativistic particle in this space. Thus, it is necessary to multiply expression (16) by $(\mathcal{P} \pm \mathcal{Q})^\nu$ and to consider that, at $\mathcal{Q}^2 = M_{\mathcal{Q}}^2$, $\mathcal{P}^2 = M_{\mathcal{P}}^2$, the following relation holds:

$$t = (\mathcal{P} - \mathcal{Q})^2 = -Q^2 = M_{\mathcal{Q}}^2 + M_{\mathcal{P}}^2 - 2\mathcal{P}\mathcal{Q}, \quad 2\mathcal{P}\mathcal{Q} = \quad (20)$$

$$= M_{\mathcal{Q}}^2 + M_{\mathcal{P}}^2 - t, \quad (\mathcal{P} + \mathcal{Q})^2 = 2(M_{\mathcal{Q}}^2 + M_{\mathcal{P}}^2) - t. \quad (21)$$

Performing integration with respect to $dk_{20}, dk_{10}, dk'_{10}$ and taking into account Eqs. (19) and (20), we obtain the following expressions for the form-factor components:

$$\begin{aligned} F^{(+)}(t) &= \frac{z_1}{(2M_{\mathcal{Q}}^2 + 2M_{\mathcal{P}}^2 - t)(4\pi)^3} \int \frac{d\tau_{\mathcal{P}} d\tau_{\mathcal{Q}} d\mathbf{k}_2 d\mathbf{k}_1 d\mathbf{k}'_1}{\sqrt{m_2^2 + \mathbf{k}_2^2} \sqrt{m_1^2 + \mathbf{k}_1^2} \sqrt{m_1^2 + \mathbf{k}'_1{}^2}} \times \\ &\times \Gamma_{\mathcal{P}}^+(k'_1, k_2; \lambda_{\mathcal{P}} \tau_{\mathcal{P}}) \frac{(\mathcal{P} + \mathcal{Q})(k_1 + k'_1)}{(\tau_{\mathcal{P}} + i\varepsilon)(\tau_{\mathcal{Q}} - i\varepsilon)} \Gamma_{\mathcal{Q}}(k_1, k_2; \lambda_{\mathcal{Q}} \tau_{\mathcal{Q}}) \times \\ &\times \delta^{(4)} \left[\left(-1 + \frac{\tau_{\mathcal{Q}}}{M_{\mathcal{Q}}} \right) \mathcal{Q} + k_1 + k_2 \right] \delta^{(4)} \left[\left(1 - \frac{\tau_{\mathcal{P}}}{M_{\mathcal{P}}} \right) \mathcal{P} - k_2 - k'_1 \right] + \\ &+ (1 \leftrightarrow 2), \end{aligned} \quad (22)$$

$$\begin{aligned}
F^{(-)}(t) = & \frac{z_1}{it(4\pi)^3} \int \frac{d\tau_{\mathcal{P}} d\tau_{\mathcal{Q}} d\mathbf{k}_2 d\mathbf{k}_1 d\mathbf{k}'_1}{\sqrt{m_2^2 + \mathbf{k}_2^2} \sqrt{m_1^2 + \mathbf{k}_1^2} \sqrt{m_1^2 + \mathbf{k}'_1^2}} \times \quad (23) \\
& \times \Gamma_{\mathcal{P}}^+(k'_1, k_2; \lambda_{\mathcal{P}} \tau_{\mathcal{P}}) \frac{(\mathcal{P} - \mathcal{Q})(k_1 + k'_1)}{(\tau_{\mathcal{P}} + i\varepsilon)(\tau_{\mathcal{Q}} - i\varepsilon)} \Gamma_{\mathcal{Q}}(k_1, k_2; \lambda_{\mathcal{Q}} \tau_{\mathcal{Q}}) \times \\
& \times \delta^{(4)} \left[\left(-1 + \frac{\tau_{\mathcal{Q}}}{M_{\mathcal{Q}}} \right) \mathcal{Q} + k_1 + k_2 \right] \delta^{(4)} \left[\left(1 - \frac{\tau_{\mathcal{P}}}{M_{\mathcal{P}}} \right) \mathcal{P} - k_2 - k'_1 \right] + (1 \leftrightarrow 2).
\end{aligned}$$

Within this approach, for the bounded system of spinless particles which are found in the motion with moment $J = 0$ the vertex functions $\Gamma_{\mathcal{Q}}(k_2, k_1; \lambda_{\mathcal{Q}} \tau_{\mathcal{Q}})$ and $\Gamma_{\mathcal{P}}(k_2, k'_1; \lambda_{\mathcal{P}} \tau_{\mathcal{P}})$ when $\lambda_{\mathcal{Q}} \uparrow\uparrow \mathcal{Q}$ and $\lambda_{\mathcal{P}} \uparrow\uparrow \mathcal{P}$ will depend each only on one the Lorentz invariant scalar parameter, as which we choose accordingly $\mathcal{Q}k_2$ and $\mathcal{P}k_2$. According to Eqs. (3), these parameters are invariant under the pure Lorentz transformations $\Lambda_{\lambda_{\mathcal{Q}, \mathcal{P}}}^{-1}$: $\Lambda_{\lambda_{\mathcal{Q}}}^{-1} \mathcal{Q} = (M_{\mathcal{Q}}; \mathbf{0})$, $\Lambda_{\lambda_{\mathcal{P}}}^{-1} \mathcal{P} = (M_{\mathcal{P}}; \mathbf{0})$; therefore, we have

$$\mathcal{Q}k_2 = \Lambda_{\lambda_{\mathcal{Q}}}^{-1}(\mathcal{Q}k_2) = M_{\mathcal{Q}} \Delta_{k_2, m_2 \lambda_{\mathcal{Q}}}^0, \mathcal{P}k_2 = \Lambda_{\lambda_{\mathcal{P}}}^{-1}(\mathcal{P}k_2) = M_{\mathcal{P}} \Delta_{k_2, m_2 \lambda_{\mathcal{P}}}^0.$$

Moreover, the application of the Lorentz transformation $\Lambda_{\lambda_{\mathcal{Q}, \mathcal{P}}}^{-1}$ to the conservation laws

$$-\mathcal{Q} + k_1 + k_2 + \lambda_{\mathcal{Q}} \tau_{\mathcal{Q}} = 0, \mathcal{P} - k_2 - k'_1 - \lambda_{\mathcal{P}} \tau_{\mathcal{P}} = 0, \quad (24)$$

yields

$$\tau_{\mathcal{Q}} = M_{\mathcal{Q}} - \Delta_{k_2, m_2 \lambda_{\mathcal{Q}}}^0 - \Delta_{k_1, m_1 \lambda_{\mathcal{Q}}}^0, \Delta_{k_1, m_1 \lambda_{\mathcal{Q}}} = -\Delta_{k_2, m_2 \lambda_{\mathcal{Q}}}; \quad (25)$$

$$\tau_{\mathcal{P}} = M_{\mathcal{P}} - \Delta_{k_2, m_2 \lambda_{\mathcal{P}}}^0 - \Delta_{k'_1, m_1 \lambda_{\mathcal{P}}}^0, \Delta_{k'_1, m_1 \lambda_{\mathcal{P}}} = -\Delta_{k_2, m_2 \lambda_{\mathcal{P}}}.$$

From Eqs. (24) and (25), it also follows that

$$k_1 + k'_1 = \lambda_{\mathcal{Q}} \sqrt{s_{\Delta_{k_2, m_2 \lambda_{\mathcal{Q}}}}} + \lambda_{\mathcal{P}} \sqrt{s_{\Delta_{k_2, m_2 \lambda_{\mathcal{P}}}}} - 2k_2,$$

where we have used the invariance of the total energy under Lorentz transformations; that is,

$$\sqrt{s_k} = \sqrt{(k_2 + k_1)^2} = \sqrt{s_{\Delta_{k_2, m_2 \lambda_{\mathcal{Q}}}}} = \sqrt{m_1^2 + \Delta_{k_2, m_2 \lambda_{\mathcal{Q}}}^2} + \sqrt{m_2^2 + \Delta_{k_2, m_2 \lambda_{\mathcal{Q}}}^2}, \quad (26)$$

$$\sqrt{s_{k'}} = \sqrt{(k_2 + k'_1)^2} = \sqrt{s_{\Delta_{k_2, m_2 \lambda_{\mathcal{P}}}}} = \sqrt{m_1^2 + \Delta_{k_2, m_2 \lambda_{\mathcal{P}}}^2} + \sqrt{m_2^2 + \Delta_{k_2, m_2 \lambda_{\mathcal{P}}}^2}.$$

Taking into account Eq. (20), we find from here that

$$\begin{aligned}
(\mathcal{P} \pm \mathcal{Q})(k_1 + k'_1) &= \frac{M_{\mathcal{Q}}^2 + M_{\mathcal{P}}^2 - t}{2M_{\mathcal{Q}}} \sqrt{s_{\Delta_{k_2, m_2 \lambda_{\mathcal{Q}}}}} \pm \quad (27) \\
&\pm \frac{M_{\mathcal{Q}}^2 + M_{\mathcal{P}}^2 - t}{2M_{\mathcal{P}}} \sqrt{s_{\Delta_{k_2, m_2 \lambda_{\mathcal{P}}}}} \pm \frac{(m_1^2 - m_2^2)M_{\mathcal{Q}}}{\sqrt{s_{\Delta_{k_2, m_2 \lambda_{\mathcal{Q}}}}} + \frac{(m_1^2 - m_2^2)M_{\mathcal{P}}}{\sqrt{s_{\Delta_{k_2, m_2 \lambda_{\mathcal{P}}}}}}.
\end{aligned}$$

Now in (22) and (23) we execute the integrations respecting of $\mathbf{k}_1, \mathbf{k}'_1, \tau_{\mathcal{P}}, \tau_{\mathcal{Q}}$. For that we execute the pure Lorentz transformations $\Lambda_{\lambda_{\mathcal{Q}}}^{-1}$ and $\Lambda_{\lambda_{\mathcal{P}}}^{-1}$ by formulas (3) in the integrals with respect to \mathbf{k}_1 and \mathbf{k}'_1 accordingly, and take into account Eq. (27) and the invariance of the delta functions involved and the integration measures $d\Omega_{\mathbf{k}_i} = m_i d\mathbf{k}_i / \sqrt{m_i^2 + \mathbf{k}_i^2}, i = 1, 2$ on the mass hyperboloids (17) under Lorentz transformations. Expressions (22) and (23) for the form-factor components can then be recast into the form

$$\begin{aligned}
F^{(+)}(t) &= \frac{z_1}{(2M_{\mathcal{Q}}^2 + 2M_{\mathcal{P}}^2 - t)(4\pi)^3} \int \frac{d\Delta_{k_2, m_2 \lambda_{\mathcal{Q}}}}{\sqrt{m_2^2 + \Delta_{k_2, m_2 \lambda_{\mathcal{Q}}}^2}} \times \quad (28) \\
&\times \frac{\Gamma_{M_{\mathcal{P}}}^+(\Delta_{k_2, m_2 \lambda_{\mathcal{P}}})}{\sqrt{m_1^2 + \Delta_{k_2, m_2 \lambda_{\mathcal{P}}}^2} (M_{\mathcal{P}} - \sqrt{s_{\Delta_{k_2, m_2 \lambda_{\mathcal{P}}}}} + i\varepsilon)} \left[\frac{M_{\mathcal{Q}}^2 + M_{\mathcal{P}}^2 - t}{2M_{\mathcal{Q}}} \sqrt{s_{\Delta_{k_2, m_2 \lambda_{\mathcal{Q}}}}} + \right. \\
&\quad \left. + \frac{M_{\mathcal{Q}}^2 + M_{\mathcal{P}}^2 - t}{2M_{\mathcal{P}}} \sqrt{s_{\Delta_{k_2, m_2 \lambda_{\mathcal{P}}}}} + (m_1^2 - m_2^2) \left(\frac{M_{\mathcal{Q}}}{\sqrt{s_{\Delta_{k_2, m_2 \lambda_{\mathcal{Q}}}}} + \right. \right. \\
&\quad \left. \left. + \frac{M_{\mathcal{P}}}{\sqrt{s_{\Delta_{k_2, m_2 \lambda_{\mathcal{P}}}}} \right) \right] \frac{\Gamma_{M_{\mathcal{Q}}}(\Delta_{k_2, m_2 \lambda_{\mathcal{Q}}})}{\sqrt{m_1^2 + \Delta_{k_2, m_2 \lambda_{\mathcal{Q}}}^2} (M_{\mathcal{Q}} - \sqrt{s_{\Delta_{k_2, m_2 \lambda_{\mathcal{Q}}}}} - i\varepsilon)} + (1 \leftrightarrow 2),
\end{aligned}$$

$$\begin{aligned}
F^{(-)}(t) &= \frac{z_1}{it(4\pi)^3} \int \frac{d\Delta_{k_2, m_2 \lambda_{\mathcal{Q}}}}{\sqrt{m_2^2 + \Delta_{k_2, m_2 \lambda_{\mathcal{Q}}}^2}} \times \quad (29) \\
&\times \frac{\Gamma_{M_{\mathcal{P}}}^+(\Delta_{k_2, m_2 \lambda_{\mathcal{P}}})}{\sqrt{m_1^2 + \Delta_{k_2, m_2 \lambda_{\mathcal{P}}}^2} (M_{\mathcal{P}} - \sqrt{s_{\Delta_{k_2, m_2 \lambda_{\mathcal{P}}}}} + i\varepsilon)} \left[\frac{M_{\mathcal{Q}}^2 + M_{\mathcal{P}}^2 - t}{2M_{\mathcal{Q}}} \sqrt{s_{\Delta_{k_2, m_2 \lambda_{\mathcal{Q}}}}} - \right. \\
&\quad \left. - \frac{M_{\mathcal{Q}}^2 + M_{\mathcal{P}}^2 - t}{2M_{\mathcal{P}}} \sqrt{s_{\Delta_{k_2, m_2 \lambda_{\mathcal{P}}}}} - (m_1^2 - m_2^2) \left(\frac{M_{\mathcal{Q}}}{\sqrt{s_{\Delta_{k_2, m_2 \lambda_{\mathcal{Q}}}}} - \right. \right. \\
&\quad \left. \left. - \frac{M_{\mathcal{P}}}{\sqrt{s_{\Delta_{k_2, m_2 \lambda_{\mathcal{P}}}}} \right) \right] \frac{\Gamma_{M_{\mathcal{Q}}}(\Delta_{k_2, m_2 \lambda_{\mathcal{Q}}})}{\sqrt{m_1^2 + \Delta_{k_2, m_2 \lambda_{\mathcal{Q}}}^2} (M_{\mathcal{Q}} - \sqrt{s_{\Delta_{k_2, m_2 \lambda_{\mathcal{Q}}}}} - i\varepsilon)} + (1 \leftrightarrow 2),
\end{aligned}$$

where we have introduced the notation $\Gamma_{\mathcal{Q}}(k_1, k_2; \lambda_{\mathcal{Q}}\tau_{\mathcal{Q}}) = \Gamma_{M_{\mathcal{Q}}}(\Delta_{k_2, m_2 \lambda_{\mathcal{Q}}})$, $\Gamma_{\mathcal{P}}(k'_1, k_2; \lambda_{\mathcal{P}}\tau_{\mathcal{P}}) = \Gamma_{M_{\mathcal{P}}}(\Delta_{k_2, m_2 \lambda_{\mathcal{P}}})$.

Within the RQP approach being considered, the two body problem under study reduces to a one-body problem formulated in terms of the RQP wave function $\Psi_{M_{\mathcal{Q}}}(\Delta_{k', m' \lambda_{\mathcal{Q}}})$ describing an effective relativistic particle and satisfying the fully covariant RQP Kadyshevsky equation (1) in the angular-momentum space. The 4-vector k' is chosen as

$$k' = (k'_0; \mathbf{k}') = \sqrt{\frac{\mathcal{K}^2}{\mathcal{K}_{\perp}^2}} \mathcal{K}_{\perp}, \quad (30)$$

where $\mathcal{K} = (m_1 k_2 - m_2 k_1)/(m_1 + m_2)$, the vector $\mathcal{K}_{\perp} = \mathcal{K} - \lambda_{\mathcal{K}}(\lambda_{\mathcal{K}}\mathcal{K})$ is the Wightman–Gording vector, and $\lambda_{\mathcal{K}} = (k_1 + k_2)/\sqrt{s_k} = \lambda_{\mathcal{Q}}$. Signifies, $(\lambda_{\mathcal{K}}\mathcal{K}_{\perp}) = 0$, but from (30) we find:

$$k'^2 = k_0'^2 - \mathbf{k}'^2 = \mathcal{K}^2 = \frac{m_1 m_2}{(m_1 + m_2)^2} [(m_1 + m_2)^2 - s_k]. \quad (31)$$

Under the Lorentz transformations (3) follows that

$$\Lambda_{\lambda_{\mathcal{Q}}}^{-1} \mathcal{K}_{\perp} = (0; \Delta_{k_2, m_2 \lambda_{\mathcal{Q}}}), \quad (32)$$

$$\Lambda_{\lambda_{\mathcal{Q}}}^{-1} \mathcal{K} = \left(\frac{m_1 \sqrt{m_2^2 + \Delta_{k_2, m_2 \lambda_{\mathcal{Q}}}^2} - m_2 \sqrt{m_1^2 + \Delta_{k_2, m_2 \lambda_{\mathcal{Q}}}^2}}{m_1 + m_2}; \Delta_{k_2, m_2 \lambda_{\mathcal{Q}}} \right).$$

Then from (26), (31) and (32) we get expression $(\Lambda_{\lambda_{\mathcal{Q}}}^{-1} k'_0 = 0)$

$$\Delta_{k', m' \lambda_{\mathcal{Q}}}^2 = -(\Lambda_{\lambda_{\mathcal{Q}}}^{-1} k')^2 = -(\Lambda_{\lambda_{\mathcal{Q}}}^{-1} \mathcal{K})^2 = \frac{m_1 m_2}{(m_1 + m_2)^2} [s_{\Delta_{k_2, m_2 \lambda_{\mathcal{Q}}}} - (m_1 + m_2)^2].$$

As direction of the vector $\Delta_{k', m' \lambda_{\mathcal{Q}}}$ in correspondence to (30) and (32), we choose the direction of the vector $\Delta_{k_2, m_2 \lambda_{\mathcal{Q}}}$:

$$\begin{aligned} \Delta_{k', m' \lambda_{\mathcal{Q}}} &= \sqrt{\frac{(\Lambda_{\lambda_{\mathcal{Q}}}^{-1} \mathcal{K})^2}{(\Lambda_{\lambda_{\mathcal{Q}}}^{-1} \mathcal{K}_{\perp})^2}} (\Lambda_{\lambda_{\mathcal{Q}}}^{-1} \mathcal{K}_{\perp}) = \frac{\Delta_{k_2, m_2 \lambda_{\mathcal{Q}}}}{|\Delta_{k_2, m_2 \lambda_{\mathcal{Q}}}|} \times \\ &\times \left[\Delta_{k_2, m_2 \lambda_{\mathcal{Q}}}^2 - \left(\frac{m_1 \sqrt{m_2^2 + \Delta_{k_2, m_2 \lambda_{\mathcal{Q}}}^2} - m_2 \sqrt{m_1^2 + \Delta_{k_2, m_2 \lambda_{\mathcal{Q}}}^2}}{m_1 + m_2} \right)^2 \right]^{1/2}. \end{aligned} \quad (33)$$

The inverse transformation have the form

$$\Delta_{k_2, m_2 \lambda_Q} = \Delta_{k', m' \lambda_Q} \frac{m'}{2\mu} \sqrt{\frac{4\mu^2 + \Delta_{k', m' \lambda_Q}^2}{m'^2 + \Delta_{k', m' \lambda_Q}^2}}. \quad (34)$$

Farther, in expression (28) and (29) we shall perform the change of variables according to Eqs. (33), (34) and take into account Eq. (4). The expressions for the components of the elastic form factor ($M_{\mathcal{P}} = M_Q = M$) then takes the form

$$\begin{aligned} F^{(+)}(t) &= \frac{(z_1 + z_2)(2M^2 - t)}{M(4M^2 - t)(2\pi)^3} \frac{2\mu}{m'} \int d\Omega_{\Delta_{k', m' \lambda_Q}} \Psi_M^*(\Delta_{k', m' \lambda_{\mathcal{P}}}) \times \\ &\times \left[\frac{f_+(\Delta_{k', m' \lambda_{\mathcal{P}}}) + f_-(\Delta_{k', m' \lambda_{\mathcal{P}}})}{2f(\Delta_{k', m' \lambda_{\mathcal{P}}})} \right] \left(\Delta_{k', m' \lambda_{\mathcal{P}}}^0 + \Delta_{k', m' \lambda_Q}^0 \right) \Psi_M(\Delta_{k', m' \lambda_Q}) + \\ &+ \frac{(z_1 - z_2)(m_1^2 - m_2^2)M}{2(4M^2 - t)(2\pi)^3} \left(\frac{2\mu}{m'} \right)^3 \int d\Omega_{\Delta_{k', m' \lambda_Q}} \Psi_M^*(\Delta_{k', m' \lambda_{\mathcal{P}}}) \times \\ &\times \left[\frac{f_+(\Delta_{k', m' \lambda_{\mathcal{P}}}) + f_-(\Delta_{k', m' \lambda_{\mathcal{P}}})}{2f(\Delta_{k', m' \lambda_{\mathcal{P}}})} \right] \left(\frac{\Delta_{k', m' \lambda_{\mathcal{P}}}^0 + \Delta_{k', m' \lambda_Q}^0}{\Delta_{k', m' \lambda_{\mathcal{P}}}^0 \Delta_{k', m' \lambda_Q}^0} \right) \Psi_M(\Delta_{k', m' \lambda_Q}), \end{aligned} \quad (35)$$

$$\begin{aligned} F^{(-)}(t) &= \frac{(z_1 + z_2)(2M^2 - t)}{iM(-t)(2\pi)^3} \frac{2\mu}{m'} \int d\Omega_{\Delta_{k', m' \lambda_Q}} \Psi_M^*(\Delta_{k', m' \lambda_{\mathcal{P}}}) \times \\ &\times \left[\frac{f_+(\Delta_{k', m' \lambda_{\mathcal{P}}}) + f_-(\Delta_{k', m' \lambda_{\mathcal{P}}})}{2f(\Delta_{k', m' \lambda_{\mathcal{P}}})} \right] \left(\Delta_{k', m' \lambda_{\mathcal{P}}}^0 - \Delta_{k', m' \lambda_Q}^0 \right) \Psi_M(\Delta_{k', m' \lambda_Q}) + \\ &+ \frac{(z_1 - z_2)(m_1^2 - m_2^2)M}{2i(-t)(2\pi)^3} \left(\frac{2\mu}{m'} \right)^3 \int d\Omega_{\Delta_{k', m' \lambda_Q}} \Psi_M^*(\Delta_{k', m' \lambda_{\mathcal{P}}}) \times \\ &\times \left[\frac{f_+(\Delta_{k', m' \lambda_{\mathcal{P}}}) + f_-(\Delta_{k', m' \lambda_{\mathcal{P}}})}{2f(\Delta_{k', m' \lambda_{\mathcal{P}}})} \right] \left(\frac{\Delta_{k', m' \lambda_{\mathcal{P}}}^0 - \Delta_{k', m' \lambda_Q}^0}{\Delta_{k', m' \lambda_{\mathcal{P}}}^0 \Delta_{k', m' \lambda_Q}^0} \right) \Psi_M(\Delta_{k', m' \lambda_Q}), \end{aligned} \quad (36)$$

where

$$\begin{aligned} f_{\pm}(\Delta_{k', m' \lambda_Q}) &= \frac{\sqrt{m'^2 + \Delta_{k', m' \lambda_Q}^2}}{m'^2 + \Delta_{k', m' \lambda_Q}^2 \pm m' \sqrt{m'^2 - 4\mu^2}}, \\ f(\Delta_{k', m' \lambda_Q}) &= \frac{\sqrt{4\mu^2 + \Delta_{k', m' \lambda_Q}^2}}{m'^2 + \Delta_{k', m' \lambda_Q}^2}, \end{aligned}$$

and we have defined the wave function for the system in the angular-momentum space as

$$\Psi_M(\Delta_{k',m'\lambda_Q}) = \frac{f(\Delta_{k',m'\lambda_Q})\Gamma_M(\Delta_{k',m'\lambda_Q})}{2^{3/2}\sqrt{m'}\left(\frac{2\mu M}{m'} - 2\Delta_{k',m'\lambda_Q}^0\right)},$$

and are introduced the notations

$$\Gamma_{M_Q}(\Delta_{k_2,m_2\lambda_Q}) = \Gamma_M(\Delta_{k',m'\lambda_Q}), \Gamma_{M_P}(\Delta_{k_2,m_2\lambda_P}) = \Gamma_M(\Delta_{k',m'\lambda_P}).$$

It should be noted that the factor $[f_+ + f_-]/2f(\Delta_{k',m'\lambda_P})$ possible to be simplified to the form

$$\begin{aligned} \frac{f_+(\Delta_{k',m'\lambda_P}) + f_-(\Delta_{k',m'\lambda_P})}{2f(\Delta_{k',m'\lambda_P})} &\approx 1 + \frac{m'^2 - 4\mu^2}{2\Delta_{k',m'\lambda_P}^{02}}, \\ \frac{m'\sqrt{m'^2 - 4\mu^2}}{\Delta_{k',m'\lambda_P}^{02}} &< 1, \quad \frac{m'^2 - 4\mu^2}{\Delta_{k',m'\lambda_P}^{02}} < 1, \end{aligned}$$

and the vector $\Delta_{k',m'\lambda_P}$ from the Lobachevsky space arising on the upper mass-hyperboloid sheet (2) can be represented in the form

$$\begin{aligned} \Delta_{k',m'\lambda_P} &= \Lambda_{\lambda_P}^{-1}\mathbf{k}' = (\Lambda_{\lambda_P}^{-1}\Lambda_{\lambda_Q}\Lambda_{\Delta_{P,Q}}) \left(\Lambda_{\Delta_{P,Q}}^{-1}\Delta_{k',m'\lambda_Q} \right) = \\ &= V(\Lambda_{\lambda_Q}, \mathcal{P})\Delta_{k',m'\lambda_Q}(-) \frac{m'}{M}\Delta_{P,Q}. \end{aligned} \quad (37)$$

Here $\Delta_{P,Q} = \Lambda_{\lambda_Q}^{-1}\mathcal{P}$ is the 4-momentum transfer in the Lobachevsky space; that is,

$$\Delta_{P,Q} = \Lambda_{\lambda_Q}^{-1}\mathcal{P} = \mathcal{P} - \frac{\mathcal{Q}}{M} \left(\mathcal{P}_0 - \frac{\mathcal{P} \cdot \mathcal{Q}}{Q_0 + M} \right) = M \sinh \chi_{\Delta} \mathbf{n}_{\Delta}, \quad (38)$$

$$\Delta_{P,Q}^0 = (\Lambda_{\lambda_Q}^{-1}\mathcal{P})^0 = \frac{\mathcal{P}_0 Q_0 - \mathcal{P} \cdot \mathcal{Q}}{M} = \frac{\mathcal{P} Q}{M} = M \cosh \chi_{\Delta},$$

$$\mathcal{P} = M \sinh \chi_P \mathbf{n}_P, \quad \mathcal{Q} = M \sinh \chi_Q \mathbf{n}_Q,$$

$$\mathcal{P}_0 = M \cosh \chi_P, \quad Q_0 = M \cosh \chi_Q,$$

$$|\mathbf{n}_P| = |\mathbf{n}_Q| = |\mathbf{n}_{\Delta}| = 1, \quad \Delta_{P,Q}^{02} - \Delta_{P,Q}^2 = M^2,$$

where $V(\Lambda_{\lambda_{\mathcal{Q}}}, \mathcal{P}) = \Lambda_{\lambda_{\mathcal{P}}}^{-1} \Lambda_{\lambda_{\mathcal{Q}}} \Lambda_{\Delta_{\mathcal{P}, \mathcal{Q}}}$ is Wigner's rotation matrix and χ_{Δ} , $\chi_{\mathcal{P}}$, $\chi_{\mathcal{Q}}$ are the respective rapidities. From Eqs. (3) and (38), it follows that

$$\Delta_{k', m' \lambda_{\mathcal{P}}}^0 \gtrsim \frac{m'^2 \Delta_{\mathcal{P}, \mathcal{Q}}^0}{2M \Delta_{k', m' \lambda_{\mathcal{Q}}}^0}, \quad (39)$$

and the square of the 4-momentum transfer, $Q^2 = -t = -(\mathcal{P} - \mathcal{Q})^2$, is related to the 3-momentum transfer $\Delta_{\mathcal{P}, \mathcal{Q}}$ by the equation

$$Q^2 = -t = -2M^2 + 2M \sqrt{M^2 + \Delta_{\mathcal{P}, \mathcal{Q}}^2} = 2M^2 (\cosh \chi_{\Delta} - 1). \quad (40)$$

Consequently, the components $F^{(\pm)}(t)$ of the elastic form factor in (35) and (36) can be considered as functions of the invariant variable $\Delta_{\mathcal{P}, \mathcal{Q}}^2$, which is the square of the momentum-transfer vector in the Lobachevsky space. Then, taking into consideration Eqs. (3), (3) and (39), they are convolutions of the wave functions in this space. It follows that, by employing the Shapiro transformation in (10), the addition theorem for relativistic plane waves (5) in the form [18]

$$\int d\omega_n \xi \left(\Delta_{k', m' \lambda_{\mathcal{Q}}}(-) \frac{m'}{M} \Delta_{\mathcal{P}, \mathcal{Q}}, \mathbf{r} \right) = \int d\omega_n \xi(\Delta_{k', m' \lambda_{\mathcal{Q}}}, \mathbf{r}) \xi^* \left(\frac{m'}{M} \Delta_{\mathcal{P}, \mathcal{Q}}, \mathbf{r} \right), \quad (41)$$

the completeness condition in (7), equation (8), and the Hermitian of operator of the free Hamiltonian (9), one can recast expressions (35) and (36) into the form of relativistic Fourier transforms of covariant RQP wave functions in the coordinate representation²⁾:

$$\begin{aligned} F^{(+)}(Q^2) &\approx \quad (42) \\ &\approx \left\{ \frac{(z_1 + z_2)(2M^2 + Q^2)}{M(4M^2 + Q^2)} \frac{2\mu}{m'} + \frac{2M^3(z_1 - z_2)(m_1^2 - m_2^2)}{m'^2(4M^2 + Q^2)(2M^2 + Q^2)} \left(\frac{2\mu}{m'} \right)^3 \right\} \times \\ &\quad \times \left\{ \int d\mathbf{r} \xi^* \left(\frac{m'}{M} \Delta_{\mathcal{P}, \mathcal{Q}}, \mathbf{r} \right) \text{Re}[\psi_M^*(\mathbf{r}) \widehat{H}_0 \psi_M(\mathbf{r})] + \right. \\ &\quad \left. + \frac{2M^4(m'^2 - 4\mu^2)}{m'^4(2M^2 + Q^2)^2} \int d\mathbf{r} \xi^* \left(\frac{m'}{M} \Delta_{\mathcal{P}, \mathcal{Q}}, \mathbf{r} \right) \text{Re} \left[\left(\widehat{H}_0 \psi_M(\mathbf{r}) \right)^* \widehat{H}_0^2 \psi_M(\mathbf{r}) \right] \right\}, \end{aligned}$$

²⁾ A similar expression for the case of two particles of equal mass was obtained in [16].

$$F^{(-)}(Q^2) \approx \quad (43)$$

$$\approx \left\{ \frac{(z_1 + z_2)(2M^2 + Q^2)}{MQ^2} \frac{2\mu}{m'} + \frac{2M^3(z_1 - z_2)(m_1^2 - m_2^2)}{m'^2 Q^2 (2M^2 + Q^2)} \left(\frac{2\mu}{m'} \right)^3 \right\} \times$$

$$\times \left\{ \int d\mathbf{r} \xi^* \left(\frac{m'}{M} \Delta_{\mathcal{P}, \mathcal{Q}}, \mathbf{r} \right) \text{Im} [\psi_M(\mathbf{r}) (\hat{H}_0 \psi_M(\mathbf{r}))^*] + \right.$$

$$\left. + \frac{2M^4(m'^2 - 4\mu^2)}{m'^4 (2M^2 + Q^2)^2} \int d\mathbf{r} \xi^* \left(\frac{m'}{M} \Delta_{\mathcal{P}, \mathcal{Q}}, \mathbf{r} \right) \text{Im} \left[\left(\hat{H}_0 \psi_M(\mathbf{r}) \right) \left(\hat{H}_0^2 \psi_M(\mathbf{r}) \right)^* \right] \right\},$$

where possibility to applicability of the addition theorem (41) follows from independence of the wave RQP-function $\psi_M(\mathbf{r})$ in the case of $J = 0$ from direction of the vector \mathbf{r} .

We note that, if the RQP wave function $\psi_M(\mathbf{r})$ is a real-valued function of the variable r and corresponds to a real-valued quasipotential $V(r)$, then, according to Eq. (12), the quantity $\psi_M(\mathbf{r}) (\hat{H}_0 \psi_M(\mathbf{r}))^*$ is also real-valued. It follows that, in this case and at equal masses ($m_1 = m_2 = m$), the transverse component $F^{(-)}(t)$ of the elastic form factor vanishes. For s -state ($\ell = 0$) the radial wave function $\varphi_0(r, \chi_n)$ corresponding to a real-valued quasipotential $V(r)$ is real-valued, the quantities $\frac{\varphi_0^*(r, \chi_n)}{r} \hat{H}_{0, \ell=0} \frac{\varphi_0(r, \chi_n)}{r}$ and $\left(\hat{H}_{0, \ell=0} \frac{\varphi_0(r, \chi_n)}{r} \right)^* \hat{H}_{0, \ell=0}^2 \frac{\varphi_0(r, \chi_n)}{r}$ are also real-valued. It follows that, in this case, the transverse component $F^{(-)}(t)$ of the elastic form factor for the s -wave state vanishes even for unequal masses ($m_1 \neq m_2$).

For s -state ($\ell = 0$) of the composite system the integrations in (42) respecting of angular variables gives

$$F_{\ell=0}^{(+)}(Q^2) = \quad (44)$$

$$= \left\{ \frac{8\pi\mu(z_1 + z_2)(2M^2 + Q^2)}{m' M (4M^2 + Q^2)} + \frac{8\pi M^3(z_1 - z_2)(m_1^2 - m_2^2)}{m'^2 (4M^2 + Q^2)(2M^2 + Q^2)} \left(\frac{2\mu}{m'} \right)^3 \right\} \frac{\chi_\Delta}{\sinh \chi_\Delta} \times$$

$$\times \left\{ \int_0^\infty dr \frac{r \sin(rm'\chi_\Delta)}{m'\chi_\Delta} \text{Re} \left[\frac{\varphi_0^*(r, \chi_n)}{r} \hat{H}_{0, \ell=0} \frac{\varphi_0(r, \chi_n)}{r} \right] + \frac{2M^4(m'^2 - 4\mu^2)}{m'^4 (2M^2 + Q^2)^2} \times \right.$$

$$\left. \times \int_0^\infty dr \frac{r \sin(rm'\chi_\Delta)}{m'\chi_\Delta} \text{Re} \left[\left(\hat{H}_{0, \ell=0} \frac{\varphi_0(r, \chi_n)}{r} \right)^* \hat{H}_{0, \ell=0}^2 \frac{\varphi_0(r, \chi_n)}{r} \right] \right\},$$

where are used decompositions (13) for wave function $\psi_M(\mathbf{r})$ and the expansion for the relativistic plane wave (5) in the form

$$\xi(\mathbf{p}', \mathbf{r}) = \sum_{\ell=0}^{\infty} (2\ell + 1) i^\ell p_\ell(r, \cosh \chi_{p'}) P_\ell \left(\frac{\mathbf{p}' \cdot \mathbf{r}}{p' r} \right).$$

Here the rapidity χ_n corresponds to the level n bound state with energy $M = M_n = (m'^2/\mu) \cosh \chi_n$; the function

$$p_\ell(\rho, \cosh \chi_{p'}) = \sqrt{\frac{\pi}{2 \sinh \chi_{p'}}} \frac{(-1)^{\ell+1}}{\rho} (-\rho)^{(\ell+1)} P_{-1/2+i\rho}^{-1/2-\ell}(\cosh \chi_{p'}), \quad \rho = r m',$$

is a solution of the equation (8), where the function $(-\rho)^{(\ell+1)} = i^{l+1} \Gamma(l+1+i\rho)/\Gamma(i\rho)$ is called the generalized power [18], and $\Gamma(z)$ is a gamma function.

4 Root-mean-square radius and form factor for the Coulomb interaction

Now let us consider the expression for the invariant root-mean-square radius of a composite system, which has the group-theoretical meaning of an eigenvalue of the Casimir operator of the Lorentz group and according to Eqs. (6) and (44) has the form

$$\begin{aligned} & \langle r_0^2 \rangle = \\ & = \frac{6\partial F_{\ell=0}^{(+)}(t)/\partial t|_{t=0}}{F_{\ell=0}^{(+)}(0)} = \frac{1}{M^2} + \left(\frac{m'}{M}\right)^2 \frac{\int_0^\infty dr r^2 \left(r^2 - \frac{3}{2m'^2}\right) \left(R_1 + \frac{m'^2-4\mu^2}{2m'^4} R_2\right)}{\int_0^\infty dr r^2 \left(R_1 + \frac{m'^2-4\mu^2}{2m'^4} R_2\right)} + \\ & + \frac{3(m'^2 - 4\mu^2) \int_0^\infty dr r^2 R_2}{m'^4 M^2 \int_0^\infty dr r^2 \left(R_1 + \frac{m'^2-4\mu^2}{2m'^4} R_2\right)} + \frac{3(z_1 - z_2)(m_1^2 - m_2^2) (2\mu/m')^2}{m'^2 M^2 \left[z_1 + z_2 + \frac{(z_1 - z_2)(m_1^2 - m_2^2)(2\mu/m')^2}{2m'^2} \right]}, \end{aligned}$$

where

$$R_1 = \text{Re} \left[\frac{\varphi_0^*(r, \chi)}{r} \widehat{H}_{0,\ell=0} \frac{\varphi_0(r, \chi)}{r} \right], \quad R_2 = \text{Re} \left[\left(\widehat{H}_{0,\ell=0} \frac{\varphi_0(r, \chi)}{r} \right)^* \widehat{H}_{0,\ell=0}^2 \frac{\varphi_0(r, \chi)}{r} \right].$$

Thus, it is necessary to consider the composite particle as a dipole and that the wave function of s -state describes not all structure of the composite particle, but only the region which be upon distances that larger its of the Compton wavelength $1/M$. The root-mean-square radius of the composite system includes not only the central sphere of radius $r_0 = 1/M$, where the relative motion of the quarks forming this system proceeds, but also terms generated by the difference in the masses of the quarks and in their coupling constants. At $m_1 = m_2$, these terms vanish.

As example, we consider the form factor in the case of the attractive Coulomb field

$$V(r) = -\frac{\alpha}{r}, \alpha > 0. \quad (45)$$

The radial wave function of exact solution of the RQP-equation (14) with interaction (45) for the s -state and ground level ($n = 0$) with the energy M_0 has the form [19–21]

$$\varphi_0(r, i\kappa_0) = N_{0,0}(\kappa_0) r m' \exp \left[-r m' \kappa_0 + \frac{i\tilde{\alpha}\kappa_0}{2 \sin \kappa_0} \right],$$

where $\tilde{\alpha} = 2\mu\alpha/m'$, $M_0 = (m'^2/\mu) \cos \kappa_0$, κ_0 defines by the following quantization condition $\tilde{\alpha}/(2 \sin \kappa_0) = 1$, $0 \leq \kappa_0 < \pi/2$, and $N_{0,0}^2(\kappa_0) = m' \kappa_0^3/\pi$ is the normalization factor.

The form factor (44) for the ground level of the bound s -state with the energy M_0 then assumes the form

$$\begin{aligned} F_{\ell=0, n=0}^{(+)}(Q^2) &= \frac{16\mu\kappa_0^3 \sin \kappa_0 (2M_0^2 + Q^2)}{M_0(4M_0^2 + Q^2)\chi_\Delta \sinh \chi_\Delta} \times \quad (46) \\ &\times \left[z_1 + z_2 + \frac{2(z_1 - z_2)M_0^4(m_1^2 - m_2^2)}{m'^2(2M_0^2 + Q^2)^2} \left(\frac{2\mu}{m'} \right)^2 \right] \left\{ \frac{1}{1 + (2\kappa_0/\chi_\Delta)^2} + \right. \\ &+ \frac{4\kappa_0}{\chi_\Delta^2 \tan \kappa_0 (1 + (2\kappa_0/\chi_\Delta)^2)^2} + \frac{4\pi M_0^4(m'^2 - 4\mu^2)\chi_\Delta \sin 2\kappa_0}{m'^2(2M_0^2 + Q^2)^2} \times \\ &\times \left[1 - \frac{2}{\pi} \arctan \frac{2\kappa_0}{\chi_\Delta} + \frac{3}{\pi\chi_\Delta \tan \kappa_0 (1 + (2\kappa_0/\chi_\Delta)^2)} + \right. \\ &\left. \left. + \frac{4\kappa_0}{\pi\chi_\Delta^3 \tan^2 \kappa_0 (1 + (2\kappa_0/\chi_\Delta)^2)^2} \right] \right\}. \end{aligned}$$

For large Q^2 the rapidity $\chi_\Delta \approx \ln(Q^2/M_0^2)$ and, consequently, the leading behavior of form factor (46) gives by expression

$$F_{\ell=0,n=0}^{(+)}(Q^2) \approx 8(z_1 + z_2) \left(\frac{2\mu}{m'}\right)^2 \frac{\kappa_0^3 \tan \kappa_0}{(Q/M_0)^2 \ln(Q/M_0)^2}, \quad (47)$$

i.e. either as in [16]. Such behavior of the form factor under large $t = -Q^2$ differs from prediction of the nonrelativistic model based on the Coulomb potential, which gives the dipole decrease of the pion form factor: $F_\pi \sim t^{-2}$. However, the nonrelativistic result contradicts the prediction of the dimensional quark counting rules [1], which gives the decrease of the pion form factor under the law $F_\pi \sim t^{-1}$.

5 Conclusions

For the case of a vector current, the new covariant expressions for the components of the elastic form factor for a bound system of two relativistic spinless particles of arbitrary masses m_1 and m_2 are obtained. The components of the elastic form factor are functions of the invariant variable $\Delta_{p,Q}^2$, which is the square of the momentum-transfer vector in the Lobachevsky space. The consideration is conducted within the framework of relativistic quasipotential approach on the basis of covariant Hamiltonian formulation of quantum field theory [5, 6] by transition to the three-dimensional relativistic configurational representation in the case of two interacting relativistic spinless particles of arbitrary masses m_1, m_2 [17, 18]. In this approach, the invariant relativistic relative coordinate r is conjugated to the rapidity $m'\chi_\Delta$, and it is the distance in the Lobachevsky space.

It has been shown that expressions (35) and (36) for the form-factor components are convolutions of the RQP wave functions in the space of Lobachevsky angular momenta. This makes it possible to express them in terms of relativistic Fourier transforms of covariant RQP wave functions in the configuration representation [expressions (42)–(44)]. It has also been found that, for a real-valued RQP wave function $\psi_M(\mathbf{r})$, corresponding to a real-valued quasipotential $V(r)$ and in the case of equal masses ($m_1 = m_2 = m$), the transverse component $F^{(-)}(t)$ of the elastic form factor vanishes. Under the same real-valued conditions for the s -state ($\ell = 0$) of the radial wave function $\varphi_0(r, \chi_n)$ and the quasipotential, the transverse component $F_{\ell=0}^{(-)}(t)$ of the elastic form factor also vanishes even in the case of unequal masses ($m_1 \neq m_2$).

Using of the three-dimensional relativistic configurational representation for the system of two relativistic spinless particles with arbitrary masses has allowed to install that the wave function of s -state describes not whole structure of the composite particle, but only the region which be upon distances that larger its of the Compton wavelength $1/M$. The executed analysis has shown, that the leading contribution to structure of the composite particle from the central sphere of radius $r_0 = 1/M$ is proportional to $\chi_\Delta/\sinh \chi_\Delta$ and that the correction terms correspond to the dipole contribution associated with the difference in the masses of the particles constituting this system and in their coupling constants. In the nonrelativistic limit this the relativistic geometric factor go to 1, while the correction terms in expression (44) under $m_1 = m_2$ vanish.

As example, the expression (46) for the longitudinal component of the form factor for relativistic two-particles bound system that have arbitrary masses and in the case of Coulomb quasipotential was obtained. It is installed that the covariant wave RQP-function of attractive Coulomb quasipotential for larges Q^2 gives the decrease for this form factor under the law $F_\pi \sim t^{-1}$, which predicts the dimensional quark counting rules [1].

Acknowledgments

I an grateful to O.P. Solovtsova for her attention to this work, support, and enlightening comments and to E.A. Kuraev, A.E. Dorokhov, Yu.A.Kurochkin, and I.S. Satsunkevich for their interest in this study and valuable discussions on its results.

Partial support of the work by the International Program of Cooperation between Republic of Belarus and the Joint Institute of Nuclear Research (JINR, Dubna).

References

- [1] V. A. Matveev, R. M. Muradyan, and A. N. Tavkhelidze, *Lett. Nuovo Cimento* **5**, 907 (1973).
- [2] J. G. Korner and M. Kuroda, *Phys. Rev. D* **16**, 2165 (1977).
- [3] S. Dubnicka, *Nuovo Cimento A* **103**, 1417 (1991).
- [4] A. A. Logunov and A. N. Tavkhelidze, *Nuovo Cimento* **29**, 380 (1963).
- [5] V. G. Kadyshevsky, *Sov. Phys. JETP* **19**, 443, 597 (1964); *Sov. Phys. Dokl.* **10**, 46 (1965).
- [6] V. G. Kadyshevsky, *Nucl. Phys. B* **6**, 125 (1968).

- [7] V. A. Matveev, R. M. Muradyan, and A. N. Tavkhelidze, Preprint No. E2-3498, JINR (Dubna, 1967); No. P2-3900, JINR (Dubna, 1968).
- [8] V. R. Garsevanishvili, A. N. Kvinikhidze, V. A. Matveev, A. N. Tavkhelidze, and R. N. Faustov, *Theor. Math. Phys.* **23**, 533 (1975).
- [9] A. L. Khelashvili, Preprint No. P2-8750, JINR (Dubna, 1976).
- [10] R. N. Faustov, *Theor. Math. Phys.* **3**, 478 (1970).
- [11] R. N. Faustov, *Ann. Phys.* **78**, 176 (1973).
- [12] S. I. Bilenkaya, N. B. Skachkov, and I. L. Solovtsov, *Yad. Fiz.* **26**, 1051 (1977).
- [13] V. G. Kadyshevsky, R. M. Mir-Kasimov, and N. B. Skachkov, *Nuovo Cimento A* **55**, 233 (1968).
- [14] N. B. Skachkov and I. L. Solovtsov, Preprint No. E2-11678, JINR (Dubna, 1978); *Teor. Mat. Fiz.* **41**, 205 (1979).
- [15] N. B. Skachkov and I. L. Solovtsov, Preprint No. E2-11727, JINR (Dubna, 1978); *Yad. Fiz.* **30**, 1079 (1979).
- [16] N. B. Skachkov and I. L. Solovtsov, *Teor. Mat. Fiz.* **43**, 330 (1980).
- [17] V. G. Kadyshevsky, M. D. Mateev, and R. M. Mir-Kasimov, *Yad. Fiz.* **11**, 692 (1970).
- [18] V. G. Kadyshevsky, R. M. Mir-Kasimov, and N. B. Skachkov, *Fiz. Elem. Chastits At. Yadra* **2**, 635 (1972).
- [19] Yu. D. Chernichenko, in *Proceedings "Nonlinear Dynamics and Applications" of the XVI Annual Seminar NPCS'2009, Minsk, Belarus, May 18-22, 2009* (Minsk, 2010), V. 16, P. 26.
- [20] O. P. Solovtsova and Yu. D. Chernichenko, *Theor. Math. Phys.* **166**, 194 (2011).
- [21] Yu. D. Chernichenko, *Relativistic quasipotential approach in the scattering problems*. (Izdat. centr UO GGTU im. P. O. Sukhogo, Gomel, 2011).
- [22] Yu. D. Chernichenko, *Izv. Nats. Akad. Nauk Belarusi. Ser. fiz.-mat. nauk* **1**, 62 (2012).

The Quark Potential Model in Theory of Resonances

Mikhail N. Sergeenko*

Gomel State Medical University

Abstract

The potential approach is used to study meson resonances as relativistic quasi-bound states. The interaction of quarks in the bound state is described by the QCD motivated funnel-type potential with the distance-dependent value of the strong coupling. Two exact asymptotic solutions of the relativistic quasi-classical wave equation for the modified Cornell potential are used to derive the resonance's complex-mass formula. The resonances' masses of some light and heavy mesons are calculated.

Introduction

Hadron data listed in the Particle Data Group tables [1] represent the purest imprint of the hadron world. A thorough understanding of the physics summarized by the PDG is related to the concept of a resonance. The number of known hadrons is constantly increasing with the growing energies of accelerators and proposed experiments on LHC [2, 3].

At the present time, there is no fundamental dynamic theory of hadron resonances. Calculations of hadron properties are frequently carried out with the help of phenomenological quark models [4]; one of the simplest among them is the Regge method. All mesons and baryons in this approach are associated with Regge poles which move in the complex angular momentum J plane. Moving poles are described by the Regge trajectories,

*E-mail:msergeen@usa.com

$\alpha(s)$, which are the functions of the invariant squared mass $s = W^2$ (Mandelstam's variable), where $W = E^*$ is the c. m. rest energy. Hadrons and resonances populate their Regge trajectories which contain all the dynamics of hadron interaction.

Apparent form of the quarkonium Regge trajectories as analytic functions of s was obtained in [5, 6]. It was shown that trajectories are the analytic nonlinear “saturating” at large negative s functions. In this work, two exact asymptotic solutions of the relativistic quasi-classical (QC) wave equation for the Coulomb-type and linear terms of the modified Cornell potential are considered. On this basis, we obtain the interpolating mass formula for the masses of $Q\bar{q}$ meson resonances. The mass spectra of some meson resonances are calculated.

1 Resonances and their definitions

Impressive successes of the quark potential models in quarkonium physics require a strict relativistic consideration of the potential approach in the theory of resonances. There is the lack of a precise definition of what is meant by mass and width of a resonance. There are two well-known definitions of these resonance's parameters, both widely used in hadron physics [7]. One definition, known as the conventional approach, is based on the behavior of the resonance's *phase shift* $\delta(E)$ as a function of the energy, while the other, known as the *pole approach*, is based on the pole position of the resonance and includes several approaches [8].

In particle physics resonances arise as unstable intermediate states with complex masses [9]. Resonances in quantum field theory are described by the complex-mass poles of the scattering matrix [10]. The rigorous quantum-mechanical definition of a resonance requires determining the pole position in the second Riemann sheet of the analytically continued partial-wave scattering amplitude in the complex Mandelstam s variable plane [11]. A Riemann surface $\mathcal{M} = \pm\sqrt{s}$ is obtained by replacing the s -plane with a surface made up of two sheets R_0 and R_1 , each cut along the positive real axis [12]. The resonance positions are symmetrically located in the Riemann \mathcal{M} -surface (Fig. 1): if $\mathcal{M}_p = M_p - i\Gamma_p^{\text{TOT}}/2$ is a pole in the fourth quadrant of the surface $\pm\sqrt{s}$, then $\mathcal{M}_p = -M_p - i\Gamma_p^{\text{TOT}}/2$ is also a pole, but in the third quadrant (antiparticle) [9], where the total width, $\Gamma_p^{\text{TOT}} = -2\text{Im } \mathcal{M}_p$, is given by the imaginary-part of the invariant mass \mathcal{M}_p . The formula for Γ_p^{TOT} is related to the particle's decay rate

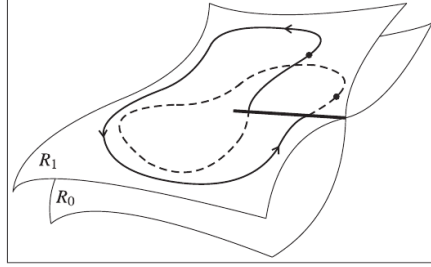


Figure 1: The two-sheet Riemann surface $\mathcal{M} = \pm\sqrt{s}$. The lower edge of the slit in R_0 is joined to the upper edge of the slit in R_1 , and the lower edge of the slit in R_1 is joined to the upper edge of the slit in R_0 .

by the optical theorem [10]. The complex eigenmasses correspond to a first-order pole of the S-matrix.

There are two basic problems in quantum physics: the scattering problem and bound state problem. Resonances are usually studied in scattering experiment, for example, potential scattering. But, resonances are quasi-bound states in the s -channel at $s > 0$; this means that one can use another approach to consider resonances, i. e., the bound state problem in the potential approach.

2 The modified Cornell potential

The Cornell potential [13] incorporates the basic physical quantities of the strong interaction: one-gluon exchange at small distances and the string tension at large ones. The potential is fixed in an extremely simple manner in terms of very small number of parameters. This potential, if considered in the complex-mass scheme, results in the resonance's complex eigenmasses [14].

However, the strong coupling α_S in the Cornell potential is a free parameter. This potential can be modified by introducing the $\alpha_S(r)$ dependence [15]:

$$V_{QCD}(r) = -\frac{4}{3} \frac{\alpha_S(r)}{r} + \sigma r, \quad \alpha_S(r) = \frac{1}{b_0 \ln[1/(\Lambda r)^2 + (2\mu_g/\Lambda)^2]}. \quad (1)$$

where $b_0 = (33 - 2n_f)/12\pi$, n_f is number of flavors, $\mu_g = \mu(q^2)$ — gluon mass at $q^2 = 0$, Λ is the QCD scale parameter. The running coupling

$\alpha_S(r)$ in (1) is frozen in soft regime ($r \rightarrow \infty$) and is in agreement with the asymptotic freedom properties [$\alpha_S(r \rightarrow 0) \rightarrow 0$]. The spin-dependent corrections to the potential (1) can also be included [6]. In this work, the modified funnel-type potential (1) is considered to be Lorentz-scalar in order to confine quarks and gluons inside hadrons.

3 The relativistic QC equation

Relativistic description of two-body systems is usually based on the four-dimensional covariant Bethe-Salpeter equation [16]. It is a problem to find the analytic solution of this equation for the potential (1). Instead, we solve the QC wave equation [17, 18]. For two equal-mass bound particles (quarkonia, glueballs) in the c.m. rest frame this gives the complex-mass formula ($\hbar = c = 1$) [14, 19]:

$$\mathcal{M}_N^2 = 4 \left[\left(\sqrt{2\sigma\tilde{N}} + \frac{i\tilde{\alpha}_n}{N} \right)^2 + \left(m - i\sqrt{2\tilde{\alpha}_n\sigma} \right)^2 \right] \equiv 4 [(\pi_n)^2 + \mu^2], \quad (2)$$

which has the form of the squared mass of two free relativistic particles with the complex eigenmomenta π_n and complex mass μ . Here in (2) $\tilde{\alpha}_n = \frac{4}{3}\alpha_S(r) = \frac{2}{3}[b_0 \ln(2\mu_g/\Lambda)]^{-1}$ at $r \rightarrow \infty$, $\tilde{N} = N + n_r + \frac{1}{2}$, $N = n_r + l + 1$; n_r and l are the radial and orbital quantum numbers. The real part of (2) exactly coincides with the universal mass formula obtained independently with the use of the two-point Padé approximant [5, 6].

In case of different quark masses, the relativistic two-particle QC wave equation in the c.m. rest frame is [17, 18]:

$$\left\{ \sum_{i=1}^3 \left(\frac{\partial}{g_{ii}\partial q_i} \right)^2 + \frac{s - m_-^2}{s} \left[\frac{s}{4} - \left(\frac{m_+}{2} + V_r \right)^2 \right] - \frac{M_l^2}{r^2} \right\} \tilde{\psi}(\vec{r}) = 0, \quad (3)$$

where the canonical operator given by the sum in (3) is expressed via the elements of the metric tensor, g_{ii} . In the spherical coordinates, for our case, $q_i = r, \theta, \varphi$; $m_+ = m_1 + m_2$, $m_- = m_1 - m_2$, $V_r = V_{QCD}(r)$ (1), $M_l = l + \frac{1}{2}$ are the angular momentum eigenvalues, which are found from solution of the angular QC equation [17, 18]. The eigenvalues M_l are universal for all central potentials and not any Langer-type corrections are required.

4 Solution of the QC equation

The problem for the potential (1) has four turning points and cannot be solved analytically by standard methods. However, the QC equation (3) can be solved by the QC method in the complex plane. The QC quantization condition appropriate to (3) in the complex plane is [17, 18]:

$$I = \oint_C \sqrt{\frac{s - m_-^2}{s} \left[\frac{s}{4} - \left(\frac{m_+}{2} + V_r \right)^2 \right] - \frac{M_l^2}{r^2}} dr = 4\pi \left(n_r + \frac{1}{2} \right). \quad (4)$$

The phase integral (4) is considered separately at small distances, where the Coulomb term in (1) dominates, and large distances for the linear term.

The Coulomb-term contribution. The QC wave equation (3) for the Coulomb term in (1) has two turning points. The phase-space integral (4) is found in the complex plane with the use of the method of stereographic projection [14]; the QC quantization condition is:

$$I = 2\pi \left\{ \tilde{\alpha}_n m_+ \left[\frac{s - m_-^2}{s(-s + m_+^2)} \right]^{1/2} - M_l \right\} = 2\pi \left(n_r + \frac{1}{2} \right), \quad (5)$$

which gives, for the eigenmasses ($v_N = \tilde{\alpha}_n/N$, $N = n_r + l + 1$):

$$s_N = W_N^2 = \frac{m_+^2}{2} \left[(1 - v_N^2) + \sqrt{(1 - v_N^2)^2 + (2m_- v_N / m_+)^2} \right]. \quad (6)$$

In the case of equal quark masses ($m_- = 0$), we have, from (6): $W_N^2 = 4m^2(1 - v_N^2)$, which is the well known result for quarkonia.

The linear-term contribution. Large distances in hadron physics are related to the problem of confinement. The problem has four turning points, i. e., two cuts between these points. The phase-space integral (4) is found by the same method of stereographic projection as above; this results in the cubic equation: $s^3 + a_1 s^2 + a_2 s + a_3 = 0$, where $a_1 = 16\tilde{\alpha}_n \sigma - m_-^2$, $a_2 = 64\sigma^2 (\tilde{\alpha}_n^2 - \tilde{N}^2 - \tilde{\alpha}_n m_-^2 / 4\sigma)$, $a_3 = -(8\tilde{\alpha}_n \sigma m_-)^2$, $\tilde{N} = N + n_r + \frac{1}{2}$. The first root of this equation gives the physical solution (complex eigenmasses), $s_N \equiv W_N^2 = W_1^2(N)$, for the squared invariant mass. The real part of the root, $\text{Re}\{W_N^2\}$, contributes in the centered mass and the imaginary part, $\text{Im}\{W_N^2\}$, contributes in the total widths, $\Gamma_N^{\text{TOT}} = -2 \text{Im} W_N$, of the resonance [14, 19].

5 The masses of $Q\bar{q}$ meson resonances

Two exact asymptotic solutions, i. e., (6) and the first root of the cubic equation above, are used to derive the resonance's mass formula. The interpolation procedure for these two solutions is used [5, 6] to derive the resonance's mass formula:

$$W_N^2 = \frac{m_+^2}{2} \left[(1 - v_N^2) + \sqrt{(1 - v_N^2)^2 + (2m_-v_N/m_+)^2} \right] + \text{Re}\{W_N^2\}. \quad (7)$$

To demonstrate its efficiency we calculate the leading-state masses of the ρ and D^* meson resonances (see tables, where masses are in MeV). The free

Table 1: The masses of the $\rho^\pm(u\bar{d})$ -meson resonances

Meson	J^{PC}	E_n^{ex}	E_n^{th}	Parameters in (7)
$\rho(1S)$	1^{--}	776	776	$\Lambda = 500$ MeV
$a_2(1P)$	2^{++}	1318	1314	$\mu_g = 416$ MeV
$\rho_3(1D)$	3^{--}	1689	1689	$\sigma = 0.139$ GeV ²
$a_4(1F)$	4^{++}	1996	1993	$m_d = 276$ MeV
$\rho(1G)$	5^{--}		2255	$m_u = 129$ MeV
$\rho(2S)$	1^{--}	1717	1682	
$\rho(2P)$	2^{++}		1990	
$\rho(2D)$	3^{--}		2254	

Table 2: The masses of the $D^{*\pm}(c\bar{d})$ -meson resonances

Meson	J^{PC}	E_n^{ex}	E_n^{th}	Parameters in (7)
$D^*(1S)$	1^{--}	2010	2010	$\Lambda = 446$ MeV
$D_2^*(1P)$	2^{++}	2460	2464	$m_g = 416$ MeV
$D_3^*(1D)$	3^{--}		2845	$\sigma = 0.249$ GeV ²
$D_4^*(1F)$	4^{++}		3178	$m_c = 1163$ MeV
$D_5^*(1G)$	5^{--}		3478	$m_d = 271$ MeV
$D^*(2S)$	1^{--}	1820	2821	
$D^*(2P)$	2^{++}	2011	3166	
$D^*(2D)$	3^{--}		3471	

fit to the data show a good agreement for the light and heavy $Q\bar{q}$ meson resonances. Note, that the gluon mass in the independent fitting is

the same, $m_g = 416$ MeV. Besides, it is the same for glueballs [15]. The d quark effective mass is also practically the same, i. e., $m_d \simeq 273$ MeV, for the light and heavy resonances.

Conclusion

The constituent quark picture could be questioned since potential models have serious difficulties because the potential is non-relativistic concept. However, in spite of non-relativistic phenomenological nature, the potential approach is used with success to describe mesons as bound states of quarks.

We have modeled meson resonances to be the quasi-bound states of two quarks interacting by the QCD-inspired funnel-type potential with the coordinate dependent strong coupling, $\alpha_S(r)$. We have shown here the results only for unflavored and charmed meson resonances, however, we have obtained a good description for strange and beauty mesons as well. The mass formula (7), if considered in the complex-mass scheme, can be generalized to the complex eigenmasses, i. e. centered masses and total widths. These calculations will be considered elsewhere.

I would like to thank Yu.A. Kurochkin for support.

This work was done in the framework of investigations for the experiment ATLAS (LHC), code 02-0-1081-2009/2013, “Physical explorations at LHC” (JINR-ATLAS).

References

- [1] J. Beringer *et al.* (Particle Data Group), Phys. Rev. D **86**, 010001 (2012).
- [2] ATLAS: Technical proposal for a general-purpose pp experiment at the Large Hadron Collider at CERN. W.W. Armstrong, ... M. N. Sergeenko [et al.] (ATLAS Collaboration), CERN-LHCC-94-43. December, 1994. – 289 p.
- [3] CMS: the Compact Muon Solenoid. Letter of intent for a general purpose detector at the LHC. Letter of Intent, M. Markytan, ... M. N. Sergeenko [et al.] (CMS Collaboration), – CERN/LHCC 92-03, CERN-LHCC-I-1. – 112 p.

- [4] D. Ebert, R.N. Faustov, V.O. Galkin, Eur. Phys. J. C. **71**, 1825 (2011).
- [5] M.N. Sergeenko, Phys. At. Nucl. **56**, 365 (1993).
- [6] M.N. Sergeenko, Z. Phys. C, **64**, 315 (1994).
- [7] A. Bernicha, G.L. Castro and J. Pestieau, Nucl. Phys. A, **597**, 623 (1996) [arXiv:hep-ph/9508388].
- [8] D. Morgan and M.R. Pennington, Phys. Rev. D, **48**, 1185 (1993).
- [9] N. Moiseyev, Phys. Rep. **302**, 211 (1998).
- [10] J.R.Taylor, the Quantum Theory of Nonrelativistic Collisions, Dover Publications, 2006, 496 pages.
- [11] J. Nieves, E. R. Arriola, Phys. Lett. B, **679(5)**, 449 (2009).
- [12] J.W. Brown and R.V. Churchill, Complex Variables and Applications, 7th edition, New York NY: McGraww Hill, (2003).
- [13] E. Eichten, S. Godfrey, H. Mahlke and J.L. Rosner, Rev. Mod. Phys. **80**, 1161 (2008).
- [14] M.N. Sergeenko, Adv. in High Ener. Phys. Vol. **2013**, Article ID 325431.
- [15] M.N. Sergeenko, Euro. Phys. J. C, **72(8)**, 2128 (2012).
- [16] E. E. Salpeter, H. A. Bethe, Phys. Rev. **84**, 1232 (1951);
E. E. Salpeter, Phys. Rev. **87**, 328 (1952).
- [17] M.N. Sergeenko, Mod. Phys. Lett. A, **12**, 2859 (1997).
- [18] M.N. Sergeenko, Phys. Rev. A, **53**, 3798 (1996); [arXiv:quant-ph/9911075]; Mod. Phys. Lett. **A15** (2000) 83; [arXiv:quant-ph/9912069]; Mod. Phys. Lett. **A13** (1998) 33.
- [19] M.N. Sergeenko, Nonlin. Phen. in Compl. Sys. **17(4)**, 433 (2014); **16(4)**, 403 (2013).

Interactions of Strange Mesons at Low Energies

E.Z.Avakyan*, S.L.Avakyan†

Sukhoi State Technical University of Gomel

Abstract

Analytical expressions for the vector and scalar form factors of semileptonic decays K_{l3} have been obtained in the Quark Confinement Model. The contribution from the direct diagrams, as well as that one from the intermediate vector states in the form factors are examined. The performed investigation proves that the semileptonic kaon decays can be successfully described in the framework of QCM. We need no additional parameters and assumptions for adequate description of this kind of decays. Well known CTMOP relation, obtained in the current algebra approach, reproduces in QCM with 10% accuracy. Numerical values for slope parameters $\lambda'_+ = 0.031$ and $\lambda'_0 = 0.0165$ are in satisfactory agreement with experimental data. We also study the radiative decays of neutral kaons $K_{L,S}^0 \rightarrow \gamma\gamma$ in the framework of effective weak lagrangian approach. It is shown that the dominant contribution to $K_L^0 \rightarrow \gamma\gamma$ amplitude is given by the weak transitions of kaons into π, η and η' mesons. It should also be noted that the amplitudes associated with the operator O_5 , are strengthened in comparison with other. Decay $K_S^0 \rightarrow \gamma\gamma$ is completely described by graphs with intermediate scalar states. Received values $Br(K_L^0 \rightarrow \gamma\gamma) = 5.58 \times 10^{-4}$ and $Br(K_S^0 \rightarrow \gamma\gamma) = 2.083 \times 10^{-6}$ are in a good agreement with experimental data.

*E-mail:mikot@tut.by

†E-mail:avakyan@tut.by

1 Introduction

Study of kaon decays has attracted the attention of researchers for decades. The reason is that kaon decays involve an intricate interplay between weak, electromagnetic and strong interactions. These decays are of extraordinary interest as a source of information about a New Physics beyond Standard Model. From this point of view it is very important to have trustworthy quantitative estimations of parameters of mentioned decays in the framework of Standard model. The problem is that calculation of hadronic matrix elements in the most of theoretical approaches needs a great number of additional parameters and model assumptions. Kaon decays have been treated in several reviews and lecture notes during the past 20 years [1].

Pure leptonic and semileptonic decays are among the theoretically cleanest K decays. From this point of view it is very important to have trustworthy quantitative estimations of parameters of mentioned decays in the framework of Standard model.

The aim of this work is theoretical study of semileptonic and electromagnetic interactions of kaons by means of effective Lagrangians proposed in [2], [3],[4]. The calculation of hadronic matrix elements are performed in the Quark Confinement Model (QCM) [5]. This model based on the certain assumptions about nature of quark confinement and hadronization allows to describe the electromagnetic, strong and weak interactions of light (nonstrange and strange) mesons from a unique point of view. Basic low-energy properties of kaons in QCM were considered by us in [6]. The undoubted dignity of model is that further study of kaon decays doesn't need no more additional assumptions and no more additional parameters.

2 Quark Interactions

The hadronic interactions will be described in the QCM. This model is based on the following assumptions [5]:

The hadron fields are assumed to arise after integration over gluon and quark variables in the QCM generating function. The transition of hadrons to quarks and vice versa is given by the interaction Lagrangian. In particular necessary interaction Lagrangians for π^\pm and K mesons look

like:

$$\mathcal{L}_M = \frac{g_M}{\sqrt{2}} M \bar{q}^a \Gamma \lambda^m q^a \quad (1)$$

where Γ - Dirak matrix, λ^m - is a corresponding SU(3)-matrix, q - quark vector

$$q_j^a = \begin{pmatrix} u^a \\ d^a \\ s^a \end{pmatrix}$$

In order to quantify the mixing in the η, η' system, one have to define appropriate mixing parameters, which can be related to physical observables. In the [8] the best agreement with experimental data was achieved with the

$$\varphi = 39.3^\circ \quad (2)$$

The properties of scalars are not well established and its description needs an additional assumptions. We use the Lagrangian with additional interaction with derivative [9]:

$$L_S = \frac{g_s}{\sqrt{2}} s(x) \bar{q}(x) (I - i \frac{H}{\Lambda} (\overleftarrow{\partial} - \overrightarrow{\partial})) \lambda_S q(x) \quad (3)$$

with

$$\begin{aligned} & \text{diag}(1, -1, 0) \Rightarrow a_0(980) \\ \lambda_S = & \text{diag}(\cos \delta_s, \cos \delta_s, -\sqrt{2} \sin \delta_s) \Rightarrow \sigma(600) \\ & \text{diag}(-\sin \delta_s, -\sin \delta_s, -\sqrt{2} \cos \delta_s) \Rightarrow f_0(980) \end{aligned}$$

We use the values of additional parameters H, δ_s fixed in [9]:

$$H = 0.54; \quad \delta_s = 17^\circ \quad (4)$$

The coupling constants g_M for meson-quark interaction are defined from so-called compositeness condition. It us convenient to use interaction constant in a form:

$$h_M = \frac{3g_M^2}{4\pi^2} = -\frac{1}{\tilde{\Pi}'_M(m_M)} \quad (5)$$

instead of g_M in the further calculations. All hadron-quark interactions are described by quark diagrams induced by S matrix averaged over vacuum backgrounds.

The confinement ansatz in the case of one-loop quark diagrams consists in following replacement:

$$\int d\sigma_{VAC} Tr |M(x_1)S(x_1, x_2|B_{VAC}) \dots M(x_n)S(x_n, x_1|B_{VAC})| \longrightarrow \int d\sigma_v Tr |M(x_1)S_v(x_1 - x_2) \dots M(x_n)S_v(x_n - x_1)|, \quad (6)$$

where

$$S_v(x_1 - x_2) = \int \frac{d^4 p}{i(2\pi)^4} e^{-ip(x_1 - x_2)} \frac{1}{v\Lambda_q - \hat{p}} \quad (7)$$

The parameter Λ_q characterizes the confinement rang of quark with flavor number $q = u, d, s$. The measure $d\sigma_v$ is defined as:

$$\int \frac{d\sigma_v}{v - \hat{z}} = G(z) = a(-z^2) + \hat{z}b(-z^2) \quad (8)$$

The function $G(z)$ is called the confinement function. $G(z)$ is independent on flavor or color of quark. $G(z)$ is an entire analytical function on the z -plane. $G(z)$ decreases faster then any degree of z in Euclidean region. The choice of $G(z)$, or as the same of $a(-z^2)$ and $b(-z^2)$, is one of model assumptions. In the note [5] $a(-z^2)$ and $b(-z^2)$ are chosen as:

$$\begin{aligned} a(u) &= a_0 e^{-u^2 - a_1 u} \\ b(u) &= b_0 e^{-u^2 - b_1 u} \end{aligned} \quad (9)$$

The request of satisfaction of Ward anomaly identity in QCM gives the additional correlation between $a(0)$ and $b(0)$: $b(0) = -a'(0)$, $a(0) = 2$. Using $a(u)$ and $b(u)$ as (9), one can receive: $a_0 = 2$, $a_1 = \frac{b_0}{4}$. So, the free parameters of the model are Λ_q , b_0 , b_1 . The model parameters for nonstrange quarks were fixed by fitting the well-established constants of low-energy physics in [6]

$$\begin{aligned} \Lambda_u &= 460 \text{ MeV}, & \Lambda_s &= 506 \text{ MeV}, \\ b_0 &= 2, & b_1 &= 0.2, \\ a_0 &= 2, & a_1 &= 0.5. \end{aligned} \quad (10)$$

We put $\Lambda_u = \Lambda_d$ in the most of decays.

Semileptonic transitions are mediated by the effective Lagrangian

$$\mathcal{L}_{eff} = -\frac{G_F}{\sqrt{2}} S_{EW}^{1/2} [\bar{l}\gamma_\mu(1 - \gamma_5)\nu_l][\bar{u}_i\gamma^\mu(1 - \gamma_5)V_{ij}d_j] + h.c. \quad (11)$$

where V_{ij} denotes the ij element of CKM matrix [10], $G_F = 1.1663788(7) \times 10^{-5} GeV^{-2}$ [11] is the Fermi constant as extracted from muon decay. The universal short distance factor

$$S_{EW} = 1 + \frac{2\alpha}{\pi} \left(1 - \frac{\alpha_s}{4\pi}\right) \ln \frac{M_Z}{M_\rho} + \mathcal{O}\left(\frac{\alpha\alpha_s}{\pi^2}\right) = 1.0223 \pm 0.0005 \quad (12)$$

encodes electroweak corrections not included in G_F and small QCD effects [12].

Electromagnetic quark interaction is described in the standard form:

$$L_q^{em} = eA_\mu \bar{q} Q \gamma^\mu q. \quad (13)$$

the notation is adopted

$$q = \begin{pmatrix} u \\ d \\ s \end{pmatrix}$$

$$Q = \begin{pmatrix} 2/3 & 0 & 0 \\ 0 & -1/3 & 0 \\ 0 & 0 & -1/3 \end{pmatrix}$$

The quark weak interaction is described by effective Lagrangian \mathcal{L}_w^{eff} for $\Delta S = 1$ -transitions (the $K^+ \rightarrow \gamma\gamma$ decays are of this type). This Lagrangian is a sum of usual four-quark operators [3] :

$$\mathcal{L}_w^{eff} = \frac{G_F}{2\sqrt{2}} V_{ud} V_{us}^* \sum_{i=1}^6 c_i O_i \quad (14)$$

where four-quark local operators O_i are chosen in following way:

$$\begin{aligned} O_1 &= (\bar{d}O_L^\mu s)(\bar{u}O_L^\mu u) - (\bar{d}O_L^\mu u)(\bar{u}O_L^\mu s) \\ O_2 &= (\bar{d}O_L^\mu u)(\bar{u}O_L^\mu s) + (\bar{d}O_L^\mu s)(\bar{u}O_L^\mu u) + 2(\bar{d}O_L^\mu s)(\bar{d}O_L^\mu d) + 2(\bar{d}O_L^\mu s)(\bar{s}O_L^\mu s) \\ O_3 &= (\bar{d}O_L^\mu u)(\bar{u}O_L^\mu s) + (\bar{d}O_L^\mu s)(\bar{u}O_L^\mu u) - (\bar{d}O_L^\mu s)(\bar{s}O_L^\mu s) \\ O_4 &= (\bar{d}O_L^\mu u)(\bar{u}O_L^\mu s) + (\bar{d}O_L^\mu s)(\bar{u}O_L^\mu u) - (\bar{d}O_L^\mu s)(\bar{d}O_L^\mu d) \\ O_5 &= (\bar{d}O_L^\mu \lambda^a s) \sum_{q=u,d,s} (\bar{q}O_R^\mu \lambda^a q) \\ O_5 &= (\bar{d}O_L^\mu s) \sum_{q=u,d,s} (\bar{q}O_R^\mu q) \end{aligned} \quad (15)$$

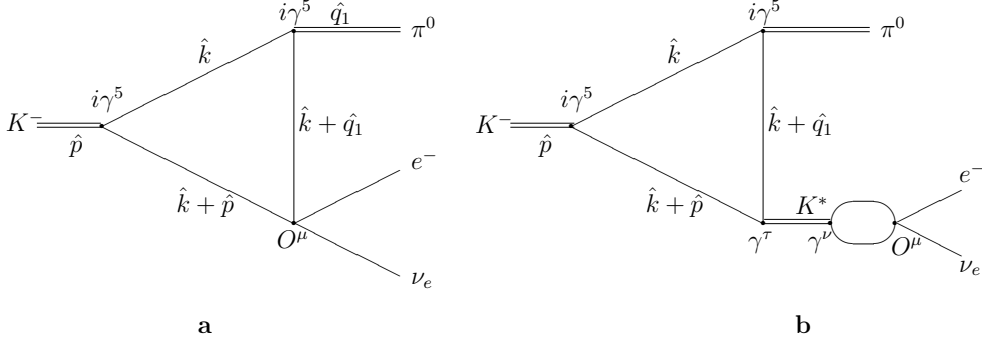


Figure 1: Graphs define K_{l3} matrix element. Indexes a and b indicate the contributions of direct graph (a) and graph with intermediate K^* resonance(b).

Here $O_{R,L}^\mu = \gamma^\mu(1 \pm \gamma^5)$, λ^a -Gell-Mann matrices, acting in colour space. The numerical values of c_i depend on QCD parameters μ_s α_s [4]. In this note we use the set of coefficients c_i corresponding $\mu_s = 0.25$ GeV, $\alpha_s = 0.45$:

$$c_1 = -1.97 \quad c_2 = 0.12 \quad c_3 = 0.093 \quad c_4 = 0.47 \quad c_5 = -0.036 \quad (16)$$

3 K_{l3} Decay

Matrix element of K_{l3} decay is determined by graphs shown in Figure 1. and can be written as

$$M^\mu = F_+(t)(p_1 + p_2)^\mu + F_-(t)(p_1 - p_2)^\mu \quad (17)$$

where

$$\begin{aligned} F_+(t) &= F_+^a(t) + F_+^b(t) \\ F_-(t) &= F_-^a(t) + F_-^b(t) \\ t &= (p_1 - p_2)^2 \end{aligned} \quad (18)$$

Contribution from graph (1a) have been obtained in following form:

$$\begin{aligned} F_+^a(t) &= \sqrt{2h_K h_\pi} F_{VPP}^-(t, m_K^2, m_\pi^2, \Lambda_s, \Lambda_u, \Lambda_u) \\ F_-^a(t) &= \sqrt{2h_K h_\pi} F_{VPP}^+(t, m_K^2, m_\pi^2, \Lambda_s, \Lambda_u, \Lambda_u) \end{aligned} \quad (19)$$

where h_K, h_π - K, π -quark interaction constants calculated by (5).

$F_{VPP}^\pm(t, m_K^2, m_\pi^2, \Lambda_s, \Lambda_u, \Lambda_v)$ -loop integrals for triangle graph, describing $V \rightarrow PP$ transition:

$$\begin{aligned}
F_{VPP}^+(p^2, k_1^2, k_2^2, \Lambda_1, \Lambda_2, \Lambda_3) &= \tag{20} \\
&= \frac{\Delta p^2}{16\Lambda^2} \int_0^{u_\Delta} du u b(-\frac{p^2}{4\Lambda^2}) \sqrt{1-u + (\frac{\Delta u}{2})^2} + \\
&+ \frac{1}{2} \int \int \int_0^1 d\alpha_1 d\alpha_2 d\alpha_3 \delta(1-\alpha_1-\alpha_2-\alpha_3) \times \\
&\times \frac{P \cdot [(\alpha_1 - \alpha_2)(\Lambda_1 - \Lambda_2)(\Lambda_2 - \Lambda_3) + \Lambda_3(\Lambda_1 - \Lambda_2)] + \alpha_1 k_1^2 + \alpha_2 k_2^2}{\alpha_1 \Lambda_1^2 + \alpha_2 \Lambda_2^2 + \alpha_3 \Lambda_3^2}
\end{aligned}$$

$$\begin{aligned}
F_{VPP}^-(p^2, k_1^2, k_2^2, \Lambda_1, \Lambda_2, \Lambda_3) &= \tag{21} \\
&= \frac{1}{2} \int_0^\infty du b(u) + \frac{p^2}{8\Lambda^2} \int_0^{u_\Delta} du b(-\frac{p^2}{4\Lambda^2}) \sqrt{1-u + (\frac{\Delta u}{2})^2} + \\
&+ \frac{1}{2} \int \int \int_0^1 d\alpha_1 d\alpha_2 d\alpha_3 \delta(1-\alpha_1-\alpha_2-\alpha_3) \times \\
&\times \frac{P \cdot [(\alpha_1 + \alpha_2)(\Lambda_1 - \Lambda_3)(\Lambda_2 - \Lambda_3) + \Lambda_3(\Lambda_1 + \Lambda_2 - \Lambda_3)] + \alpha_1 k_1^2 + \alpha_2 k_2^2}{\alpha_1 \Lambda_1^2 + \alpha_2 \Lambda_2^2 + \alpha_3 \Lambda_3^2}
\end{aligned}$$

The following notations have been introduced:

$$\begin{aligned}
\Lambda^2 &= \frac{1}{2}(\Lambda_1^2 + \Lambda_2^2) \tag{22} \\
\Delta &= \frac{\Lambda_2^2 - \Lambda_1^2}{\Lambda_1^2 + \Lambda_2^2} \\
u_\Delta &= \frac{2}{1 + \sqrt{1 - \Delta^2}} \\
P &= \frac{\alpha_1 \alpha_2 p^2 + \alpha_1 \alpha_3 k_1^2 + \alpha_2 \alpha_3 k_2^2}{\alpha_1 \Lambda_1^2 + \alpha_2 \Lambda_2^2 + \alpha_3 \Lambda_3^2}
\end{aligned}$$

For sequential account of the intermediate vector meson the contribution the so-called chain approximation have been used for its propagator:

$$h_V G^{\mu\nu}(p^2) = \frac{1}{\Pi_1(p^2) - \Pi_1(m_V^2)} \left\{ -g^{\mu\nu} + \frac{p^\mu p^\nu \Pi_2(p^2)}{\Pi_1(p^2) - \Pi_1(m_V^2) + p^2 \Pi_2(p^2)} \right\} \tag{23}$$

where $\Pi_{1,2}(p^2)$ are transverse and longitudinal parts of vector polarization operator.

So, after standard transformations, we obtain the following expressions for $F_{\pm}^b(t)$:

$$\begin{aligned} F_+^b(t) &= -F_+^b(t) \frac{t}{\Pi_1(t) - \Pi_1(m_{K^*}^2)} F_{VV}(t) \\ F_-^b(t) &= F_-^b(t) \frac{m_k^2 + m_\pi^2}{\Pi_1(t) - \Pi_1(m_{K^*}^2)} F_{VV}(t) \end{aligned} \quad (24)$$

$F_{VV}(t)$ is a loop integral, corresponding the transverse part of vector polarization operator.

The very simple relationship between $F_+(m_K^2)$ and $F_-(m_K^2)$ was established by C.G. Callan and S.B.Treiman [13], V.Mattur, S.Okubo and L.Pandit [14] by means of current algebra:

$$F_+(m_K^2) + F_-(m_K^2) = f_k/f_\pi \quad (25)$$

In QCM we can obtain analogous relationship without any additional without any additional assumptions. So after calculating $F_+(t)$ and $F_-(t)$ with $t = m_K^2$, ($m_\pi^2 = 0$), one obtains

$$F_+(m_K^2) + F_-(m_K^2) = 0.9f_k/f_\pi \quad (26)$$

i.e. QCM with 10% accuracy reproduces CTMOP relation. One have to mention the cancelation of resonance graphs.

The vector form factor $F_+(t)$ deined in (17) represents the p-wave projection of the crossed-channel matrix element $\langle 0|\bar{s}\gamma^\mu u|K\pi\rangle$ whereas the s-wave projection is described by the scalar form factor [15]

$$F_0(t) = F_+(t) + \frac{t}{m_K^2 - m_\pi^2} F_-(t) \quad (27)$$

It is convenient to normalize all the form factors to $F_+(0)$, so

$$f_{+,0}(t) = \frac{F_{+,0}(t)}{F_+(0)} \quad (28)$$

In the analysis of experimental data form factors usually parameterized in the form [16]

$$f_{+,0}(t) = 1 + \lambda'_{+,0} \frac{t}{m_\pi^2} + \frac{1}{2} \lambda''_{+,0} \left(\frac{t}{m_\pi^2}\right)^2 + \dots \quad (29)$$

Slope parameters can be calculated as follows:

$$\lambda'_{+,-,0} = m_\pi^2 f'_{+,-,0}(0) \quad (30)$$

For K_{e3} decays, recent measurements of the quadratic slope parameters of the vector form factor (λ', λ'') from (refeq:tey) are available from KTeV [17], KLOE [18], ISTRA+ [19], and NA48 [20]. Calculated values for slope parameters λ' and averaged experimental data are displayed in table 1

Table 1.

λ'	QCM	Experiment
$\lambda'_+ \times 10^{-3}$	31	25.2 ± 0.9
$\lambda'_- \times 10^{-3}$	3	0
$\lambda'_0 \times 10^{-3}$	16.5	11.7 ± 1.4

4 $K(p) \rightarrow \gamma^* \gamma^*$ Transition

The amplitude of a transition

$$K \rightarrow \gamma^*(q_1) \gamma^*(q_2) \quad (31)$$

can be written in the general form compatible with gauge invariance as [15]

$$\begin{aligned} M^{\mu\nu} = & [g^{\mu\nu} - \frac{q_1^\mu q_1^\nu}{q_1^2} - \frac{q_2^\mu q_2^\nu}{q_2^2} + \frac{q_1 \cdot q_2}{q_1^2 q_2^2} q_1^\mu q_2^\nu] m_K^2 f_1(q_1^2, q_2^2) + \\ & + [q_2^\mu q_1^\nu - q_1 \cdot q_2 (\frac{q_1^\mu q_1^\nu}{q_1^2} + \frac{q_2^\mu q_2^\nu}{q_2^2} - \frac{q_1 \cdot q_2}{q_1^2 q_2^2} q_1^\mu q_2^\nu)] f_2(q_1^2, q_2^2) + \\ & + i \varepsilon^{\mu\nu\rho\sigma} q_{1\rho} q_{2\sigma} f_3(q_1^2, q_2^2) \end{aligned} \quad (32)$$

When one of the photons is on-shell ($q_1^2 = 0$ for instance) $M^{\mu\nu}$ is described by two invariant amplitudes

$$M^{\mu\nu} = (q_2^\mu q_1^\nu - q_1 \cdot q_2 g^{\mu\nu}) f_2(0, q_2^2) + i \varepsilon^{\mu\nu\rho\sigma} q_{1\rho} q_{2\sigma} f_3(0, q_2^2) \quad (33)$$

The (33) remains valid for both photons on-shell.

The $K_L^0 \rightarrow \gamma\gamma$ decay produces photons with perpendicular polarisation ($\varepsilon_{\mu\nu\rho\sigma} F^{\mu\nu} F^{\rho\sigma}$) and then only $f_3(0, 0)$ in (33) contributes to the width. Let denote it as

$$f_3(0, 0) = M(K_L^0 \rightarrow \gamma\gamma)$$

Amplitude of the studied decay can be written in the form:

$$M(K_L^0 \rightarrow \gamma\gamma) = \frac{G_F}{2\sqrt{2}} V_{ud} V_{us}^* \sum_{i=1}^6 c_i [T_{K_L^0 \gamma\gamma}^i + \sum_{P=\pi,\eta,\eta'} T_{KP}^i D_P(m_K^2) g_{P\gamma\gamma}(m_K^2)] \quad (34)$$

The following notation has been adopted:

$$T_{K_L^0 \gamma\gamma}^i = \int dy dx_1 dx_2 dx_3 e^{ip_1 x_1 + ip_2 x_2 + ip_3 x_3} \langle 0 | T(L_q^{em}(x_1) L_q^{em}(x_2) L_K(x_3) O^i(y)) | 0 \rangle \quad (35)$$

$$T_{KP}^i = \int dy dx_1 dx_2 e^{ip_1 x_1 + ip_2 x_2} \langle 0 | T(L_P(x_1) \mathcal{L}_K(x_2) O^i(y)) | 0 \rangle \quad (36)$$

$L_q^{em}(x)$, $\mathcal{L}_P(x)$ are defined by (13) and (1) correspondingly. We use the chain approximation for propagator of pseudoscalar meson P $D_P(m_K^2)$:

$$h_P D_P(p^2) = \frac{1}{\Pi_P(p^2) - \Pi_P(m_P^2)}. \quad (37)$$

where $\Pi_P(p^2)$ -mass operator of P .

$g_{P\gamma\gamma}(m_K^2)$ -form factor of $P \rightarrow \gamma\gamma$ decay:

$$g_{P\gamma\gamma}(x) = \frac{1}{\Lambda} \frac{\sqrt{3h_P}}{9\pi} F_{PVV}\left(\frac{x}{\Lambda^2}\right) Tr\{\lambda_P Q^2\} \quad (38)$$

$F_{PVV}\left(\frac{x}{\Lambda^2}\right)$ is the loop integral (20) with $p^2 = x$, $q_1^2 = q_2^2 = 0$, $\Lambda_1 = \Lambda_2 = \Lambda_u$.

Analytical expressions for invariant amplitudes $T_{K_L^0 \gamma\gamma}^i$ and T_{KP}^i obtained in the QCM are given in the Table 2 and the numerical values are shown in Table 3.

The table 3 shows that the dominant contribution is given by the weak transitions of kaons into π, η and η' mesons. This is consistent with [15]. It should also be noted that the amplitudes associated with the operator O_5 , are strengthened in comparison with other.

T	Analytical expression
$T_{K_L^0\gamma\gamma}^1$	$-\frac{16}{3}\sqrt{\frac{h_K}{6}}\frac{\alpha}{3\pi^2}\Pi_{PA}(m_K^2, \Lambda_u, \Lambda_s)F_{AVV}(m_K^2)$
$T_{K_L^0\gamma\gamma}^5$	$\sqrt{\frac{h_K}{6}}\frac{\alpha}{3\pi^2}\left[\frac{\Lambda_u^3+\Lambda_s^3}{2\Lambda^2}\cdot(F_{PVVI}(m_K^2, \Lambda_s, \Lambda_s, \Lambda_s, \Lambda_u)+F_{PVVI}(m_K^2, \Lambda_s, \Lambda_s, \Lambda_s, \Lambda_u))+F_{PVIV}(m_K^2, \Lambda_s, \Lambda_s, \Lambda_u, \Lambda_u)\right]-\Lambda_s\frac{4}{3}\Pi_{PA}(m_K^2, \Lambda_u, \Lambda_s)F_{PVV}\left(\frac{m_K^2}{\Lambda_u^2}\right)+\frac{\Lambda_s^2}{\Lambda_u}\frac{4}{27}\Pi_{PP}(m_K^2, \Lambda_u, \Lambda_s)F_{PVV}\left(\frac{m_K^2}{\Lambda_u^2}\right)]$
$T_{K_L^0\pi}^1$	$\sqrt{\frac{h_\pi h_K}{2}}/\pi^2\Pi_{PA}(m_K^2, \Lambda_u, \Lambda_s)F_P\left(\frac{m_K^2}{\Lambda_u^2}\right)m_K^2\Lambda_u\sqrt{\Lambda_u^2+\Lambda_s^2}$
$T_{K_L^0\pi}^5$	$\frac{\sqrt{\Lambda_u^2+\Lambda_s^2}}{\pi^2}\frac{16}{3}[\Pi_{PP}(m_K^2, \Lambda_u, \Lambda_s)\Pi_{PP}(m_K^2, \Lambda_u, \Lambda_u)\frac{\Lambda_u^2(\Lambda_u^2+\Lambda_s^2)}{2}+F_{IPP}(0, m_K^2, m_\pi^2, \Lambda_u, \Lambda_u, \Lambda_s)(\Lambda_u^3+\Lambda_s^3)C_A^{(1)}]$
$T_{K_L^0\eta'}^1$	$\sqrt{h_{\eta'}h_K}/\pi^2\Pi_{PA}(m_K^2, \Lambda_u, \Lambda_s)F_P\left(\frac{m_K^2}{\Lambda_u^2}\right)m_K^2\Lambda_u\sqrt{\frac{\Lambda_u^2+\Lambda_s^2}{2}}\cos\varphi$
$T_{K_L^0\eta'}^2$	$\sqrt{h_{\eta'}h_K}/\pi^2m_K^2\sqrt{\frac{\Lambda_u^2+\Lambda_s^2}{2}}\Pi_{PA}(m_K^2, \Lambda_u, \Lambda_s)\times[-6\cos\varphi\Lambda_uF_P\left(\frac{m_K^2}{\Lambda_u^2}\right)+4\sqrt{2}\sin\varphi\Lambda_sF_P\left(\frac{m_K^2}{\Lambda_s^2}\right)]$
$T_{K_L^0\eta'}^3$	$\sqrt{h_{\eta'}h_K}/\pi^2m_K^2\sqrt{\frac{\Lambda_u^2+\Lambda_s^2}{2}}\Pi_{PA}(m_K^2, \Lambda_u, \Lambda_s)\times[-6\cos\varphi\Lambda_uF_P\left(\frac{m_K^2}{\Lambda_u^2}\right)-6\sqrt{2}\sin\varphi\Lambda_sF_P\left(\frac{m_K^2}{\Lambda_s^2}\right)]$
$T_{K_L^0\eta'}^5$	$\frac{\sqrt{h_{\eta'}h_K}}{\pi^2}\frac{16}{3}[\cos\varphi(\Lambda_u^2\frac{\Lambda_u^2+\Lambda_s^2}{2}\Pi_{PP}(m_K^2, \Lambda_u, \Lambda_s)\times\Pi_{PP}(m_K^2, \Lambda_s, \Lambda_s)+F_{IPP}(0, m_K^2, m_{\eta'}^2, \Lambda_u, \Lambda_u, \Lambda_s)(\Lambda_u^3+\Lambda_s^3)C_A^{(1)})-\sqrt{2}\sin\varphi(\Lambda_s^2\frac{\Lambda_u^2+\Lambda_s^2}{2}\Pi_{PP}(m_K^2, \Lambda_u, \Lambda_s))F_{PP}\left(\frac{m_K^2}{\Lambda_s^2}\right)+F_{IPP}(0, m_K^2, m_{\eta'}^2, \Lambda_s, \Lambda_s, \Lambda_u)(\Lambda_u^3+\Lambda_s^3)C_A^{(1)}]$
$T_{K_L^0\eta}^1$	$-\sqrt{h_\eta h_K}/\pi^2\Pi_{PA}(m_K^2, \Lambda_u, \Lambda_s)F_P\left(\frac{m_K^2}{\Lambda_u^2}\right)m_K^2\Lambda_u\sqrt{\frac{\Lambda_u^2+\Lambda_s^2}{2}}\sin\varphi$
$T_{K_L^0\eta}^2$	$\sqrt{h_\eta h_K}/\pi^2m_K^2\sqrt{\frac{\Lambda_u^2+\Lambda_s^2}{2}}\Pi_{PA}(m_K^2, \Lambda_u, \Lambda_s)\times[6\sin\varphi\Lambda_uF_P\left(\frac{m_K^2}{\Lambda_u^2}\right)+4\sqrt{2}\cos\varphi\Lambda_sF_P\left(\frac{m_K^2}{\Lambda_s^2}\right)]$
$T_{K_L^0\eta}^3$	$\sqrt{h_\eta h_K}/\pi^2m_K^2\sqrt{\frac{\Lambda_u^2+\Lambda_s^2}{2}}\Pi_{PA}(m_K^2, \Lambda_u, \Lambda_s)\times[\sin\varphi\Lambda_uF_P\left(\frac{m_K^2}{\Lambda_u^2}\right)-6\sqrt{2}\cos\varphi\Lambda_sF_P\left(\frac{m_K^2}{\Lambda_s^2}\right)]$

Table 2: Analytical expressions for invariant amplitudes

T	Analytical expression
$T_{K_L^0 \eta}^5$	$\frac{\sqrt{h_\eta h_K}}{\pi^2} \frac{16}{3} [\sin \varphi(\Lambda_u^2 \frac{\Lambda_u^2 + \Lambda_s^2}{2} \Pi_{PP}(m_K^2, \Lambda_u, \Lambda_s) \Pi_{PP}(m_K^2, \Lambda_u, \Lambda_u) -$ $- F_{IPP}(0, m_K^2, m_{\eta'}^2, \Lambda_u, \Lambda_u, \Lambda_s)(\Lambda_u^3 + \Lambda_s^3) C_A^{(1)}) +$ $+ \sqrt{2} \cos \varphi(\Lambda_s^2 \frac{\Lambda_u^2 + \Lambda_s^2}{2} \Pi_{PP}(m_K^2, \Lambda_u, \Lambda_s) \Pi_{PP}(m_K^2, \Lambda_s, \Lambda_s) -$ $- F_{IPP}(0, m_K^2, m_{\eta'}^2, \Lambda_s, \Lambda_s, \Lambda_u)(\Lambda_u^3 + \Lambda_s^3) C_A^{(1)}]$
$T_{K_s^0 a_0}^5$	$\frac{\sqrt{h_k h_{a_0}}}{\pi^2} \frac{16}{3} (\Pi_{PP}(m_K^2, \Lambda_u, \Lambda_s) \Pi_{IS}(\frac{m_K^2}{\Lambda_u^2}) \Lambda_u^2 \frac{\Lambda_u^2 + \Lambda_s^2}{2} +$ $+ F_{SPP}(m_{a_0}^2, 0, m_K^2, \Lambda_u, \Lambda_s, \Lambda_u)(\Lambda_s^3 - \Lambda_u^3) C_a^{(1)})$
$T_{K_s^0 \sigma}^5$	$\frac{\sqrt{h_k h_\sigma}}{\pi^2} \frac{16}{3} [\cos \delta_S (\Pi_{PP}(m_K^2, \Lambda_u, \Lambda_s) \Pi_{IS}(m_K^2, \Lambda_u, \Lambda_u) \Lambda_u^2 \frac{\Lambda_u^2 + \Lambda_s^2}{2} +$ $+ F_{SPP}(m_\sigma^2, 0, m_K^2, \Lambda_u, \Lambda_s, \Lambda_u)(\Lambda_s^3 - \Lambda_u^3) C_a^{(1)}) -$ $- \sqrt{2} \sin \delta_S (\Pi_{PP}(m_K^2, \Lambda_u, \Lambda_s) \Pi_{IS}(m_K^2, \Lambda_s, \Lambda_s) \Lambda_s^2 \frac{\Lambda_u^2 + \Lambda_s^2}{2} +$ $+ F_{SPP}(m_\sigma^2, 0, m_K^2, \Lambda_s, \Lambda_u, \Lambda_s)(\Lambda_s^3 - \Lambda_u^3) C_a^{(1)})]$
$T_{K_s^0 f_0}^5$	$\frac{\sqrt{h_k h_\sigma}}{\pi^2} \frac{16}{3} [\sin \delta_S (\Pi_{PP}(m_K^2, \Lambda_u, \Lambda_s) \Pi_{IS}(m_K^2, \Lambda_u, \Lambda_u) \Lambda_u^2 \frac{\Lambda_u^2 + \Lambda_s^2}{2} +$ $+ F_{SPP}(m_{f_0}^2, 0, m_K^2, \Lambda_u, \Lambda_s, \Lambda_u)(\Lambda_s^3 - \Lambda_u^3) C_a^{(1)}) -$ $+ \sqrt{2} \cos \delta_S (\Pi_{PP}(m_K^2, \Lambda_u, \Lambda_s) \Pi_{IS}(m_K^2, \Lambda_s, \Lambda_s) \Lambda_s^2 \frac{\Lambda_u^2 + \Lambda_s^2}{2} +$ $+ F_{SPP}(m_{f_0}^2, 0, m_K^2, \Lambda_s, \Lambda_u, \Lambda_s)(\Lambda_s^3 - \Lambda_u^3) C_a^{(1)})]$

Table 2: Analytical expressions for invariant amplitudes (continue)

T	Numerical value	T	Numerical value
$T_{K_L^0 \gamma \gamma}^1$	$-1.06 \cdot 10^{-5} \text{ GeV}$	$T_{K_L^0 \gamma \gamma}^5$	$-1.43 \cdot 10^{-4} \text{ GeV}$
$T_{K_L^0 \pi}^1$	$9.69 \cdot 10^{-3} \text{ GeV}^4$	$T_{K_L^0 \pi}^5$	$2.1 \cdot 10^{-1} \text{ GeV}^4$
$T_{K_L^0 \eta'}^1$	$5.49 \cdot 10^{-3} \text{ GeV}^4$	$T_{K_L^0 \eta'}^2$	$-6.6 \cdot 10^{-2} \text{ GeV}^4$
$T_{K_L^0 \eta'}^3$	$1.71 \cdot 10^{-2} \text{ GeV}^4$	$T_{K_L^0 \eta}^1$	$6.3 \cdot 10^{-3} \text{ GeV}^4$
$T_{K_L^0 \eta}^2$	$-2.04 \cdot 10^{-2} \text{ GeV}^4$	$T_{K_L^0 \eta}^3$	$9.15 \cdot 10^{-2} \text{ GeV}^4$
$T_{K_L^0 \eta}^5$	$4.07 \cdot 10^{-1} \text{ GeV}^4$	$T_{K_s^0 a_0}^5$	0.22 GeV^4
$T_{K_s^0 \sigma}^5$	0.36 GeV^4	$T_{K_s^0 f_0}^5$	0.22 GeV^4

Table 3: Numerical values for invariant amplitudes

The photons $K_S^0 \rightarrow \gamma\gamma$ decay have parallel polarisation ($F_{\mu\nu} F^{\mu\nu}$), so its amplitude is determined by $f_2(0, 0)$ from (33) and, up to one loop, there is no short- distance contribution due to Furry's theorem. We denote

$$f_s(0, 0) = M(K_S^0 \rightarrow \gamma\gamma)$$

Matrix element of the studied decay can be written in the form:

$$M(K_s^0 \rightarrow \gamma\gamma) = \frac{G_F}{2\sqrt{2}} V_{ud} V_{us}^* \cdot c_5 \cdot \sum_{S=a_0, \sigma(600), f_0(980)} T_{KS}^5 D_S(m_K^2) g_{S\gamma\gamma}(m_K^2) \quad (39)$$

where $g_{S\gamma\gamma}(m_K^2)$ -form factor of scalar radiative decay at $m_S^2 = m_K^2$:

$$g_{S\gamma\gamma}(m_s^2) = \alpha \sqrt{6h_s(H)} \frac{1}{\Lambda} \text{Tr} \{Q^2 \lambda_s\} [F_{SVV}^1(m_s^2) + H F_{SVV}^2(m_s^2)] \quad (40)$$

$F_{SVV}^{1,2}(m_s^2)$ are defined in following way:

$$F_{SVV}^1(m_s^2) = \frac{x}{4} \int_0^1 du a \left(-u \frac{x}{4}\right) (1+u) \ln \left(\frac{1+\sqrt{1-u}}{1-\sqrt{1-u}}\right) \quad (41)$$

$$F_{SVV}^2(m_s^2) = \frac{x}{4} \int_0^1 du b \left(-u \frac{x}{4}\right) u \ln \left(\frac{1+\sqrt{1-u}}{1-\sqrt{1-u}}\right) \quad (42)$$

Table 2 represents analytical expressions obtained in QCM for T_{KS}^5 , while the numerical value are displayed in Table 3.

The decay width of $K^0 \rightarrow \gamma\gamma$ decay is given by

$$\Gamma(K^0 \rightarrow \gamma\gamma) = \frac{m_K^3}{64\pi} |M((K^0 \rightarrow \gamma\gamma))|^2 \quad (43)$$

Matrix elements $M((K^0 \rightarrow \gamma\gamma))$ is defined (34) and (39). Numerical value of obtained in the QCM invariant amplitudes $T_{K_L^0\gamma\gamma}^i$, T_{KP}^i and T_{KS}^5 are given in Tables 2,3. We use the set of coefficients c_i (16) and numerical values $G_F = 1.1664 \times 10^{-5} \text{GeV}^{-2}$ for Fermi constant [11], $|V_{ud}| = 0.97425$, $|V_{us}| = 0.2253$ for CKM matrix elements [7].

Table 4 summarizes our values of branching ratios $K_{L,S}^0 \rightarrow \gamma\gamma$

Decay	QCM	Experiment[7]
$K_L^0 \rightarrow \gamma\gamma$	5.58×10^{-4}	$(5.47 \pm 0.04) \times 10^{-4}$
$K_S^0 \rightarrow \gamma\gamma$	2.083×10^{-6}	$(2.63 \pm 0.17) \times 10^{-6}$

Table 4: The values of branching ratios $K_{L,S}^0 \rightarrow \gamma\gamma$

The table shows that the obtained numerical values are in good agreement with modern experimental data. It should be noted that intermediate hadron states give the main contribution to the amplitude. We were able to describe $K_S^0 \rightarrow \gamma\gamma$ due to the correct account of the intermediate scalar mesons.

References

- [1] Artuso, M. *B, D and K Decays* / Artuso, M., et al., Eur. Phys. J. C57 (2008) 309-492.
- [2] Gilman, F.J. *$K \rightarrow \pi e^+ e^-$ in the six-quark model* / Gilman F.J. and M.B. Wise.- Phys. Rev. D 21 (1980) 3150-3165
- [3] Shifman, M.A. Asymptotic freedom, light quarks and the origin of the $\Delta T = \frac{1}{2}$ rule in the non-leptonic decays of strange particles / Shifman M.A., A.I. Vainstein and V.I. Zakharov.- Nucl. Phys. B120 (1976) 316-324
- [4] Buras, A. J., Weak Hamiltonian, CP violation and rare decays / Buras, A.J.- in 'Probing the Standard Model of Particle Interactions', F.David and R. Gupta, eds., 1998, Elsevier Science B.V. Amsterdam, 281-539
- [5] Efimov, G.V. Confinement and Quark Structure of Light Hadrons / G.V. Efimov, M.A. Ivanov.- Internat. J. Mod. Phys. A, 4, (1989) 2031-2061.
- [6] Avakyan, E.Z. Polarizability Of π Mesons In The Quark Confinement Model / Avakyan, E.Z. et al.- Soviet Journ. of Nucl. Phys. v.49(1989), 867-872
- [7] Beringer, J. Review of Particle Physics (RPP) / J. Beringer et al.- Phys. Rev. D86, (2012) 010001
- [8] Avakyan, E. Mixing Parameters of η and η' Mesons / E. Avakyan, S. Avakyan . – Physics of Particles and Nuclei Letters- 2010- Vol. 7, No. 6- P.391-396.
- [9] Avakyan, E.Z. Decays of Light Scalar Mesons in the Quark Confinement Model. / E.Z. Avakyan, S.L. Avakyan, Proceedings of the Academy of Sciences of Belarus, Series of Physical-Mathematical Sciences v3, 70-75, 2008. (in Russian)
- [10] Kobayashi, M. CP Violation in the Renormalizable Theory of Weak Interaction / Kobayashi, M., and T. Maskawa.- Prog. Theor. Phys. 49 (1973) 652-657

- [11] Webber, D. M., Measurement of the Positive Muon Lifetime and Determination of the Fermi Constant to Part-per-Million Precision/Webber, D. M., et al. (MuLan Collab).- Phys. Rev. Lett. 106,(2011) 041803.
- [12] Marciano, W. J. Radiative corrections to π_{l2} decays/Marciano, W. J., and A. Sirlin.-Phys. Rev. Lett. 71,(1993) 3629-3632
- [13] Callan, C.G. Equal Time Commutators and K Meson Decays / C.G. Callan, S.B. Treiman. Phys. Rev. Lett. 16,(1966) 153-157.
- [14] Mattur, V. Algebra of Currents and K_{l3} Decay /Mattur V., Okubo S. and Pandit L.-Phys. Rev. Lett. 16,(1966) 371-374,601
- [15] Cirigliano, V. Kaon Decays in the Standard Model/Cirigliano, V. et al.-Rev.Mod.Phys. 84 (2012) 399-449
- [16] Antonelli, M. Flavor Physics in the Quark Sector/Antonelli, M. et al.-Phys.Rept. 494 (2010) 197-414
- [17] Alexopoulos, T. Measurements of Semileptonic K_l Decay Form Factors/F. Ambrosino, et al.-Phys. Rev. D70 (2004) 092007.
- [18] Ambrosino, F. Measurement of the form-factor slopes for the decay $K_L \rightarrow \pi^\pm e \nu$ with the KLOE detector /F. Ambrosino, et al.-Phys. Lett. B636 (2006) 166-172.
- [19] Yushchenko, O.P. High statistic measurement of the $K^- \rightarrow \pi^0 e^- \nu$ decay form-factors/Yushchenko, O.P. et al.-Phys. Lett. B589 (2004) 111-117.
- [20] Lai, A. Measurement of K_{e3}^0 form factors/ Lai, A. et al.-Phys. Lett. B604 (2004) 1-10.

Low Energy Hadron Interaction of Tau Lepton

E.Z.Avakyan*, S.L.Avakyan†

Sukhoi State Technical University of Gomel

Abstract

Hadronic decays of τ -lepton have been investigated in the framework of Quark Confinement Model. Branching ratios of τ decays with one pseudoscalar, vector or axial vector meson and with two pions in the final state have been calculated. The numerical results are in a satisfactory agreement with experimental data.

1 Introduction

Since opening in 1975 [1] τ -lepton is an essential tool for testing the fundamental aspects of the electroweak interaction. In particular, due to the large mass of τ -lepton hadronic decays are cinematically . This makes it possible further study as a phenomenon related to the strong interaction, as well as phenomena associated with the weak interaction. Unlike a well-known process of hadrons, which gives an indication only of the electromagnetic vector current, semi-leptonic decays lepton provide an opportunity to study both vector and axial currents. Unlike a well-known process $e^+e^- \rightarrow \gamma$ and hadrons, which gives an indication only of the electromagnetic vector current, semi-leptonic decays of τ -lepton provide an opportunity to study both vector and axial currents. This kind of decays were studied in different theoretical approaches [2] Currently hadron decays of heavy lepton are studied by such collaborations as ALEPH [3], BaBar[4], CLEO[5], BELLE[6]. The study of hadron decays requires attraction of additional models of strong interactions at low energies. In the

*E-mail:mikot@tut.by

†E-mail:avakyan@tut.by

present investigation we we study τ - lepton decays in Quark Confinement Model (QCM) [7]. This model based on the certain assumptions about nature of quark confinement and hadronization allows to describe the electromagnetic, strong and weak interactions of light (nonstrange and strange) mesons from a unique point of view.

2 Two particle τ -Decays with Pseudoscalar Mesons in the Final State

The hadron fields in QCM are assumed to arise after integration over gluon and quark variables in the QCM generating function. The transition of hadrons to quarks and vice versa is given by the interaction Lagrangian. In particular necessary interaction Lagrangians for π and K mesons look like:

$$\mathcal{L}_P = \frac{g_M}{\sqrt{2}} P \bar{q}^a i \gamma_5 \lambda^m q^a \quad (1)$$

λ^m - is a corresponding SU(3)-matrix, q - quark vector

$$q_j^a = \begin{pmatrix} u^a \\ d^a \\ s^a \end{pmatrix}$$

The coupling constants g_M for meson-quark interaction are defined from so-called compositeness condition. It is convenient to use interaction constant in a form:

$$h_M = \frac{3g_M^2}{4\pi^2} = -\frac{1}{\tilde{\Pi}'_M(m_M)} \quad (2)$$

instead of g_M in the further calculations.

a) $\tau \rightarrow \pi \nu_\tau$ Decay

The matrix element of this decay can be written as

$$M(\tau \rightarrow \pi \nu_\tau) = \frac{G_F}{\sqrt{2}} f_\pi \cos \theta_C p^\mu \bar{\nu}(\hat{q}) \gamma^\mu (1 - \gamma^5) \tau(\hat{k}) \quad (3)$$

where

$$f_\pi = \frac{\sqrt{3} \Lambda F_P(\mu_\pi^2)}{\pi \sqrt{2 F_{PP}(\mu_\pi^2)}} \quad (4)$$

with $\mu_\pi^2 = \frac{m_\pi^2}{\Lambda^2}$

$$\Gamma(\tau \rightarrow \pi \nu_\tau) = \frac{1}{16\pi} G_F^2 f_\pi^2 \cos^2 \theta_C m_\tau^3 \left(1 - \frac{m_\pi^2}{m_\tau^2}\right)^2 \quad (5)$$

Structure integrals $F_P(x), F_{PP}(x)$ has the following form

$$F_P(x) = \int_0^\infty du a(u) + \frac{x}{4} \int_0^1 du a\left(-\frac{ux}{4}\right) \sqrt{1-u} \quad (6)$$

$$F_{PP}(x) = \int_0^\infty du b(u) + \frac{x}{4} \int_0^1 du b\left(-\frac{ux}{4}\right) \frac{1-\frac{u}{2}}{\sqrt{1-u}} \quad (7)$$

Functions $a(u)$ and $b(u)$ are QCM confinement functions:

$$\begin{aligned} a(u) &= a_0 e^{-u^2 - a_1 u} \\ b(u) &= b_0 e^{-u^2 - b_1 u} \end{aligned} \quad (8)$$

Decay width for $\tau \rightarrow P\nu_\tau$ is written as:

$$\Gamma(\tau \rightarrow P\nu_\tau) = \frac{1}{16\pi} G_F^2 g_{\tau\nu P}^2 V_{ij}^2 m_\tau^3 \left(1 - \frac{m_P^2}{m_\tau^2}\right)^2 \quad (9)$$

where V_{ij} denotes the ij element of CKM matrix [8]. In case of $\tau \rightarrow P\nu_\tau$ $V_{ij} = V_{ud}$ Branching ratio of this decay have been recieved

b) $\tau \rightarrow K\nu_\tau$ Decay

To describe the interaction of heavy lepton with kaons it is necessary to take into account the difference in the parameters of the non-strange and strange quark. The matrix element of this decay can be written as

$$M(\tau \rightarrow K\nu_\tau) = \frac{G_F}{\sqrt{2}} g_{\tau\nu K} \sin\theta_C p^\mu \bar{\nu}(\hat{q}) \gamma^\mu (1 - \gamma^5) \tau(\hat{k}) \quad (10)$$

Form factor $g_{\tau\nu K}$ have been recieved as

$$g_{\tau\nu K} = \frac{\Lambda}{\pi} \sqrt{\frac{3h_K}{2}} F_P(\mu_K^2, \Lambda_u, \Lambda_s) \quad (11)$$

where h_K is defined by (2) Loop integral F_P in this case is:

$$\begin{aligned} F_P(\mu_K^2, \Lambda_u, \Lambda_s) &= \frac{\delta}{2} \left(\int_0^\infty du a(u) + s \int_0^{u_\Delta} du a(-us) \sqrt{1-u + \left(\frac{u\Delta}{2}\right)^2} \right) + \\ &+ \frac{\Delta}{4} \delta s^2 \int_0^{u_\Delta} du u a(-us) \sqrt{1-u + \left(\frac{u\Delta}{2}\right)^2} \end{aligned} \quad (12)$$

The following notations in (12) have been introduced:

$$\Lambda^2 = \frac{\Lambda_s^2 + \Lambda_u^2}{2}; \Delta = \frac{\Lambda_s^2 - \Lambda_u^2}{\Lambda_s^2 + \Lambda_u^2}; \delta = \sqrt{1-\Delta} + \sqrt{1+\Delta}. \quad (13)$$

The decay width $\tau \rightarrow K\nu_\tau$ can be calculated by (9) with $V_{ij} = V_{sd}$

3 τ Lepton Interaction with Vector mesons

The study of τ - lepton decay in vector particles is very important due to the fact that the ρ - mesons channel is the main channel of heavy lepton decays. Interaction Lagrangians for ρ and K^* mesons in QCM is:

$$\mathcal{L}_V = \frac{g_V}{\sqrt{2}} V^\mu \bar{q}^a \gamma_\mu \lambda^m q^a \quad (14)$$

a) $\tau \rightarrow \rho \nu_\tau$ Decay

The matrix element of this decay can be written in the following way:

$$M^{\mu\nu} = [g^{\mu\nu} q^2 - q^\mu q^\nu] F_{\tau\rho\nu}(q^2) \quad (15)$$

where

$$F_{\tau\rho\nu}(q^2) = \frac{G_F}{\sqrt{2}} V_{ud} \Lambda^2 \frac{\sqrt{3} h_\rho}{2\pi} \Pi_\rho(q^2) \quad (16)$$

Constant of ρ - quark interactions h_ρ can be calculated by (2). Form factor $\Pi_\rho(x)$ have been received as

$$\Pi_\rho(x) = \frac{1}{3\Lambda^2} \left(\int_0^\infty du b(u) + \frac{x}{4} \int_0^1 du b\left(-\frac{ux}{4}\right) \sqrt{1-u} \right) \quad (17)$$

b) $\tau \rightarrow K^* \nu_\tau$ Decay

Matrix element of $\tau \rightarrow K^* \nu_\tau$ decay can be written in a form similar to (15) and (16), with V_{ud} changed to V_{sd} .

$$M^{\mu\nu} = [g^{\mu\nu} q^2 - q^\mu q^\nu] F_{\tau K^* \nu}(q^2) \quad (18)$$

$$F_{\tau K^* \nu}(q^2) = \frac{G_F}{\sqrt{2}} V_{sd} \Lambda^2 \frac{\sqrt{3} h_{K^*}}{2\pi} \Pi_{K^*}(q^2) \quad (19)$$

We have taken into account difference between nonstrange and strange quarks, so form factor $\Pi_{K^*}^*(x)$ is written as

$$\begin{aligned} \Pi_{K^*}^*(x) &= \left(\sqrt{1 - \Delta^2} - 1 \right) \times \quad (20) \\ &\times \left(\int_0^\infty du u b(u) - \left(\frac{x}{4} \right)^2 \int_0^1 du u b\left(-\frac{ux}{4}\right) \sqrt{1-u + \left(\frac{u\Delta}{2} \right)^2} \right) - \\ &- \left(\frac{x\Delta}{8} \right)^2 \int_0^1 du u^2 b\left(-\frac{ux}{4}\right) \sqrt{1-u + \left(\frac{u\Delta}{2} \right)^2} + \\ &+ \frac{4}{3\Lambda^2} \left(\int_0^\infty du b(u) + \frac{x}{4} \int_0^1 du u b\left(-\frac{ux}{4}\right) \sqrt{1-u + \left(\frac{u\Delta}{2} \right)^2} \right) \end{aligned}$$

The widths of $\tau \rightarrow V\nu_\tau$ can be calculated in standard way and can be written using (15)-(17) and (18)-(20) as

$$\Gamma(\tau \rightarrow V\nu_\tau) = \frac{3G_F^2 V_{ij}^2 h_V \Lambda^4}{128\pi^3 m_V^2} m_\tau^3 \left(1 - \frac{m_V^2}{m_\tau^2}\right)^2 \left(1 + \frac{2m_V^2}{m_\tau^2}\right) \Pi_V^2(m_V^2) \quad (21)$$

4 Interaction of τ -Lepton with Axial a_1 Meson

The study of τ - lepton interactions with axial vector meson is extremely interesting from the point of view of studying its decay into $(2n + 1)$ meson, as well as a testing of model because the calculation of the decay constants can not be linked with the phenomenological constants of the low-energy physics, as is done in most of the approaches in the case of final pseudoscalar and vector states. In the QCM axial vector meson-quark interactions are described by

$$i\gamma_\mu \gamma_5 \lambda^m q^a \quad (22)$$

Matrix element for $\tau \rightarrow a_1\nu_\tau$ is written as

$$M^{\mu\nu}(\tau \rightarrow a_1\nu_\tau) = \frac{G_F}{\sqrt{2}} V_{ud} \Lambda^2 \frac{\sqrt{3h_{a_1}}}{2\pi} [g^{\mu\nu} q^2 F_1^A(q^2) - q^\mu q^\nu F_2^A(q^2)] \quad (23)$$

where form factors $F_1^A(x)$ and $F_2^A(x)$ have been obtained in a form

$$F_1^A(x) = \quad (24)$$

$$= -2 \int_0^\infty du ub(u) - \frac{x}{3} \left(\int_0^\infty dub(u) + \frac{x}{4} \int_0^1 dub\left(-\frac{ux}{4}\right) (2u-1)\sqrt{1-u} \right)$$

$$F_2^A(x) = \frac{1}{3\Lambda^2} \left(\int_0^\infty dub(u) + \frac{x}{4} \int_0^1 dub\left(-\frac{ux}{4}\right) \sqrt{1-u} \right) \quad (25)$$

The decay width is calculated by the formula:

$$\Gamma(\tau \rightarrow a_1\nu_\tau) = \frac{3G_F^2 V_{ud}^2 h_{a_1} \Lambda^4}{128\pi^3 m_{a_1}^2} m_\tau^3 \left(1 - \frac{m_{a_1}^2}{m_\tau^2}\right)^2 \left(1 + \frac{2m_{a_1}^2}{m_\tau^2}\right) (F_1^A(m_{a_1}^2))^2 \quad (26)$$

5 Three Particles Decays

Decay $\tau \rightarrow \pi\pi\nu_\tau$ is one of the main modes of heavy lepton decays. The matrix element is defined by the contact graph and graphs with an intermediate vector meson.

Contribution from the contact graph can be written as

$$M_{dir}^\mu(\tau \rightarrow \pi\pi\nu_\tau) = G_F V_{ud} h_\pi (q_1 - q_2)^\mu F_-(s, q_1^2, q_2^2) \quad (27)$$

where $s = (p_\tau - p_{\nu_\tau})^2$.

Form factor $F_-(s, q_1^2, q_2^2)$ have been obtained as

$$F_-(s, q_1^2, q_2^2) = \frac{1}{2} \left(\int_0^\infty dub(u) + \frac{s}{4\Lambda^2} \int_0^1 dub\left(-\frac{us}{4\Lambda^2}\right) \sqrt{1-u} \right) + \quad (28)$$

$$+ \frac{1}{2\Lambda^2} \int_0^1 d^3\alpha \cdot \delta\left(1 - \sum_{i=1}^3 \alpha_i\right) \left(s\alpha_1\alpha_2 + q_1^2\alpha_1(1 + \alpha_3) + q_2^2(1 + \alpha_3) \right) b(-Q)$$

where

$$Q = \frac{s\alpha_1\alpha_2 + q_1^2\alpha_1\alpha_3 + q_2^2\alpha_2\alpha_3}{\Lambda^2} \quad (29)$$

Intermediate vector meson contribution to the matrix element in the general case can be written as

$$M_{int}^\mu(\tau \rightarrow \pi\pi\nu_\tau) = M_{\tau \rightarrow \rho\nu_\tau}^{\mu\lambda}(s) D_\rho^{\lambda\sigma}(s) (q_1 - q_2)^\sigma F_-(s, q_1^2, q_2^2) \quad (30)$$

$M_{\tau \rightarrow \rho\nu_\tau}^{\mu\lambda}(s)$ and $F_-(s, q_1^2, q_2^2)$ are defined by (27) and (28).

$M_{\tau \rightarrow \rho\nu_\tau}^{\mu\lambda}(s) D_\rho^{\lambda\sigma}(s)$ contents $h_\rho D_\rho^{\mu\nu}(p^2)$. Its analytical expression in chain approximation have to be modified due of ρ -resonance. The following form have been used

$$h_\rho D_\rho^{\mu\nu}(p^2) = \frac{1}{\Pi_{1\rho}(p^2) - \Pi_{1\rho}(m_\rho^2) + im_\rho\Gamma_\rho} \times$$

$$\times \left(-g^{\mu\nu} + p^\mu p^\nu \frac{\Pi_{2\rho}(p^2)}{\Pi_{1\rho}(p^2) - \Pi_{1\rho}(m_\rho^2) + p^2\Pi_{2\rho}(p^2)} \right) \quad (31)$$

where m_ρ and Γ_ρ are mass and full width of ρ resonance. Matrix element of $\tau \rightarrow \pi\pi\nu_\tau$ is a sum of mentioned above contributions. So it have been

obtained in the form:

$$M^\mu(\tau \rightarrow \pi\pi\nu_\tau) = G_F V_{ud} h_\pi (q_1 - q_2)^\mu F_-(s, q_1^2, q_2^2) \times \left(\frac{\Pi_{1\rho}(p^2)}{\Pi_{1\rho}(p^2) - \Pi_{1\rho}(m_\rho^2) + im_\rho\Gamma_\rho} - 1 \right) \quad (32)$$

The width of the decay have been received under standard transformations is written in the following way

$$\Gamma(\tau \rightarrow \pi\pi\nu_\tau) = \frac{G_F^2 h_\pi^2 V_{ud}^2}{64\pi^3 m_\tau} \times \int_{4m_\pi^2}^{m_\tau^2} \frac{ds}{s} \lambda(s, m_\tau^2, 0) \lambda^{\frac{3}{2}}(s, m_\pi^2, m_\pi^2) \left(1 + \frac{2s}{m_\tau^2}\right) F_-^2(s, q_1^2, q_2^2) \quad (33)$$

6 Numerical Results

The following QCM parameters were used for calculation of numerical values of matrix elements [9]

$$\begin{aligned} \Lambda_u &= 460 \text{ MeV} \\ \Lambda_s &= 506 \text{ MeV} \\ b_0 &= 2 \quad b_1 = 0.2 \\ a_0 &= 2 \quad a_1 = 0.5 \end{aligned} \quad (34)$$

Branching rations calculated by

$$Br(\tau \rightarrow M\nu_\tau) = \frac{\Gamma(\tau \rightarrow M\nu_\tau)}{\Gamma_{tot}} \quad (35)$$

are given in Table.

τ -Decays	Br (QCM)	Br (Experiment) [10]
$\tau \rightarrow \pi\nu_\tau$	11, 25%	(10, 83 \pm 0.06) %
$\tau \rightarrow K\nu_\tau$	$7, 6 \cdot 10^{-3}$	(7, 0 \pm 0.1) $\cdot 10^{-3}$
$\tau \rightarrow \rho\nu_\tau$	23, 5%	(25, 52 \pm 0, 09) %
$\tau \rightarrow K^*\nu_\tau$	1, 68%	(1, 20 \pm 0, 07) %
$\tau \rightarrow a_1\nu_\tau$	10, 4%	-
$\tau \rightarrow \pi\pi\nu_\tau$	23, 7%	(25, 24 \pm 0, 16) %

The table shows that our values are in reasonable agreement with the experimental data.

References

- [1] Perl, M.L. Evidence for Anomalous Lepton Production in e^+e^- Annihilation / Martin L. Perl et. al. Phys.Rev.Lett. 35 (1975) 1489-1492
- [2] Pich,A.Theoretical overview on tau physics/ A. Pich Int.J.Mod.Phys. A21 (2006) 5652-5659
- [3] Davier, M.Update of the ALEPH non-strange spectral functions from hadronic τ decays/M.Davier et. al.Eur.Phys.J. C74 (2014) 2803-2814
- [4] Lees J.P. Search for CP Violation in the Decay $\tau \rightarrow \pi^- K_S^0(\geq 0)\nu_\tau$ /BaBar Collaboration(J.P. Lees et al.)Phys.Rev. D85 (2012) 031102
- [5] Andersen S.Hadronic Structure in the Decay $\tau \rightarrow \pi^- \pi_S^0 \nu_\tau$ /CLEO Collaboration (Andersen S. et. al.)Phys.Rev. D61 (2000) 112002-112042
- [6] Fujikawa M. High-Statistics Study of the $\tau \rightarrow \pi^- \pi_S^0 \nu_\tau$ Decay Belle Collaboration (M. Fujikawa et al.). Phys.Rev. D78 (2008) 072006
- [7] Efimov,G.V.Confinement and Quark Structure of Light Hadrons / G. V. Efimov, M. A. Ivanov.- Internat. J. Mod. Phys. A, 4, (1989) 2031-2061.
- [8] Kobayashi, M.CP Violation in the Renormalizable Theory of Weak Interaction/ Kobayashi, M., and T. Maskawa.-Prog.Theor.Phys. 49 (1973) 652-657
- [9] Avakyan,E.Z. Polarizability Of π Mesons In The Quark Confinement Model/ Avakyan,E.Z.et al.- Soviet Journ.of Nucl.Phys.v.49(1989),867-872
- [10] Olive K.2015 Review of Particle Physics / K.A. Olive et al.(Particle Data Group), Chin. Phys. C, 38, 090001 (2014)

4 Physics In and Beyond the Frame of the Standard Model

Some NNLO contribution to the Drell-Yan differential cross section

Ya.Dydyshka V.Yermolchyk
J.Suarez Gonzalez

Institute for Nuclear Problems of Belarusian State University

Abstract

In this work we report our preliminary results in two-loop mixed EW-QCD correction calculation. We hardly exploit computer algebra systems and perform the two most time-consuming operations: traces and kinematics (with FORM) and scalar integral reduction (with FIRE). The third step is to evaluate master-integrals and we made all essential preparations for this task.

Drell-Yan process is one of the most investigated and thus widely exploited for precise measurements of the Standard Model parameters and for the various detector calibrations. From the theoretical point of view mixed electroweak (EW) and QCD effects are the only remaining source of uncertainties of the perturbative nature and thus at present attract attention of various groups [1, 2]. But most calculations were made in so-called “pole-approximation” i.e. neglecting box-type diagrams. In this work we do not make such simplifications.

Mixed EW-QCD contribution can be separated into two parts: contribution with photon-gluon loops and with massive weak boson(MWB)-gluon loops. Former part we denote as QED-QCD contribution and latter as MWB-QCD.

Next, we separate 2-loop corrections onto contributions from weak- and strong-connected diagrams. Weak-connected diagram contribution needs calculation of product of two one-loop diagrams. In dimensional regularization it is necessary to expand these integrals to higher order in $\epsilon = (4 - d)/2$. Such expansion is known in most cases.

For strong-connected diagrams needs calculation of the additional set of integrals. We collect them according to number of propagators in loop. It is known in advance that maximal number of propagators will be in the integrals with maximal number of external (relative to loop) legs. For Drell-Yan process maximal number of external legs is number of external particles i.e. 4. We call integrals with 4 legs and maximal number of propagators (which is 7) two-loop boxes. Diagrams with lower number of legs and lower number of propagators can be obtained from two-loop boxes by contraction of one or more propagator lines to a point (and merging their vertexes). The only exception is two-loop corrections to the self-energies of external and internal lines, but they are rather well-investigated[3, 4]

Let's consider contribution from two-loop boxes:

$$\begin{aligned} \frac{d\sigma_{u\bar{u}}^{BX}}{dy} &= \frac{\pi\alpha^2}{3s} \frac{\alpha}{4\pi} \frac{\alpha_s}{4\pi} \times \\ &\times 2\text{Re} \left[2T_1(s, t, u, M_Z) + 2T_1(s, u, t, M_Z) + 2T_1(s, u, t, M_W) + \right. \\ &\quad + T_2(s, t, u, M_Z) + T_2(s, u, t, M_Z) + T_2(s, u, t, M_W) + \\ &\quad \left. + T_3(s, t, u, M_Z) + T_3(s, u, t, M_Z) + T_3(s, u, t, M_W) \right] \quad (1) \end{aligned}$$

where $y = -t/s$, and factors $T_i(s, t, u, M)$ are determining all the dynamics of the process and corresponds to diagrams 1,2,3 of Fig.1.

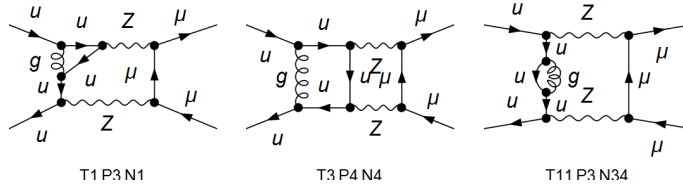


Figure 1: Diagrams for T_1 , T_2 and T_3 .

Generic topology 2 has to be represented as union of three diagrams, which are closed with respect to tensor reduction. They have chosen in such a way that irreducible numerators from one diagram are coincide with propagators from another which fixes them uniquely.

Introducing notations for combinations of coupling constants and inte-

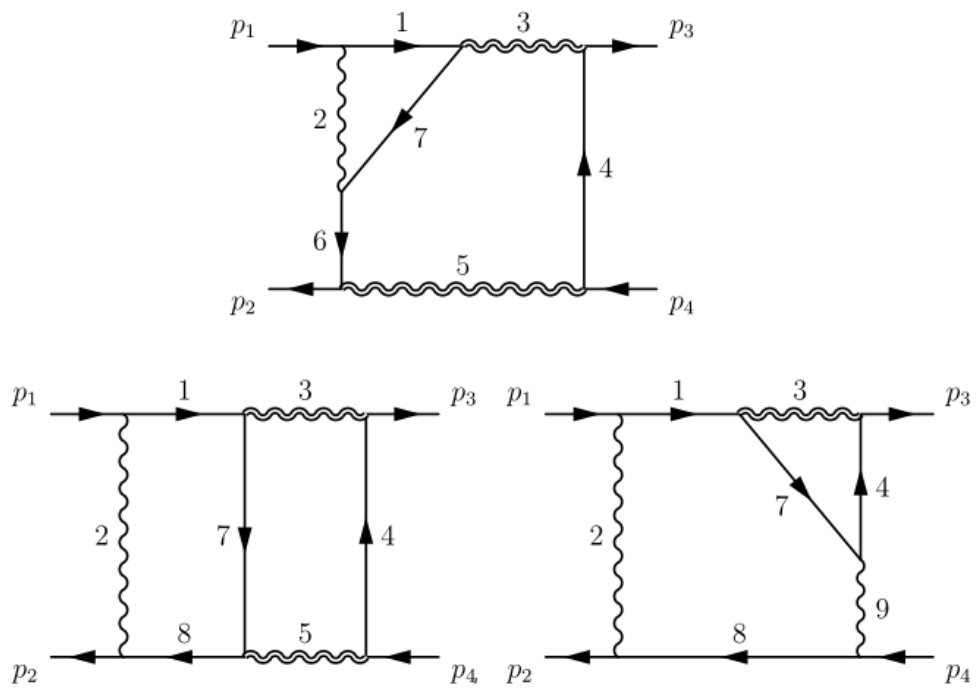


Figure 2: 2-loop box diagram; momenta p_1 and p_2 - incoming, p_3 and p_4 - outgoing.

grals

$$\Lambda_1 = g_L(q)^3 g_R(l)^3 + g_R(q)^3 g_L(l)^3 \quad (2)$$

$$\Lambda_2 = g_L(q)^3 g_L(l)^3 + g_R(q)^3 g_R(l)^3 \quad (3)$$

$$\begin{aligned} \begin{bmatrix} a_1 a_3 \\ a_2 a_7 a_4 \\ a_6 a_9 \\ a_8 a_5 \end{bmatrix} &= \int d^d q_1 d^d q_2 \frac{1}{[q_1^2]^{a_1}} \frac{1}{[(p_1 + q_1)^2]^{a_2}} \times \\ &\times \frac{1}{[q_2^2 + M_Z^2]^{a_3}} \frac{1}{[(k_1 - q_2)^2]^{a_4}} \frac{1}{[(p_1 + p_2 - q_2)^2 - M_Z^2]^{a_5}} \times \\ &\times \frac{1}{[(p_1 - q_2)^2]^{a_6}} \frac{1}{[(q_1 + q_2)^2]^{a_7}} \frac{1}{[(p_1 + p_2 + q_1)^2]^{a_8}} \frac{1}{[(k_1 + q_1)^2]^{a_9}} \end{aligned} \quad (4)$$

we evaluate factors $T_i(s, t, u, M)$ using FORM [5].

$$\begin{aligned} T_1(s, t, u, M_Z) &= \frac{s\Lambda_1}{2(s - M_Z^2)} \left[\left(- \begin{bmatrix} 11 \\ 111 \\ 10 \\ 01 \end{bmatrix} M_Z^2 + \begin{bmatrix} 01 \\ 111 \\ 10 \\ 01 \end{bmatrix} - \begin{bmatrix} 10 \\ 111 \\ 10 \\ 01 \end{bmatrix} + \begin{bmatrix} 11 \\ 101 \\ 10 \\ 01 \end{bmatrix} \right) t^3 + \\ &+ \left(\left(2 \begin{bmatrix} 11 \\ 011 \\ 10 \\ 01 \end{bmatrix} + \begin{bmatrix} 11 \\ 110 \\ 10 \\ 01 \end{bmatrix} \right) M_Z^2 - \begin{bmatrix} 01 \\ 011 \\ 10 \\ 01 \end{bmatrix} - \begin{bmatrix} 01 \\ 111 \\ 00 \\ 01 \end{bmatrix} + 2 \begin{bmatrix} 01 \\ 101 \\ 10 \\ 01 \end{bmatrix} - \begin{bmatrix} 01 \\ 111 \\ 11 \\ 01 \end{bmatrix} + 2 \begin{bmatrix} 10 \\ 011 \\ 10 \\ 01 \end{bmatrix} - \begin{bmatrix} 11 \\ 010 \\ 10 \\ 01 \end{bmatrix} - \begin{bmatrix} 11 \\ 001 \\ 10 \\ 01 \end{bmatrix} + \right. \\ &\quad \left. + 2 \begin{bmatrix} 11 \\ 011 \\ 11 \\ 01 \end{bmatrix} + \begin{bmatrix} 10 \\ 110 \\ 10 \\ 01 \end{bmatrix} - \begin{bmatrix} 11 \\ 100 \\ 10 \\ 01 \end{bmatrix} - \begin{bmatrix} 11 \\ 111 \\ 01 \\ 01 \end{bmatrix} - \begin{bmatrix} 11 \\ 101 \\ 11 \\ 01 \end{bmatrix} \right) t^2 + \\ &\quad + \left(\left(- \begin{bmatrix} 11 \\ 010 \\ 10 \\ 01 \end{bmatrix} + 2 \begin{bmatrix} 11 \\ 011 \\ 11 \\ 01 \end{bmatrix} + \begin{bmatrix} 11 \\ 110 \\ 11 \\ 01 \end{bmatrix} - \begin{bmatrix} 11 \\ 111 \\ 12 \\ 01 \end{bmatrix} - \begin{bmatrix} 11 \\ 111 \\ 10 \\ 01 \end{bmatrix} \right) M_Z^2 - \begin{bmatrix} 01 \\ 010 \\ 10 \\ 01 \end{bmatrix} + \begin{bmatrix} 01 \\ 011 \\ 00 \\ 01 \end{bmatrix} + \right. \\ &\quad + \begin{bmatrix} 01 \\ 110 \\ 00 \\ 01 \end{bmatrix} + \begin{bmatrix} 01 \\ 110 \\ 11 \\ 01 \end{bmatrix} - \begin{bmatrix} 01 \\ 111 \\ 01 \\ 01 \end{bmatrix} - \begin{bmatrix} 01 \\ 111 \\ 10 \\ 01 \end{bmatrix} - \begin{bmatrix} 10 \\ 010 \\ 10 \\ 01 \end{bmatrix} + 2 \begin{bmatrix} 10 \\ 011 \\ 11 \\ 01 \end{bmatrix} - \begin{bmatrix} 11 \\ 010 \\ 11 \\ 01 \end{bmatrix} - \begin{bmatrix} 11 \\ 011 \\ 01 \\ 01 \end{bmatrix} + \begin{bmatrix} 11 \\ 011 \\ 10 \\ 01 \end{bmatrix} + \\ &\quad \left. + \begin{bmatrix} 10 \\ 110 \\ 11 \\ 01 \end{bmatrix} - \begin{bmatrix} 10 \\ 111 \\ 12 \\ 01 \end{bmatrix} - \begin{bmatrix} 11 \\ 110 \\ 01 \\ 01 \end{bmatrix} + \begin{bmatrix} 11 \\ 111 \\ 02 \\ 01 \end{bmatrix} - \begin{bmatrix} 10 \\ 111 \\ 10 \\ 01 \end{bmatrix} + \begin{bmatrix} 11 \\ 110 \\ 10 \\ 01 \end{bmatrix} \right) t \Big] + \frac{s\Lambda_2}{2(s - M_Z^2)} \left[\dots \right] \end{aligned} \quad (5)$$

Expressions for T_2 and T_3 have similar form. All of them contains more than 200 different expressions of the form $\begin{bmatrix} a_1 a_3 \\ a_2 a_7 a_4 \\ a_6 a_9 \\ a_8 a_5 \end{bmatrix}$. But they are not independent and obey linear relations following from integration-by-parts identities[6]. We use program FIRE [7] implementing Laporta's algorithm [8] to solve these relations.

As a result we obtain expressions like this

$$\begin{aligned}
T_1(s, t, u, M_Z) = & \frac{\Lambda_1}{1-z} \left[\left(-\frac{y^2}{6\epsilon^4} - \right. \right. \\
& - \frac{\left(3(7-8y)yz^3 + ((51y-41)y-4)z^2 + (29-32y)y^2z - 8(1-y)y^2 \right) y^2}{24(1-y) \left(y^2 + 2(1-2y)zy + z^2 \right) \epsilon^3} - \\
& - \frac{y^2}{48(1-y) \left(y^2 + 2(1-2y)zy + z^2 \right) \epsilon^2} \left(3(7-8y)yz^3 + \right. \\
& + (16 - (61 - 51y)y)z^2y^2 + y(40 - (91 - 48y)y)z + 12(1-y)y^2 \Big) + \\
& + \frac{5 \left(-3(7-8y)z^3 + (45 - 51y)z^2 + (-(5 - 16y)y - 8)z + 4(1-y)y \right) y^3}{48(1-y) \left(y^2 + 2(1-2y)zy + z^2 \right) \epsilon} - \\
& - \frac{y^2}{48(1-y) \left(y^2 + 2(1-2y)zy + z^2 \right)} \left(21(7-8y)yz^3 + \right. \\
& + (32 - (347 - 357y)y)z^2 + y(120 - (157 - 16y)y)z + 4(1-y)y^2 \Big) \Big) g_1 + \\
& \dots \\
& + \left(\dots \right) g_{21} \Big] + \frac{\Lambda_2}{1-z} \left[\dots \right] \quad (6)
\end{aligned}$$

Functions $g_1 \dots g_{21}$ in this expression are master-integrals and shown in Fig. 3.

For the analytical evaluation of the master-integrals we construct system of the differential equations which they obey[9]. Then we are going to solve it up to the desired order in ϵ . For the elimination of the typical radicals at the threshold of the production of two massive bosons we apply substitution $z = (1+x)(1+1/x)$.

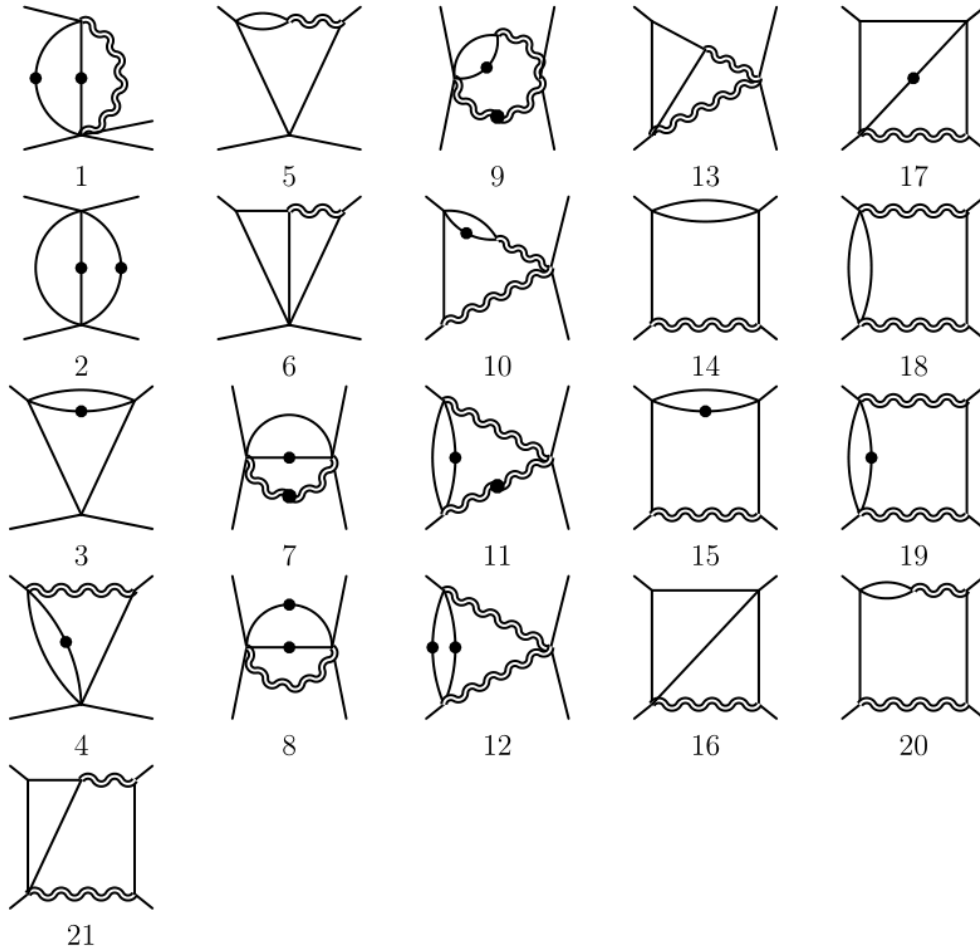


Figure 3: Diagrams for master-integrals. Solid dots denote squared propagators.

For example, master-integral g_{14} obey following differential equation

$$\begin{aligned}
\frac{dg_{14}}{dx} = & +g_{14} \left[-\frac{2}{(x+1)^3(x^2y+2xy-x+y)} + \frac{3\epsilon(x^2+x-1)}{2(x+1)^3} + \right. \\
& + \frac{-3x^3\epsilon - 9x^2\epsilon - 9x\epsilon - 3\epsilon + 4}{2(x+1)^3((x^2+2x+1)y-x)} - \\
& \left. - \frac{\epsilon}{x(x+1)(y-1)} - \frac{3\epsilon}{2x(x+1)^3} - \frac{2(x+2)}{(x+1)^3} - \frac{2}{x(x+1)^3} \right] + \\
+ g_{15} & \left[\frac{(x^2+x+1)\epsilon}{x(x+1)^3(y-1)(2\epsilon-1)} - \frac{(x^2+x+1)\epsilon}{2(x+1)^2(2\epsilon-1)((x^2+2x+1)y-x)} \right. \\
& \left. + \frac{(x^2+x+1)\epsilon}{2x(x+1)^5(2\epsilon-1)} + \frac{x^4(-\epsilon) - 2x^3\epsilon - x^2\epsilon + \epsilon}{2(x+1)^5(2\epsilon-1)} \right] + \\
+ g_7 & \left[\frac{x^2(-\epsilon) - 4x\epsilon - \epsilon}{2x(2\epsilon-1)((x^2+2x+1)y-x)} - \frac{\epsilon}{x(x+1)(y-1)(2\epsilon-1)} \right] + \\
& + \frac{g_8(x^2+x+1)\epsilon}{2x(2\epsilon-1)(x^2y+2xy-x+y)} + \\
+ g_3 & \left[-\frac{3\epsilon}{2(2\epsilon-1)((x^2+2x+1)y-x)} - \frac{\epsilon}{x(x+1)(y-1)(2\epsilon-1)} - \right. \\
& \left. - \frac{(3x+5)\epsilon}{2x(x+1)(2\epsilon-1)} \right]. \quad (7)
\end{aligned}$$

To solve such system of equations we need initial conditions. They can be obtained at special limits of the kinematic variables. Sometimes it is useful to perform rescaling of master-integrals and multiply them by some powers of ϵ so their expansion do not contain negative powers in this parameter.

$$\begin{aligned}
g_1(x, y) &= \varepsilon^2 \frac{1 - \varepsilon M^2}{1 + \varepsilon} \frac{1}{2} \text{ (diagram) } = & (8) \\
&= -\frac{1}{2} - \frac{3}{2} \varepsilon^2 \zeta_2 + \frac{4}{3} \varepsilon^3 \zeta_3 - \frac{63}{8} \varepsilon^4 \zeta_4 + O(\varepsilon^5)
\end{aligned}$$

$$\begin{aligned}
g_2(x, y) &= \varepsilon^2 \frac{t}{2} \text{ (diagram) } = & (9) \\
&= -(xy)^{-2\varepsilon} \left[-\frac{1}{2} + \frac{1}{2} \varepsilon^2 \zeta_2 + \frac{16}{3} \varepsilon^3 \zeta_3 + \frac{57}{8} \varepsilon^4 \zeta_4 + O(\varepsilon^5) \right]
\end{aligned}$$

$$\begin{aligned}
g_3(x, y) &= \varepsilon^3 t \text{ (diagram) } = & (10) \\
&= -(xy)^{-2\varepsilon} \left[\frac{1}{4} + \frac{1}{4} \varepsilon^2 \zeta_2 - \frac{13}{6} \varepsilon^3 \zeta_3 - \frac{41}{16} \varepsilon^4 \zeta_4 + O(\varepsilon^5) \right]
\end{aligned}$$

$$\begin{aligned}
g_4(x, y) &= \varepsilon^3 t \text{ (diagram) } = \varepsilon^2 t C_0(t, M) + O(\varepsilon^3) = O(M^{-1}) & (11)
\end{aligned}$$

$$\begin{aligned}
g_5(x, y) &= \varepsilon^3 (1 - 2\varepsilon) t \text{ (diagram) } = -\varepsilon^2 t C_0(t, M) + O(\varepsilon^3) = O(M^{-1}) & (12) \\
&\dots
\end{aligned}$$

Conclusion

Important intermediate results of the calculation of two-loop mixed EW-QCD corrections was presented. Computer algebra systems were hardly exploited to perform the two most time-consuming operations: evaluation of Dirac traces with kinematic simplifications (by FORM) and reduction of the scalar integrals to master-integrals (by FIRE). For the third step i.e. evaluation of the master-integrals all essential preparations were made.

References

- [1] Dittmaier S., Huss A. and Schwinn C. *Nuclear Physics B* **885**, (2014) 318 – 372.
- [2] Scherbakova E., Quantum corrections to Drell-Yan production of Z bosons.
- [3] Martin S. P. *Phys. Rev. D* **68**(7), (2003) 075002.
- [4] Martin S. P. and Robertson D. G. *Computer Physics Communications* **174**, (2006) 133 – 151.
- [5] Blmlein J., Moch S., Riemann T., Vermaseren J. and Tentyukov M. *Nuclear Physics B - Proceedings Supplements* **160**, (2006) 38 – 43.
- [6] Chetyrkin K., Kataev A. and Tkachov F. *Nuclear Physics B* **174**, (1980) 345 – 377.
- [7] Smirnov A. *Computer Physics Communications* **189**, (2015) 182 – 191.
- [8] Laporta S., *International Journal of Modern Physics A*, (2000) **15** 5087–5159.
- [9] Kotikov A., *Physics Letters B* **254**, (1991) 158 – 164.

Experimental Signatures of the Gauge-Higgs Unification Models

A.A. Babich *

Sukhoi State Technical University of Gomel

Abstract

The phenomenological predictions of the 5D gauge-Higgs unification models with $SO(5) \times U(1)$ gauge group, where the fifth dimension is compactified on an orbifold S^1/Z_2 , are discussed. Shown that the discovery of the two Z' bosons with close masses in experiments at LHC would give strong support for the gauge-Higgs unification and signal about the existence of extra dimensions.

1 Introduction

After the discovery of a Higgs boson at LHC [1]-[2] many fundamental questions remains unresolved still now. One of such questions is the hierarchy problem. Gauge-Higgs Unification (GHU) is one of the attractive scenarios beyond the Standard Model, which provide a possible solution to the hierarchy problem without supersymmetry. In this scenario, the SM Higgs boson and the gauge fields are unified into higher dimensional gauge fields. A remarkable fact is that the quantum corrections to Higgs mass and potential are UV-finite and calculable due to the higher dimensional gauge symmetry though the theory may be the non-renormalizable!

The fact that the Higgs boson is a part of gauge fields implies that Higgs interactions are governed by gauge principle and may provide specific predictions in LHC physics.

*E-mail: babich@gstu.gomel.by

2 Realistic GHU models

The idea of the gauge-Higgs unification is rather old and the one was proposed by Fairlie and by Forgacs and Manton in 1979 [3]-[6].

The first attempts have been based on embedding the SM electroweak gauge group $SU(2)_L \times U(1)_Y$ to the large simple group \mathcal{G} and thus gauge fields live in spacetime with $M^4 \times S^2$ topology. But unfortunately the models in a simple variant were unrealistic as predicted too small higgs boson mass and an incorrect the Weinberg angle θ_W (see Table 1).

\mathcal{G}	$\sin^2 \theta_W$	m_W	m_Z	m_H
$SU(3)$	3/4	44 GeV	88 GeV	88 GeV
$O(5)$	1/2	54 GeV	76 GeV	76 GeV
G_2	1/4	76 GeV	88 GeV	88 GeV

Table 1: Spectrum in the Gauge-Higgs Unification model by Manton.

New attempts of construction of realistic models are based on realization of several key ideas, such as orbifolds, warped spacetime, Hosotani mechanism of dynamical breaking gauge symmetry and some other.

Further we will shortly characterize the most promising realistic models [7]-[11].

All of these models are formulated as 5D GHU models with $SO(5) \times U(1)_X$ gauge group, where the fifth dimension is compactified on an orbifold S^1/Z_2 with a compactification radius R . The models do not contradict all precise electroweak experimental data and differ from each other by structure of fermion sector.

The gauge group choice as $SO(5) \times U(1)_X$ is caused by following reason. At first, in the EW symmetry breaking $SU(2)_L \times U(1)_Y \rightarrow U(1)_{EM}$ the Higgs field is an $SU(2)_L$ doublet in the fundamental representation. In the Gauge-Higgs Unification scheme the Higgs field is a part of gauge fields which are in the adjoint representation of the gauge group \mathcal{G} . So this implies that one needs to start with a larger gauge group \mathcal{G} which contains $SU(2)_L \times U(1)_Y$ as a subgroup. At second, group $SO(5)$ is minimal group which contain SM custodial symmetry group $SO(4) \cong SU(2)_L \times SU(2)_R$ as subgroup that allows to make control over the corrections to S and T electroweak parameters. And at third, factor $U(1)_X$ allows to make control over the correct value of Weinberg angle due to additional gauge coupling

constant.

The models are defined in the 5D Randall-Sundrum (RS) warped space $M^4 \times S^1/Z_2$ with orbifold topology in the fifth dimension. The metric is written as

$$ds^2 = e^{-2\sigma(y)} \eta_{\mu\nu} dx^\mu dx^\nu + dy^2, \quad (1)$$

where $\eta_{\mu\nu} = \text{diag}(-1, 1, 1, 1)$, $\sigma(y) = \sigma(y + 2L) = \sigma(-y)$, and $\sigma(y) = k|y|$ for $|y| \leq L$.

The RS space is viewed as bulk AdS space ($0 < y < L$) with AdS curvature $\Lambda = -6k^2$ sandwiched by the Planck (or UV) brane at $y = 0$ and the TeV (or IR) brane at $y = L$. The warp factor $z_L = e^{kL} \gg 1$ is very large ($\sim 10^{15}$). The KK mass scale is given by $m_{\text{KK}} = \pi k / (z_L - 1) \sim \pi k z_L^{-1}$.

In the fundamental region $0 \leq y \leq L$ the metric can be written in terms of the useful conformal coordinate $z = e^{ky}$ as

$$ds^2 = \frac{1}{z^2} \left(\eta_{\mu\nu} dx^\mu dx^\nu + \frac{dz^2}{k^2} \right). \quad (2)$$

The 5D Lagrangian density has following structure:

$$\begin{aligned} \mathcal{L} = & \mathcal{L}_{\text{bulk}}^{\text{gauge}}(A, B) + \mathcal{L}_{\text{bulk}}^{\text{fermion}}(\Psi_a, \Psi_F, A, B) \\ & + \mathcal{L}_{\text{brane}}^{\text{fermion}}(\hat{\chi}_\alpha, A, B) + \mathcal{L}_{\text{brane}}^{\text{scalar}}(\hat{\Phi}, A, B) + \mathcal{L}_{\text{brane}}^{\text{int}}(\Psi_a, \hat{\chi}_\alpha, \hat{\Phi}), \end{aligned} \quad (3)$$

where A_M and B_M are $SO(5)$ and $U(1)_X$ gauge fields with the two associated gauge coupling constants g_A and g_B , respectively; $\Psi_a, a = 1, 2, 3, 4$ are the 5D bulk fermions in the vector representation of $SO(5)$ which contains usual leptons and quarks; Ψ_F are n_F the 5D bulk fermions in the spinor representation of $SO(5)$; $\hat{\chi}_\alpha$ the Planck ($y = 0$) brane fermions in the fundamental representation of $SO(4) \cong SU(2)_L \times SU(2)_R$ (in particular with these brane fermions all 4D anomalies in $SO(4) \times U(1)_X$ are cancelled); $\hat{\Phi}$ are the Planck brane scalars which induces symmetry breaking $SU(2)_R \times U(1)_X$ to $U(1)_Y$ on UV brane $y = 0$.

The explicit view of the all lagrangian density parts can be found in

[7]-[11]. For example, the sum of the bulk matter parts can be written as

$$\begin{aligned}
\mathcal{L}_{\text{bulk}}^{\text{gauge}} + \mathcal{L}_{\text{bulk}}^{\text{fermions}} &= -\text{Tr} \left(\frac{1}{4} F^{(A)MN} F_{MN}^{(A)} + \frac{1}{2\xi_A} (f_{\text{gf}}^{(A)})^2 + \mathcal{L}_{\text{gh}}^{(A)} \right) - \\
&\quad - \left(\frac{1}{4} F^{(B)MN} F_{MN}^{(B)} + \frac{1}{2\xi_B} (f_{\text{gf}}^{(B)})^2 + \mathcal{L}_{\text{gh}}^{(B)} \right) +, \quad (4) \\
&\quad + \sum_a \bar{\Psi}_a \mathcal{D}(c_a) \Psi_a + \sum_{i=1}^{n_F} \bar{\Psi}_{F_i} \mathcal{D}(c_{F_i}) \Psi_{F_i}, \\
\mathcal{D}(c) &= \Gamma^A e_A{}^M \left(\partial_M + \frac{1}{8} \omega_{MBC} [\Gamma^B, \Gamma^C] - \right. \\
&\quad \left. -ig_A A_M - ig_B Q_X B_M \right) - c\epsilon(y), \quad (5)
\end{aligned}$$

where the gauge fixing and ghost terms are denoted as functionals with subscripts gf and gh, respectively. The gauge field strengths are $F_{MN}^{(A)} = \partial_M A_N - \partial_N A_M - ig_A [A_M, A_N]$, $F_{MN}^{(B)} = \partial_M B_N - \partial_N B_M$. The gauge fixing function is taken as $f_{\text{gf}}^{(A)} = z^2 \{ \eta^{\mu\nu} \mathcal{D}_\mu A_\nu + \xi_A k^2 z \mathcal{D}_z^c (A_z^q/z) \}$ with a background field A_z^c ($A_z = A_z^c + A_z^q$), $B_z^c = 0$. In this paper we take $\xi_A = \xi_B = 1$.

The $SO(5)$ gauge fields A_M are decomposed as

$$A_M = \sum_{a_L=1}^3 A_M^{a_L} T^{a_L} + \sum_{a_R=1}^3 A_M^{a_R} T^{a_R} + \sum_{\hat{a}=1}^4 A_M^{\hat{a}} T^{\hat{a}}, \quad (6)$$

where T^{a_L, a_R} ($a_L, a_R = 1, 2, 3$) and $T^{\hat{a}}$ ($\hat{a} = 1, 2, 3, 4$) are the generators of $SO(4) \simeq SU(2)_L \times SU(2)_R$ and $SO(5)/SO(4)$, respectively.

The electric charge satisfies to following equality

$$Q_{\text{EM}} = T^{3L} + T^{3R} + Q_X. \quad (7)$$

In the fermion part we have $\bar{\Psi} = i\Psi^\dagger \Gamma^0$, and Γ^M matrices are given by

$$\Gamma^\mu = \begin{pmatrix} & \sigma^\mu \\ \bar{\sigma}^\mu & \end{pmatrix}, \quad \Gamma^5 = \begin{pmatrix} 1 & \\ & -1 \end{pmatrix}, \quad \sigma^\mu = (1, \vec{\sigma}), \quad \bar{\sigma}^\mu = (-1, \vec{\sigma}). \quad (8)$$

The $c\epsilon(y)$ term in the action, where $\epsilon(y) \equiv \text{sign}(y)$, gives a bulk kink mass. The dimensionless parameter c plays an important role in controlling profiles of fermions wave functions.

The orbifold boundary conditions at $y_0 = 0$ and $y_1 = L$ points are given by following relations

$$\begin{aligned}
\begin{pmatrix} A_\mu \\ A_y \end{pmatrix} (x, y_j - y) &= P_{\text{vec}} \begin{pmatrix} A_\mu \\ -A_y \end{pmatrix} (x, y_j + y) P_{\text{vec}}^{-1}, \\
\begin{pmatrix} B_\mu \\ B_y \end{pmatrix} (x, y_j - y) &= \begin{pmatrix} B_\mu \\ -B_y \end{pmatrix} (x, y_j + y), \\
\Psi_a(x, y_j - y) &= P_{\text{vec}} \Gamma^5 \Psi_a(x, y_j + y), \\
\Psi_{F_i}(x, y_j - y) &= (-1)^j P_{\text{sp}} \Gamma^5 \Psi_{F_i}(x, y_j + y), \\
P_{\text{vec}} &= \text{diag}(-1, -1, -1, -1, +1), \quad P_{\text{sp}} = \text{diag}(+1, +1, -1, -1). \quad (9)
\end{aligned}$$

The Lagrangian density remains invariant under the parity transformations. The $SO(5)$ symmetry is reduced to $SO(4) \simeq SU(2)_L \times SU(2)_R$ by the orbifold boundary conditions. At this stage the four-dimensional components A_μ of the five-dimensional gauge fields A_M have zero modes only in $SO(4) \times U(1)_X$ block, whereas the extra-dimensional components A_y have zero modes only in $SO(5)/SO(4)$ block. The latter contains the four-dimensional Higgs field, which is a doublet concerning both $SU(2)_L$ and $SU(2)_R$ groups:

$$SO(5) : A_y = \begin{pmatrix} \phi_1 \\ \phi_2 \\ \phi_3 \\ \phi_4 \\ -\phi_1 & -\phi_2 & -\phi_3 & -\phi_4 \end{pmatrix}, \quad \Phi = \begin{pmatrix} \phi_1 + i\phi_2 \\ \phi_4 - i\phi_3 \end{pmatrix}. \quad (10)$$

After determination mass spectra of all boson and fermion fields we can find Coleman–Weinberg effective potential. Should be note that 4D Higgs field associated with nontrivial Wilson line phase. The Wilson line phase for the zero modes is defined as

$$e^{i\Theta_H/2} \sim P \exp \left\{ ig_A \int_0^L dy A_y \right\}. \quad (11)$$

At the tree level the value of the Θ_H is not determined, as it gives vanishing field strengths. At the quantum level its effective potential V_{eff} becomes nontrivial. The value of Θ_H is determined by the location of the

minimum of V_{eff} . Without loss of generality one can assume that $(A_y)_{45}$ component develops a non-vanishing expectation value. Let us denote the corresponding component of Θ_H by θ_H . If θ_H takes a non-vanishing value, the electroweak symmetry breaking takes place.

Further for the extra-dimensional component $A_z = (kz)^{-1}A_y$, which contains the four-dimensional Higgs field $H(x)$, we can write down following expansion

$$A_z^{\hat{4}}(x, z) = \{\theta_H f_H + H(x)\} u_H(z) + \dots ,$$

$$u_H(z) = \sqrt{\frac{2}{k(z_L^2 - 1)}} z \quad \text{for } 1 \leq z \leq z_L . \quad (12)$$

The value of θ_H is determined by the location of the global minimum of the effective potential $V_{\text{eff}}(\theta_H)$. The Higgs boson mass is given by

$$m_H^2 = \frac{1}{f_H^2} \left. \frac{d^2 V_{\text{eff}}}{d\theta_H^2} \right|_{\text{min}} , \quad f_H = \frac{2}{g_w} \sqrt{\frac{k}{L(z_L^2 - 1)}} . \quad (13)$$

Let us consider the case in which all $SO(5)$ -spinor fermions Ψ_{F_i} are degenerate at the tree level, so $c_{F_i} = c_F$ ($i = 1, \dots, n_F$). At the one-loop level only the KK towers whose mass spectra depend on θ_H contribute to the effective potential $V_{\text{eff}}(\theta_H)$. These spectra are given for the gauge W and Z tower, for the top and the bottom quark tower, and for D and fermion F tower. Contributions of other quarks and leptons turn out exponentially suppressed and negligible.

The relevant parameters of the model are $k, z_L, g_A, g_B, c_t, \tilde{\mu}/\mu_2, c_F$ and n_F . Other brane mass parameters are irrelevant so long as $\mu_\alpha, \tilde{\mu}, w \gg m_{\text{KK}}$. These eight parameters are chosen such that $m_Z, \alpha_w, \sin^2 \theta_W, m_t, m_b$, and m_H take the observed values. This procedure leaves two parameters z_L and n_F free.

With those given parameters, the one-loop effective potential is given by

$$V_{\text{eff}}(\theta_H, c_t, r_t, c_F, n_F, k, z_L, \theta_W) = 4I[Q_W] + 2I[Q_Z] + 3I[Q_D]$$

$$- 12\{I[Q_{\text{top}}] + I[Q_{\text{bottom}}]\} - 8n_F I[Q_F] ,$$

$$I[Q(q; \theta_H)] = \frac{(kz_L^{-1})^4}{(4\pi)^2} \int_0^\infty dq q^3 \ln\{1 + Q(q; \theta_H)\} ,$$

$$\begin{aligned}
Q_W &= \cos^2 \theta_W Q_Z = \frac{1}{2} Q_D = \frac{1}{2} Q_0[q; \frac{1}{2}] \sin^2 \theta_H , \\
Q_{\text{top}} &= \frac{Q_{\text{bottom}}}{r_t} = \frac{Q_0[q; c_t]}{2(1+r_t)} \sin^2 \theta_H , \\
Q_F &= Q_0[q; c_F] \cos^2 \frac{1}{2} \theta_H , \\
Q_0[q; c] &= \frac{z_L}{q^2 \hat{F}_{c-\frac{1}{2}, c-\frac{1}{2}}(qz_L^{-1}, q) \hat{F}_{c+\frac{1}{2}, c+\frac{1}{2}}(qz_L^{-1}, q)} , \\
\hat{F}_{\alpha, \beta}(u, v) &= I_\alpha(u) K_\beta(v) - e^{-i(\alpha-\beta)\pi} K_\alpha(u) I_\beta(v) , \tag{14}
\end{aligned}$$

where $r_t = (\tilde{\mu}/\mu_2)^2$ and K_α and I_α are modified Bessel functions.

The value $\theta_H = \theta_1$ at the minimum is determined as $\theta_H(z_L, n_F)$. All other quantities such as the mass spectra of all KK towers, gauge couplings of all particles, and Yukawa couplings of all fermions are determined as functions of z_L and n_F .

The example of profile $V_{\text{eff}}(\theta_H)$ is depicted in Fig. 1 with red curves. For comparison V_{eff} in the case of $n_F = 0$ is also plotted with a blue curve. When $n_F = 0$ and $z_L = 10^7$, the minima are located at $\theta_H = \pm \frac{1}{2}\pi$.

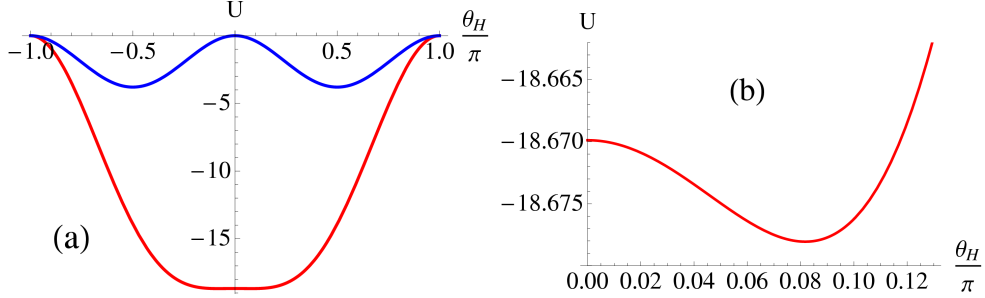


Figure 1: The effective potential $V_{\text{eff}}(\theta_H)$ for $z_L = 10^7$. $U = 16\pi^6 m_{\text{KK}}^{-4} V_{\text{eff}}$ is plotted. The red curves are for $n_F = 3$ with $m_H = 126$ GeV. V_{eff} has minima at $\theta_H = \pm 0.258$ and $m_{\text{KK}} = 3.95$ TeV. The blue curve is for $n_F = 0$ in which case $m_H = 87.9$ GeV and $m_{\text{KK}} = 993$ GeV.

Determined values for θ_H , m_{KK} , $m_{Z^{(1)}}$, etc. are tabulated in Table 2 in the case of $n_F = 5$.

Table 2: Parameters and masses in the case of degenerate dark fermions with $n_F = 5$. All masses and k are given in units of TeV.

z_L	θ_H	m_{KK}	k	c_t	c_F	$m_{F^{(1)}}$	$m_{Z_R^{(1)}}$	$m_{Z^{(1)}}$	$m_{\gamma^{(1)}}$
10^9	0.473	2.50	7.97×10^8	0.376	0.459	0.353	1.92	1.97	1.98
10^8	0.351	3.13	9.97×10^7	0.357	0.445	0.502	2.40	2.48	2.48
10^7	0.251	4.06	1.29×10^7	0.330	0.430	0.735	3.11	3.24	3.24
10^6	0.172	5.45	1.74×10^6	0.292	0.410	1.11	4.17	4.37	4.38
10^5	0.114	7.49	2.38×10^5	0.227	0.382	1.75	5.73	6.07	6.08
10^4	0.0730	10.5	3.33×10^4	0.037	0.333	2.91	8.00	8.61	8.61

3 Phenomenological predictions

One of the distinctive predictions of the $SO(5) \times U(1)$ gauge-Higgs unification is the existence of the KK excited modes of neutral gauge bosons and photon. There are four kinds of neutral gauge bosons at the TeV scale. They are the first KK mode of Z boson $Z^{(1)}$ ($Z^{(0)} \equiv Z^{\text{SM}}$), the first KK mode of photon $\gamma^{(1)}$ ($\gamma^{(0)} \equiv \gamma^{\text{SM}}$), the $Z_R^{(1)}$ boson ($Z_R^{(0)}$ is not exist), the $A^{\hat{4}}$ boson.

Among them the $A^{\hat{4}}$ boson does not couple to SM particles so that it escapes from detection in the Z' search. $Z^{(1)}$, $\gamma^{(1)}$, and $Z_R^{(1)}$ are the candidates for Z' bosons.

To evaluate the production and decay rates of Z' bosons is needed to know four-dimensional Z' couplings of quarks and leptons. They are obtained from the five-dimensional gauge interaction terms by inserting wave functions of gauge bosons and quarks or leptons and integrating over the fifth-dimensional coordinate. The couplings of the photon, Z boson

and $Z_R^{(1)}$ boson KK towers can be written as

$$\begin{aligned}
\mathcal{L} \supset \sum_{n,i} A_\mu^{\gamma^{(n)}} & \left[g_{u^i L}^{\gamma^{(n)}} \bar{u}_L^i \gamma^\mu u_L^i + g_{u^i R}^{\gamma^{(n)}} \bar{u}_R^i \gamma^\mu u_R^i + g_{d^i L}^{\gamma^{(n)}} \bar{d}_L^i \gamma^\mu d_L^i + g_{d^i R}^{\gamma^{(n)}} \bar{d}_R^i \gamma^\mu d_R^i \right. \\
& \left. + g_{e^i L}^{\gamma^{(n)}} \bar{e}_L^i \gamma^\mu e_L^i + g_{e^i R}^{\gamma^{(n)}} \bar{e}_R^i \gamma^\mu e_R^i \right] \\
& + \sum_{n,i} Z_\mu^{(n)} \left[g_{u^i L}^{Z^{(n)}} \bar{u}_L^i \gamma^\mu u_L^i + g_{u^i R}^{Z^{(n)}} \bar{u}_R^i \gamma^\mu u_R^i + g_{d^i L}^{Z^{(n)}} \bar{d}_L^i \gamma^\mu d_L^i + g_{d^i R}^{Z^{(n)}} \bar{d}_R^i \gamma^\mu d_R^i \right. \\
& \left. + g_{\nu^i L}^{Z^{(n)}} \bar{\nu}_L^i \gamma^\mu \nu_L^i + g_{\nu^i R}^{Z^{(n)}} \bar{\nu}_R^i \gamma^\mu \nu_R^i + g_{e^i L}^{Z^{(n)}} \bar{e}_L^i \gamma^\mu e_L^i + g_{e^i R}^{Z^{(n)}} \bar{e}_R^i \gamma^\mu e_R^i \right] \\
& + \sum_{n,i} Z_{R\mu}^{(n)} \left[g_{u^i L}^{Z_R^{(n)}} \bar{u}_L^i \gamma^\mu u_L^i + g_{u^i R}^{Z_R^{(n)}} \bar{u}_R^i \gamma^\mu u_R^i + g_{d^i L}^{Z_R^{(n)}} \bar{d}_L^i \gamma^\mu d_L^i + g_{d^i R}^{Z_R^{(n)}} \bar{d}_R^i \gamma^\mu d_R^i \right. \\
& \left. + g_{\nu^i L}^{Z_R^{(n)}} \bar{\nu}_L^i \gamma^\mu \nu_L^i + g_{\nu^i R}^{Z_R^{(n)}} \bar{\nu}_R^i \gamma^\mu \nu_R^i + g_{e^i L}^{Z_R^{(n)}} \bar{e}_L^i \gamma^\mu e_L^i + g_{e^i R}^{Z_R^{(n)}} \bar{e}_R^i \gamma^\mu e_R^i \right],
\end{aligned}$$

where the superscript i denotes the generation, i.e., $(u^1, u^2, u^3) = (u, c, t)$, etc. The four-dimensional gauge couplings are obtained by overlapping integrals of wave functions (which contains the combination of Bessel functions) and cannot be written in simple analytical form. Explicit formulas for the gauge couplings can be found in papers cited above.

The relevant couplings of the Z' bosons for fixing θ_H parameter are tabulated in Table 3 and Table 4.

Table 3: Masses, total decay widths and couplings of the Z' bosons to SM particles in the first generation for $\theta_H = 0.114$. Couplings to μ are approximately the same as those to e .

Z'	$m(\text{TeV})$	$\Gamma(\text{GeV})$	$g_{uL}^{Z'}$	$g_{dL}^{Z'}$	$g_{eL}^{Z'}$	$g_{uR}^{Z'}$	$g_{dR}^{Z'}$	$g_{eR}^{Z'}$
Z	0.0912	2.44	0.257	-0.314	-0.200	-0.115	0.0573	0.172
$Z_R^{(1)}$	5.73	482	0	0	0	0.641	-0.321	-0.978
$Z^{(1)}$	6.07	342	-0.0887	0.108	0.0690	-0.466	0.233	0.711
$\gamma^{(1)}$	6.08	886	-0.0724	0.0362	0.109	0.846	-0.423	-1.29
$Z^{(2)}$	9.14	1.29	-0.0073	0.0089	0.0056	0.0055	0.00274	0.0086

Table 4: Masses, total decay widths and couplings of the Z' bosons to SM particles in the first generation for $\theta_H = 0.073$.

Z'	$m(\text{TeV})$	$\Gamma(\text{GeV})$	$g_{uL}^{Z'}$	$g_{dL}^{Z'}$	$g_{eL}^{Z'}$	$g_{uR}^{Z'}$	$g_{dR}^{Z'}$	$g_{eR}^{Z'}$
$Z_R^{(1)}$	8.00	553	0	0	0	0.588	-0.294	-0.896
$Z^{(1)}$	8.61	494	-0.100	0.123	0.078	-0.426	0.213	0.650
$\gamma^{(1)}$	8.61	1040	-0.0817	0.041	0.123	0.775	-0.388	-1.18

The decay width of the Z' boson is given by

$$\Gamma_{Z'} = \sum_i \frac{m_{Z'}}{12\pi} \left(\frac{(g_{iL}^{Z'})^2 + (g_{iR}^{Z'})^2}{2} + 2g_{iL}^{Z'}g_{iR}^{Z'} \frac{m_i^2}{m_{Z'}^2} \right) \sqrt{1 - \frac{4m_i^2}{m_{Z'}^2}}. \quad (15)$$

Here i runs over all fermions including SM fermions and exotic fermions. The contribution of its decay to W^+W^- is very small and can be neglected. The evaluated $\Gamma_{Z'}$ for $\theta_H = 0.114$ is summarized in Table 3. It is seen that all of $Z_R^{(1)}$, $Z^{(1)}$, and $\gamma^{(1)}$ have large decay widths (300 ~ 900 GeV) in quite contrast to the narrow width of the Z boson. It is mainly due to the large couplings of right-handed quarks and leptons.

Now consider the dilepton production cross sections through the Z' boson exchange together with the SM processes mediated by the Z boson and photon. The dependence of the cross section on the final state dilepton invariant mass $M_{\ell\ell}$ is described as

$$\begin{aligned} \frac{d\sigma(pp \rightarrow \ell^+\ell^- X)}{dM_{\ell\ell}} &= \sum_q \int_{-1}^1 d\cos\theta \int_{\frac{M_{\ell\ell}^2}{E_{\text{CMS}}^2}}^1 dx_1 \frac{2M_{\ell\ell}}{x_1 E_{\text{CMS}}^2} \\ &\times f_q(x_1, M_{\ell\ell}^2) f_{\bar{q}} \left(\frac{M_{\ell\ell}^2}{x_1 E_{\text{CMS}}^2}, M_{\ell\ell}^2 \right) \frac{d\sigma(\bar{q}q \rightarrow \ell^+\ell^-)}{d\cos\theta} \end{aligned} \quad (16)$$

where E_{CMS} is the center-of-mass energy of the LHC and f_q 's are the parton distribution functions(PDFs) for q quark.

Figure 2 shows the differential cross section for $pp \rightarrow \mu^+\mu^-$ together with the SM cross section mediated by the Z boson and photon for $\theta_H = 0.114$ ($n_F = 5$, $z_L = 10^5$). The deviation from the SM is very small below 3 TeV because the couplings of the Z boson or photon to SM fermions

are almost the same as in the SM. For this reason it is difficult to see the signals of the gauge-Higgs unification at 8 TeV LHC experiments. In the case of $\theta_H = 0.251$ ($n_F = 5$, $z_L = 10^7$), the deviation from the SM is large and this value is excluded by the 8 TeV LHC experiments.

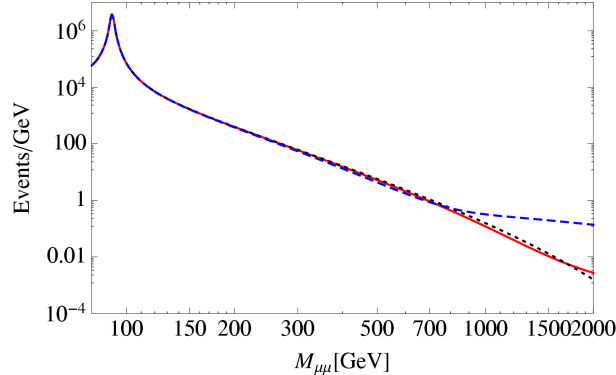


Figure 2: The differential cross section multiplied by an integrated luminosity of 20.6 fb^{-1} for $pp \rightarrow \mu^+ \mu^- X$ at the 8 TeV LHC for $\theta_H = 0.114$ (red solid curve) and for $\theta_H = 0.251$ (blue dashed curve). The black dashed line represents the SM background.

On the other hand, at 14 TeV LHC experiments, we expect the signals. Figure 3 shows the differential cross section $d\sigma/dM_{\mu\mu}$ in the range $3 \text{ TeV} < M_{\mu\mu} < 9 \text{ TeV}$ for $\theta_H = 0.114$ and 0.073 . The contributions from $Z^{(2)}$ boson and higher KK modes are negligible because the couplings are very small and the widths are very narrow (see Table 4). One sees a very large deviation from the SM, which can be detected at the upgraded LHC.

4 Conclusion and remarks

In the $SO(5) \times U(1)$ gauge-Higgs unification the three gauge bosons, $Z_R^{(1)}$, $Z^{(1)}$, and $\gamma^{(1)}$, appear as Z' bosons in dilepton events at LHC. It is interesting that the masses of these bosons turn out around 6 (8 TeV) for $\theta_H = 0.114$ (0.073), which is exactly in the region explored at the 14 TeV LHC.

As right-handed quarks and leptons have large couplings to those Z' bosons, the widths of those bosons become large; the decay widths of $Z_R^{(1)}$,

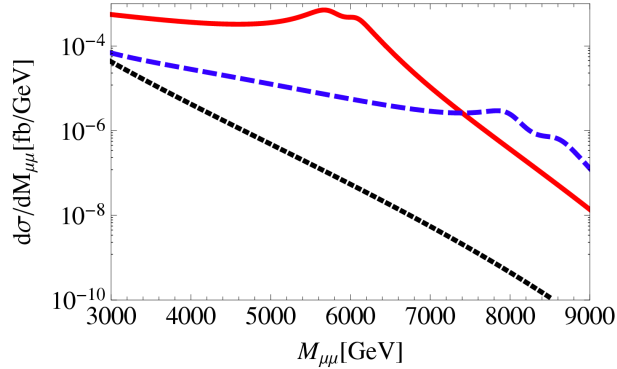


Figure 3: The differential cross section for $pp \rightarrow \mu^+ \mu^- X$ at the 14 TeV LHC for $\theta_H = 0.114$ (red solid curve) and for $\theta_H = 0.073$ (blue dashed curve) . The nearly straight line represents the SM background.

$Z^{(1)}$ and $\gamma^{(1)}$ are 482, 342 and 886 GeV for $\theta_H = 0.114$.

As the difference in masses of $Z^{(1)}$ and $\gamma^{(1)}$ is small, there should appear two peaks in dilepton events. Due to the large widths the excess of events over those expected in the SM should be seen in much wider range of energies. For $\theta_H = 0.114$ an excess due to the broad widths of the Z' resonances should be observed above 3 TeV in the dilepton invariant mass. The discovery of the Z' bosons in the 3-9 TeV range would give strong support for the gauge-Higgs unification, signaling the existence of extra dimensions.

Let's give some remarks concerning Higgs interactions. In realistic GHU models all Higgs couplings HWW , HZZ , $Hc\bar{c}$, $Hb\bar{b}$, $H\tau\bar{\tau}$ are suppressed by a factor $\cos\theta_H$ at the tree level, moreover coupling $HZ\gamma$ is absent on 1-loop level. The corrections to $\Gamma[H \rightarrow \gamma\gamma]$ and $\Gamma[H \rightarrow gg]$ due to KK states amount only to 0.2% for $\theta_H = 0.114$. Hence may conclude that $Br(H \rightarrow j) \sim Br^{\text{SM}}(H \rightarrow j)$, where $j = WW, ZZ, \gamma\gamma, gg, b\bar{b}, c\bar{c}, \tau\bar{\tau}$ and $\sigma^{\text{prod}}(H) \cdot Br(H \rightarrow \gamma\gamma) \sim (\text{SM}) \times \cos^2\theta_H$. The signal strength in the $\gamma\gamma$ production relative to the SM is about $\cos^2\theta_H$. It is about 0.99 for $\theta_H \sim 0.1$. This contrasts to the prediction in the UED models in which the contributions of KK states can add up in the same sign.

References

- [1] G. Aad *et al.* [ATLAS Collaboration], Phys. Lett. B **716**, 1 (2012) [arXiv:1207.7214 [hep-ex]].
- [2] S. Chatrchyan *et al.* [CMS Collaboration], Phys. Lett. B **716**, 30 (2012) [arXiv:1207.7235 [hep-ex]].
- [3] D. B. Fairlie, Phys. Lett. B **82**, 97 (1979).
- [4] D. B. Fairlie, J. Phys. G **5**, L55 (1979).
- [5] P. Forgacs and N. S. Manton, Commun. Math. Phys. **72**, 15 (1980).
- [6] N. S. Manton, Nucl. Phys. B **158**, 141 (1979).
- [7] A. D. Medina, N. R. Shah and C. E. M. Wagner, Phys. Rev. D **76**, 095010 (2007) [arXiv:0706.1281 [hep-ph]].
- [8] M. Carena, A. D. Medina, B. Panes, N. R. Shah and C. E. M. Wagner, Phys. Rev. D **77** (2008) 076003 [arXiv:0712.0095 [hep-ph]].
- [9] Y. Hosotani, K. Oda, T. Ohnuma and Y. Sakamura, Phys. Rev. D **78**, 096002 (2008) [Erratum-ibid. D **79**, 079902 (2009)] [arXiv:0806.0480 [hep-ph]].
- [10] Y. Hosotani, S. Noda and N. Uekusa, Prog. Theor. Phys. **123** (2010) 757 [arXiv:0912.1173 [hep-ph]].
- [11] S. Funatsu, H. Hatanaka, Y. Hosotani, Y. Orikasa and T. Shimotani, Phys. Lett. B **722** (2013) 94 [arXiv:1301.1744 [hep-ph]].

Electromagnetic Decays of Light Vector Mesons

Andreev V.V ^{*}, Gavrish V.Yu. [†]

F.Skorina Gomel State University

Abstract

This work dedicated to describing two-body compounded system of quarks (meson) in point form of Poincare invariant quantum mechanics with potential, which was offered by so-called Mock-meson model. Authors shows process of calculation the basis parameters of the model by the variational method and followed applications for radiative decay processes. For such calculation authors use the simplest radiative decay scheme. Comparing results with experimental data was shown how to calculate the anomalous part of quark magnetic moment.

1 Introduction

The radiative processes, in particular the decays of vector mesons has been a convenient tool for studying the structure of hadrons. There are quite a number of approaches for the model to describe radiative transitions mesons(see,[1, 2, 3, 4]). In our work, the calculation of the form-factor of the radiative decay conducted within the constituent relativistic quark model based on the point form of Poincare invariant quantum mechanics (about Poincare invariant quantum mechanics, see, eg [5, 6]).

^{*}E-mail:vik.andreev@gsu.by

[†]E-mail:mez0n@inbox.ru

2 Elements of quark model, based on Poincare invariant quantum mechanics

For the our relativistic quark model, based on the Poincare invariant quantum mechanics, using the potential proposed by the so-called Mock-meson model [7] using a model parameterization running coupling constant of the strong interaction, modified in [8]:

$$\alpha_S(Q^2) = \sum_{k=1}^7 \alpha_k \exp(-Q^2/4\gamma_k^2) . \quad (1)$$

The interquark potential in coordinate representation from [7] is used, which is considered a sum of Coulomb, linear confinement, and spin-spin parts for pseudoscalar and vector mesons:

$$\hat{V}(\mathbf{r}) = \hat{V}_{\text{Coul}}(\mathbf{r}) + \hat{V}_{\text{conf}}(\mathbf{r}) + \hat{V}_{\text{SS}}(\mathbf{r}) \quad (2)$$

where

$$\hat{V}_{\text{Coul}}(r) = -\frac{4}{3} \frac{\alpha_S(r)}{r} = -\frac{4}{3r} \sum_{k=1}^7 \alpha_k \text{erf}(\tau_k r) , \quad (3)$$

$$\hat{V}_{\text{conf}}(\mathbf{r}) = w_0 + \sigma r \left(\frac{\exp(-b^2 r^2)}{\sqrt{\pi} b r} + \left(1 + \frac{1}{2b^2 r^2} \right) \text{erf}(br) \right) \quad (4)$$

and

$$\hat{V}_{\text{SS}}(\mathbf{r}) = -\frac{32 (\mathbf{S}_q \mathbf{S}_{\bar{Q}})}{9\sqrt{\pi} m_q m_{\bar{Q}}} \sum_{k=1}^7 \alpha_k \tau_k^4 \exp(-\tau_k^2 r^2) . \quad (5)$$

Potential has following free parameters: gluon string tension parameter σ , parameter of perturbative part w_0 and masses of quarks $m_{q,\bar{Q}}$. Parameter τ_k determined from relation

$$\tau_k^2 = \frac{\gamma_k^2}{\gamma_k^2 + b} b , \quad (6)$$

where b is smearing parameter [7].

Parameter of linear part of the potential in most number of models lies in limits $\sigma = (0.18 \div 0.20) \text{ GeV}^2$, that's why we assume, that

$$\sigma = \bar{\sigma} \pm \Delta\sigma = (0.19 \pm 0.01) \text{ GeV}^2 . \quad (7)$$

The parameters α_k, γ_k are fixed on the basis of requirements, consistent with experimental data for the difference in the first moments of the proton and neutron spin structure functions (QCD-modified Bjorken sum rule [9])[8].

In work [10] were calculated integral representation of decay constant for pseudoscalar and vector meson in framework of point form of Poincare invariant quantum mechanics:

$$f_P(m_q, m_{\bar{Q}}, \beta) = \frac{3}{\sqrt{2\pi}} \int_0^\infty dk k^2 \Phi(k, \beta) \sqrt{\frac{M_0^2 - (m_q - m_Q)^2}{\omega_{m_q}(k) \omega_{m_Q}(k)} \frac{(m_q + m_Q)}{M_0^{3/2}}}, \quad (8)$$

$$\begin{aligned} f_V(m_q, m_Q) &= \\ &= \frac{3}{\sqrt{2\pi}} \int_0^\infty dk k^2 \Phi(k, \beta) \frac{\sqrt{(\omega_{m_q}(k) + m_q)(\omega_{m_Q}(k) + m_Q)}}{\sqrt{\omega_{m_q}(k) + \omega_{m_Q}(k)} \sqrt{\omega_{m_q}(k) \omega_{m_Q}(k)}} \times \\ &\times \left(1 + \frac{k^2}{3(\omega_{m_q}(k) + m_q)(\omega_{m_Q}(k) + m_Q)} \right), \end{aligned} \quad (9)$$

where $M_0 = \omega_{m_q}(k) + \omega_{m_{\bar{Q}}}(k)$ and $\omega_m(k) = \sqrt{k^2 + m^2}$.

Using equations (2)-(5) and (8),(9) we get the following system of equations [8]:

$$M_P(m_q, m_{\bar{Q}}, w_0, \beta) = M_P^{\text{exp}} \pm \Delta M_P, \quad (10)$$

$$M_V(m_q, m_{\bar{Q}}, w_0, \beta) = M_V^{\text{exp}} \pm \Delta M_V, \quad (11)$$

$$M_V(m_q, m_{\bar{Q}}, w_0, \beta) - M_P(m_q, m_{\bar{Q}}, w_0, \beta) = M_V^{\text{exp}} - M_P^{\text{exp}} \pm \delta M_{V,P}^{\text{exp}}, \quad (12)$$

$$f_P(m_q, m_{\bar{Q}}, \beta) = f_P^{\text{exp}} \pm \Delta f_P^{\text{exp}}, \quad (13)$$

$$f_V(m_q, m_{\bar{Q}}, \beta) = f_V^{\text{exp}} \pm \Delta f_V^{\text{exp}}, \quad (14)$$

where $M_P^{\text{exp}}, M_V^{\text{exp}}$ are experimental value of pseudoscalar and vector mesons, respectively. The last two equations (13)-(14) express condition of equality lepton coupling constants for the pseudoscalar and vector mesons, calculated in the framework of Poincare covariant model, with experimental values of decay constants. It's should be notice, that during the calculation the wave function was taken in form

$$\Phi(k, \beta) = \frac{2}{\sqrt{3}\pi^{1/4}\beta^{3/2}} \exp\left(-\frac{k^2}{2\beta^2}\right). \quad (15)$$

After solving the system of equations (10)-(14) for light mesons we have following values of quark masses and β -parameters of wave function:

$$\begin{aligned} m_u &= (239.9 \pm 2.3) \text{ MeV}, \quad m_d = (243.8 \pm 2.3) \text{ MeV}, \\ m_s &= (466.6 \pm 28) \text{ MeV}, \\ \beta_{uu} &\simeq \beta_{dd} \simeq \beta_{ud} = (328.78 \pm 2.1) \text{ MeV}, \quad \beta_{us} \simeq (360.3 \pm 12.1) \text{ MeV}. \end{aligned} \quad (16)$$

Thus, we have fixed all basic parameters of the model by equation (16).

3 Radiative decay of vector mesons

Matrix element of the radiative decay process $V \rightarrow P\gamma^*$ could be parameterized using 4-velocity of the vector and pseudoscalar mesons by expression:

$${}_P\langle Q', M_P | \hat{J}^\alpha | Q, M_V \rangle_V = \frac{e}{(2\pi)^3} g_{VP\gamma^*}(t) K^\alpha(\mu) \frac{\sqrt{M_V M_P}}{\sqrt{4V_0 V'_0}}, \quad (17)$$

where $K^\alpha(\mu) = i\epsilon^{\alpha\nu\rho\sigma} \varepsilon_\nu(\mu) V_\rho V'_\sigma$ and $e = \sqrt{4\pi\alpha_{\text{QED}}}$.

In framework of Poincare invariant quantum mechanics we consider mesons P and V as relativistic constituent quark-antiquark system. In such approach decay caused by the emission of quark a γ^* -quantum. In generalized Breit system it's easy to show, that

$$\begin{aligned} g_{VP\gamma^*}(t) &= \frac{1}{4\pi\sqrt{M_V M_P}} \int d\mathbf{k} \ k^2 \Phi(\mathbf{k}, \beta) \sqrt{\frac{1}{\omega_{m_q}(\mathbf{k}) \omega_{m_{\bar{q}}}(\mathbf{k})}} \times \\ &\times \sqrt{\frac{3 + 4\nu_1(\lambda - \nu_1)}{2}} \nu'_1 \times \left[\Phi(\mathbf{k}_2, \beta) \sqrt{\frac{\omega_{m_{\bar{q}}}(\mathbf{k}_2)}{\omega_{m_q}(\mathbf{k}_2)}} \bar{u}_{\nu'_1}(\mathbf{k}_2, m_q) B^{-1}(\mathbf{v}_{\mathbf{Q}}) \times \right. \\ &\times \frac{(\Gamma_2 \cdot K^*)}{(K \cdot K^*)} u_{\nu_1}(\mathbf{k}, m_q) D_{-\nu'_1, \lambda - \nu_1}^{1/2}(\mathbf{n}_{W_2}(\mathbf{k}, \mathbf{v}_{\mathbf{Q}})) + \Phi(\mathbf{k}_2, \beta) \sqrt{\frac{\omega_{m_q}(\mathbf{k}_2)}{\omega_{m_{\bar{q}}}(\mathbf{k}_2)}} \times \\ &\left. \times \bar{v}_{\lambda - \nu_1}(\mathbf{k}, m_{\bar{q}}) \frac{(\Gamma_1 \cdot K^*)}{(K \cdot K^*)} B(\mathbf{v}_{\mathbf{Q}}) v_{-\nu'_1}(\mathbf{k}_2, m_{\bar{q}}) D_{\nu'_1, \nu_1}^{1/2}(\mathbf{n}_{W_1}(\mathbf{k}, \mathbf{v}_{\mathbf{Q}})) \right], \end{aligned} \quad (18)$$

where \mathbf{k} is relative momentum and

$$\mathbf{n}_{W_{2,1}} = -\frac{[\mathbf{k}, \mathbf{V}]}{\omega_{m_q, \bar{q}} + m_{q, \bar{q}} - (\mathbf{k} \mathbf{V})}, \quad (19)$$

$$\Gamma_{1,2}^\mu = F_1(t)\gamma^\mu + iF_2(t)\frac{\sigma^{\mu\nu}(k_{1,2} - k)}{2m_{q,\bar{q}}}. \quad (20)$$

In relation (20) form-factors $F_1(t)$ and $F_2(t)$ normalized in the natural units magnetic μ_q and anomalous magnetic moments of quarks κ_q :

$$F_1(t=0) + F_2(t=0) = \mu_q, \quad F_2(t=0) = \kappa_q. \quad (21)$$

It's also should be notice, than in (18) relation for \mathbf{k}_2 and $\omega_{m_{q,\bar{q}}}(\mathbf{k}_2)$ given by:

$$\mathbf{k}_2 = \mathbf{k} + \mathbf{v}_Q \left((\varpi + 1)\omega_{m_{q,\bar{q}}} + \sqrt{\varpi^2 - 1} k \cos \theta_k \right), \quad (22)$$

$$\omega_{m_{q,\bar{q}}}(\mathbf{k}_2) = \omega_{m_{q,\bar{q}}}(\mathbf{k})\varpi - \sqrt{\varpi^2 - 1} k \cos \theta_k \quad (23)$$

and

$$\varpi = \frac{M_0^2 + M_0'^2 - t}{2M_0M_0'}. \quad (24)$$

Using experimental data for radiative decay of light vector mesons ρ^+ , K^\pm and K^* [11] and carrying numerical integration from (18) and (21) we obtain following values of magnetic moments of u , d and s quarks in units μ_N (nuclear magneton)(Table (1)):

Table 1: Quarks magnetic moments, μ_N

Magnetic moment	This work	[12]	[13]
μ_u	2.080 ± 0.082	2.066	2.08 ± 0.07
μ_d	-1.261 ± 0.015	-1.110	-1.31 ± 0.06
μ_s	-0.621 ± 0.011	-0.633	-0.77 ± 0.06

4 Conclusion and remarks

The work conducted within the framework of the relativistic quark model based on the point form of the Poincare-invariant quantum mechanics to obtain an integral representation for the form factor of the $V \rightarrow P\gamma$ transition. From the condition of compliance with model calculations decay width of experimental values found values of the magnetic moments of quarks, which are correlated with the data obtained using the experimental values of the magnetic moments of baryons.

5 Acknowledgments

We are grateful to the organizational and material support to the organizers of the Conference DSPIN'15. This work was supported by the Belarusian Republican Foundation for Basic Research.

References

- [1] Gerasimov S 1989 (*Preprint* JINR-E2-89-837)
- [2] Jaus W 1991 *Phys.Rev.* **D44** 2851–2859
- [3] Ebert D, Faustov R and Galkin V 2002 *Phys.Lett.* **B537** 241–248 (*Preprint* hep-ph/0204089)
- [4] Choi H M 2007 *Phys.Rev.* **D75** 073016 (*Preprint* hep-ph/0701263)
- [5] Krutov A and Troitsky V 2009 *Physics of Particles and Nuclei* **40** 136–161
- [6] Polyzou W N, Huang Y, Elster C, Glockle W, Golak J, Skibinski R, Witala H and Kamada H 2011 *Few Body Syst.* **49** 129–147 (*Preprint* hep-ph/1008.5215)
- [7] Godfrey S and Isgur N 1985 *Phys.Rev.* **D32** 189–231
- [8] Andreev V 2013 (*Preprint* hep-ph/1305.4266)
- [9] Bjorken J 1970 *Phys.Rev.* **D1** 1376–1379
- [10] Andreev V 1998 (*Preprint* hep-ph/9912286)
- [11] Olive K and Group P D 2014 *Chinese Physics C* **38** 090001
- [12] Bijker R, Santopinto E and Santopinto E 2009 *Phys. Rev.* **C80** 065210 (*Preprint* hep-ph/0912.4494)
- [13] Dothan Y 1982 *Physica* **114A** 216–220

The Polarized Semi-inclusive Lepton-Nucleon DIS with Charged Current

E.A.Degtyareva*, S.I.Timoshin

Sukhoi State Technical University of Gomel

Abstract

This paper discusses the polarization asymmetry of semi-inclusive deep inelastic scattering of leptons on nucleons. Numerical results of asymmetries and radiative corrections to lepton current are provided.

1 Introduction

A study of the spin structure of the nucleon is one of the main problems of particle physics [1]. This problem is called "spin crisis". Semi-inclusive processes are sources of new data on the spin structure of the nucleon. Using data that can give these experiments can provide information for each quark flavor. Spin nucleon problem is not yet solved completely and therefore further research of all the contributions into nucleon spin is necessary.

2 The semi-inclusive deep inelastic lN -scattering

Consider the process of semi-inclusive lepton-nucleon deep inelastic scattering of leptons on nucleons with a charged current

$$\ell + N \rightarrow \nu + h + X. \quad (1)$$

*E-mail:dekaterinaa@mail.ru

The differential cross section for scattering of a lepton is defined as case of a lepton:

$$\begin{aligned} & \left(\frac{d^3\sigma_{\ell^-}}{dx dy dz} \right)^h = \tag{2} \\ & = 2\rho x \left\{ \sum_{q_i, q_j} q_i(x, Q^2) D_{q_j}^h(z, Q^2) + y_1^2 \sum_{\bar{q}_j, \bar{q}_i} \bar{q}_j(x, Q^2) D_{\bar{q}_i}^h(z, Q^2) + \right. \\ & \left. P_N \left(\sum_{q_i, q_j} \Delta q_i(x, Q^2) D_{q_j}^h(z, Q^2) - y_1^2 \sum_{\bar{q}_j, \bar{q}_i} \Delta \bar{q}_j(x, Q^2) D_{\bar{q}_i}^h(z, Q^2) \right) \right\}, \end{aligned}$$

where $q_i = d, s, b, q_j = u, c, t, \bar{q}_i = \bar{d}, \bar{s}, \bar{b}, \bar{q}_j = \bar{u}, \bar{c}, \bar{t}$;
the case of antilepton

$$\begin{aligned} & \left(\frac{d^3\sigma_{\ell^+}}{dx dy dz} \right)^h = \tag{3} \\ & 2\rho x \left\{ y_1^2 \sum_{q_i, q_j} q_i(x, Q^2) D_{q_j}^h(z, Q^2) + \sum_{\bar{q}_j, \bar{q}_i} \bar{q}_j(x, Q^2) D_{\bar{q}_i}^h(z, Q^2) + \right. \\ & \left. + P_N \left(\sum_{q_i, q_j} \Delta q_i(x, Q^2) D_{q_j}^h(z, Q^2) - \sum_{\bar{q}_j, \bar{q}_i} \Delta \bar{q}_j(x, Q^2) D_{\bar{q}_i}^h(z, Q^2) \right) \right\} \end{aligned}$$

where $q_i = u, c, t, q_j = d, s, b, \bar{q}_i = \bar{u}, \bar{c}, \bar{t}, \bar{q}_j = \bar{d}, \bar{s}, \bar{b}$.

Here $\rho = \frac{G^2 s}{2\pi} \left(\frac{m_w^2}{m_w^2 + Q^2} \right)^2$, $y_1 = 1 - y$, G is Fermi constant, m_w is the W-boson mass, $x = \frac{Q^2}{2p \cdot q}$, $y = \frac{p \cdot q}{p \cdot k}$, $Q^2 = -q^2 = -(k - k')^2$, $s = 2p \cdot k$, $k(k')$ and p are the initial (final) lepton and proton 4-momenta, respectively, P_N is the degree of longitudinal polarization of proton,

$$q(x)(\Delta q(x))/\bar{q}(x)(\Delta \bar{q}(x))$$

are the unpolarized (polarized) quark/antiquark distribution functions, $D_q^h(z, Q^2)(D_{\bar{q}}^h(z, Q^2))$ are the fragmentation functions of quark (antiquark) with flavor q to the hadron h .

Consider the asymmetry. These asymmetries have been offered in the [3]. We consider the asymmetry, which are constructed as a combination

of different cross-sections in the following form [2]

$$A_{\ell^-}^{h^+-h^-} = \frac{\left(\frac{d^3\sigma_{e\ell^-}^{\downarrow\uparrow}}{dx dy dz}\right)_{h^+-h^-} - \left(\frac{d^3\sigma_{e\ell^-}^{\downarrow\downarrow}}{dx dy dz}\right)_{h^+-h^-}}{\left(\frac{d^3\sigma_{e\ell^-}^{\downarrow\uparrow}}{dx dy dz}\right)_{h^+-h^-} + \left(\frac{d^3\sigma_{e\ell^-}^{\downarrow\downarrow}}{dx dy dz}\right)_{h^+-h^-}}, \quad (4)$$

$$A_{\ell^+}^{h^+-h^-} = \frac{\left(\frac{d^3\sigma_{e\ell^+}^{\uparrow\uparrow}}{dx dy dz}\right)_{h^+-h^-} - \left(\frac{d^3\sigma_{e\ell^+}^{\uparrow\downarrow}}{dx dy dz}\right)_{h^+-h^-}}{\left(\frac{d^3\sigma_{e\ell^+}^{\uparrow\uparrow}}{dx dy dz}\right)_{h^+-h^-} + \left(\frac{d^3\sigma_{e\ell^+}^{\uparrow\downarrow}}{dx dy dz}\right)_{h^+-h^-}}, \quad (5)$$

$$\begin{aligned} A_{\pm}^{h^+-h^-} &= \\ &= \frac{\left[\left(\frac{d^3\sigma_{l^-}^{\downarrow\uparrow}}{dx dy dz}\right)_{h^+-h^-} \pm \left(\frac{d^3\sigma_{l^+}^{\uparrow\uparrow}}{dx dy dz}\right)_{h^+-h^-}\right] - \left[\left(\frac{d^3\sigma_{l^-}^{\downarrow\downarrow}}{dx dy dz}\right)_{h^+-h^-} \pm \left(\frac{d^3\sigma_{l^+}^{\uparrow\downarrow}}{dx dy dz}\right)_{h^+-h^-}\right]}{\left[\left(\frac{d^3\sigma_{l^-}^{\downarrow\uparrow}}{dx dy dz}\right)_{h^+-h^-} \pm \left(\frac{d^3\sigma_{l^+}^{\uparrow\uparrow}}{dx dy dz}\right)_{h^+-h^-}\right] + \left[\left(\frac{d^3\sigma_{l^-}^{\downarrow\downarrow}}{dx dy dz}\right)_{h^+-h^-} \pm \left(\frac{d^3\sigma_{l^+}^{\uparrow\downarrow}}{dx dy dz}\right)_{h^+-h^-}\right]}, \end{aligned} \quad (6)$$

where $\sigma^{h^+-h^-} = \sigma^{h^+} - \sigma^{h^-}$.

The first arrow corresponds to the helicity of the initial lepton (\downarrow) or antilepton (\uparrow) and the second – to the polarization degree of the proton: $\uparrow (P_N = +1)$, $\downarrow (P_N = -1)$.

Let us consider the case π -meson. With the correlations for π - meson fragmentation functions [3]

$$D_d^{\pi^+-\pi^-} = -D_u^{\pi^+-\pi^-}, D_u^{\pi^+-\pi^-} = -D_{\bar{u}}^{\pi^+-\pi^-},$$

$$D_s^{\pi^+-\pi^-} = D_{\bar{s}}^{\pi^+-\pi^-} = 0, D_c^{\pi^+-\pi^-} = D_{\bar{c}}^{\pi^+-\pi^-} = 0,$$

we obtain for the proton target asymmetry in the form of

$$A_{\ell^-p}^{\pi^+-\pi^-} = \frac{\Delta u(x, Q^2) - y_1^2 \Delta \bar{d}(x, Q^2)}{u(x, Q^2) + y_1^2 \bar{d}(x, Q^2)}, \quad (7)$$

$$A_{\ell^+p}^{\pi^+-\pi^-} = \frac{y_1^2 \Delta d(x, Q^2) - \Delta \bar{u}(x, Q^2)}{y_1^2 d(x, Q^2) + \bar{u}(x, Q^2)}, \quad (8)$$

$$A_{+,p}^{\pi^+-\pi^-} = \frac{\Delta u(x, Q^2) + \Delta \bar{u}(x, Q^2) - y_1^2 (\Delta d(x, Q^2) + \Delta \bar{d}(x, Q^2))}{u_V(x, Q^2) - y_1^2 d_V(x, Q^2)}, \quad (9)$$

$$A_{-,p}^{\pi^+-\pi^-} = \frac{\Delta u_V(x, Q^2) + y_1^2 \Delta d_V(x, Q^2)}{u(x, Q^2) + \bar{u}(x, Q^2) + y_1^2 (d(x, Q^2) + \bar{d}(x, Q^2))}, \quad (10)$$

where $u_V(x, Q^2) = u(x, Q^2) - \bar{u}(x, Q^2)$, $d_V(x, Q^2) = d(x, Q^2) - \bar{d}(x, Q^2)$.

For the case of the neutron

$$A_{\ell^- n}^{\pi^+ - \pi^-} = \frac{\Delta d(x, Q^2) - y_1^2 \Delta \bar{u}(x, Q^2)}{d(x, Q^2) + y_1^2 \bar{u}(x, Q^2)}, \quad (11)$$

$$A_{\ell^+ n}^{\pi^+ - \pi^-} = \frac{y_1^2 \Delta u(x, Q^2) - \Delta \bar{d}(x, Q^2)}{y_1^2 u(x, Q^2) + \bar{d}(x, Q^2)}, \quad (12)$$

$$A_{+,n}^{\pi^+ - \pi^-} = \frac{\Delta d(x, Q^2) + \Delta \bar{d}(x, Q^2) - y_1^2 (\Delta u(x, Q^2) + \Delta \bar{u}(x, Q^2))}{d_V(x, Q^2) - y_1^2 u_V(x, Q^2)}, \quad (13)$$

$$A_{-,n}^{\pi^+ - \pi^-} = \frac{\Delta d_V(x, Q^2) + y_1^2 \Delta u_V(x, Q^2)}{d(x, Q^2) + \bar{d}(x, Q^2) + y_1^2 (u(x, Q^2) + \bar{u}(x, Q^2))}. \quad (14)$$

With the help of these asymmetries can be obtained distribution function. The expressions for $(\Delta u + \Delta \bar{u})$, $(\Delta d + \Delta \bar{d})$ we obtain from asymmetries (9),(13); for $\Delta \bar{d}$, Δu from (7) and (12); for $\Delta \bar{u}$, Δd from (8) and (11); for Δu_V , Δd_V from (10), (14). The considered asymmetries have no dependence on fragmentation function which is very useful for the analysis of proton spin structure.

Of interest are the limiting cases for y . We consider the case when $y \rightarrow 1$. Asymmetry (7)-(14) take the form of

$$\begin{aligned} A_{\ell^- p}^{\pi^+ - \pi^-} &= \frac{\Delta u(x, Q^2)}{u(x, Q^2)}, & A_{+,p}^{\pi^+ - \pi^-} &= \frac{\Delta u(x, Q^2) + \Delta \bar{u}(x, Q^2)}{u_V(x, Q^2)}, \\ A_{\ell^+ p}^{\pi^+ - \pi^-} &= \frac{-\Delta \bar{u}(x, Q^2)}{\bar{u}(x, Q^2)}, & A_{-,p}^{\pi^+ - \pi^-} &= \frac{\Delta u_V(x, Q^2)}{u(x, Q^2) + \bar{u}(x, Q^2)}, \\ A_{\ell^- n}^{\pi^+ - \pi^-} &= \frac{\Delta d(x, Q^2)}{d(x, Q^2)}, & A_{+,n}^{\pi^+ - \pi^-} &= \frac{\Delta d(x, Q^2) + \Delta \bar{d}(x, Q^2)}{d_V(x, Q^2)}, \\ A_{\ell^+ n}^{\pi^+ - \pi^-} &= \frac{-\Delta \bar{d}(x, Q^2)}{\bar{d}(x, Q^2)}, & A_{-,n}^{\pi^+ - \pi^-} &= \frac{\Delta d_V(x, Q^2)}{d(x, Q^2) + \bar{d}(x, Q^2)}. \end{aligned}$$

For the analysis of nucleon spin structure we introduce the first moments of parton distributions as follows

$$\begin{aligned} \Delta q(Q^2) &= \int_0^1 \Delta q(x, Q^2) dx, \\ \Delta \bar{q}(Q^2) &= \int_0^1 \Delta \bar{q}(x, Q^2) dx, \end{aligned}$$

which correspond to the quark q (antiquark \bar{q}) contributions to the spin of nucleon.

With the first moments of parton distributions can be obtained quark contributions to the nucleon spin. Semi-inclusive process is interesting because it can be individually receive contributions of quarks.

3 Numerical results and conclusions

To analyze the distribution of the nucleon spin structure used distribution quarks and antiquarks in the nucleon [6]. The numerical results of obtained asymmetries are presented on Fig.1, Fig.2. The asymmetry $A_{\ell-p}^{\pi^+-\pi^-}$ shows a significant dependence on y in the $x \leq 0.5$. The asymmetry $A_{\ell^+}^{\pi^+-\pi^-}$ in almost the entire region depend on y and the measured region reaches about 60% – 80%. The asymmetry $A_{\ell-n}^{\pi^+-\pi^-}$ is negative, weakly dependent on the y . The asymmetry $A_{\ell+n}^{\pi^+-\pi^-}$ is largely dependent on the y at low and medium x . The asymmetries $A_{+,p}^{\pi^+-\pi^-}$ and $A_{-,p}^{\pi^+-\pi^-}$ are of the order of 70%, the asymmetry $A_{-,p}^{\pi^+-\pi^-}$ has a significant dependence on the y in the all kinematic region.

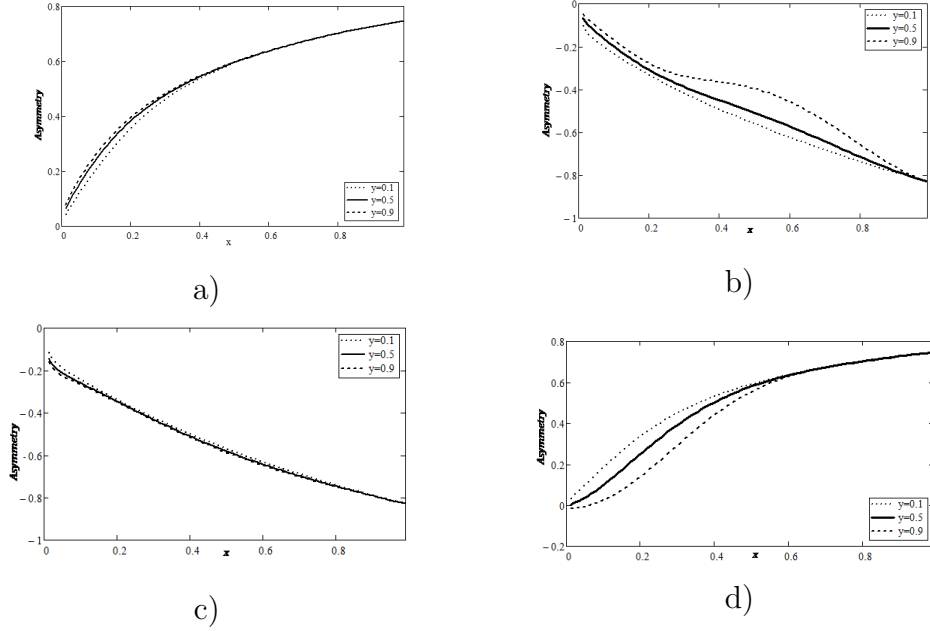


Figure 1: Obtained asymmetries a) $A_{\ell-p}^{\pi^+-\pi^-}(x, y)$, b) $A_{\ell^+}^{\pi^+-\pi^-}(x, y)$, c) $A_{\ell-n}^{\pi^+-\pi^-}(x, y)$, d) $A_{\ell+n}^{\pi^+-\pi^-}(x, y)$.

We discuss the radiative corrections. Calculated the electromagnetic corrections to lepton current. Numerical results are presented in Fig. 3. It can be seen that the correction for asymmetry $A_{\ell-p}^{\pi^+-\pi^-}$ decreases rapidly for large values of x and less than 1%, and for small values of x , it is heavily

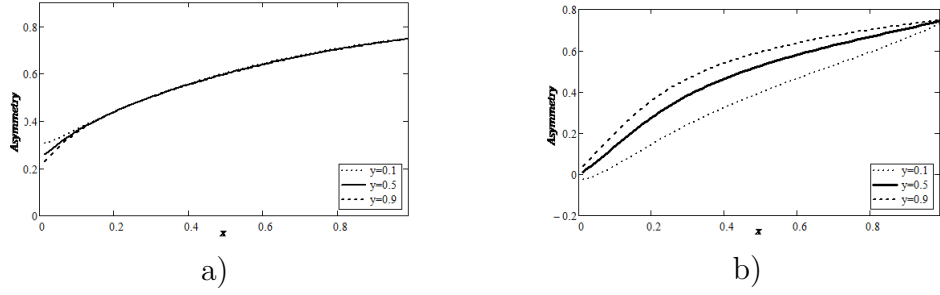


Figure 2: Obtained asymmetries: a) $A_{+,p}^{\pi^+-\pi^-}(x, y)$, b) $A_{-,p}^{\pi^+-\pi^-}(x, y)$.

dependent on y . A similar behavior of a correction for asymmetry $A_{\ell-n}^{\pi^+-\pi^-}$. For large values of x , it is insignificant, but for small x up to 4 – 10%. QCD corrections were evaluated in the work [7] and appeared small. The amendments can be neglected, and the main contribution electromagnetic corrections.

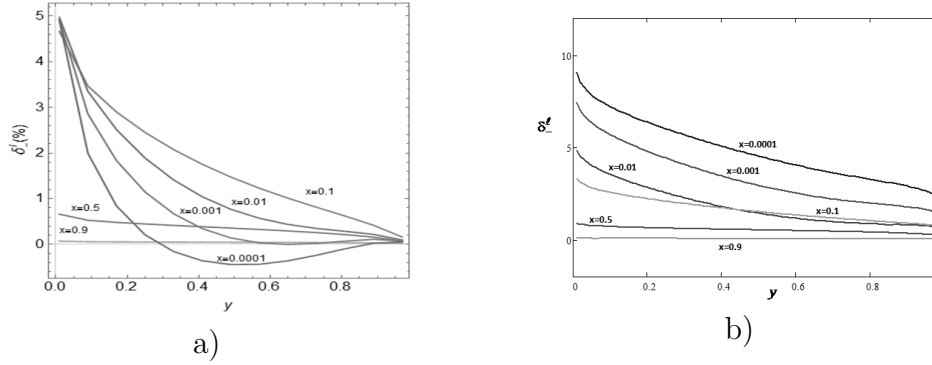


Figure 3: QED correction $\delta_{\ell}^{\ell}(\%)$ a) for $A_{+,p}^{\pi^+-\pi^-}(x, y)$, b) for $A_{-,p}^{\pi^+-\pi^-}(x, y)$.

In this paper we consider the asymmetry that do not depend on the fragmentation functions. With the help of these asymmetries can be obtained of the distribution function, and then deposits quarks and antiquark in the nucleon spin. The advantage of semi-inclusive processes is the ability to receive individual contributions quarks and antiquarks. Radiative corrections were evaluated and they were small except for small values x .

References

- [1] Burkardt, M [et al.] Spin-polarized high-energy scattering of charged leptons on nucleons, - 2008. – 103 p. (ArXiv: hep-ph/0812.2208).
- [2] Timoshin S.I. The spin and electroweak effects in the lepton-nucleon scattering: Gomel : GSTU , 2002. – 121 p.
- [3] Christova E., Leader E. A Strategy for the Analysis of Semi-Inclusive Deep Inelastic Scattering / E. Christova, E. Leader // Nucl.Phys. B607 (2001). P369.
- [4] Sissakian, A.N. [et al.] NLO QCD procedure of the SIDIS data analysis with respect to light quark polarized sea / A.N. Sissakian et al. 2004. – 20p. (ArXiv: hep-ph/0312084).
- [5] Bass, S.D. [et al.] Towards an understanding of nucleon spin structure: from hard to soft scales / S.D. Bass, C.A. Aidala. 2006. 19p. (ArXiv: hep-ph/0606269).
- [6] Kurzela, M. [et al] Phenomenological analysis of data on inclusive and semi-inclusive spin asymmetries / M.Kurzela et al.1998.–16p. (ArXiv:hep-ph/9807355).
- [7] Blumlein, J. Prog.Part Nucl. Phys.2013. V69.P28.

One-Loop Radiative Corrections of Two-Photon Production Processes of the Leptons at Colliders

A. Manko ^{*},

Institute of Physics, National Academy of Sciences of Belarus

R. Shulyakovsky [†]

Institute of Applied Physics, National Academy of Sciences of Belarus

Abstract

The one-loop radiative corrections of two-photon production of the leptons at colliders are considered. We obtain total and differential cross sections for the processes depending on various variables and parameters.

1 Introduction

The processes of two-photon production of leptons at hadrons colliders are studied in the next-leading order in this paper. This process is very important to study, because it can be used to calibrate the collider's luminosity and to search the effects of "new physics". It has the small background and the process can be used to measure the parameters of Standard Model. This background is small for this process, as the final leptons are measured at the main detector, the final hadrons are measured at the forward-detector. The process of particle production at colliders by two-photon mechanism were investigated previously at the leading order [1, 2, 3, 4, 10]. The key moment is the possibility of using the equivalent

^{*}e-mail: andrej.j.manko@gmail.com

[†]e-mail: shul@ifanbel.bas-net.by

photon method (Weizsacker-Williams approximation) for ultrarelativistic collisions, which allows us to consider virtual photons as real ones and essentially simplifies the calculation of observable values. The processes of lepton pair production by two-photon mechanism can be measured with high accuracy at modern colliders [5, 6, 7, 8] and have bright signature. It should be noted that processes with two-photon mechanism of pair production have the cross-section of the order α^4 ($\alpha \approx \frac{1}{137}$ - fine coupling constant) while "one-photon mechanism" (Drell-Yan processes) leads to the $\sigma \sim \alpha^2$. However, at high energies ($\sqrt{s} \gg 1$ GeV) corresponding cross-section of Drell-Yan processes decreases as $\frac{1}{s}$ while two-photon mechanism leads to large logarithmic growth with energy. Two-photon mechanism can be used as mechanism of lepton pair production at Tevatron and LHC energies in certain kinematic regions. As this process can be calculated with accuracy about 1% in the leading order and can be calculated with accuracy more 1% in the next-leading order, it is necessary to calculate this process with accuracy more 1% in the next-leading order to study at modern colliders. The elastic case was studied in the next-leading order in this paper. The elastic case also was studied in the leading order in these papers [8, 9, 10, 11].

2 The amplitudes and the matrix elements

The Weizsacker-Williams approximation (equivalent-photon method) [12, 13, 14] was used to study the process of lepton pairs production by mean of two-photon production in hadron collisions at LHC and Tevatron in next-to-leading order. We studied this process in the elastic case in the paper. The diagram of the full process are shown at fig. 1. The diagrams of the subprocess in leading order are shown at fig. 2. The one of self-energies diagrams and the one of boxes diagrams are shown at fig. 3. The two of vertex diagrams are shown at fig. 4. The bosons: W^+ , W^- , Z ; the unphysical particles: ϕ^+ , ϕ^- and the Faddeev Popov ghosts u^\pm , \bar{u}^\pm , u^γ , \bar{u}^γ , u^Z and \bar{u}^Z were used in our investigation, as the two-photon production process of leptons were studied. We used the 't Hooft Feynman gauge in our consideration, as the particles: ϕ^+ , ϕ^- , u^\pm , \bar{u}^\pm , u^γ , \bar{u}^γ , u^Z and \bar{u}^Z were used. The program Mathematica [15] and package FeynArts 3.4 [16] were used to calculate the subprocesses's amplitudes in the leading and the next-leading order. The regularization scheme proposed by 't Hooft [17, 18, 19, 20] and Veltman [21, 22, 23] and the renormalization on-

shell scheme developed by Denner [24] were used to calculate UV-finite amplitudes. We also used the program Mathematica and package FeynCalc [25] to calculate the square module of matrix for this process.

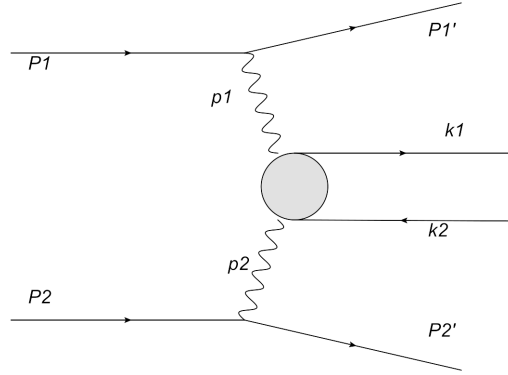


Figure 1: Feynman diagrams of the considered processes. P_1 (P_1') and P_2 (P_2') are 4-momenta of initial (final) hadrons; k_1 , k_2 are 4-momenta of leptons.

$$\gamma \quad \gamma \rightarrow e \quad e$$

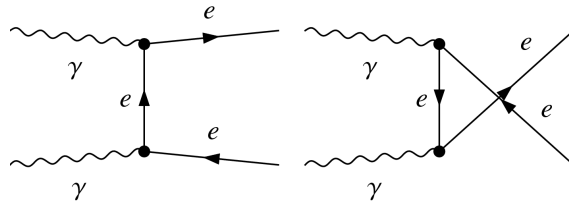


Figure 2: Feynman diagrams of the considered subprocesses in the leading order.

3 Cross and differential section

The library LoopTools [26] was used to calculate numerical the loop's integrals. The Library is based on the package FF [27] and provides

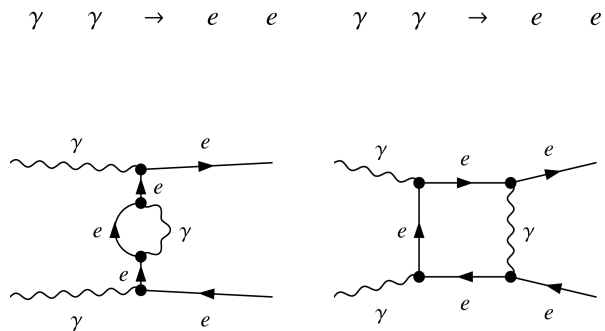


Figure 3: Feynman diagrams of the considered subprocesses in the next-leading order: the diagram of self-energies(left), the box diagram(right).

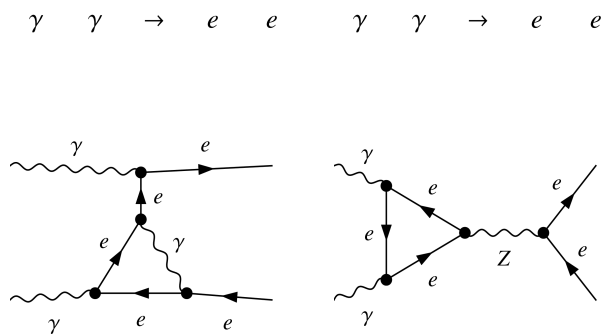


Figure 4: Feynman diagrams of the considered subprocesses in the next-leading order: the two vertex diagrams.

in addition to the scalar integrals of FF also the tensor coefficients in the conventions of the work [24]. The monte-carlo generator [28, 29] TwoPhotonGen written on C++ was used to calculate numerical total and differential cross sections. The cuts for Tevatron shown at tab. 1 and the cuts for ATLAS shown at tab. 2 were used to calculate total and differential cross sections. The results of the numerical calculation of total cross sections at the different collision energies are shown at tab. 3 for electron-positron pair in the leading and the next-leading order for the elastic case. The differential cross section of e^+e^- production as a function the invariant mass e^+e^- and the distribution as a function the electron's

pseudorapidity η are shown for Tevatron at fig. 5. The differential cross section of e^+e^- production as a function the invariant mass e^+e^- and the distribution as a function the electron's pseudorapidity η are shown for ATLAS(LHC) for different collisons' energies at fig. 6– 9. There is a solid line for the leading order at fig. 6– 9. There is a dashed line for the next-leading order at fig. 6– 9.

Cut	Value
$m_{e^-e^+}$	10 GeV
E_t	5 GeV
$ \eta $	2.0
Forward detector: $ \eta_p $	$3.6 < \eta_p < 5.2$

Table 1: The cuts for Tevatron

Cut	Value
$m_{e^-e^+}$	24 GeV
p_t	12 GeV
$ \eta $	2.4
Forward detector: $ \eta_p $	$4.3 < \eta_p < 4.9$

Table 2: The cuts for ATLAS

Collider	LO	NLO
Tevatron $\sqrt{s} = 1.96$ TEV	1.7013(54)	1.647(11)
LHC $\sqrt{s} = 7$ TEV	5.5327(13)	4.123(14)
LHC $\sqrt{s} = 8$ TEV	6.088(11)	4.469(15)
LHC $\sqrt{s} = 13$ TEV	7.825(17)	5.847(69)
LHC $\sqrt{s} = 14$ TEV	8.205(16)	6.089(23)

Table 3: Total Cross sections σ pb

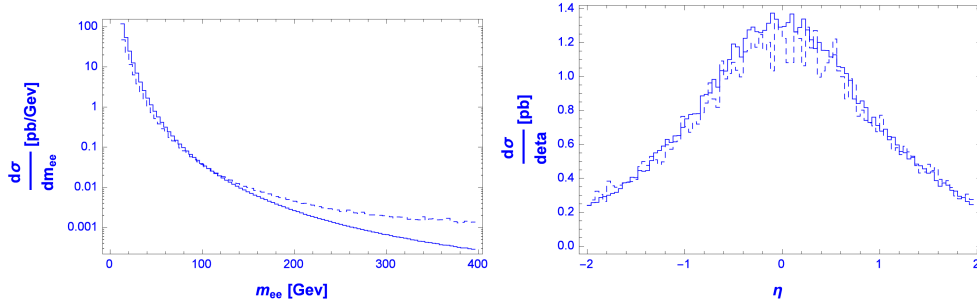


Figure 5: The Distribution as a function the invariant mass e^-e^+ for Tevatron(left) and the distribution depends on the electron's pseudorapidity for Tevatron(right).

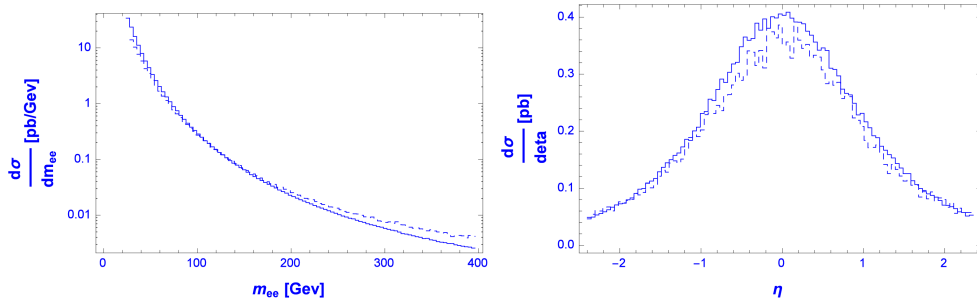


Figure 6: The Distribution as a function the invariant mass e^-e^+ (left) and the distribution depends on the electron's pseudorapidity(right) for ATLAS(LHC) at $\sqrt{s} = 7.0$ TeV.

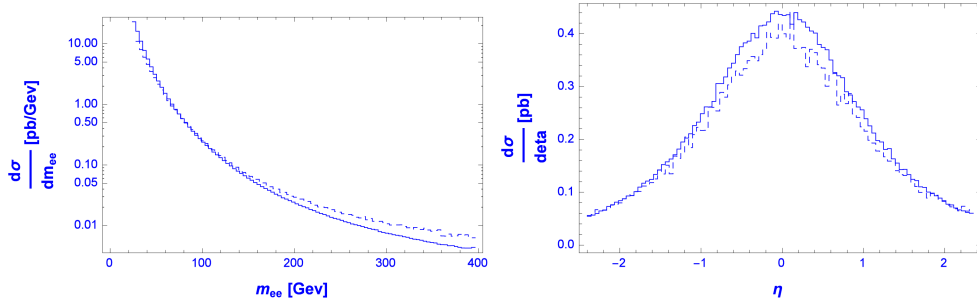


Figure 7: The Distribution as a function the invariant mass e^-e^+ (left) and the distribution depends on the electron's pseudorapidity(right) for ATLAS(LHC) at $\sqrt{s} = 8.0$ TeV.

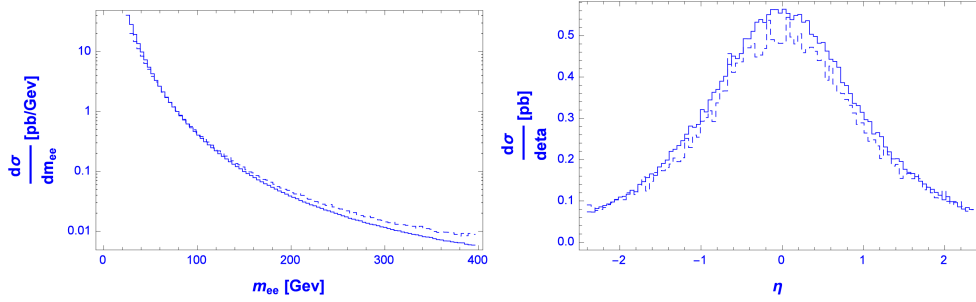


Figure 8: The Distribution as a function the invariant mass e^-e^+ (left) and the distribution depends on the electron's pseudorapidity(right) for ATLAS(LHC) at $\sqrt{s} = 13.0$ TeV.

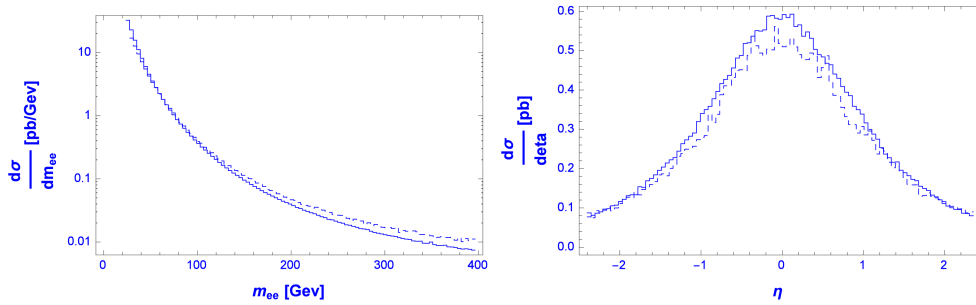


Figure 9: The Distribution as a function the invariant mass e^-e^+ (left) and the distribution depends on the electron's pseudorapidity(right) for ATLAS(LHC) at $\sqrt{s} = 14.0$ TeV.

4 Conclusion

The two-photon mechanism of lepton pairs production was studied in the next-leading order in this article. The total and differential cross sections were obtained for Tevatron and ATLAS(LHC) using the cuts for Tevatron and ATLAS(LHC) in this article. The total cross sections for next-leading order is less than the total cross section for leading order. It was shown what the process of two-photon production leptons can be use to calibrate collider's luminosity, to search the effects of "new physics" and to measure the parameters of Standard Model.

References

- [1] V.M. Budnev et al., JETP Letters. **12**, 249 (1970).
- [2] V.M. Budnev et al., PEPAN. **4**, 239 (1973).
- [3] V.E.Balakin et al., JETP Letters. **11**, 559 (1970).
- [4] C.Pisano. The Polarized and unpolarized photon content of the nucleon /thesis/, hep-ph:0512306.
- [5] CDF Collaboration. Observation Exclusive Charmonium Production and $\gamma\gamma \rightarrow \mu^-\mu^+$ in $p\bar{p}$ Collisions at $\sqrt{s} = 1.96 TeV$, hep-ex:0902.1271v4.
- [6] CMS Collaboration. Observation of Exclusive Electron-Positron Production in Hadron-Hadron Collisions, hep-ex:0611040v2.
- [7] CMS Collaboration. Exclusive diphoton production of dimuon pairs in proton-proton collisions at $\sqrt{s} = 7.0 TeV$, hep-ex:1111.5536v1.
- [8] I.Satsunkevich, Dz.Shoukavy and A.Khilkevich. Nonlinear Dynamics and Application, **17** (2011), 130.
- [9] A.G. Shamov, V.I. Telnov, Nucl. Instr. and Meth. in Phys. Res. **A494**, 51 (2002).
- [10] I.Satsunkevich, R. Shulyakovsky, A. Manko, NPCS **16** no. 1, 72 (2013).
- [11] J.A.M. Vermaseren, Nucl. Phys. **229** 347 (1983).
- [12] C.F.Weizsäcker, Z.Phys. **88**, 612 (1934).
- [13] E.J.Williams, Phys. Rev. **45**, 729 (1934).
- [14] V.M.Budnev et al., Phys.Rep. **C15**, 181 (1975).
- [15] Sal Mangano, *Mathematica Cookbook* (O'Reilly Media Sebastopol 2010).
- [16] Thomas Hahn, Comput. Phys. Commun. **140**, 418 (2001).
- [17] G. 't Hooft, Nucl. Phys. **B33**, 173 (1971).

- [18] G. 't Hooft, Nucl. Phys. **B35**, 167 (1971).
- [19] G. 't Hooft, Nucl. Phys. **B61**, 455 (1973).
- [20] G. 't Hooft, Nucl. Phys. **B62**, 444 (1973).
- [21] G. 't Hooft and M. Veltman, Nucl. Phys. **B44**, 189 (1972).
- [22] G. 't Hooft and M. Veltman, Nucl. Phys. **B50**, 318 (1972).
- [23] G. 't Hooft and M. Veltman, Nucl. Phys. **B153**, 365 (1979).
- [24] A. Denner, Fortsch. Phys. **4**(4) 307 (1994).
- [25] R. Mertig, M. Böhm, A. Denner, Comp. Phys. Comm. **64**, 345 (1991).
- [26] T. Hahn and M Perez-Victoria, Comp. Phys. Comm. **118**, 153 (1999).
- [27] G.J. van Oldenborgh and J.A.M. Vermaseren, Z. Phys. **C46**, 425 (1990).
- [28] S. Weinzierl. arXiv:0006229v1[hep-ph].
- [29] E. Byckling, K. Kajantie, Particle Kinematics. John Wiley and sons, 1973.

5 Nuclear Energy

Numerical Simulation of Flow and Heat Transfer around of Spherical Fuel Elements

L. Babichev^{1)*}, S. Bakhanovitch^{2)†}, G. Gromyko^{2)‡},
A. Zherelo^{1),2)§}

¹⁾*Joint Institute for Power and Nuclear Research - Sosny
of the NAS of Belarus*

²⁾*Institute of Mathematics of the NAS of Belarus*

Abstract

Numerical simulation of flow and heat transfer around of spherical fuel elements from a pebble-bed reactor by new 3D code is presented.

1 Introduction

The pebble-bed reactor (PBR) is a graphite-moderated, gas-cooled nuclear reactor. It is a type of very-high-temperature reactor (VHTR), one of the six classes of nuclear reactors in the Generation IV initiative [1]. The basic feature of pebble-bed reactors are spherical fuel elements called pebbles. Heightened interest to gas-cooled pebble-bed reactor is determined by their improved safety features. However, from the viewpoint of the safety of the reactor, it is important to accurately predict the maximum fuel temperature during the normal operation of the reactor. In the case of the PBR, the random distribution of the spherical fuel pebbles causes

*E-mail: babichev@sosny.bas-net

†E-mail: bsv@im.bas-net.by

‡E-mail: grom@im.bas-net.by

§E-mail: ant@sosny.bas-net.

a highly complicated flow regime which finally results in differences in the degree of local cooling. Such flow-induced local hot spot analyses in the PBR core were recently performed by several authors. In [2] the flow distribution in an aligned pebble geometry consisting of 27 pebble spheres was investigated. The local heat transfer due to complexity of the flow distribution in a body-centered cubical (BCC) structure of pebble beds was also studied [3].

In high-temperature gas-cooled reactors as limiting factors are the maximum allowable temperature of fuel and the pressure drop attributable to the core that characterizes the allowable energy costs for pumping coolant. Thus, it is necessary for the same maximum fuel temperature to develop such a core, which would have minimal hydrodynamic resistance under given geometrical dimensions of the core, and heat capacity of coolant gas parameters.

Until now, research reactors with pebble bed is considered to be a daunting task. Of particular difficulty cause local hot spots that appear in the fuel, is heated to the melting point of graphite moderator surrounding the fuel. Due to the complex non-uniform core structure of the reactor cooling gas flow has a complex turbulent character. Nuclear engineers use a simulation with help of variety of CFD-codes to examine of safety of gas-cooled pebble bed reactor. In this paper we study the gas flow in system with sphere fuel elements by means solving 3D Navier-Stokes equations. The calculations are made taking into account the turbulent flow of the stream, the calculation of eddy viscosity was carried out using Smagorinsky model.

2 Numerical method

For 3D simulations of the turbulent flow and heat transfer around sphere fuel elements in the different cases, the special supercomputer software was created.

The main purpose of creating new software is optimization of simulation on distributed memory supercomputers using standard MPI. The proposed architecture of software allows us to set an arbitrary set of operators that implement the selected circuit solutions or create new ones if it is necessary. To unify the approach the initial and boundary conditions are also implemented as operators.

Currently we implemented in the software package explicit schemes for

solving Navier-Stokes equations using Smagorinsky subgrid-scale (SGS) model that represents one of the trips to modeling using the of large-eddy simulation (LES) method. The boundary condition is the no-slip condition at a solid boundary.

It should be noted that the proposed architecture allows us to implement solutions and different approaches to solving this problem, such as the method of direct numerical simulation.

We use GDML language for description the geometry of bodies in flow, which allows us to specify the body of complex geometry, including an ensemble of several bodies.

3 Simulation of gas flow through cell with two spherical fuel elements

Let's consider the 3D modeling of flow in cell with two spherical fuel elements. The geometry for the numerical analysis is similar to that considered in article [4] (see Fig. 1.) There are two neighboring spheres aligned to each other.

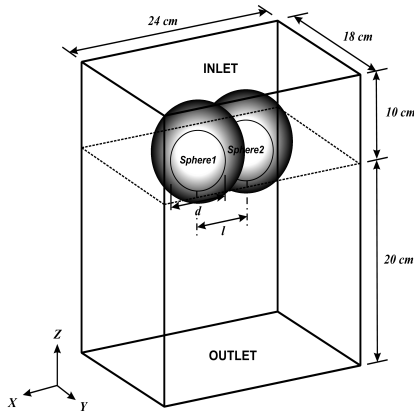


Figure 1: Geometry for simulations

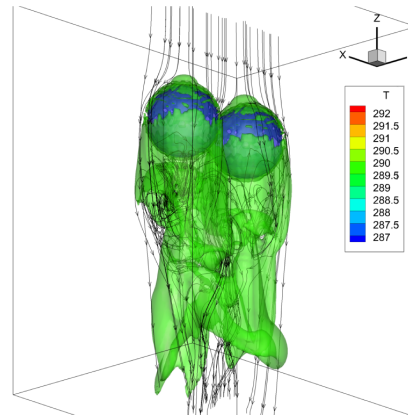


Figure 2: The temperature isosurface with flow visualization $T = 290 K$.

The incoming gas flow is directed strictly along the Z axis in the opposite direction, flow rate is $0.2 M$, which is $68 m/c$ ($u = 0, v = 0, w = -0.68$), body and flow temperatures are $T = 288.15 K$, density is

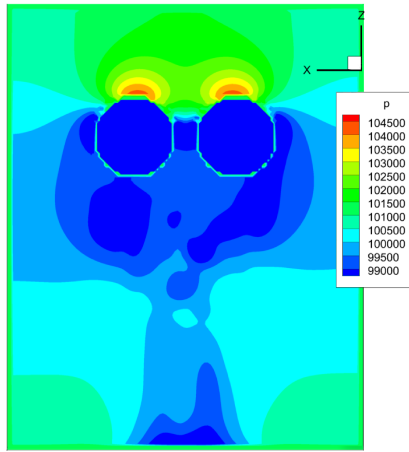


Figure 3: Pressure distribution, XZ , $y = 0$ cross section.

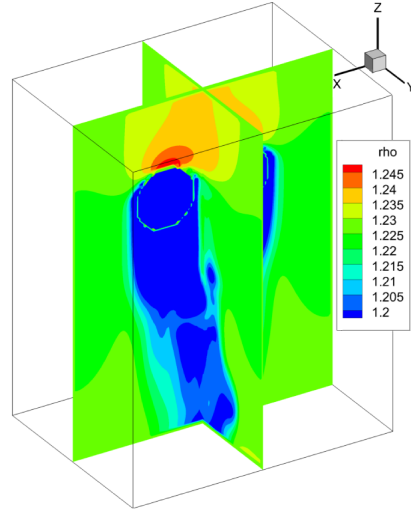


Figure 4: The density distribution, XZ , $y = 0$ and YZ , $x = 0$ cross sections.

$\rho = 1.225$, pressure is $P = 101325$, molecular viscosity is $\mu = 1.4607 \cdot 10^{-5}$.

4 Results

The times for calculations were from 0 to 0.15 *sec* with the time discretization of 10^{-7} *sec*. Processor: AMD Opteron (tm) 6376, 202 cores (198 cores for calculations and 4 cores to support exchanges and collection data). Interconnect: GigabitEthernet. The sizes of the simulation region are: $X : 24 \text{ cm}$, $Y : 18 \text{ cm}$, $Z : 30 \text{ cm}$. Origin of the coordinate system $(0, 0, 0)$ is located in the center of XY plane and at the distance of 20 *cm* from the bottom of the simulation region. Mesh Size: $212 \times 90 \times 150$, cell size $2 \text{ mm} \times 2 \text{ mm} \times 1.5 \text{ mm}$. The diameter of spheres: $d = 60 \text{ mm}$. The distance between centers of the spheres is $l = 68 \text{ mm}$. Time accounts for $t = 0.15 \text{ sec}$ duration was 7 days.

After the simulation we find the following quantities: temperature, pressure, density, viscosity, effective turbulent viscosity, thermal conductivity in each cell of computing the volume and velocity fields. Some results of our calculations are presented on Figures 2 – 4.

5 Conclusion

Simulation of flow around the pebbles in the PBMR core sell was performed with turbulence modeling using a new software for supercomputer with distributive memory and *MPI*.

The presence of turbulent gas flow for the pebbles are shown.

Temperature, pressure, density, viscosity, effective turbulent viscosity, thermal conductivity in each cell of computing the volume and velocity fields are calculated.

References

- [1] M.J. Driscoll, P. Hejzlar. Reactor physics challenges in Gen-IV reactor design. Nucl. Eng. Tech. V. 37. – 2005.– P. 1-10.
- [2] Y.A. Hassan, G. Yesilyurt. Flow distribution of pebble bed high temperature of gas cooled reactors using large eddy simulation. In: Proceedings of the 1st International Topical Meeting on High Temperature Reactor Technology, Petten, Netherlands, 22-24 Apr 2002. – 2002.– 6 p.
- [3] G. Yesilyurt, Y.A. Hassan. LES simulation in pebble bed modular reactor core through randomly distributed fuel elements. In: Proceedings of the International Conference on Global Environment and Advanced Nuclear Power Plants, Kyoto, Japan, September, Sep . 15-19, – Paper 1 204.– 2003. – 13 p.
- [4] Jung-Jae Lee, Goon-Cherl Park, Kwang-Yong Kimb, Won-Jae Lee. Numerical treatment of pebble contact in the flow and heat transfer analysis of a pebble bed reactor core. Nuclear Engineering and Design V. 237. – 2007. – P. 2183-2196.

The Estimation of Efficiency of the Control Rods in the Reactor with Sodium Coolant using Monte Carlo Simulation

L.F. Babichev*, G.W. Karpovich†

*Joint Institute for Power and Nuclear Research - Sosny
of the NAS of Belarus*

Abstract

The full-scale three-dimensional Monte Carlo model of BN-600 type reactor with plutonium fuel is created. The basic characteristics of the control system of the reactor are calculated.

1 Introduction

Knowledge of the efficiency of a control rod to absorb excess reactivity in a nuclear reactor, i.e. knowledge of its reactivity worth, is very important from many points of view. These include the analysis and the assessment of the shutdown margin of new core configurations (upgrade, conversion, refuelling, etc.) as well as several operational needs, such as calibration of the control rods, e.g. in case that reactivity insertion experiments are planned. There has been no change in the view that energy production with breeding of fissile materials is the main goal of fast reactor development to ensure long-term fuel supply [1]. However, before the breeding role of fast reactors is recognized economically, due to the increasingly available low-cost uranium from the 1980s onwards, the emphasis of fast reactor development shifted to incineration of stock-piled plutonium and

*E-mail: babichev@sosny.bas-net.by

†E-mail: gleb3452006@rambler.ru

partitioning and transmutation of nuclear wastes to meet contemporary demands.

2 Description of the model

Let us consider a model of the fast breeder reactor corresponding design of the BN-600 with plutonium fuel. A fast neutron reactor or simply a fast reactor is a category of nuclear reactor in which the fission chain reaction is sustained by fast neutrons. Such a reactor needs no neutron moderator, but must use fuel that is relatively rich in fissile material when compared to that required for a thermal reactor. The BN-600 reactor is a sodium-cooled fast breeder reactor, built at the Beloyarsk Nuclear Power Station, in Zarechny, Sverdlovsk Oblast, Russia [2]. The plant is a pool-type reactor, where the reactor, coolant pumps, intermediate heat exchangers and associated piping are all located in a common liquid sodium pool. The reactor core is 1.03 meters tall with a diameter of 2.05 meters. It has 369 fuel assemblies, mounted vertically, each consisting of 127 fuel rods enriched to between $17 \div 26\%$ ^{235}U . In comparison, normal enrichment in other Russian reactors is between 34% ^{235}U . The control and scram system comprises 27 reactivity control elements including 19 shim rods, two automatic control rods, and six automatic emergency shut-down rods. On-power refueling equipment allows for charging the core with fresh fuel assemblies, repositioning and turning the fuel assemblies within the reactor, and changing control and scram system elements remotely. Now we investigate the efficiency of the control rods in the reactor of BN-600 type with plutonium fuel. The horizontal cross section of the model of core configuration used in this work is shown in Figure 1.

3 Control rods worth estimation

BN-600 model core has been simulated by the Monte Carlo code MCU-PD using a stochastic approach. For the control rods worth estimation, the procedure insertions of positive and negative reactivity, avoiding, however, very small rod displacements which might cause Δk_{eff} of the order of the Monte Carlo statistical error. After the rise of the test control rod to the height h the inserted reactivity is calculated by the formula

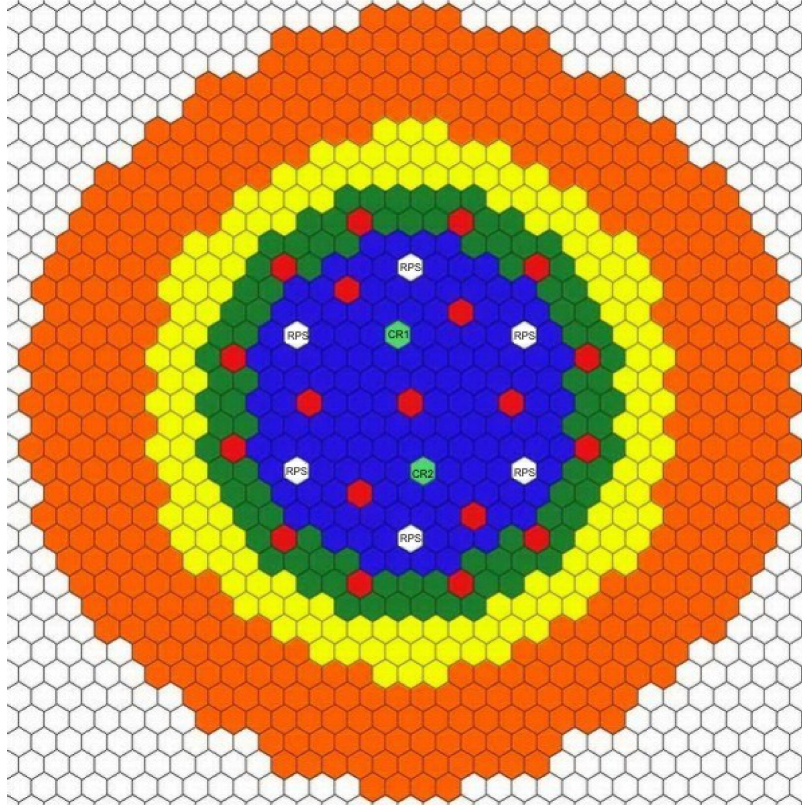


Figure 1: Horizontal cross section of the BN-600 model core. Blue areas correspond to fuel assemblies with 8% ^{239}Pu , dark-green areas correspond to fuel assemblies with 12% ^{239}Pu , yellow areas correspond to fuel assemblies with 17% ^{239}Pu , orange areas correspond fuel assemblies of breeding zone, red areas correspond to shim rods, light green correspond to control rods ($CR1$, $CR2$), white areas with RPS (Reactor Protection System) correspond to automatic emergency shut-down rods.

$$\Delta\rho_h = \rho_h - \rho_0 = \frac{k_{eff,h} - k_{eff,0}}{k_{eff,h} \cdot k_{eff,0}} \quad (1)$$

where $k_{eff,h}$ is the multiplication factor calculated for the rod raised to a height of h and $k_{eff,0}$ is the multiplication factor computed for fully inserted rod.

4 Numerical calculations

We made numerical calculations with MCU-PD code. MCU-PD is a general purpose, three dimensional, polykinetic, transport computer code. It uses the Monte Carlo method to simulate neutron, photon, electron and positron behavior in three dimensional geometries [3]. The code provides the ability of a detailed description of the geometrical elements (surface-based and/or combinatorial geometries) and very precise representation of basic nuclear data (point wise representation of cross sections), although the code also allows multigroup homogenized cross sections. It also provides easy-to-use powerful variance-reduction tools that help the user to solve deep penetration problems. For the purposes of this work, a detailed description of the BN-600 geometry was provided, using both combinatorial geometry (for the description of the reactor pool, the reflectors, the fuel elements and the control rods). The MDBPD50 nuclear data library was used for this simulation. Full-scale MCU-PD model of BN-600 reactor with plutonium fuel was developed (see Figures 2, 3).

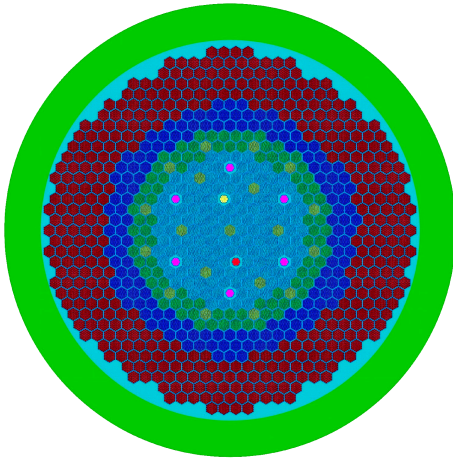


Figure 2: Monte Carlo model, XY cross section

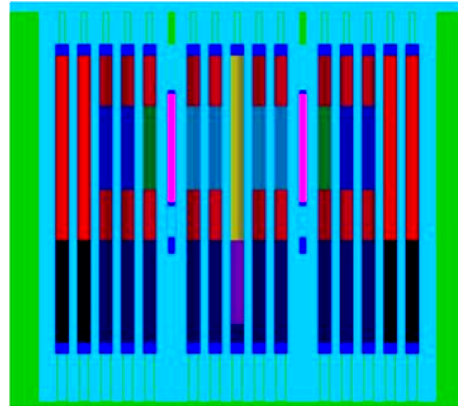


Figure 3: Monte Carlo model, XZ cross section

5 Calculation results

MCU-PD applications were performed using a number of events considered suitable for reliable results acquisition; with this statistics, each step of

the rod worth calculation (i.e. positive and negative reactivity insertion) required about 72 hours of computational time in a IBM Blade Servers HS22, 2.33 GHz, 24×8 node with 128 GB RAM, Linux machine. Thus, the complete computation of a rod worth curve requires machine time that may exceed 1 month. The results of calculations are presented in Tables 1, 2 and in Figure 4 (for $\beta_{eff} = 3.617 \cdot 10^{-3} \pm 1 \cdot 10^{-6}$).

Table 1: The basic characteristics of the control system of the reactor

Core state	k_{eff}	$\Delta\rho_H$	$\Delta\rho_H/\beta_{eff}$
All CR are extracted	1.06734 $\pm 9.0373 \cdot 10^{-5}$	-	-
CR1 is down	1.06297 $\pm 9.0003 \cdot 10^{-5}$	$3.8517 \cdot 10^{-3}$ $\pm 3.6149 \cdot 10^{-4}$	1.064 $\pm 3.62 \cdot 10^{-4}$
CR2 is down	1.06300 $\pm 9.0006 \cdot 10^{-5}$	$3.8254 \cdot 10^{-3}$ $\pm 3.6148 \cdot 10^{-4}$	1.058 $\pm 3.62 \cdot 10^{-4}$
RPS is down	1.03701 $\pm 8.7805 \cdot 10^{-5}$	0.027409 $\pm 3.5122 \cdot 10^{-4}$	7.578 $\pm 3.52 \cdot 10^{-4}$

Table 2: The characteristics of the CR1 control rod depending on h

h, cm	0	31.8	63.6	127.35
k_{eff}	1.06297 $\pm 9.0003 \cdot 10^{-5}$	1.06395 $\pm 9.0086 \cdot 10^{-5}$	1.06647 $\pm 9.0300 \cdot 10^{-5}$	1.06734 $\pm 9.0373 \cdot 10^{-5}$
$\Delta\rho_h$	0	$8.6653 \cdot 10^{-4}$ $\pm 3.6034 \cdot 10^{-4}$	$3.0874 \cdot 10^{-3}$ $\pm 3.6120 \cdot 10^{-4}$	$3.8517 \cdot 10^{-3}$ $\pm 3.6149 \cdot 10^{-4}$

6 Conclusion

In this paper we have described algorithms for calculation of the efficiency of the control rods in the fast breeder reactor, with sodium coolant using Monte Carlo simulation. The full-scale three-dimensional Monte Carlo

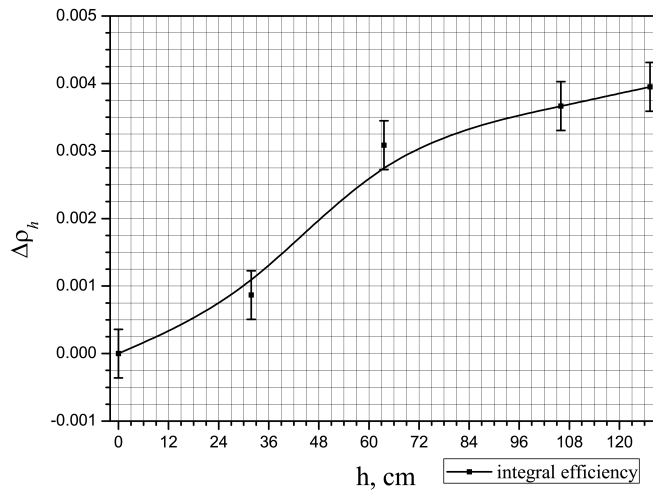


Figure 4: Integral worth of *CR1* control rod.

model of BN-600 type reactor with plutonium fuel is created. The basic characteristics of the control system of the reactor are calculated.

References

- [1] Frank von Hippel et al. Fast Breeder Reactor Programs: History and Status. International Panel on Fissile Materials. 2010. ISBN 978-0-9819275-6-5. – 128 p.
- [2] Yu.E. Bagdasarov, O.M. Saraev, N.N. Oshkanov. Reactor BN-600 power unit No 3 of Beloyarsk nuclear power plant. – Obninsk: FEI, 1992. – 40 p.
- [3] V.G. Dementiev, S.S. Gorodkov, D.S. Oleynik. Full-scale VVER-1000 model for Monte Carlo calculation of neutron characteristics of core. MCU-PD and BIPR-7A results comparison. 19th AER Symposium on VVER Reactor Physics and Reactor Safety, September 20-27, StSt. Constantine and Elena, Bulgaria, 2009. – 8 p.

Steps in Creation of Educational and Research Web-Portal of Nuclear Knowledge BelNET

S.Charapitsa¹, I.Dubovskaya², I.Kimlenko²,
A.Kovalenko¹, A.Lobko¹, A.Mazanik¹, N.Polyak¹,
T.Savitskaya², T.Sidorovich³, S.Sytova^{1*}, A.Timoschenko²

¹*Research Institute for Nuclear Problems of Belarusian State University*

²*Belarusian State University, Minsk, Belarus*

³*Brest State Technical University, Brest, Belarus*

Abstract

Belarusian State University is currently developing the educational and research web portal of nuclear knowledge BelNET (Belarusian Nuclear Education and Training Portal). In the future, this specialized electronic portal could grow into a national portal of nuclear knowledge. The concept, structure and taxonomy of BelNET portal are developed. The requirements and conditions for its functioning are analyzed. The information model and architecture of the portal, as well as algorithms and methods of software are realized. At present, BelNET software implemented all the basic functions of this portal, including the ability to remotely (via the Internet) open content editing, sorting, filtering, etc. Filling the BelNET by knowledge is at the beginning.

1 Introduction

The International Atomic Energy Agency (IAEA) [1]–[4] pays close attention to the problems of nuclear knowledge management. Nowadays,

*E-mail:sytova@inp.bsu.by

numerous national and international portals of nuclear knowledge were created in Europe, Asia, Africa and America under the patronage of the IAEA. It is planned to develop an international network of information resources on nuclear knowledge. This means that a unified information space in the field of nuclear knowledge is being formed in the world. Every developed country with its own nuclear industry has to create and maintain a national portal of nuclear knowledge, integrated into a global system of nuclear knowledge management. In the light of creation of Belarusian nuclear industry and construction of Belarusian nuclear power plant, development of electronic portal of nuclear knowledge is an insistent need for Belarus.

The development of computer technology, new requirements for the volume, complexity and speed of information transfer, as well as the rapid growth of mobile applications with specific requirements on the amount and form of presentation of information demand new effective algorithmic, architectural and software solutions. The portal of nuclear knowledge should be a complex programming system based on such modern technologies. Also, in the light of rapid growth of popularity of free software in the world, it would be good if the portal was developed on the Belarusian free software. So, creating such a portal is not just the development of a simple website, like such as millions in the Internet. The portal must meet the requirements of safety, reliability, efficiency and performance and reflect the national features of nuclear knowledge content.

The educational and research web-portal of nuclear knowledge BelNET (**B**elarusian **N**uclear **E**ducation and **T**raining) has the following objectives: acceleration of search and access to necessary data and information, creation of new knowledge, promotion of participation in research, education and training programs in nuclear industry, management of information resources, knowledge and competencies of nuclear industry in Belarus.

The basis of BelNET software is “Electronic document management system eLab” [5] developed on free software by the Laboratory of analytical research of the Research Institute for Nuclear Problems of Belarusian State University. eLab is implemented in the educational process of leading Belarusian universities: Belarusian State University, Belarusian State Technological University, Belarusian National Technical University. It is introduced in the Chemical-toxicological laboratory of the Minsk Drug Treatment Clinic. eLab has been a basis of management of specimens, measurements and passports of fuels and lubricants of Belarusian Army

since 2012 and Belarusian branch of Russian company GazPromNeft since 2013. Software eLab is protected by four Certificates of the National Intellectual Property Center of the Republic of Belarus.

eLab software is an electronic system of client-server architecture, designed on the basis of free software: Debian GNU / Linux, Web-server Apache, the Firebird database server using the application server PHP. It works under Windows and Linux through widely used browsers reliably without interruption. It is also completely secure from unauthorized access. eLab has a fast response to user requests, providing visibility and accessibility of information through a single interface for a wide range of integrated applications for users with different rights of access. It proved to be a system easily upgradable to conditions of the project.

2 BelNET principles of operation

In Fig.1, the main principles of BelNET operation are depicted in a simple form. Users with different rights of access from high school and university students to university professors and specialists visit on-line BelNET portal from their computers and laptops. Depending on the rights of access they can read documents available in open access, limited access or restricted access areas. With a user name and a password with appropriate rights, one can enter new documents on-line, or edit the existing ones etc.

BelNET components presented in Fig.2 as eLab system architecture are as follows:

- 1) Control computer (application server) running Linux, Unix or Windows;
- 2) Database server – cross-platform database management system (DBMS) Firebird;
- 3) User databases (DB);
- 4) Server of web-applications – Apache HTTP Server;
- 5) Code of web-application in PHP and JavaScript;
- 6) Library of access to databases ADOdb for PHP;
- 7) XAJAX library for building interactive user interfaces and web-applications;
- 8) Explorer (web-browser of client) for the following user categories: user with restricted access, user with limited access, user with open access;
- 9) eLab administrator;
- 10) System administrator.

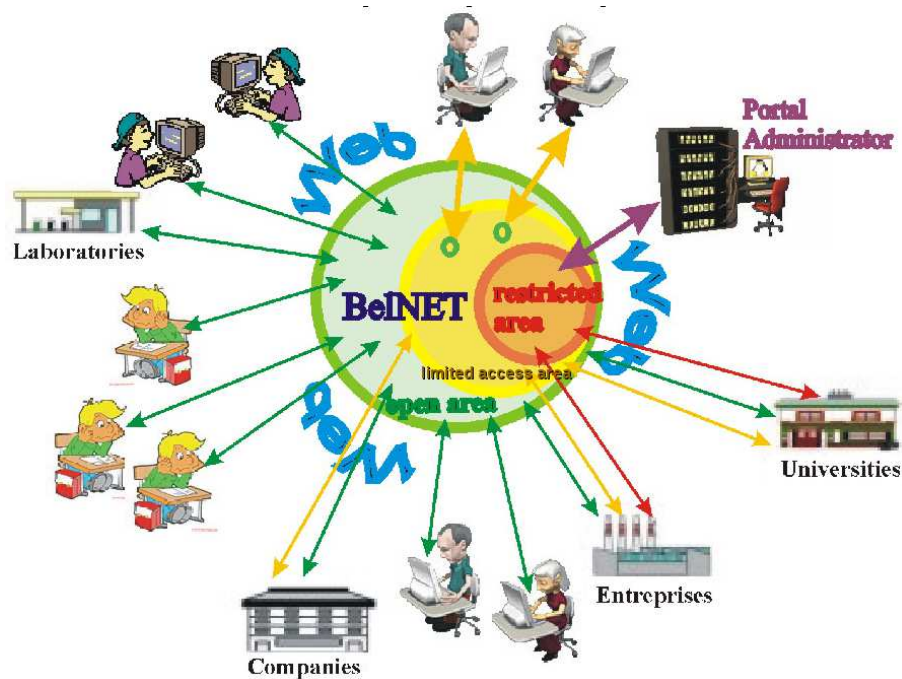


Figure 1: BelNET principles of operation

Data streams in eLab are the following:

- A. Data streams between the database server Firebird and user DB;
- B. Data streams at ADOdb library and the DBMS Firebird;
- C. Interaction of web-based applications eLab with user DB through ADOdb library and the Firebird;
- D. Implementation of XAJAX library in web-application eLab;
- E. Formation and processing of HTTP(S) requests by server of web-applications Apache;
- F. Data transfer from the server to the client and back through the web-server of applications;
- G. Interaction of eLab administrator with eLab system;
- H. Interaction of system administrator with the application server and eLab.

The interaction of these data streams (from Fig.1) are presented in other form in Fig.3.

BelNET and data content are placed on the host computer of the network (the application server) by the system administrator. The system

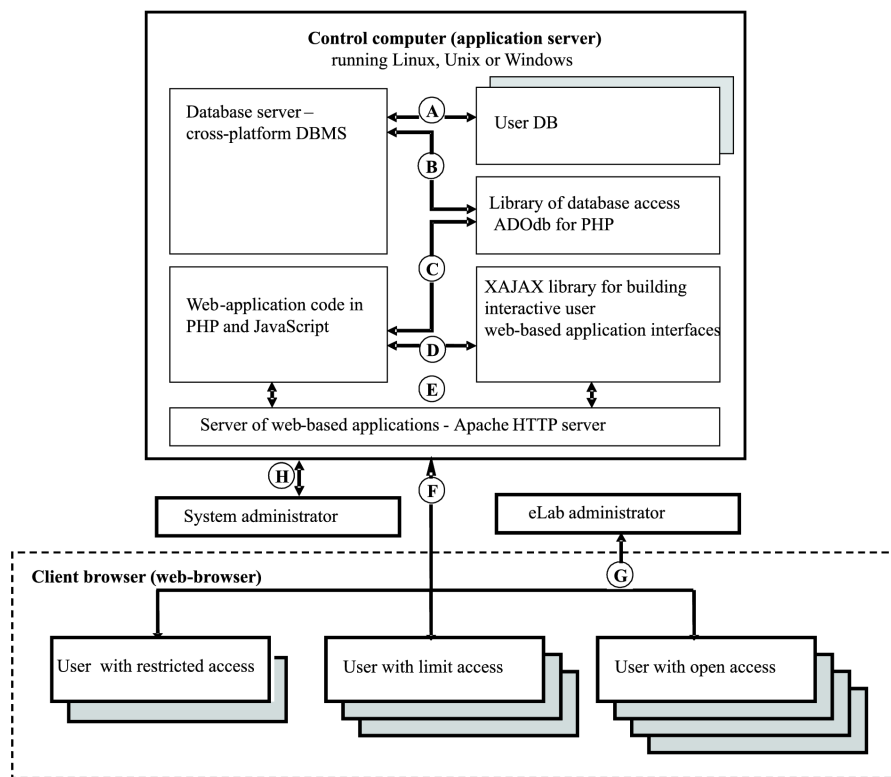


Figure 2: eLab system architecture

administrator has a full and direct access to the application server, including BelNET with its databases. The system administrator is responsible for operation, safety, and protection of server applications and data.

BelNET users, including the administrators of web-application (portal administrators) are clients of the system. They interact with the system and data over the Internet or the internal (corporate) network through a browser that is installed and used on the user's workstation. Personal desktop computers, laptops, tablets, or smartphones can be used as a workstation. Data streams between clients and web-application in both directions are carried out via the web-server Apache which provides validation, filtering and redirection of HTTP(S) requests. An interactive user interface is generated on the application server and displayed in a browser window on a workstation via the server (in PHP) and client (in JavaScript) of the interlayer XAJAX in accordance with the HTTP(S) user requests.

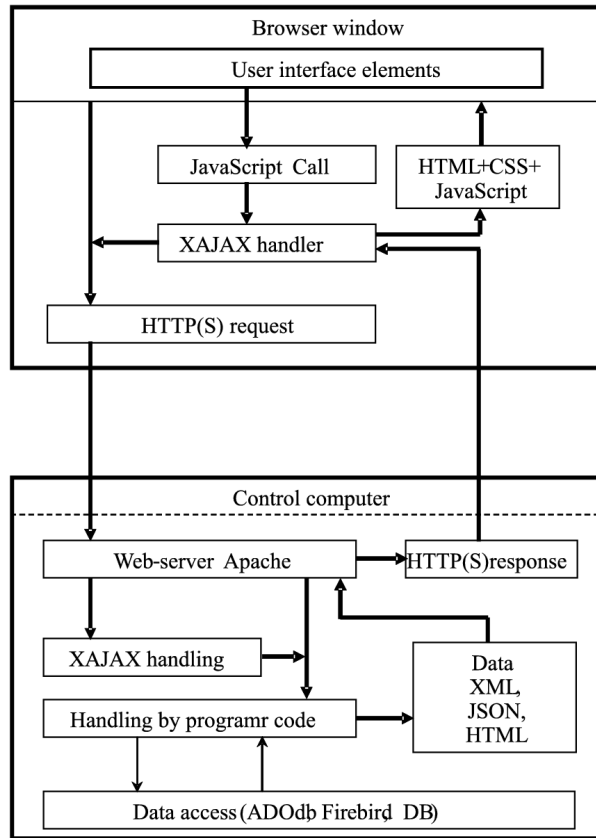


Figure 3: eLab data streams

The interface includes custom elements: links, buttons, lists, tables and other DOM-elements. Dynamic calls to the server with technology AJAX are supported allowing the modification of contents of the browser without reloading the entire page (the window contents).

3 Pilot version of BelNET

The pilot version of BelNET is depicted in part in [6]–[9] and available here: <http://lar.inpnet.net/el/belnet/> (see screenshot of its start page in Fig.4).

At present, BelNET software implements all basic functions of the portal, including the ability to remotely (via the Internet) open content editing, different sorting functions, filters, etc. (see Fig.5–6). So, we can say

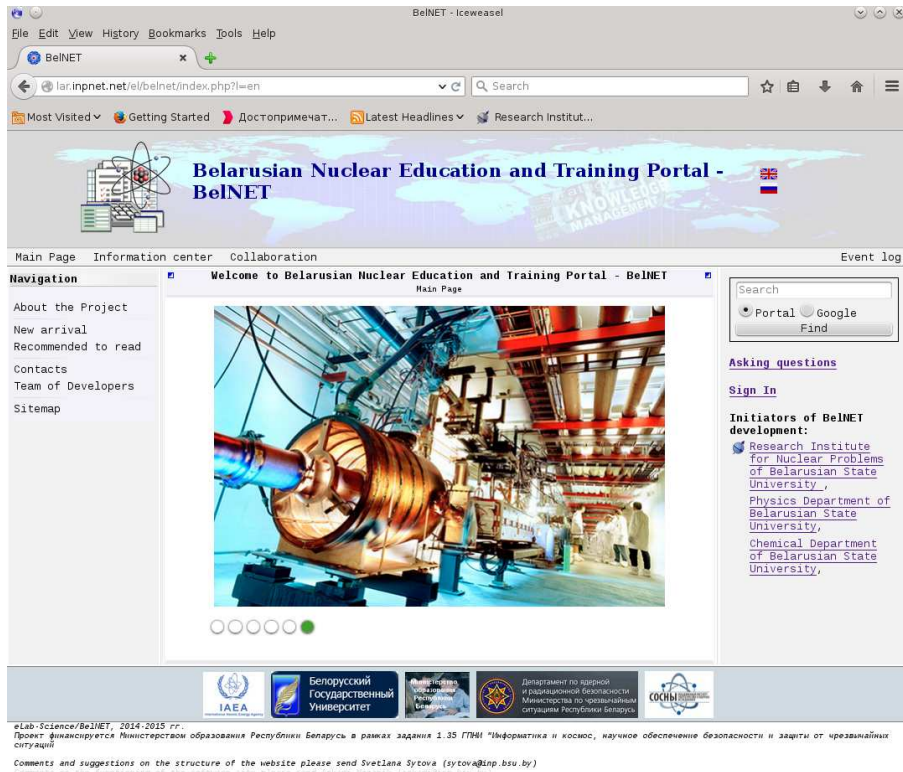


Figure 4: Start page of BelNET

that in the frame of this work the original content management system (CMS) was created. It includes the possibility to input texts and formulae in LaTeX-similar form and load different types of files, references, video, photos and pictures. On the basis of this CMS educational and scientific portals of various profiles can be created. Filling BelNET with information is underway.

4 Lab practice for students

We emphasize that filling the portal with information as well as developing special materials for a distance learning system is a time-consuming and long process. In this sense, the work on BelNET is at the beginning.

Currently, a glossary of nuclear physics terminology and lab practice for students are developed. Definitions included in the glossary are

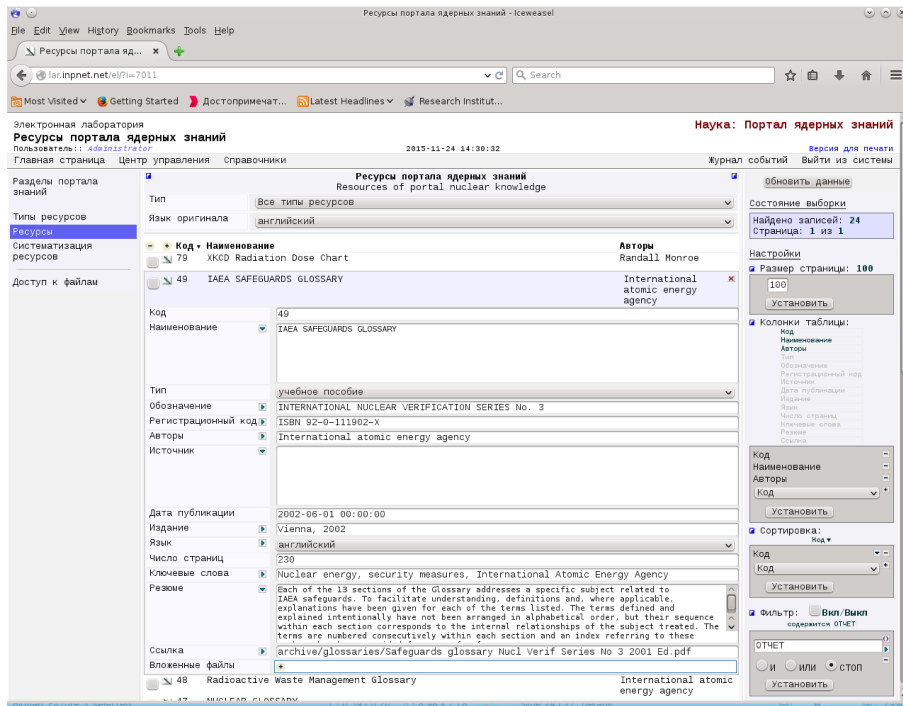


Figure 5: Editing of BelNET resources

formed on the basis of traditions prevailing in the scientific community, national and interstate regulatory documents with the account of the IAEA recommendations and the views of draftsmen. The articles contain term definitions, area of application and, if appropriate, analysis of differences between the given definitions and common or standard ones.

In high school, nuclear physics is traditionally presented only by a small theoretical section, which does not provide for implementation of lab work because the sources of ionizing radiation are forbidden by sanitary norms. However, the practical skills that students receive in performing lab work allow them to better understand the characteristics of ionizing radiation passing through matter and the dangers associated with the use of radioactive substances and principles of radiation protection. This is very important because of ionizing radiation and radioactive sources are widely used in medicine, engineering and other areas. Now requirements for basic knowledge of radiation principles and its impact on the environment are high in the light of development of nuclear industry in Belarus. The necessity to the general public of at least a minimum level of knowledge in

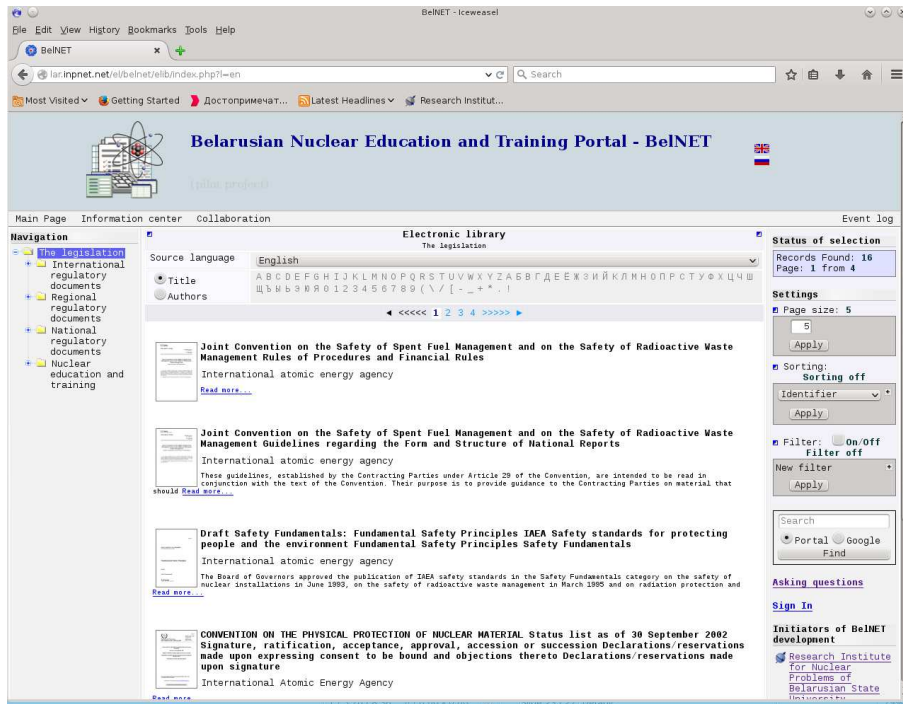


Figure 6: BelNET- Informations center - Legislation

this area was confirmed by the history of the Chernobyl disaster.

As a part of BelNET content, it was decided to develop a series of on-line guides for lab work on ionizing radiation passing through matter. These lab works are oriented to high school and university students as well as to anyone interested in this topic. The general part of the series is an introduction with brief information on nuclear physics and nuclear spectrometry. It includes the description of main features of the phenomenon of radioactivity. The work of detectors of ionizing radiation is explained as well as the principles of formation and interpretation of experimental energy radiation spectra. The formulae for estimating statistical errors of the experiment are given. Practical part includes five lab works: "Determination of the activity of radioactive source by a relative method", "Absorption of electrons in matter", "Absorption of gamma rays in matter", "Study of the penetrating power of gamma rays of different energies", "Natural decay chains". Each practice includes a brief description of the studied processes, necessary for understanding the experimental part of the work, as well as analysis of the obtained results. As a separate section

of each work, a guide on the order of experimental data processing, calculation and analysis of finite quantities is given. The experimental data (energy spectra of specific ionizing radiation) obtained using the spectrometer of ionizing radiation of the Department of Nuclear Physics of Belarusian State University are available in the form of text files. Video files demonstrate the spectrum set-up. This allows performing the lab work using only a computer with a standard set of programs. Using a computer calculator (eg. MS Excel), one can process the experimental spectra, calculate the necessary values and present the obtained results in graphical form. At the end of the series a test program is given in order to check the correctness of obtained results, as well as the level of understanding of the studied processes by the user and his willingness to use the results, for example, to estimate the parameters, necessary for protection against ionizing radiation.

5 Conclusion

Belarusian educational and research portal of nuclear knowledge BelNET is developed by the efforts of the best experts and professorate in the field of nuclear knowledge of the Republic of Belarus. The aim of the work is the promotion of nuclear knowledge, the formation positive image of nuclear science and attraction here the most able young people. Created original CMS allows developing educational and scientific portals of various profiles.

References

- [1] International Atomic Energy Agency GC(47)/RES/10. Strengthening of the Agency's Activities Related to Nuclear Science, Technology and Applications. Part B: Nuclear Knowledge. 2003.
- [2] Knowledge management for nuclear research and development organizations. IAEA-TECDOC-1675. 2012.
- [3] The Impact of Knowledge Management Practices on NPP Organizational Performance - Results of a Global Survey IAEA-TECDOC-1711, ISBN:978-92-0-143110-3, 2013.

- [4] Nuclear Engineering Education: A Competence-based Approach in Curricula Development Nuclear Energy Series No.NG-T-6.4, 2014.
- [5] Charapitsa S.V. et al. Electronic Management System of Accredited Testing Laboratory E-Lab. Abstr. 17 Int. Conf. Mathematical Modelling and Analysis, Tallinn, Estonia. P.30.
- [6] Charapitsa S.V. et al. Structure of Belarusian educational and research web portal of nuclear knowledge. LANL e-print arXiv: 1404.1338.
- [7] Charapitsa S.V. et al. Implementation of portal of nuclear knowledge BelNET, 11th Workshop on European Collaboration for Higher Education and Research in Nuclear Engineering and Radiological Protection. Minsk, 2015. P.21.
- [8] Charapitsa S.V. et al. Steps in creation of educational and research web-portal of nuclear knowledge BelNET "Mathematics of XXI Century & Natural Science". Book of Abstracts: Int. Symposium (September 29 – October 3, 2015). St. Petersburg, 2015. P. 31.
- [9] Sytova S. et al. Formation of the content of teaching and research portal nuclear knowledge BelNET. V Congress of physicists Belarus (October 27-30, 2015): Collection of scientific works. Minsk, 2015. P. 255-256.

6 List of Participants

Konstantin Afanaciev	NC PHEP BSU, Minsk
Azad Ahmadov	JINR, Dubna
Victor Andreev	GSU, Gomel
Victor Anishchik	BSU, Minsk
Elena Avakyan	GSTU, Gomel
Sergey Avakyan	GSTU, Gomel
Alexander Babich	GSTU, Gomel
Konstantin Babich	GSU, Gomel
Leanid Babicheu	JIPNR-Sosny, Minsk
Eugene Bagashov	JIPNR-Sosny, Minsk
Aleksey Bajajin	JINR, Dubna
Aliaksandr Baran	IP NASB, Minsk
Vladimir Baryshevsky	RINP BSU, Minsk
Konstantin Batrakov	RINP BSU, Minsk
Leonardo Benucci	Ghent University
Andrej Bernadskiy	GSU, Gomel
Oleg Boyarkin	BSPU, Minsk
Galina Boyarkina	BSPU, Minsk
Yury Bystritskiy	JINR, Dubna
Vassily Chaikovskiy	NC PHEP BSU, Minsk
Xin Chen	Tsinghua University, Beijing
Yurii Chernichenko	GSTU, Gomel
Elena Chernjavskaya	NC PHEP BSU, Minsk
Ekaterina Degtyareva	GSTU, Gomel
Oksana Deryuzhkova	GSU, Gomel
Eugeny Dey	GSU, Gomel
Alexander Dorokhov	JINR, Dubna
Alexander Drapezo	VIST GroupSensor Ltd., Minsk
Yahor Dydyshka	NC PHEP BSU, Minsk
Ekaterina Efimova	JINR, Dubna
Igor Emeliantchik	NC PHEP BSU, Minsk
Dmitriy Ermak	NC PHEP BSU, Minsk
Ilya Feranchuk	BSU, Minsk
Mikhail Galynskii	JIPNR-Sosny, Minsk
Vadim Gavrish	GSTU, Gomel
Valentin Gilewsky	JIPNR-Sosny, Minsk
Igor Golutvin	JINR, Dubna
Alexander Gribovskiy	GSU, Gomel
Yury Grischechkin	GSU, Gomel
Viktar Haurylavets	RINP BSU, Minsk
Aliaksei Hrynevich	NC PHEP BSU, Minsk

Laszlo Jenkovszky	BITP, Kiev
Valery Kapshai	GSU, Gomel
Ehor Kazitskiy	JIPNR-Sosny, Minsk
Viacheslav Khandramai	GSTU, Gomel
I. Kiselev	GSTU, Gomel
Alexander Kisselev	IHEP, Protvino
Elena Kokoulina	JINR, Dubna
Nikolai Kravchuk	JINR, Dubna
Sergey Kuchin	Bryansk SU, Bryansk, Novozybkov
Nikolay Kuchinskiy	JINR, Dubna
Yurii Kurochkin	IP NASB, Minsk
Semen Kuten	RINP BSU, Minsk
Viacheslav Kuvshinov	JIPNR-Sosny, Minsk
Vasiliy Lashkevich	GSTU, Gomel
Aliaksandr Leonau	BSU, Minsk
Michael Levchuk	IP NASB, Minsk
Alexander Litomin	NC PHEP BSU, Minsk
Alexander Lobko	RINP BSU, Minsk
Wolfgang Lohmann	DESY, Zeuthen
Svetlana Lukashevich	GSU, Gomel
Vladimir Makarenko	NC PHEP BSU, Minsk
Kristina Makarevich	RINP BSU, Minsk
Nikolay Maksimenko	GSU, Gomel
Andrej Man'ko	IP NASB, Minsk
Illia Maroz	RINP BSU, Minsk
Anastasiya Melnik	BSU, Minsk
Vladimir Mossolov	NC PHEP BSU, Minsk
Sergey Movchan	JINR, Dubna
Valentin Orlovich	NASB, Minsk
Mila Pandurovic	Vinča Institute of Nuclear Sciences, Belgrade
Alexander Pankov	GSTU, Gomel
Yuri Pleskachevsky	GB NASB, Gomel
Alexander Pobijakha	GSU, Gomel
Vladimir Ponariadov	BSU, Minsk
Elena Povprits	Bryansk SU, Bryansk, Novozybkov
Dmitry Prokopenko	GSTU, Gomel
Valerii Prokoshin	BSU, Minsk
Marina Prudnikova	JINR, Dubna
Alexander Rogachev	GSU, Gomel
Oleg Rogachevskiy	JINR, Dubna

Anatoli Rouba	RINP BSU, Minsk
Elena Russakovich	JINR, Dubna
Nikolai Russakovich	JINR, Dubna
Nikolai Sakhno	GSU, Gomel
Maria Savina	JINR, Dubna
Sergey Savitskiy	PUE "ARTMASH", Minsk
Sergey Sedykh	JINR, Dubna
Anatoliy Serdyukov	GSU, Gomel
Maria Serdyukova	GSU, Gomel
Inna Serenkova	GSTU, Gomel
Mikhail Sergeenko	GSMU, Gomel
Alexey Sery	Brest SU, Brest
Alexander Shalyt-Margolin	NC PHEP BSU, Minsk
Sergej Shashkov	SOL Instruments Ltd., Minsk
Sergei Shmatov	JINR, Dubna
Dzmitry Shoukavy	IP NASB, Minsk
Nikolai Shumeiko	NC PHEP BSU, Minsk
Alexander Shumilin	SCST, Minsk
Alexander Silenko	RINP BSU, Minsk
Vladimir Skalozub	DNU, Dnepropetrovsk
Olga Solovtsova	GSTU, Gomel
Siarhej Son	GSTU, Gomel
Victor Stankevich	GEI of MES, Gomel
Vassily Strazhev	BSU, Minsk
Alexei Sytov	BSU, Minsk
Svetlana Sytova	RINP BSU, Minsk
Andrey Terletskiy	JINR, Dubna
Viktor Tikhomirov	RINP BSU, Minsk
Evgeniy Timoshin	GSTU, Gomel
Sergey Timoshin	GSTU, Gomel
Lev Tomilchik	IP NASB, Minsk
Gennadiy Tyumenkov	GSU, Gomel
Sergey Tyutyunnikov	JINR, Dubna
Elena Vakulina	Bryansk SU, Bryansk, Novozybkov
Elena Velicheva	JINR, Dubna
Vladimir Voronin	JINR, Dubna
Vitaly Yermolchik	NC PHEP BSU, Minsk
Aleksandr Zhuk	Odessa Univ., Odessa
Ihar Zhuk	JIPNR-Sosny, Minsk
Vladimir Zykunov	BelSUT, Gomel